

8-2009

Experimental characterization and modeling of isothermal and nonisothermal physical aging in glassy polymer films.

Yunlong Guo 1977-
University of Louisville

Follow this and additional works at: <https://ir.library.louisville.edu/etd>

Recommended Citation

Guo, Yunlong 1977-, "Experimental characterization and modeling of isothermal and nonisothermal physical aging in glassy polymer films." (2009). *Electronic Theses and Dissertations*. Paper 547.
<https://doi.org/10.18297/etd/547>

This Doctoral Dissertation is brought to you for free and open access by ThinkIR: The University of Louisville's Institutional Repository. It has been accepted for inclusion in Electronic Theses and Dissertations by an authorized administrator of ThinkIR: The University of Louisville's Institutional Repository. This title appears here courtesy of the author, who has retained all other copyrights. For more information, please contact thinkir@louisville.edu.

EXPERIMENTAL CHARACTERIZATION AND MODELING OF
ISOTHERMAL AND NONISOTHERMAL PHYSICAL AGING IN
GLASSY POLYMER FILMS

By

Yunlong Guo

B.S., Tsinghua University, 2000
M.S., Tsinghua University, 2003

A Dissertation
Submitted to the Faculty of the
Graduate School of the University of Louisville
in Partial Fulfillment of the Requirements
for the Degree of

Doctor of Philosophy

Department of Mechanical Engineering
University of Louisville
Louisville, Kentucky

August 2009

EXPERIMENTAL CHARACTERIZATION AND MODELING OF
ISOTHERMAL AND NONISOTHERMAL PHYSICAL AGING IN
GLASSY POLYMER FILMS

By

Yunlong Guo
B.S., Tsinghua University, 2000
M.S., Tsinghua University, 2003

A Dissertation Approved on

May 13, 2009

By the following Dissertation Committee:

Dr. Roger D. Bradshaw, Dissertation Director, Department of Mechanical Engineering

Dr. Lubov P. Andrusiv, Department of Mechanical Engineering

Dr. Thomas A. Berfield, Department of Mechanical Engineering

Dr. William P. Hnat, Department of Mechanical Engineering

Dr. James C. Watters, Department of Chemical Engineering

Dr. Julius P. Wong, Department of Mechanical Engineering

DEDICATION

This dissertation is dedicated to my parents

Mr. Mingren Guo

and

Mrs. Xiuzhen Zhao

for their unconditional love and support

For my wife Jianting

Her love and companionship

made me keep optimism and gallantry

ACKNOWLEDGEMENT

First and foremost, I would like to express my sincere appreciation to my advisor, Professor Roger Bradshaw, for his exceptional understanding, insight, guidance and continuous encouragement throughout my research at University of Louisville. His industrial experience of composite materials in aerospace engineering combined with his solid fundamental knowledge and excellent academic achievement on polymer mechanics have greatly influenced my learning.

I would like to thank the other members of my proposal and examination committees: Dr. Lubov Andrusiv, Dr. Thomas Berfield, Dr. William Hnat, Dr. James Watters and Dr. Julius Wong. Their valuable comments and suggestions definitely made this dissertation better than it would have otherwise been.

I would also like to thank Dr. Gregory McKenna of Texas Tech University, and Dr. Wolfgang Knauss of California Institute of Technology, for their helpful suggestions and kind encouragement regarding this research.

I want to thank other students at Professor Bradshaw's research group, Rajeswara Resapu and Ni Wang, for introducing the Dynamic Mechanical Analyzer and performing some experimental work, respectively.

Finally, I would like to recognize the Grosscurth Fellowship for the financial

support of my graduate study, the Kentucky Science and Engineering Foundation (KSEF) for sponsorship of this project under grant number KSEF-148-502-05-136, and Scott Cione of GE Advanced Materials for supplying the film materials used in this dissertation.

ABSTRACT

EXPERIMENTAL CHARACTERIZATION AND MODELING OF ISOTHERMAL AND NONISOTHERMAL PHYSICAL AGING IN GLASSY POLYMER FILMS

Yunlong Guo

May 13, 2009

Fiber-reinforced polymer matrix composites (PMCs) using high-temperature thermoplastics as the matrix material represent a lightweight design solution for applications above 250°F. This is often required for aircraft structures subjected to supersonic airflows. While thermoplastic matrix PMCs may be successfully designed for such temperatures, they generally exhibit a time-dependent material response which must be well understood for successful design. One important aspect of this response is physical aging, which causes the viscoelastic behavior of amorphous polymers below their glass transition temperature to change with time. While isothermal physical aging has been extensively studied, physical aging during a varying temperature history has received less scrutiny.

This dissertation focuses on nonisothermal physical aging of polymers from both experimental and theoretical aspects. The study concentrates on pure polymers rather than fiber-reinforced composites; this step removes several complicating factors to

simplify the study. It is anticipated that the findings of this work can then be applied to composite materials applications.

The physical aging tests in this work are performed using a dynamic mechanical analyzer (DMA). The viscoelastic response of glassy polymers under various loading and thermal histories are observed as stress-strain data at a series of time points. The first stage of the experimental work involves the characterization of the isothermal physical aging behavior of two advanced thermoplastics. The second stage conducts tests on the same materials with varying thermal histories and with long-term test duration. This forms the basis to assess and modify a nonisothermal physical aging model (KAHR- a_{te} model). Based on the experimental findings, the KAHR- a_{te} model has been revised by new correlations between aging shift factors and volume response; this revised model performed well in predicting the nonisothermal physical aging behavior of glassy polymers.

In the work on isothermal physical aging, short-term creep and stress relaxation tests were performed at several temperatures within 15-35 °C below the glass transition temperature (T_g) at various aging times, using the short-term test method established by Struik. Stress and strain levels were such that the materials remained in the linear viscoelastic regime. These curves were then shifted together to determine momentary master curves and shift rates. In order to validate the obtained isothermal physical aging behavior, the results of creep and stress relaxation testing were compared and shown to be consistent with one another using appropriate interconversion of the viscoelastic material functions. Time-temperature superposition of the master curves was also performed. The temperature shift factors and aging shift rates for both PEEK and PPS

were consistent for both creep and stress relaxation test results.

Nonisothermal physical aging was monitored by sequential short-term creep tests after a series of temperature jumps; the resulting strain histories were analyzed to determine aging shift factors (a_{te}) for each of the creep tests. The nonisothermal aging response was predicted using the KAHR- a_{te} model, which combines the KAHR model of volume recovery with a suitable linear relationship between aging shift factors and specific volume. The KAHR- a_{te} model can be utilized to both predict aging response and to determine necessary model parameters from a set of aging shift factor data. For the PEEK and PPS materials considered in the current study, predictions of mechanical response were demonstrated to be in good agreement with the experimental results for several complicated thermal histories. In addition to short-term nonisothermal aging, long-term creep tests under identical thermal conditions were also analyzed. Effective time theory was utilized to predict long-term response under both isothermal and nonisothermal temperature histories. The long-term compliance after a series of temperature changes was predicted by the KAHR- a_{te} model, and the theoretical predictions and experimental data showed good agreement for various thermal histories.

Lastly, physical aging behavior of PPS near the glass transition temperature was investigated, in order to observe the mechanical response in the process of the evolution of the material into equilibrium. At several temperatures near T_g , the time need to reach equilibrium were determined by the creep test results at various aging times. In addition to isothermal physical aging, mechanical shift factors in the period of approaching equilibrium at a common temperature after temperature up-jumps and down-jumps are monitored from creep tests; prior to these temperature jumps, the materials were aged to

reach equilibrium states. From these tests, asymmetry of approaching equilibrium phenomenon in a_{te} was observed, which is first-time reported in the literature. This finding shows the similarity between the thermodynamic and mechanical properties during structural relaxation. This work will lead to improved understanding of the viscoelastic behavior of glassy polymers, which is important for better understanding and design of PMCs in elevated temperature applications.

With the above findings, this dissertation deals with nonisothermal physical aging of glassy polymers, including both experimental characterization and constructing a framework for predictions of mechanical behavior of polymeric materials under complicated thermal conditions.

TABLE OF CONTENTS

	PAGE
DEDICATION.....	iii
ACKNOWLEDGEMENT.....	iv
ABSTRACT.....	vi
TABLE OF CONTENTS.....	x
LIST OF TABLES.....	xiv
LIST OF FIGURES.....	xvi
CHAPTER 1 INTRODUCTION.....	1
1.1 Polymeric Materials.....	1
1.2 Physical Aging of Polymers.....	2
1.3 Scope of This Dissertation.....	5
CHAPTER 2 POLYMER VISCOELASTICITY.....	9
2.1 Classification of Polymers.....	9
2.2 Glass Transition of Polymers.....	11
2.2.1 Phenomenology of the Glass Transition.....	11
2.2.2. Free Volume Theory on Glass Transition.....	17
2.3 Linear Polymer Viscoelasticity.....	19
2.3.1 Creep and Stress Relaxation.....	19
2.3.2 Boltzmann Superposition Principle and Linearity.....	22
2.3.3 Dynamic Viscoelastic Functions.....	24
2.3.4 Interrelations among Viscoelastic Properties.....	26
2.4 Time and Temperature Behavior of Polymers.....	29

2.4.1	Viscoelastic Models and Materials Response Functions	29
2.4.2	Time-Temperature Superposition Principle	35
2.4.3	Thermorheologically Simple Materials	37
CHAPTER 3	EXPERIMENTAL METHOD AND MATERIALS	39
3.1	RSA III Dynamic Mechanical Analyzer	39
3.1.1	Background	39
3.1.2	RSA III DMA Components and Specifications.....	40
3.2	Experimental Methodology by DMA	43
3.2.1	Temperature Sweep	43
3.2.2	Creep and Stress Relaxation Test Method- Physical Aging.....	51
3.2.3	Creep and Stress Relaxation Test – DMA settings.....	56
3.3	Materials in This Dissertation.....	60
3.3.1	Specimen Configuration	61
3.3.2	Normalization of Experimental Results due to Dimension Variation.....	65
3.4	Other Aspects Related Experiments	67
3.4.1	Actual Temperature Ramp Rate	67
3.4.2	Test Temperatures	68
3.4.3	Linear Regions	70
CHAPTER 4	ISOTHERMAL PHYSICAL AGING OF PEEK AND PPS	73
4.1	Background.....	73
4.2	Results of Glass Transition Temperature	77
4.3	Creep and Stress Relaxation Test Details.....	78
4.4	Time-Aging Time Superposition and PHYAGE.....	79
4.5	Creep and Stress Relaxation Results	82
4.5.1	Isothermal Creep Test Results	82
4.5.2	Compliance Variation between Specimens	86
4.5.3	Creep Data Analysis	87
4.5.4	Isothermal Stress Relaxation Test Results.....	89
4.5.5	Stress Relaxation Data Analysis	93
4.6	Temperature Shift Factors	95

4.7 Comparison of Creep and Stress Relaxation via Interconversion	99
CHAPTER 5 NONISOTHERMAL PHYSICAL AGING OF PEEK AND PPS.....	105
5.1 Background.....	105
5.2 Experimental Results on Single Temperature Up-jump Tests.....	113
5.3 Results for Complex Thermal Treatments.....	122
5.4 Long-term Nonisothermal Aging Response	124
5.4.1 Background.....	124
5.4.2 Long-term Creep Results During Nonisothermal Aging.....	126
CHAPTER 6 MODELING NONISOTHERMAL PHYSICAL AGING	130
6.1 Background.....	130
6.2 KAHR- a_{te} Model	132
6.2.1 The KAHR Model	132
6.2.2 KAHR- a_{te} Model of Aging Shift Factor	133
6.2.3 KAHR- a_{te} Model Solution Algorithm	134
6.2.4 Optimal KAHR- a_{te} Model Parameters.....	136
6.3 Application of KAHR- a_{te} Model to Nonisothermal Data.....	137
6.3.1 KAHR- a_{te} Model Parameters.....	137
6.3.2 KAHR- a_{te} Model Parameter Identification.....	139
6.3.3 Aging Shift Factor Predictions for Up-jump Tests.....	140
6.3.4 Aging Shift Factor Predictions for Complex Thermal Histories.....	147
6.4 Optimization of KAHR- a_{te} Model Parameters	150
6.4.1 Optimization Procedure	151
6.4.2 Optimal Parameter Determination.....	156
6.4.3 Aging Shift Factor Prediction.....	162
6.4.4 Prediction of Compliance after Temperature Jumps.....	165
6.5 Prediction of Aging Shift Factors at Various Temperatures.....	167
6.6 Prediction of Long-Term Response of PPS in Nonisothermal Aging	171
6.6.1 Effective Time Theory.....	172
6.6.2 Determination of μ^* and λ^*	173
6.6.3 Predictions Long-term Response for Various Thermal Histories.....	176

CHAPTER 7 PHYSICAL AGING NEAR GLASS TRANSITION TEMPERATURE	183
7.1 Aging into Equilibrium under Isothermal Conditions	183
7.1.1 Background	184
7.1.2 Test Method	185
7.1.3 Results and Discussion	187
7.2 Asymmetry of Approaching Equilibrium	193
7.3 Effective Relaxation Time Paradox	195
7.4 Comparison of Mechanical and Volumetric Phenomenology	200
CHAPTER 8 SUMMARY AND CONCLUSIONS	204
REFERENCES	209
CURRICULUM VITAE	218

LIST OF TABLES

TABLE	PAGE
1. Viscoelastic functions of Maxwell-Wiechert and Voigt-Kelvin model	35
2. Specifications of TA Instruments RSA III DMA	43
3. Parameter set for the T_g tests	47
4. Average storage modulus over a temperature range for normalization.....	67
5. Upper stress/strain limits of linear viscoelastic range ($t_e = 5/16$ hours)	72
6. Reference (master) curve parameters obtained during isothermal creep tests at indicated temperature ($t_{eref} = 20$ hours, average values for 3+ replicates in each case).....	88
7. Reference (master) curve parameters obtained during isothermal stress relaxation tests at indicated temperature ($t_{eref} = 20$ hours, average values for 2+ replicates in each case)	94
8. Optimal reference (master) curve parameters for PEEK and PPS obtained from time-temperature superposition at indicated temperature and aging time $t_{eref} = 20$ hours.....	99
9. Optimal parameters of KAHR- a_{te} model from single temperature up-jump tests.....	140
10. RMS error between data and prediction of KAHR- a_{te} model, $K = 1$	145
11. Parameters of KAHR- a_{te} model, one-element retardation function	156
12. Parameters of KAHR- a_{te} model, PPS; with $c_0 = 0.633$, $c_1 = 12.422$	159
13. KAHR- a_{te} model values ζ and b , PPS; with $c_0 = 0.633$, $c_1 = 12.422$, $\tilde{\tau} = 477.289$, and $\tilde{\beta} = 0.0916$	161

14. KAHR- a_{te} model values ζ and b , PEEK; with $c_0 = 0.568$, $c_1 = 4.447$, $\tilde{\tau} = 986.831$, and $\tilde{\beta} = 0.155$	162
15. RMS error between data and prediction of KAHR- a_{te} model	163
16. Optimal KAHR- a_{te} model parameters for PPS obtained from three up-jump data sets by an optimization procedure.....	164
17. Parameters of Kohlrausch function to fit short-term creep response	177
18. Time required to reaching equilibrium t^* and shift rates changing before and after t^* for PPS.....	192

LIST OF FIGURES

FIGURE	PAGE
Figure 1. Volumetric response during constant rate cooling from above T_g ; evolution leads to volume path shown if temperature is maintained constant. (Bradshaw, 1997)	4
Figure 2. A simple classification of polymers	11
Figure 3. Five regions of viscoelastic behavior of a thermoplastic polymer (Brinson and Brinson, 2008).....	13
Figure 4. Viscosity-temperature dependence for an amorphous polymer (Riande et al., 2000)	14
Figure 5. Various points in temperature dependencies of heat capacity used to determine T_g (Mazurin and Gankin, 2007)	14
Figure 6. Temperature dependence of PVAc volume measured dilatometrically at cooling rate $q = 0.2$ K /min. Evaluation of T_g is indicated by the dashed lines (Svoboda et al., 2008)	15
Figure 7. T_g determined by the onset of the storage modulus E' change, the maximum of loss modulus E'' , and the maximum of phase factor $\tan \delta$ (Herzog et al., 2005)	16
Figure 8. Free volume v_f and its dependence on temperature for polymers	18
Figure 9. Creep and recovery test of elastic, plastic and viscoelastic materials (Finley et al., 1976).....	20
Figure 10. Relaxation test: strain (above) and corresponding qualitative stress (below) (Scherer, 1986)	21
Figure 11. Schematic of the strain response of a viscoelastic material to the stresses applied sequentially	23

Figure 12. Dynamic relaxation modulus and creep compliance functions.....	26
Figure 13. Maxwell-Wiechert model (Mehta and Monteiro, 1993)	30
Figure 14. Voigt-Kelvin model (Mehta and Monteiro, 1993).....	32
Figure 15. An illustration of the time temperature superposition principle with the poly(isobutylene) data (Catsiff and Tobolsky, 1955).....	36
Figure 16. RSA3 Dynamic Mechanical Analyzer (Resapu, 2005).....	41
Figure 17. Components and Subsystems of RSA III DMA (TA Instruments, 2003).....	42
Figure 18. Normalized dynamic waveforms and vectors (TA Instruments, 2003)	44
Figure 19. Dynamic temperature ramp test set-up screen	46
Figure 20. Effects of protection of auto tension adjustment (TA Instruments, 2003).....	48
Figure 21. The setting of auto tension adjustment.....	49
Figure 22. End of test settings of dynamic temperature sweep test.....	51
Figure 23. Short-term test method of isothermal creep testing (Bradshaw and Brinson, 1997e).....	54
Figure 24. Schematic of up-jump nonisothermal creep test (Guo et al., 2009).....	55
Figure 25. Test sequence design in RSA III DMA.....	58
Figure 26. Multiple extension mode test set up screen for single creep-recovery test.....	58
Figure 27. Stress relaxation test setting screen.....	59
Figure 28. Auto tension setting screen for stress relaxation test.....	60
Figure 29. Tools for preparing the sample.....	62
Figure 30. Specimen was mounted in the film/fiber tension clamps. (a) PPS specimen between top/bottom clamps; (b) Film and fiber tool component.....	63
Figure 31. Specimen geometry input.....	64
Figure 32. Tool constants input screen	64

Figure 33. Temperature change during quench of PPS	68
Figure 34. Linearity tests for PEEK at 130°C (te = 5/16 hours).....	72
Figure 35. Representative glass transition temperature (T_g) test results: (a) PEEK film; (b) PPS film.....	78
Figure 36. Isothermal creep test results for PEEK at 110°C.....	83
Figure 37. Isothermal creep test results for PEEK at 120°C.....	83
Figure 38. Isothermal creep test results for PEEK at 130°C.....	84
Figure 39. Isothermal creep test results for PPS at 57°C	84
Figure 40. Isothermal creep test results for PPS at 67°C	85
Figure 41. Isothermal creep test results for PPS at 73°C	85
Figure 42. Isothermal creep test results for PPS at 77°C	86
Figure 43. Variation between PEEK specimens in isothermal creep at 130°C	87
Figure 44. Shift factors and associated shift rates obtained from the creep tests for PEEK films at the temperatures indicated	88
Figure 45. Shift factors and associated shift rates obtained from the creep tests for PPS films at the temperatures indicated	89
Figure 46. Isothermal stress relaxation test results for PEEK at 110°C	90
Figure 47. Isothermal stress relaxation test results for PEEK at 120°C	90
Figure 48. Isothermal stress relaxation test results for PEEK at 130°C	91
Figure 49. Isothermal stress relaxation test results for PPS at 57°C.....	91
Figure 50. Isothermal stress relaxation test results for PPS at 67°C.....	92
Figure 51. Isothermal stress relaxation test results for PPS at 73°C.....	92
Figure 52. Isothermal stress relaxation test results for PPS at 77°C.....	93
Figure 53. Shift factors and associated shift rates obtained from the stress relaxation tests for PEEK films at the temperatures indicated	94

Figure 54. Shift factors and associated shift rates obtained from the stress relaxation tests for PPS films at the temperatures indicated.....	95
Figure 55. Time–temperature superposition of PPS creep master curves ($t_{ref}= 20$ hours,	97
Figure 56. Time–temperature superposition of PEEK creep master curves ($t_{ref}= 20$ hours, $T_{ref}= 130^{\circ}\text{C}$, temperature shift factors a_T as noted).....	97
Figure 57. Time–temperature superposition of PPS stress relaxation master curves ($t_{ref}= 20$ hours, $T_{ref}= 77^{\circ}\text{C}$, temperature shift factors a_T as noted)	98
Figure 58. Time–temperature superposition of PEEK stress relaxation master curves ($t_{ref}= 20$ hours, $T_{ref}= 130^{\circ}\text{C}$, temperature shift factors a_T as noted)	98
Figure 59. Comparison of compliance obtained by creep testing and stress relaxation testing for PPS isothermally aged at 77°C	100
Figure 60. Comparison of compliance obtained by creep testing and stress relaxation testing for PEEK isothermally aged at 120°C	101
Figure 61. Compliances of creep test and inverted from stress relaxation in PPS and 73°C	102
Figure 62. Shift rate comparison of creep and stress relaxation tests in PPS and 73°C	102
Figure 63. Comparison of shift rates obtained by creep and stress relaxation: (a) PEEK; (b) PPS.....	103
Figure 64. Comparison of temperature shift factors obtained by creep and stress relaxation: (a) PEEK; (b) PPS	104
Figure 65. Compliance and shift factors for PVC after aging 120 hours at a lower temperature (30°C , 40°C) followed by jump to 50°C as performed by Struik(Bradshaw and Brinson, 1997c; Struik, 1988).....	108
Figure 66. Single temperature up-jump test on volume recovery after aging at a lower temperature, studied by Struik for both volume and mechanical response (Struik, 1978).....	109
Figure 67. Correlation between a_{te} and specific volume v for polycarbonate during temperature up-jump histories (above T_g , quench to T_l and hold 120 hr, jump to T_e) (Struik, 1988).....	109

Figure 68. Aging shift factor a_{te} and effective aging time t_e^{eff} determined from the effective time for CSF method. Thermal history: aged 68 hours at 215°C, followed by up-jump to 225°C (Bradshaw, 1997).....	112
Figure 69. Creep compliance of PEEK after aging at 110°C for 14 h then jump to 130°C	114
Figure 70. Creep compliance of PEEK after aging at 118°C for 14 h then jump to 130°C	114
Figure 71. Creep compliance of PEEK after aging at 120°C for 14 h then jump to 130°C	115
Figure 72. Creep compliance of PEEK after aging at 125°C for 14 h then jump to 130°C	115
Figure 73. Creep compliance of PPS after aging at 57°C for 14 h then jump to 73°C ...	117
Figure 74. Creep compliance of PPS after aging at 63°C for 14 h then jump to 73°C ...	118
Figure 75. Creep compliance of PPS after aging at 67°C for 14 h then jump to 73°C ...	118
Figure 76. Average aging shift factors from three PEEK tests after aging at 118°C for 14 h followed by jump to 130°C; error bars indicate a 90% confidence level	120
Figure 77. Aging shift factors of creep tests after temperature up-jump to 130°C for PEEK; isothermal aging shift factors at the same temperature reported for comparison	121
Figure 78. Aging shift factors of creep tests after temperature up-jump to 73°C for PPS; isothermal aging shift factors at the same temperature reported for comparison.....	121
Figure 79. Mechanical shift factors during physical aging after multiple temperature steps for PPS with end temperature of 73 °C; experimental data are the average of three data sets of sequenced creep experiments.....	123
Figure 80. Mechanical shift factors during physical aging after multiple temperature steps for PPS with end temperature of 67 °C; experimental data are the average of three data sets of sequenced creep experiments.....	123
Figure 81. Long-term creep compliance curves of two thermal histories:	128
Figure 82. Long-term creep compliance curves of two thermal histories:	129

Figure 83. Long-term creep compliance curves of two thermal histories:	129
Figure 84. Prediction of mechanical shift factor for PEEK using KAHR- a_{te} model parameters obtained from 118-130°C.....	141
Figure 85. Prediction of mechanical shift factor for PEEK using KAHR- a_{te} model parameters obtained from 120-130°C.....	141
Figure 86. Prediction of mechanical shift factor for PPS using KAHR- a_{te} model parameters obtained from the 63-73°C tests.....	143
Figure 87. Prediction of mechanical shift factor for PPS using KAHR- a_{te} model parameters obtained from the curve fitting of the entire data points of 67-73°C tests.....	143
Figure 88. Prediction of mechanical shift factor for PPS using KAHR- a_{te} model parameters obtained from the curve fitting of 67-73°C tests except excluding the.....	144
Figure 89 Correlation between $\log a_{te}$ and δ of PEEK for several thermal histories; δ is calculated by model parameters from 120-130°C.....	146
Figure 90 Correlation between $\log a_{te}$ and δ of PPS for several thermal histories; δ is calculated by model parameters from 63-73°C.....	147
Figure 91. Aging shift factor of creep tests on PPS for thermal history 97°C → 57°C (4hr) → 67°C (10hr) → 73°C; KAHR- a_{te} model parameters obtained from the single up-jump 63-73°C, as listed in Table 9.....	148
Figure 92. Aging shift factor of creep tests on PPS, thermal history 97 °C → 67 °C (3hr) → 77 °C (7hr) → 57 °C (4hr) → 73 °C; KAHR- a_{te} model parameters obtained from the single up-jump 63-73°C, as listed in Table 9	149
Figure 93. Aging shift factor of creep tests on PPS for thermal history 97 °C → 27 °C (12hr) → 73 °C (1hr) → 27 °C (1hr) → 73 °C. KAHR- a_{te} model parameters obtained from the single up-jump 63-73°C, as listed in Table 9	150
Figure 94. Schematic representation of optimization procedure	155
Figure 95. Correlation of $\log a_{te}$ and δ for PPS, based the parameter frame of 57-73°C	157
Figure 96. Correlation of $\log a_{te}$ and δ for PPS, based the parameter frame of 63-73°C	158

Figure 97. Correlation of $\log a_{te}$ and δ for PPS, based the parameter frame of 67-73°C	158
Figure 98. Average retardation function and retardation functions of three individual up-jump thermal histories for PPS	160
Figure 99. Data and regression of $\ln(-\ln R_{avg}(z))$ vs. $\ln z$ for PPS.....	160
Figure 100. Prediction of aging shift factor for PEEK using optimal KAHR- a_{te} model parameters.....	162
Figure 101. Prediction of aging shift factor for PPS using optimal KAHR- a_{te} model parameters.....	163
Figure 102. Prediction of mechanical aging shift factor by KAHR- a_{te} model for various complex thermal histories in PPS	165
Figure 103. Compliance of experimental data and model predictions for PEEK:	166
Figure 104. Prediction of mechanical aging shift factor of PPS by KAHR- a_{te} model for thermal history: 97° C → 57° C (4hr) → 73° C (6hr) → 67° C. Reference curve is the isothermal compliance response at 67 °C with aging time = 20 hours	169
Figure 105. Prediction of mechanical aging shift factor of PPS by KAHR- a_{te} model for thermal history: 97° C → 57° C (14hr) → 67° C; reference curve is the isothermal compliance response at 67 °C with aging time = 20 hours and KAHR model uses parameters from Table 16.....	170
Figure 106. Prediction of mechanical aging shift factor of PEEK by KAHR- a_{te} model for thermal history: 148° C → 110° C (14hr) → 120° C; reference curve is the isothermal compliance response at 120 °C with aging time = 20 hours and KAHR model uses parameters from Table 16	171
Figure 107. Nonisothermal aging shift rate μ^* for complex thermal histories, values of μ^* are calculated using the predicted a_{te} from KAHR- a_{te} model	175
Figure 108. Calculated effective time for several isothermal and nonisothermal conditions.....	176
Figure 109. Long-term creep predictions by effective time theory and original Kohlrausch function from short-term response; thermal Histories: 97 °C → 57 °C → 73 °C and	178

Figure 110. Long-term creep predictions by effective time theory and original Kohlrausch function from short-term response; thermal Histories: 97 °C → 57 °C → 67 °C → 73 °C and 97 °C → 67 °C → 77 °C → 73 °C.....	178
Figure 111. Long-term creep predictions by isothermal and nonisothermal effective time theory and original Kohlrausch function from short-term response; thermal histories:	180
Figure 112. Long-term creep predictions by nonisothermal effective time theory and original Kohlrausch function from short-term response; the thermal history is:	181
Figure 113. Compliance limitation physical aging test (Wang, 2007)	186
Figure 114. Compliance curves of PPS at 82°C for aging times from 0.039 hr to 5 hr	188
Figure 115. Log a_{te} versus log t_e for PPS aged at 82°C. The transition from aging to approximate non-aging behavior is illustrated by the abrupt change of shift rate.	189
Figure 116. Compliance curves of PPS at 84°C for aging times from 0.039 hr to 1.25 hr	190
Figure 117. Log a_{te} versus log t_e for PPS aged at 84°C; the transition from aging to approximate non-aging behavior is illustrated by the abrupt change of shift rate	190
Figure 118. Linear fit of aging shift factors in aging and non-aging regions of PPS, at temperatures 81°C, 82°C, 83°C, 84°C and 85°C.....	191
Figure 119. Temperature dependence of the time necessary for attainment of equilibrium t^* of PPS, in isothermal physical aging.....	193
Figure 120. Normalized volumetric response of PVAc after single temperature jump (Kovacs, 1963)	194
Figure 121. Asymmetry of approaching equilibrium of aging shift factors of PPS	195
Figure 122. Original τ -effective plot from Kovacs for poly(vinyl acetate). Unlabeled values are equilibrium temperature before the jump, values T are temperatures after the jump, and both lines and circles are experimental data. Left part presents the results for up-jump tests; while the right part shows the results of down-jump experiments (Kovacs, 1963).....	196

Figure 123. Logarithmic effective relaxation time at 83°C for PPS, the results are obtained from mechanical test results for up-jump and down-jump from equilibrium at various temperatures. 199

Figure 124. τ -effective plot for an epoxy aging at 77 °C. The values of τ_{eff} were determined from $(d\delta/dt)$ and average δ value obtained from time t to $1.05t$ (i.e. over a logarithmic time interval of 0.02) for the volume recovery curves (Kolla and Simon, 2005) 199

Figure 125. Volume recovery in a polystyrene during isothermal physical aging at various indicated temperatures (Simon et al., 2001)201

Figure 126. The “memory effect” for volumetric response δ in a poly(vinyl acetate) on several thermal histories. (1): quench from 40°C to 30°C (isothermal aging); (2): quench from 40°C to 10°C for 160 h followed by up-jump to 30°C; (3): quench from 40°C to 15°C for 140 h followed by up-jump to 30°C and (4): quench from 40°C to 25°C for 90 h followed by up-jump to 30°C. $t - t_i$ is the time elapsed since the jump to 30°C (Kovacs, 1963).....202

CHAPTER 1

INTRODUCTION

This chapter provides a brief introduction of polymeric materials and the background of physical aging of glassy polymers. It also includes the scope of this dissertation and the organization of the following chapters.

1.1 Polymeric Materials

Polymers are widely used in the world today because of their desirable properties. These include good strength and modulus to weight ratios, chemical resistance, toughness, low thermal and electrical conductivity, ease of manufacture and low cost. As such, various forms of polymeric materials are used in the automotive industry, aerospace industry, computer industry, sporting goods, building structures and many other applications such as coatings, packaging, furniture and furnishing, etc. (Brinson and Brinson, 2008). One interesting feature of polymers is the cost to produce polymers is sometimes less than the cost to produce metals for comparable use. Crawford (Crawford, 1992) reported relative energy required to manufacture various sheet materials and the data indicates that several popular polymers (PVC, polycarbonate, polyethylene, etc.) can save more than 50% of the energy needed to manufacture similar steel sheets.

This partially explains why some traditional materials are being replaced by polymeric materials. Currently, advanced polymer-based materials, including polymer matrix composites, self-healing polymers, polymers for biomedical applications, and nano-reinforced polymers, are attracting a great deal of attention from researchers and industry all over the world.

Along with the development of many novel polymeric materials, theoretical analysis and experimental methodology in polymer physics, polymer chemistry and polymer viscoelasticity (Aklonis and MacKnight, 1983; Eisele, 1990; Hiemenz and Lodge, 2007) have been developed to aid in design and analysis of polymer-based materials. This dissertation focuses on the mechanical characterization of polymers, specifically in the area of viscoelastic behavior at elevated temperatures near the glass transition temperature of the polymer.

1.2 Physical Aging of Polymers

Understanding the mechanical behavior of polymer-based materials, especially fiber-reinforced polymeric matrix composites (PMCs) is a critical issue for many modern engineering structural applications (Ward, 1983). In such materials, strong/stiff fibers (graphite, glass, Kevlar, etc.) are held together using a softer polymer material called the matrix. In many circumstances, the polymeric matrix is the major constituent that contributes to degradation or changes in durability of PMCs subjected to long term exposure at elevated temperatures (Brinson and Gates, 1995; Sullivan, 1990; Sullivan et al., 1993). One important aspect of these changes is physical aging, which causes the

viscoelastic behavior of the polymer to vary with time spent below its glass transition temperature (T_g). The design of polymer composites for elevated temperature applications thus requires an understanding of physical aging of polymers subjected to isothermal and nonisothermal conditions (Bradshaw, 1997).

When an amorphous¹ polymer is cooled to a temperature below T_g , it enters a non-equilibrium glassy state. The material then proceeds towards equilibrium over a period of time; this phenomenon is known as structural relaxation. Structural relaxation manifests itself in several ways: volume recovery (shown in Figure 1); enthalpy relaxation, which underlies changes in thermodynamic properties, such as specific volume and enthalpy, structural relaxation is also observed in changes of mechanical properties such as compliance and modulus, in this context, structural relaxation is named physical aging by Struik (Struik, 1978).

The temperature dependence upon cooling of the specific volume, as shown in Figure 1, is pioneered by Kovacs (1963). The T_g is actually determined as the intersection of the straight line portions of the curve above and below the glass transition temperature. In Figure 1, temperature T is below T_g , the polymer is in nonequilibrium state at this temperature right after a quench from a temperature above T_g . At the beginning of physical aging, the specific volume is given by $v|_{t=0} = v^* + \alpha_g(T - T_g)$, where v^* is the

¹ The bulk state includes both amorphous (totally lacking positional order on the molecular scale) and crystalline polymers. While amorphous polymers do not contain any crystalline regions, crystalline polymers generally contains both crystalline and amorphous regions, so those are often called semicrystalline polymers. Crystalline polymers have true melting temperature (T_m) at which the ordered regions break up and become disordered (amorphous). In contrast, the amorphous regions soften over a relatively wide temperature range (always lower than T_m) known as the glass transition (T_g). Fully amorphous polymers do not exhibit T_m , of course, but all polymers exhibit T_g . Above these temperatures, polymers are liquids. See later sections for details.

specific volume at T_g , and a_g is volumetric coefficient of thermal expansion in glassy state; during physical aging, the specific volume can be expressed as $v|_{t_e>0} = v^* + \alpha_g(T - T_g) + \Delta v$, with the change of v $\Delta v = (\alpha_l - \alpha_g)(T - T_g)\gamma; \gamma \in [0,1]$, where α_l is volumetric coefficient of thermal expansion in liquid (equilibrium) state.

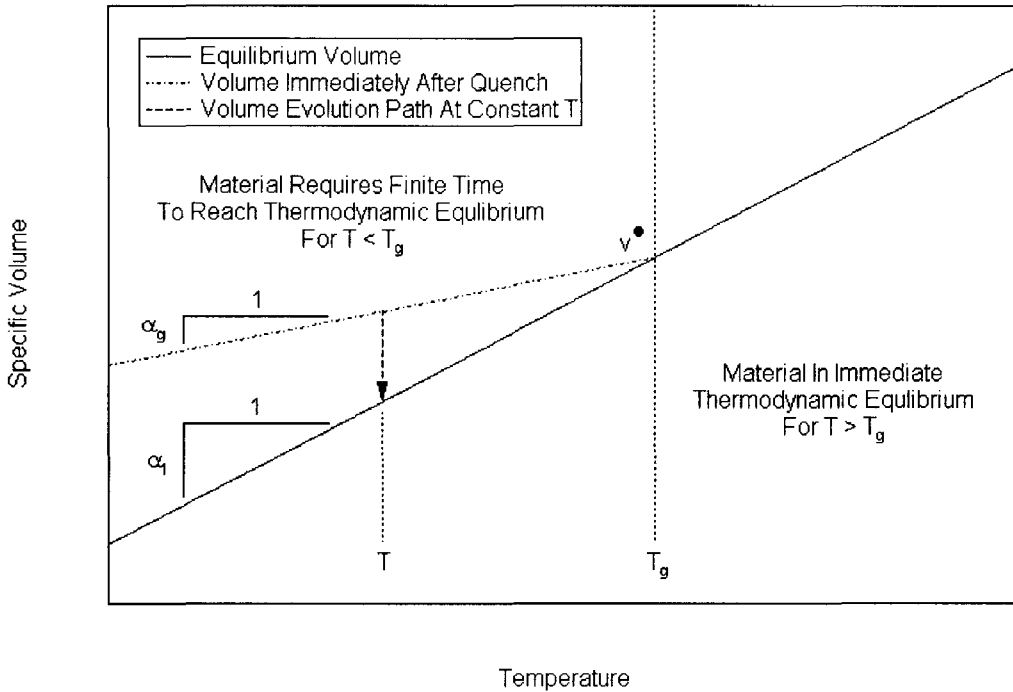


Figure 1. Volumetric response during constant rate cooling from above T_g ; evolution leads to volume path shown if temperature is maintained constant. (Bradshaw, 1997)

The behavior of a material with physical aging is governed by its aging state², which in turn depends upon the thermal history. In the case of isothermal aging, the material is quenched from $T > T_g$ (i.e. equilibrium state) to a temperature below T_g and held at that temperature thereafter. The aging time of the material (t_e) is defined as the time that has passed since the completion of the quench. In the case of nonisothermal

² For brevity, the term “aging” will be taken in this document to be synonymous with “physical aging”; no other forms of aging are considered in this dissertation.

aging, the material undergoes a varying thermal history following the quench and the aging time is less clear. This condition is typical of many PMCs structures during their service life. Due to the complex material response under varying temperature conditions, however, nonisothermal physical aging has received much less attention than its isothermal counterpart.

Although the chief interest for physical aging is to understand the effect of elevated temperature upon polymer matrix composites, this phenomenon can be studied more easily using pure polymer films. One benefit of working with films is that a dynamic mechanical analyzer (DMA) can be used to characterize material response; this instrument is designed to accurately characterize polymer viscoelastic response using a wide variety of temperature and load histories. This research investigates physical aging of polymer films under constant and varying thermal histories using a DMA and develops techniques to predict that response.

1.3 Scope of This Dissertation

This dissertation focuses on physical aging of polymers in their glassy state (below T_g) subjected to isothermal and nonisothermal conditions. The first stage involves the characterization of the isothermal physical aging behavior of two thermoplastics. The second stage consists of both experimental investigation and modeling of physical aging on the same materials with varying thermal histories. The third and final stage of this dissertation investigates physical aging near the glass transition temperature, which includes aging into equilibrium at constant temperatures and a study of the effect of the

path of approaching equilibrium via temperature up jumps and down jumps. Since aging shift factors have similar characteristics to the specific volume response observed by many researchers in last century, the physical aging behavior near T_g provides new database for future research into the relationship between the thermodynamic and mechanical properties during structural relaxation.

There are seven chapters in the dissertation following this introduction. Briefly structured, the content of these chapters is as follows:

- Chapter 2 represents background information on classification and viscoelastic behavior of polymers.
- Chapter 3 describes the experimental methods and materials in this dissertation. The experimental equipment is also introduced.
- Chapter 4 reports the experimental characterization of isothermal physical aging of PEEK and PPS films by creep and stress relaxation. In order to validate the obtained behavior, the results of creep and stress relaxation testing were compared and shown to be consistent with one another using appropriate interconversion of the viscoelastic material functions. Time-temperature superposition of the master curves was also performed. The temperature shift factors and aging shift rates for both PEEK and PPS were consistent for both creep and stress relaxation test results.
- Chapter 5 represents the experimental details, results and data analysis of nonisothermal physical aging, including the single-step temperature up

jumps and complicated thermal histories. This chapter covers both the short-term and long-term creep responses for PEEK and PPS films.

- Chapter 6 describes the work on modeling and prediction of mechanical aging shift factors during nonisothermal physical aging. The KAHR- a_{te} model, which combines the KAHR model of volume recovery with a suitable linear relationship between aging shift factors and specific volume, is introduced and utilized to both predict aging response or to determine necessary model parameters from a set of aging shift factor data. A procedure is demonstrated in this chapter to determine optimal model parameters for data sets from various temperature histories. Long term creep predictions of nonisothermal physical aging using these parameters, based on effective time theory, is also included.
- Chapter 7 investigates the physical aging near glass transition temperature of PPS. Both the isothermal and the nonisothermal aging into equilibrium testing and results are reported. The times of reaching equilibrium in isothermal physical aging were determined at several temperatures, by fitting the change of aging shift rate with increasing aging time. In this chapter, mechanical shift factors following temperature up-jump and down-jump after reaching equilibrium to a common temperature were observed, the finding of asymmetry of a_{te} for up-jump and down-jump can be used for future research on the relationship among various material properties during structural relaxation.

The work in chapters above is summarized in Chapter 8. Several conclusions are made at the end of this dissertation.

CHAPTER 2

POLYMER VISCOELASTICITY

This chapter covers several portions as a background of properties of polymers, which include classification of polymers; glass transition and characterization methods; and several general topics in linear polymer viscoelasticity such as creep and stress relaxation, Boltzmann Superposition Principle, viscoelastic models, etc .

2.1 Classification of Polymers

The word polymer literally means “many units”. A polymer is the union of two or more structural units of a simple compound. There are many ways to classify polymers based on their molecular structure. However, most polymers can be broadly classified as either thermoplastics or thermosets according to bonding types. Polymers consist of atoms joined by a combination of van der Waals bonds and chemical covalent bonds. The intrachain bonds for thermoplastics and thermosets are chemical (covalent); but thermoplastics have only van der Waals bonds between chains, while thermosets have both chemical and van der Waals bonds between chains. As such, thermosets are often called crosslinked or network polymers. Effectively, the thermoset is one large molecule with no crystalline structure.

The names thermoset and thermoplastic are not only associated with the

molecular structures of each but with their material properties as well. Thermoplastics can be cooled and reheated so therefore recycled where thermosets can only be heated once and are therefore not recyclable by melting. The reason for this is that thermoplastics have relatively weak forces of attraction between the chains, which are overcome when the material is heated. Alternately, thermosets, where the crosslinking of the molecules is by strong chemical bonds, cannot be melted.

Compared with thermoplastics, thermosets are generally harder, more rigid and more brittle, and their mechanical properties are not as heat sensitive. Thermosets are also less soluble in organic solvents. Some examples of thermosetting polymers include: epoxies, polyamines, polyurethanes. For structural PMCs, thermosets are the most common matrix material.

Thermoplastic polymers can be classified into amorphous and crystalline materials. Many polymers when cooled from the molten state form a disordered structure, which is termed the amorphous state. Amorphous polymers are usually considered to be a random tangle of molecules. Polystyrene (PS), poly (methyl methacrylate) (PMMA), polycarbonate (PC) and poly (vinyl Chloride) (PVC) are examples of amorphous thermoplastics (Brinson and Brinson, 2008). Many other polymers produce both molecular orientation and small regions of three-dimensional order, called crystallites, when they are cooled from the melt. Crystalline polymers show isotropic bulk mechanical properties in the macroscopic sense, but are not homogeneous in the microscopic sense. Crystalline polymers have often more density, hardness, corrosion resistance, and less time dependent behavior than amorphous polymers. The degree of crystallinity is rarely over 50%. Typical crystalline thermoplastics in engineering

application include: polypropylene (PP), polyamides (Nylon), poly (ether ether ketone) (PEEK), and poly (phenylene Sulfide) (PPS).

According to the discussion above, one simple classification schematic of polymers is shown in Figure 2. It should be noted that physical aging is manifested in materials with an amorphous phase; this includes virtually all polymers of interest for structural applications.

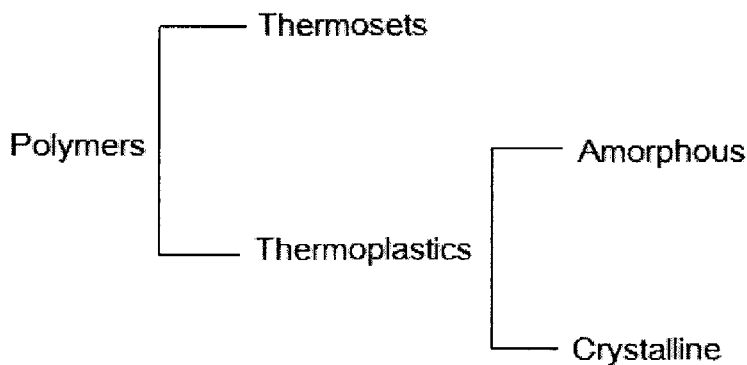


Figure 2. A simple classification of polymers

2.2 Glass Transition of Polymers

2.2.1 Phenomenology of the Glass Transition

The glass transition temperature, T_g , is the temperature at which an amorphous solid, such as glass or a polymer, becomes brittle on cooling, or soft on heating. More specifically, it defines the glass transition, a phenomenon which not only affects the modulus of polymeric materials but also the specific volume, the specific heat, the enthalpy, the entropy, the dielectric constant, etc., of such materials. It is important to

note that the glass transition temperature is a kinetic parameter; as such, it parametrically depends on the melt cooling rate, where the slower the melt cooling rate, the lower the resulting T_g . In addition, T_g depends on the measurement conditions, which are not universally defined (Mazurin and Gankin, 2007).

Below the glass transition temperature, polymeric materials are in a glassy state and maintain the disordered nature of the melt and lack molecular mobility. Due to low thermal energy and little available free volume (see next section for details), the molecular motion consist of the vibration of chain segments around fixed positions. When the temperature increases, the amplitude of the vibrations increases, transmitting a rise to intermolecular interactions, and a growing fraction of chain segments occur. Stronger modes of movement appear that involve the rotation and translation of chain terminals and chain segments or loops incorporating about ten bonds. The related temperature range of these movements is the glass transition temperature (Riande et al., 2000). Above T_g , joining bonds are broken by thermal fluctuations so that broken bonds begin to form clusters. These clusters become large facilitating the flow of material. In organic polymers, secondary, non-covalent bonds between the polymer chains become weak above T_g and polymers become soft and capable of plastic deformation without fracture.

Polymers have five regions of behavior as a function of temperature as depicted in modulus (using 10 second data³) properties in Figure 3 (Brinson and Brinson, 2008): 1) glassy region where the polymer is glassy and frequently brittle; 2) glass transition region

³ In a stress relaxation test conducted at a constant temperature, the ratio of stress to strain at a given instant in time of 10 seconds, is defined as the 10 second modulus, $E(10 \text{ sec})$.

where the polymer acts as leathery, and a few degrees of temperature change affects the stiffness of the leather; 3) rubbery plateau region where after the sharp drop that the modulus takes in the glass transition region, it becomes almost constant again in the rubbery plateau region; 4) Rubbery flow region; 5) liquid flow region (Sperling, 2005). All tests in this dissertation were performed within the first 3 regions.

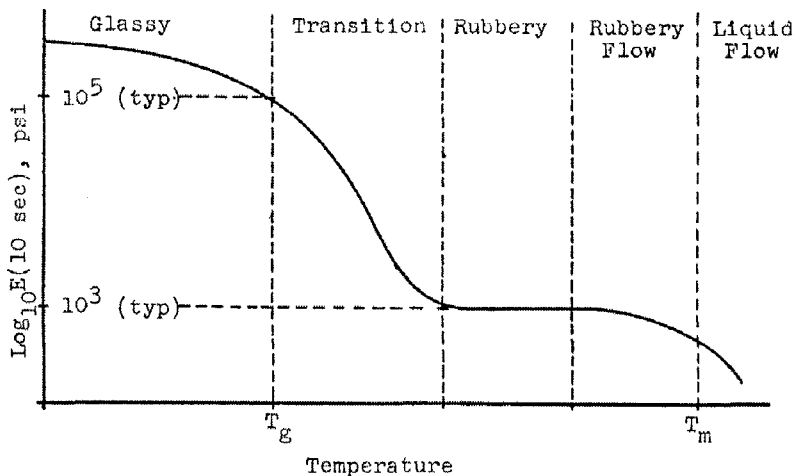


Figure 3. Five regions of viscoelastic behavior of a thermoplastic polymer (Brinson and Brinson, 2008)

The glass transition temperature can be determined experimentally by various methods. Figure 4 shows the variation of viscosity η with temperature for a polymer (Riande et al., 2000). Due to the enormous change in η in passing through the glass transition, this behavior can be used to determine the T_g as the temperature of minimum value of the derivative (rate of change) with temperature of $\log \eta$.

In contrast to the viscosity, the coefficient of thermal expansion, heat capacity, and many other properties of polymers show a relatively sudden change at the glass transition temperature. This effect is used for measurement by dilatometry and

differential scanning calorimetry (DSC). Figure 5 shows three different points on the curve of temperature dependencies of specific heat that can be used to determine T_g (Mazurin and Gankin, 2007). Although some researchers use temperature corresponding to point B or C as the glass transition temperature, it appears that the most popular way of defining T_g by DSC curves is the intersection of two tangents at the start of the apparent change of the slope of the heat capacity (point A).

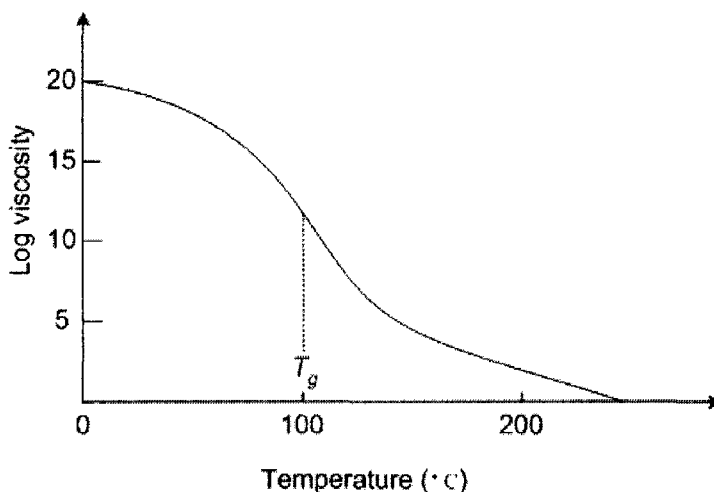


Figure 4. Viscosity-temperature dependence for an amorphous polymer (Riande et al., 2000)

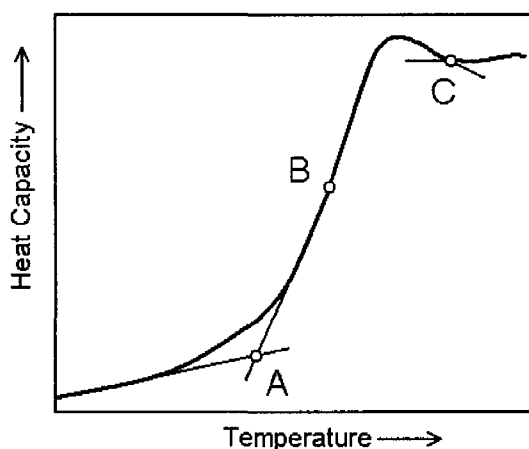


Figure 5. Various points in temperature dependencies of heat capacity used to determine T_g (Mazurin and Gankin, 2007)

In addition to calorimetry, dilatometry has been extensively employed as a classic method for the experimental determination of the glass transition temperature. In this technique, the temperature dependence upon the volume or specific volume is measure, and the temperature at the change in slope is taken as T_g . Such a plot is represented in Figure 6 (Svoboda et al., 2008). The T_g is determined at the intersection of the extension lines of volume curves below and above T_g . Note that the slope (the first derivative of volume) is the volumetric coefficient of thermal expansion, which is expressed as

$$\alpha_v = \left[\frac{1}{V} \frac{\Delta V}{\Delta T} \right]_p \quad (1)$$

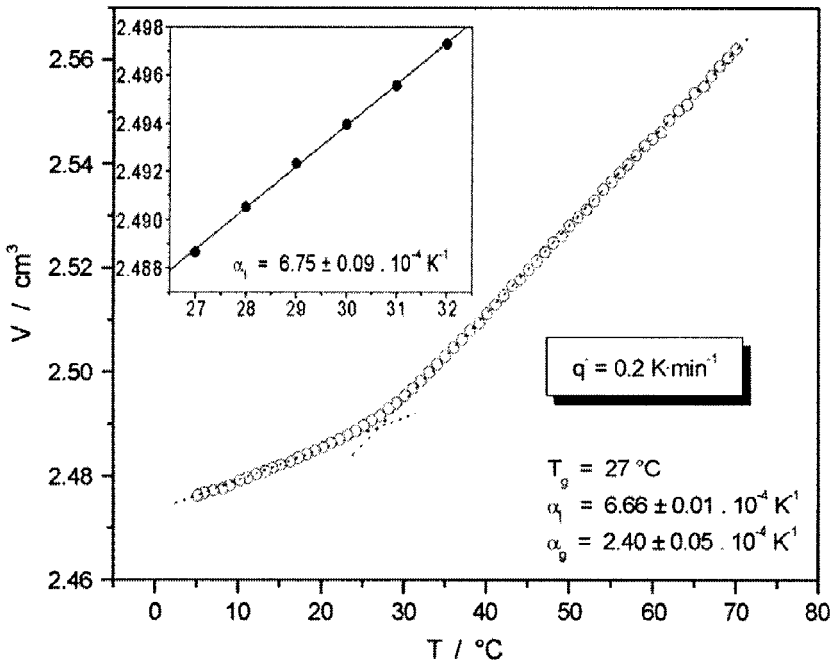


Figure 6. Temperature dependence of PVAc volume measured dilatometrically at cooling rate $q = 0.2 \text{ K/min}$. Evaluation of T_g is indicated by the dashed lines (Svoboda et al., 2008)

It can be seen that at T_g there is a discontinuous change in the thermal expansion coefficient. In Figure 6, the thermal expansion coefficient in the glassy state, α_g , is

$2.4 \times 10^{-4} K^{-1}$, and for the liquid, α_l , is $6.66 \times 10^{-4} K^{-1}$. The coefficient α exhibits a discontinuity at glass transition.

Another method to determine the glass transition temperature is the dynamic mechanical analysis. Figure 7 illustrates that the dynamic properties (these properties will be discussed in next section) change with temperature. In this approach, T_g is commonly defined as either the maximum of the damping ratio, E''/E' ($\tan \delta$), the maximum of E'' (Herzog et al., 2005), or the onset of the change in the slope of the E' curve. Each of these is illustrated in Figure 7; it is clear that these methods can produce different values for the same set of data.

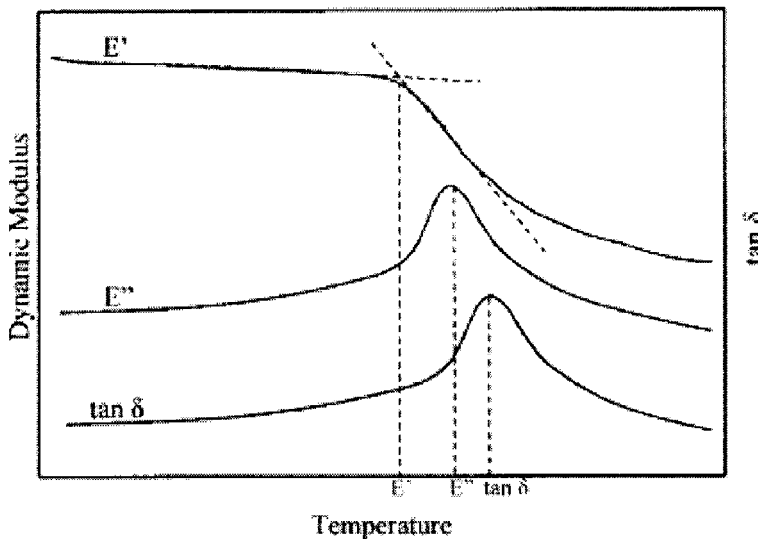


Figure 7. T_g determined by the onset of the storage modulus E' change, the maximum of loss modulus E'' , and the maximum of phase factor $\tan \delta$ (Herzog et al., 2005)

Experimental results suggest that glass transition is a second order⁴ phase

⁴ A second order transition is characterized by a discontinuity in the second partial derivatives of the free energy function with respect to the relevant state variables, but by continuity in both the free energy and its first partial derivations (McKenna, 1989). Also, a first order transition is one for which the free energy as a function of any given state variable (V, P, T) is continuous, but the first partial derivatives of the free energy with respect to the relevant state variables are discontinuous.

transition. However, the approaches to ascertain T_g often result in different T_g values ($\sim 10^\circ\text{C}$). This is due, in part, to the fact that T_g is a single temperature that represents a range over which the glass transition takes place (see Figure 3). It is also appropriate to note that the glass transition is a rate-dependent phenomenon, the cooling or heating rate need to be report when the measurement is conducted.

2.2.2. Free Volume Theory on Glass Transition

One of the most suitable approximations of analyzing the glass transition concerns free volume. The concept of free volume, v_f , and the idea that the mobility of molecules at any temperature is primarily controlled by the free volume, was brought forth by Doolittle (Doolittle, 1951; Mark et al., 2004). The free volume is the space in a solid or liquid not occupied by molecules; in other words, it is the empty space existing between molecules.

Figure 8 shows the schematic division of that total volume of the polymer into both occupied volume, v_o , and free volume v_f . The occupied volume increases uniformly with temperature. The discontinuity in the expansion coefficient at T_g then corresponds to a sudden onset of expansion in the free volume. Below the glass transition temperature, the free volume remains constant because the molecular mobility is so drastically reduced that a non-equilibrium state would become frozen. The free volume at temperatures greater than T_g is given by

$$v_f = v_g + (T - T_g) \frac{\Delta v_f}{\Delta T} \quad (2)$$

where v_g is the free volume below T_g , v_f is the free volume (see Figure 8). Note that the total volume v is the sum of occupied volume and free volume given by

$$v = v_o + v_f \quad (3)$$

The fractional free volume is defined as $f = (v - v_o)/v = v_f/v$, and is found by dividing Equation (2) by v resulting in

$$f = f_g + \alpha_f(T - T_g) \quad (4)$$

where f_g is the fractional free volume at the glass transition T_g and α_f is the thermal expansion coefficient of the free volume.

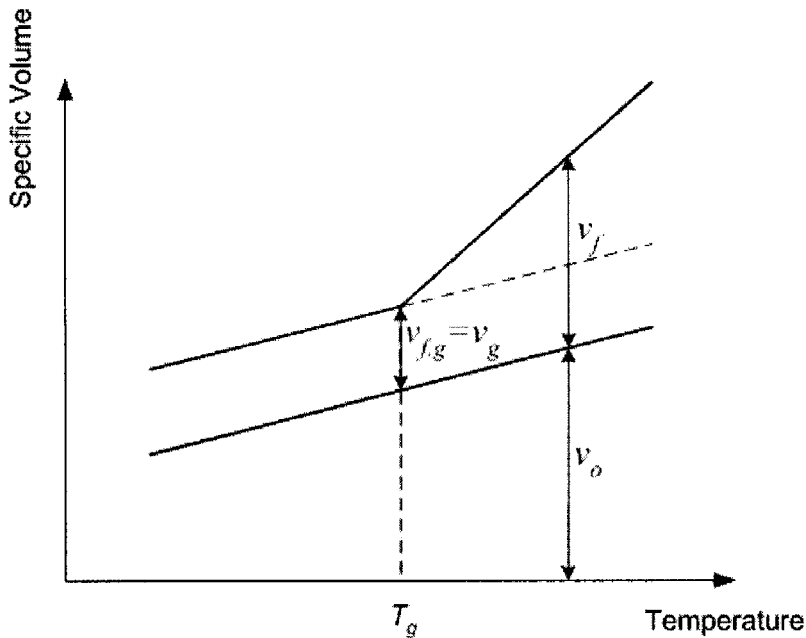


Figure 8. Free volume v_f and its dependence on temperature for polymers

Free volume theory is critical in understanding the glass transition. Because of the success of the empirical free volume relations in describing the behavior of viscoelastic materials (Turnbull and Cohen, 1961; Williams et al., 1955), there have been many

attempts to quantify the concept and make “free volume physics” (McKenna, 1989) more than a convenient way to correlate data (Haward and Young, 1997; Kovacs, 1958; Scherer, 1986; Tant and Wilkes, 1981). Among these works, the two close to the topic of this dissertation are the Robertson-Simha-Curro (RSC) molecular theory, which characterizes the kinetics of structural relaxation of polymers (Robertson et al., 1984), and the work by Knauss and Emri, in which they developed the nonlinear viscoelastic constitutive law of polymers based on free volume concepts to describe the time-dependent deformation of volume and pressure induced aging of polymers (Emri and Knauss, 1986; Knauss and Emri, 1981, 1987). These theories are discussed in later sections of this dissertation.

2.3 Linear Polymer Viscoelasticity

2.3.1 Creep and Stress Relaxation

The mechanical behavior of a viscoelastic material such as polymer exhibits both dissipation (viscous liquid) and storage (elastic solid) of energy. In a viscoelastic material, the stress depends on the time history of deformation. The materials also exhibit “fading memory”, meaning that after some finite time elapses, a polymer tends to forget the sequence of shapes that it had in the past. The basic viscoelastic effects are typically studied by creep and stress relaxation. In general, the linear viscoelastic behavior is introduced with the one-dimensional situation of creep under a uniaxial fixed load. In the test, a specimen is loaded with a constant stress for some time and the resulting strain, which increases with time, is observed in the entire test. Based on the strain and applied

stress, a quantity called (tensile) creep compliance is defined as:

$$D(t) = \frac{\varepsilon(t)}{\sigma_0} \quad (5)$$

where σ_0 is the applied stress, $\varepsilon(t)$ is the strain response. The initial compliance is:

$$D(t=0) = \frac{\varepsilon_0}{\sigma_0} \quad (6)$$

which is analogous to the behavior of an elastic solid. On the other hand, for a sufficiently long period of time the rate of change of strain becomes characteristic of a fluid. An equally important facet of a constant stress test is the recovery phenomena after the load is removed. In this condition, there is an initial elastic decrease followed by continuous recovery in strain. A classic creep and recovery test is shown in Figure 9.

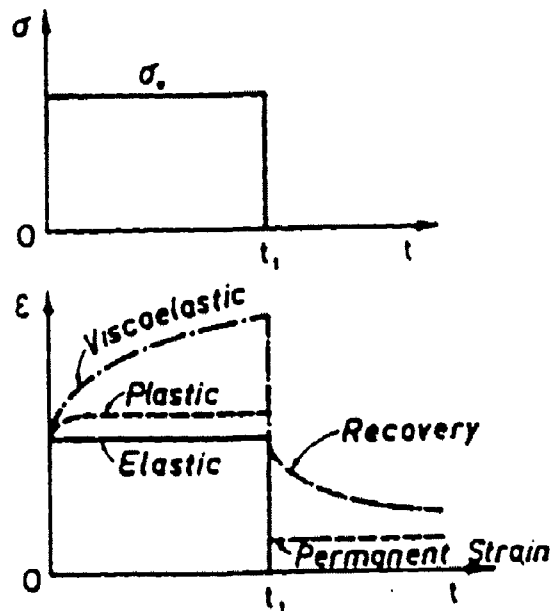


Figure 9. Creep and recovery test of elastic, plastic and viscoelastic materials (Finley et al., 1976)

Another fundamental characterization test for viscoelastic materials is the stress

relaxation test. In a stress relaxation test, the sample is suddenly deformed to a new position and subjected to a constant uniaxial strain. The decay of stress is observed as the corresponding time-dependent viscoelastic behavior. The strain input and stress output of thermoplastics in stress relaxation is illustrated in Figure 10. The relaxation modulus of the polymer is given by

$$E(t) = \frac{\sigma(t)}{\epsilon_0} \quad (7)$$

where $\sigma(t)$ is the resulting stress, and ϵ_0 is the applied strain. The initial modulus is equal to the reciprocal of initial creep compliance mathematically, $E_0 = 1/D_0$; but the modulus and compliance functions with time $E(t)$ and $D(t)$ for viscoelastic materials do not have this relationship.

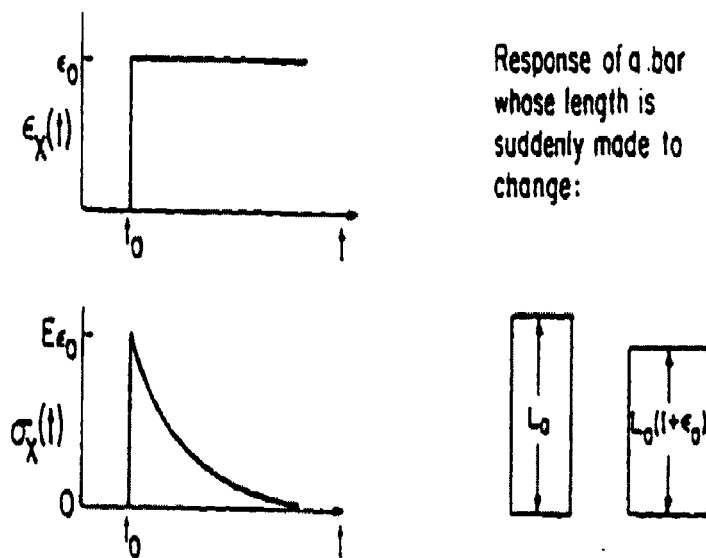


Figure 10. Relaxation test: strain (above) and corresponding qualitative stress (below) (Scherer, 1986)

2.3.2 Boltzmann Superposition Principle and Linearity

The Boltzmann superposition principle is the first statement of linear viscoelastic behavior (Ferry, 1980) and is one of the simplest but most powerful principles of polymer physics. Boltzmann proposed (1) that the creep in a polymer is a function of the entire loading history and (2) that each loading step makes an independent contribution to the final deformation and (3) that the final deformation can be obtained by the simple addition of each contribution (Aklonis and MacKnight, 1983). The creep compliance has been previously defined as relating the stress and strain in a creep test.

$$\varepsilon(t) = \sigma_0 D(t) \quad (8)$$

The stress is applied instantaneously at time equal to zero. For multiple stress portions, assume the stresses $\Delta\sigma(\theta_1)$, $\Delta\sigma(\theta_2)$ and $\Delta\sigma(\theta_3)$ are applied on the material at times θ_1 , θ_2 , and θ_3 , respectively. This stress history is shown schematically in Figure 11.

The response is written as

$$\varepsilon(t) = D(t - \theta_1)\Delta\sigma(\theta_1) + D(t - \theta_2)\Delta\sigma(\theta_2) + D(t - \theta_3)\Delta\sigma(\theta_3) \quad (9)$$

For a more complicated experiment consisting of variously discrete stress increments, the relationship between the strain and stress is expressed in a generalized form as

$$\varepsilon(t) = \sum_{\theta_i = -\infty}^{\theta_i = t} D(t - \theta_i)\Delta\sigma(\theta_i) \quad (10)$$

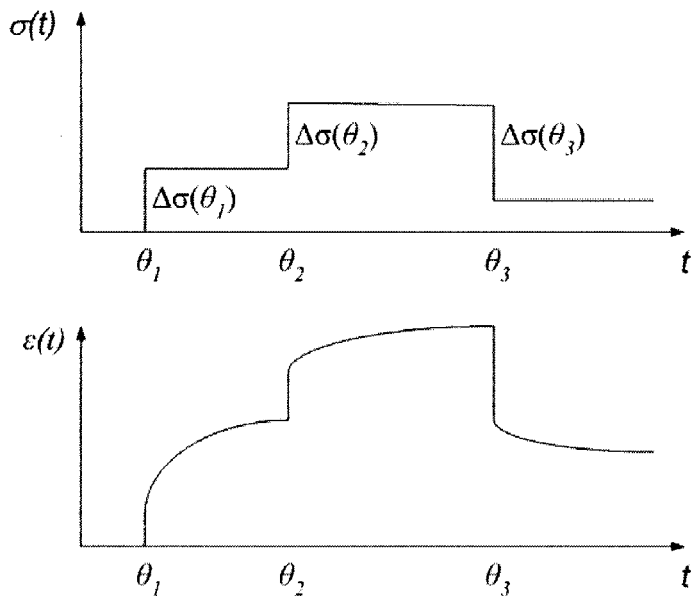


Figure 11. Schematic of the strain response of a viscoelastic material to the stresses applied sequentially

This equation is a general way of expressing the Boltzmann Superposition Principle, which indicates the effects of mechanical history are linearly additive. The summation of individual stress step represents the total applied stress at time t . Replacing the summation by integration and noting that the increment of applied stress is replaced by the derivative of continuous stress leads to

$$\varepsilon(t) = \int_{-\infty}^t \frac{\partial \sigma(\theta)}{\partial \theta} D(t-\theta) d\theta \quad (11)$$

Note that the lower limit of the integral is taken as $-\infty$, since the complete stress history contributes to the current state of stress and strain. This equation is also referred as a hereditary integral. An analogous derivation of stress output for a variable strain input yields the stress and strain relationship during stress relaxation, in discrete and continuous form as

$$\sigma(t) = \sum_{\theta_i=-\infty}^{\theta_i=t} E(t-\theta_i)\Delta\varepsilon(\theta_i) \quad (12)$$

$$\sigma(t) = \int_{-\infty}^t \frac{\partial\varepsilon(\theta)}{\partial\theta} E(t-\theta)d\theta \quad (13)$$

Linear viscoelasticity requires a linear relationship between stress and strain to be maintained. It is thus necessary for the responses to stresses applied at any time to be superposable and for responses to different stress levels to be proportional. To determine the linear regions under particular experimental conditions, isochronous (equal aging time) creep or stress relaxation tests can be performed; the results are then examined by the Boltzmann superposition principle to demonstrate that they satisfy both conditions (superposition and proportionality) of linearity. Typically, these limitations are violated once the stress level becomes too large.

2.3.3 Dynamic Viscoelastic Functions

An alternative experimental method to creep and stress relaxation testing is the dynamic mechanical test, which involves the application of an oscillatory strain to a specimen. The resulting sinusoidal stress is measured and correlated against the input strain, and the viscous and elastic properties of the sample are simultaneously measured. Thus, the strain input and stress output are given by

$$\varepsilon(t) = \varepsilon_0 \sin \omega t \quad (14)$$

$$\sigma(t) = \sigma_0 \sin(\omega t + \delta) \quad (15)$$

where ω is the angular frequency, and δ is the phase lag.

Write $\varepsilon(t) = \varepsilon_0 \exp i\omega t$ and $\sigma(t) = \sigma_0 \exp i(\omega t + \delta)$, then the complex modulus is defined as

$$E^*(\omega) = \frac{\sigma(t)}{\varepsilon(t)} = \frac{\sigma_0}{\varepsilon_0} e^{i\delta} = E'(\omega) + iE''(\omega) \quad (16)$$

The dynamic components of complex relaxation modulus are given by

$$\begin{aligned} E'(\omega) &= \frac{\sigma_0}{\varepsilon_0} \cos \delta \\ E''(\omega) &= \frac{\sigma_0}{\varepsilon_0} \sin \delta \\ \tan \delta &= \frac{E''(\omega)}{E'(\omega)} \end{aligned} \quad (17)$$

where $E'(\omega)$ and $E''(\omega)$ are called storage modulus and loss modulus respectively, since they define the energy stored in the specimen and dissipation of energy due to the applied strain, and the ratio of the loss modulus to storage modulus is the tangent of the phase angle δ between stress and strain; $\tan \delta$ is a measure of the damping property of the material.

Dynamic creep compliance functions are obtained by an analogous procedure by applying a sinusoidal stress and measuring a sinusoidal strain. The dynamic compliance components are then given by

$$\begin{aligned} D'(\omega) &= \frac{\varepsilon_0}{\sigma_0} \cos \delta \\ D''(\omega) &= \frac{\varepsilon_0}{\sigma_0} \sin \delta \\ \tan \delta &= \frac{D''(\omega)}{D'(\omega)} \end{aligned} \quad (18)$$

These expressions relate the components of the complex compliance of the amplitudes of both the perturbation and the response as well as the out-of-phase angle δ . A vectorial schematic of the components of complex modulus and compliance is shown in Figure 12.

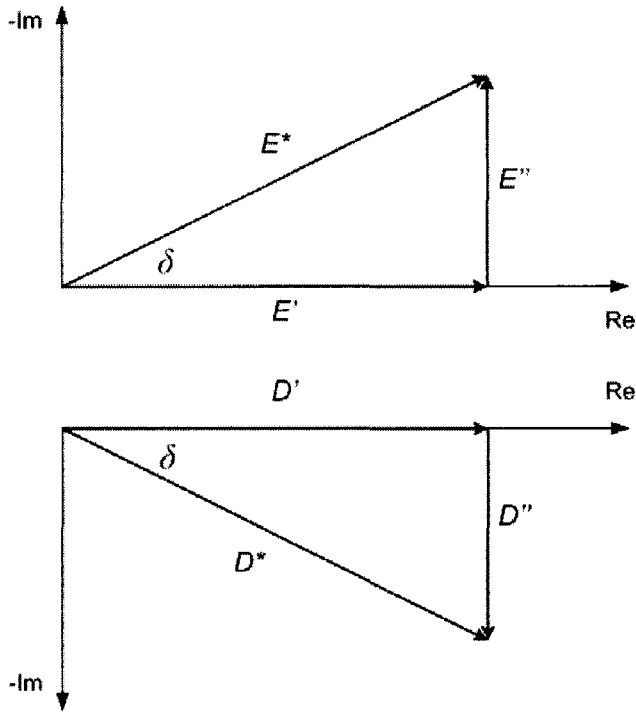


Figure 12. Dynamic relaxation modulus and creep compliance functions

2.3.4 Interrelations among Viscoelastic Properties

According to Borel's theorem, the result of Laplace transform of the hereditary integral is equal to the product of the Laplace transform of the two functions in hereditary integral (Kreyszig, 2005). Thus, the Laplace transforms of Equation (11) and (13) are,

$$\bar{\sigma}(s) = \bar{E}(s) s \bar{\epsilon}(s) \quad (19)$$

$$\bar{\varepsilon}(s) = \bar{D}(s) s \bar{\sigma}(s) \quad (20)$$

where the overbar indicates Laplace transform. These relations lead to

$$\bar{E}(s) \bar{D}(s) = \frac{1}{s^2} \quad (21)$$

which upon using the convolution theorem yields

$$\int_0^t E(t-\tau) D(\tau) d\tau = t \quad (22)$$

These equations permit the creep compliance to be obtained from the relaxation modulus and vice versa.

Another relationship between static and dynamic properties is a direct consequence of the Boltzmann superposition principle. Recall Equations (13) and (14), and set a variable change as $u = t - \theta$; the complex modulus $E^*(\omega)$ is determined as

$$E^*(\omega) = i\omega \int_0^{\infty} E(u) e^{-i\omega u} du \quad (23)$$

Substitute Equation (16) into Equation (23) and separate the modulus into two components, $E(t) = E_{\infty} + \tilde{E}(t)$ where E_{∞} represents the equilibrium modulus at $t = \infty$, either of the two dynamic modulus functions may then be calculated from the relaxation modulus in time domain as

$$\begin{aligned} E'(\omega) &= E_{\infty} + \omega \int_0^{\infty} \tilde{E}(t) \sin \omega t dt \\ E''(\omega) &= \omega \int_0^{\infty} \tilde{E}(t) \cos \omega t dt \end{aligned} \quad (24)$$

Equation (24) suggests that $E'(\omega)$ and $E''(\omega)$ are the sine and cosine Fourier transforms of the relaxation modulus, respectively. The pertinent relations are

$$\begin{aligned}\frac{E'(\omega) - E_\infty}{\omega} &= \mathcal{F}_s[E(t) - E_\infty] \\ \frac{E''(\omega)}{\omega} &= \mathcal{F}_c[E(t) - E_\infty]\end{aligned}\tag{25}$$

where \mathcal{F}_s and \mathcal{F}_c are the symbols for the sin and cosine Fourier transforms.

The relaxation modulus $E(t)$ can also be obtain from the inverse of the Fourier transform of Equation (25); the corresponding relationships to find $E(t)$ from $E'(\omega)$ and $E''(\omega)$ are

$$\begin{aligned}E(t) &= E_\infty + \frac{2}{\pi} \int_0^\infty [(E'(\omega) - E_\infty) / \omega] \sin \omega t \, d\omega \\ E(t) &= \frac{2}{\pi} \int_0^\infty (E''(\omega) / \omega) \cos \omega t \, d\omega\end{aligned}\tag{26}$$

In principle, these integrals can be performed numerically if the starting function is known over a sufficiently wide range of time or frequency. Equations (24) - (26) show the relationship of relaxation modulus in the time domain and frequency domain.

Analogous relations connect the creep compliance with the components of the complex dynamic compliance. As formulated in (Riande et al., 2000), the equations regarding creep compliance are shown in Equations (27) and (28). These relationships are important since in some particular experimental conditions, the desired material properties are difficult to determine directly, in these cases, the converting method between dynamic and static functions can be applied.

$$D'(\omega) = D_e - \omega \int_0^{\infty} [D_e - D(t)] \sin \omega t \, dt \quad (27)$$

$$D''(\omega) = \omega \int_0^{\infty} [D_e - D(t)] \cos \omega t \, dt$$

$$D(t) = D_e + \frac{2}{\pi} \int_0^{\infty} \frac{D'(\omega) - D_e}{\omega} \sin \omega t \, d\omega \quad (28)$$

$$D(t) = D_e - \frac{2}{\pi} \int_0^{\infty} \frac{D''(\omega)}{\omega} \cos \omega t \, d\omega$$

The creep compliance in these two equations is written as

$$D(t) = D_g + D_d \Psi(t) + \frac{t}{\eta} \quad (29)$$

where D_g and D_d are, respectively, the glassy and maximum elastic entropic compliance.

$\Psi(t)$ is a monotonous function with values between 0 ($t = 0$) and 1 ($t = \infty$). η is the viscosity. The compliance function D_e in Equations (27) and (28) is given by

$$D_e = D_g + D_d \quad (30)$$

which represents the maximum elasticity that in a deformed polymeric material; D_e is often called equilibrium compliance for solids and steady-state compliance for viscoelastic liquids.

2.4 Time and Temperature Behavior of Polymers

2.4.1 Viscoelastic Models and Materials Response Functions

In order to describe the viscoelastic behavior of a material over many decades of

logarithmic time, phenomenological mechanical models are developed in various forms. Among these, the most popular two are the Maxwell-Wiechert model and the Voigt-Kelvin model with sufficient elements to span the broad region of relaxation or retardation times. The Maxwell-Wiechert model is the generalized Maxwell model, consisting of an arbitrary number of Maxwell elements connected in parallel as shown in Figure 13.

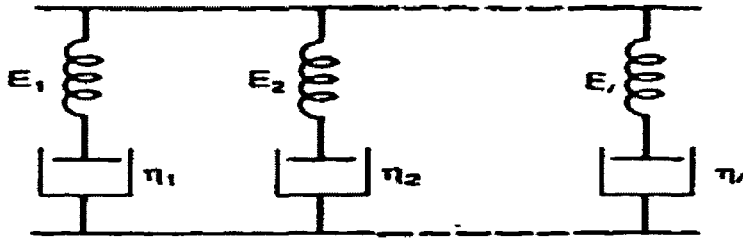


Figure 13. Maxwell-Wiechert model (Mehta and Monteiro, 1993)

Consider a Maxwell-Wiechert model with P elements subjected to a stress relaxation experiment. In all of the individual elements, the strain is the same and the total stress is the summation of the individual stresses experienced by each element. In each unit in the generalized Maxwell-Wiechert model in parallel, the stress and strain relationship is

$$\frac{d\varepsilon_p(t)}{dt} = \left[\frac{1}{E_p} \frac{d}{dt} + \frac{1}{\eta_p} \right] \sigma_p(t) \quad (31)$$

where the proportionality constant, E_p , is the Young's modulus of the spring component in the p^{th} element; η_p is the viscosity of the p^{th} element. The total stress $\sigma(t)$ is given by

$$\sigma(t) = \sum_{p=1}^P \sigma_p(t) \quad (32)$$

Integration of Equation (31) gives the partial stresses $\sigma_p(t)$, which is substituted into Equation (32) to calculate the total stress. In the stress relaxation under constant strain ε_0 , the relaxation modulus results in

$$E(t) = \frac{\sigma(t)}{\varepsilon_0} = \sum_{p=1}^P \frac{\sigma(0)_p}{\varepsilon_0} e^{-t/\tau_p} = \sum_{p=1}^P E_p e^{-t/\tau_p} \quad (33)$$

where $\sigma(0)_p$ is the stress on the p^{th} element at $t = 0$ and τ_p is the relaxation time for the p^{th} element, which becomes $\tau_p = \eta_p / E_p$. Equation (33) shows that the response of viscoelastic materials depends on a distribution of relaxation times. The equation has been found useful in modeling complex viscoelastic materials (Mehta and Monteiro, 1993).

Similar to the generalized Maxwell model, the Voigt-Kelvin model is a generalization of the Kelvin model, by connecting the Kelvin elements in series, as shown in Figure 14. In this model, the compliance functions are easily calculated, while the modulus functions are rather complicated. Since in each unit the stress is given by

$$\sigma_q(t) = \left[E_q + \eta_q \frac{d}{dt} \right] \varepsilon_q(t) \quad (34)$$

The total strain is the summarization of the strain in the individual elements, thus, the total strain in the Voigt-Kelvin model consisting of Q units is expressed as

$$\varepsilon(t) = \sum_{q=1}^Q \varepsilon_q(t) \quad (35)$$

If constant total strain is applied, the creep compliance is

$$D(t) = \frac{\varepsilon(t)}{\sigma_0} = \sum_{q=1}^Q D_q \left[1 - e^{-t/\tau_q} \right] \quad (36)$$

where $D_q = 1/E_q$ and $\tau_q = \eta_q/E_q$ is a characteristic time constant called the retardation time of the q th element. All these relationships are exactly analogous to the stress relaxation behavior in the generalized Maxwell model.

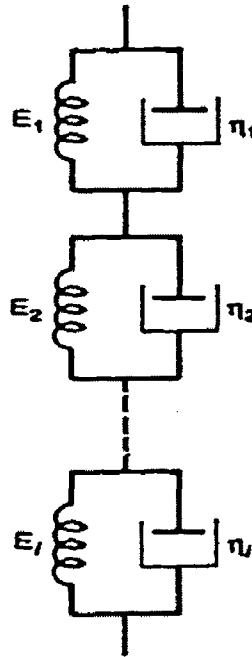


Figure 14. Voigt-Kelvin model (Mehta and Monteiro, 1993)

A general issue in working with polymeric materials is representing the measured material properties by an appropriate mathematical function (Brinson and Brinson, 2008). While viscoelastic properties can be represented by a number of forms, the exponential Prony series, as expressed in Equation (37), exactly meet the creep compliance in generalized Kelvin model and the relaxation modulus in the generalized Maxwell model.

$$\begin{aligned}
E(t) &= E_{\infty} + \sum_{i=1}^N E_i e^{-t/\tau_i} \\
D(t) &= D_0 + \sum_{j=1}^N D_j \left(1 - e^{-t/\tau_j}\right)
\end{aligned}
\tag{37}$$

The benefit of material characterization using Prony series is that the coefficients can be related to the spring and damper elements in a mechanical model. Since the experimental data for a polymer often produce compliance or modulus functions as a function of time or frequency, Equation (37) can be applied to fit any material response in complex shapes by applying sufficient number of elements. Finally, the form of Prony series ensures that its derivatives and integration of terms can be obtained analytically; this is an attractive advantage in finding the solution of a mathematical formulation. The main disadvantage of Prony series is that it is somewhat more difficult to manage since many elements may be required for complicated material response.

When the relaxation behavior is relatively simple, other material functions are often used. One of these is the Kohlrausch material function that is often used for modulus as (Kohlrausch, 1863)

$$E(t) = E_{\infty} + (E_0 - E_{\infty}) e^{-\left(\frac{t}{\tau}\right)^{\beta}} \tag{38}$$

and for compliance as (Struik, 1978)

$$D(t) = D_0 e^{-\left(\frac{t}{\tau}\right)^{\beta}} \tag{39}$$

where τ is the characteristic relaxation time of the function and β is a parameter on the order of 0 and 1 that is referred to as the stretching parameter. The Kohlrausch function is often referred to as stretched exponential function or KWW (Kohlrausch–Williams–

Watts)⁵ function by many other researchers. It is a frequently used empirical description of the relaxation rates of many physical properties of polymers. The Kohlrausch is very compact and is capable of fitting a wide variety of material function shapes by varying the parameter β , while using only a single time parameter τ . The major drawback of this approach is that a single Kohlrausch function is not sufficient for correctly describing more than one relaxation processes; to use the Kohlrausch function to describe the dynamic, material response has to be considered over a specific region of time (Apitz et al., 2004). For example, the Kohlrausch compliance function represents inadmissible viscoelastic behavior for the long term material response.

Many other material response functions can be employed in the study of linear viscoelastic behavior. In this work, the Prony series and Kohlrausch forms are considered as material response functions. This choice is made because the Kohlrausch function is most common in the study of physical aging; as such, it will be used to represent short term creep compliance and stress relaxation. However, the Prony series is a powerful function, and provides ideal curve fitting for any material response; as such, it will be used in this dissertation to fit the aging shift factors obtained from nonisothermal creep tests near the glass transition temperature.

The material properties from creep, stress relaxation and dynamic tests for the Maxwell-Wiechert model and the Voigt-Kelvin model are presented in Table 1.

⁵ The function was introduced by F.W.G. Kohlrausch in 1863 to describe the discharge of a capacitor. The stretched exponential was again used by G. Williams and D.C. Watts in 1970 to characterize the dielectric relaxation rates in polymers.

Table 1. Viscoelastic Functions of Maxwell-Wiechert and Voigt-Kelvin model (Aklonis and MacKnight, 1983)

Experiment	Maxwell-Wiechert	Voigt-Kelvin Model
Creep		$D(t) = \sum_{q=1}^Q D_q (1 - e^{-t/\tau_q})$
Stress Relaxation	$E(t) = \sum_{p=1}^P E_p e^{-t/\tau_p}$	
Dynamic	$E' = \sum_{p=1}^P \frac{E_p \omega^2 \tau_p^2}{1 + \omega^2 \tau_p^2}$	$D'(\omega) = \sum_{q=1}^Q \frac{D_q}{1 + \omega^2 \tau_q^2}$
	$E'' = \sum_{p=1}^P \frac{E_p \omega \tau_p}{1 + \omega^2 \tau_p^2}$	$D''(\omega) = \sum_{q=1}^Q \frac{D_q \omega \tau_q}{1 + \omega^2 \tau_q^2}$

2.4.2 Time-Temperature Superposition Principle

Material response functions, relaxation modulus and creep compliance, are functions of time as well as temperature. This leads one to wonder about the feasibility of finding the equivalence of measuring the material response as a function of time at a constant temperature, and a function of temperature at a constant time. Based on the experimental results, the time-temperature superposition principle (TTSP) was suggested by Leaderman (Leaderman, 1943) in which the modulus (or compliance) data at one temperature can be superimposed upon data taken at different temperatures by simply shifting the modulus curve along the time axis (Tran, 1996).

Figure 15 demonstrates the time temperature superposition principle produced for poly(isobutylene) data by Catsiff and Tobolsky (Catsiff and Tobolsky, 1955). On the left side of Figure 15, several individual modulus curves measured at different temperatures are illustrated. The superimposed continuous curve on the right side is the master curve at the reference temperature (25°C); this consists of the (horizontally) shifted data curves

from the left side.

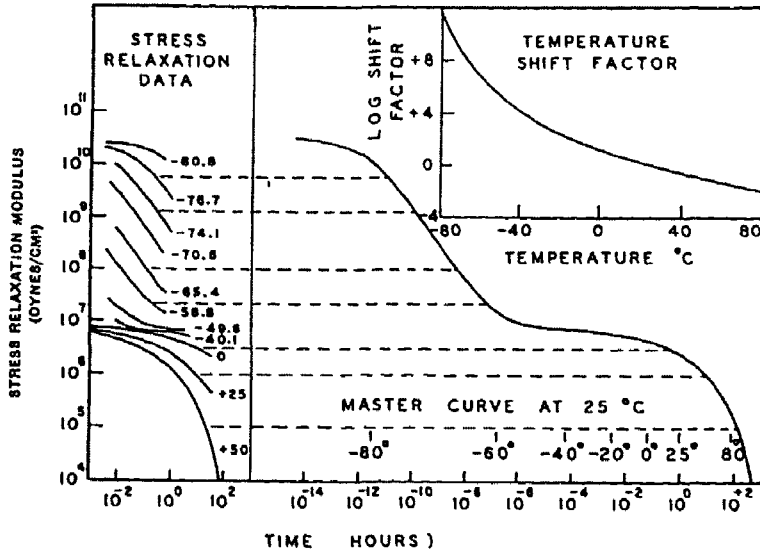


Figure 15. Illustration of time temperature superposition principle with poly(isobutylene) data (Catsiff and Tobolsky, 1955)

The master curve in Figure 15 covers more than 16 orders of magnitude. The time temperature correspondence states that this extension is identical to that which would be measured at particular temperatures on experimentally accessible time scales. This idea is expressed as

$$E(T_1, t) = E(T_2, t / a_T) \quad (40)$$

where the effect of changing temperature is identical to modify the timescale by a multiplicative factor a_T (i.e., an additive factor to the log time scale).

The mathematical development of TTSP is available at some reference books (e.g. (Brinson and Brinson, 2008)). Although the time temperature superposition was proved to be successful to many polymers, Plazek (Plazek, 1965) has shown that it is not

quantitatively correct except in limited time temperature ranges. The TTSP method is only strictly valid above the T_g ; while it is thought to be valid for temperatures below T_g , the exact lower limit is not well defined.

2.4.3 Thermorheologically Simple Materials

A fundamental characteristic of the so-called thermorheologically simple materials is that consecutive isotherms have similar habits, so they overlie each other when they are shifted horizontally along the logarithmic time axis (i.e. as in Figure 15). This assumption has been found to hold for a number of polymer systems, and is analogous to stating that the retardation/relaxation times of the material functions above are the only parameters affected by a change of temperature.

When dealing with experimental data, slight vertical shifting is often needed to build the master curve. Thus, a general relationship of the properties of polymeric materials at various temperatures is written as

$$S_T(t) = b_T S_{T_0}(a_T t) \tag{41}$$

where b_T is referred to as the vertical temperature shift factor. This expression no longer represents a thermorheologically simple relationship, but still constrains the behavior at varying temperatures to that of a single reference (master) curve.

The materials in this work often need a minor amount (within $\pm 5\%$ from the individual data curve to reference curve) vertical shift when applying the TTSP and the

time-aging time superposition (will be discussed later). This is also typically found by other researchers. Experience on an array of experimental data has shown that the lack of including of a vertical shift, even if small, can lead to substantial errors in the prediction of properties over a long time. The vertical shift may be necessary for reasons other than the temperatures/aging times for the collected data. For example, one issue leading to vertical shifting is slight specimen variation (Brinson and Brinson, 2008). Polymer film can be difficult to accurately measure the thickness and width. In the tests, compliance or modulus is often calculated by the nominal dimensions, so the variation of the specimen usually cause minor vertical shift in different data sets.

CHAPTER 3

EXPERIMENTAL METHOD AND MATERIALS

This chapter begins with an introduction of the RSA III dynamic mechanical analyzer, the test equipment used in this work. Following this part, test procedures for creep, stress relaxation, temperature sweep, etc. built by the software of the DMA are represented. Finally the materials used in this dissertation are described, several issues related to the experiments such as specimen dimension variation, temperature changes during quench, experimental thermal histories and linear viscoelastic regions at various temperatures are included as well.

3.1 RSA III Dynamic Mechanical Analyzer

3.1.1 Background

All experiments to investigate the effects of physical aging of polymers in this dissertation were performed on an RSA III commercial dynamic mechanical analyzer (DMA) manufactured by TA Instruments. Dynamic mechanical analysis, as represented in last chapter, is a technique for observing the viscoelastic nature of polymers, by applying an oscillatory force/deformation on a specimen. Commercial DMA instruments

allow the load, strain, temperature, and frequency to be selected and scanned automatically through a range in the course of the experiments. For measuring the glass transition temperature, DMA is more sensitive and yields more easily interpreted data compared with DSC. DMA as a versatile thermal analysis method is becoming more and more commonly seen in the analytical laboratory.

Early work attempting to measure the material properties by oscillatory deformation began from 1950's. The commercial success of DMA in the late 1970's started the modern period in the history of this instrument; several corporations were found but the instruments at that time were difficult to use, slow and limited in their ability to process data (Menard, 1999). This situation changed during the 1980's due to the improvement of technology and competition between vendors. The revolution in computer engineering changed the DMA to be more user-friendly as computers and control software evolved. Currently, there are many manufacturers, including TA Instruments, Perkin-Elmer, LINSEIS, SETARAM, etc., that provide advanced commercial DMAs.

3.1.2 RSA III DMA Components and Specifications

The TA Instruments Rheometric Series RSA III tests the dynamic mechanical properties of solid materials by using a servo drive linear actuator to mechanically impose an oscillatory deformation, or strain, upon the material. The sample is coupled between the motor and a transducer, which measures the resultant force generated by the sample deformation (TA Instruments, 2003).

Figure 16 shows the RSA III test station, including the motor, a transducer, and an oven. The motor is configured as a position servo, which is driven by the motor controller using command signals from the host computer, applying deformation to the specimen. The transducer is also configured as a position servo but with an input of zero. When the specimen is under load, electric current responds the resulting force on the transducer shaft to keep the transducer at the zero position. The load (force value) applied on the specimen is then calculated via the yielded current. This instrument can subject the sample to a number of thermal environments. A forced air convection oven is used to enclose the sample. A simplified block diagram of the RSA III system is showed in Figure 17.

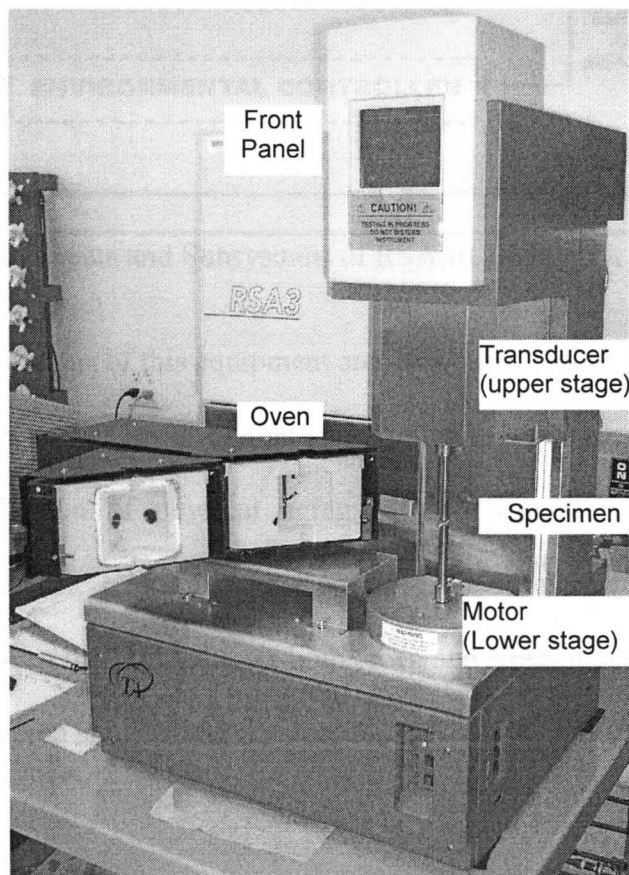


Figure 16. RSA3 Dynamic Mechanical Analyzer (Resapu, 2005)

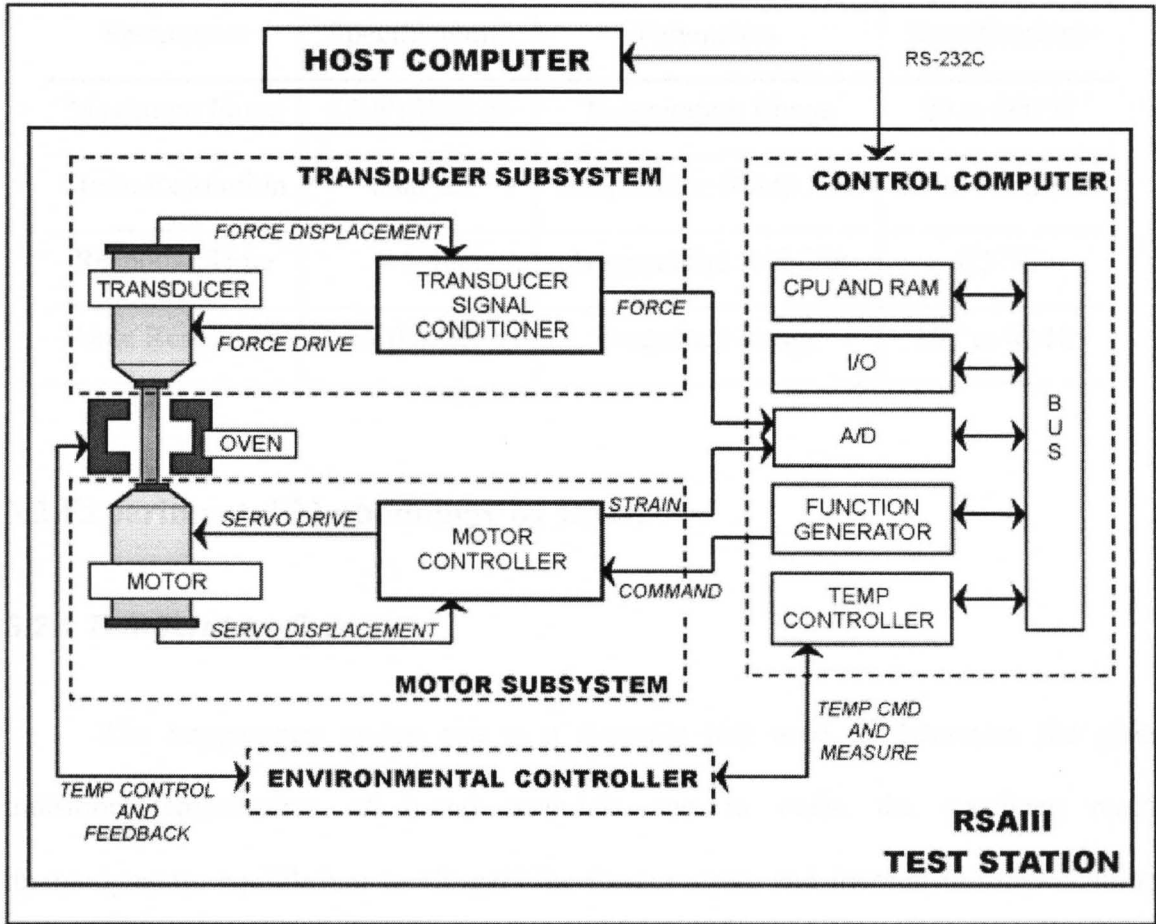


Figure 17. Components and Subsystems of RSA III DMA (TA Instruments, 2003)

The specifications of this equipment are shown in Table 2. The DMA provides the capability to accurately control either stress or strain while monitoring the other. This permits characterization of physical aging by two separate means to validate the anticipated viscoelastic relationships. This is also ideal for future polymer film characterization; since the DMA allows both creep and stress relaxation test methods, the ideal choice for a given situation can be chosen.

Table 2. Specifications of TA Instruments RSA III DMA (TA Instruments, 2003)

Parameters	Specifications	Parameters	Specifications
Maximum Force	35 N (3500 g)	Temperature Range	20 to 600°C
Strain Resolution	0.05 $\mu\epsilon$	Temperature Ramp Rate	0.1 to 50°C/min
Response Time	< 5 ms	Temperature Stability	0.5°C
Force Resolution	2 μN (0.0002 g)	Frequency Range	10 ⁻⁶ to 80 Hz

3.2 Experimental Methodology by DMA

3.2.1 Temperature Sweep

The temperature sweep test is a dynamic test used to determine the glass transition temperatures of tested materials and to make the specimen reach thermodynamic equilibrium to “forget” the former stress and thermal histories. During dynamic mechanical testing, the control computer makes a digital cross-correlation of measured strain and force by comparing the amplitude and phase shift between the imposed motion (strain) and the force (stress). The dynamic sinusoidal strain and force are measured 2048 times regardless of the test frequency to calculate the average amplitude and phase shift of both. During the measurements, two reference sine waves (command) of fixed amplitude are compared with the data; the result is a strain and force phase relative to the reference as shown in Figure 18. Using fundamental geometric techniques, the phase angle between strain and force is determined using the force-strain vector relationship in the complex plane. The complex dynamic material properties, represented in Chapter II, are then obtained from Figure 18. According to Equation (16)

and (17), the complex modulus, E^* , which indicates the total energy required to deform the material, is calculated by dividing the stress by the strain. Multiplying E^* by the cosine of the phase angle gives the in-phase component of the stress, E' , which is proportional to the energy stored elastically. Multiplying E^* by the sine of the phase angle gives the out-of-phase component of the stress, E'' , which is proportional to the amount of energy lost to viscous dissipation.

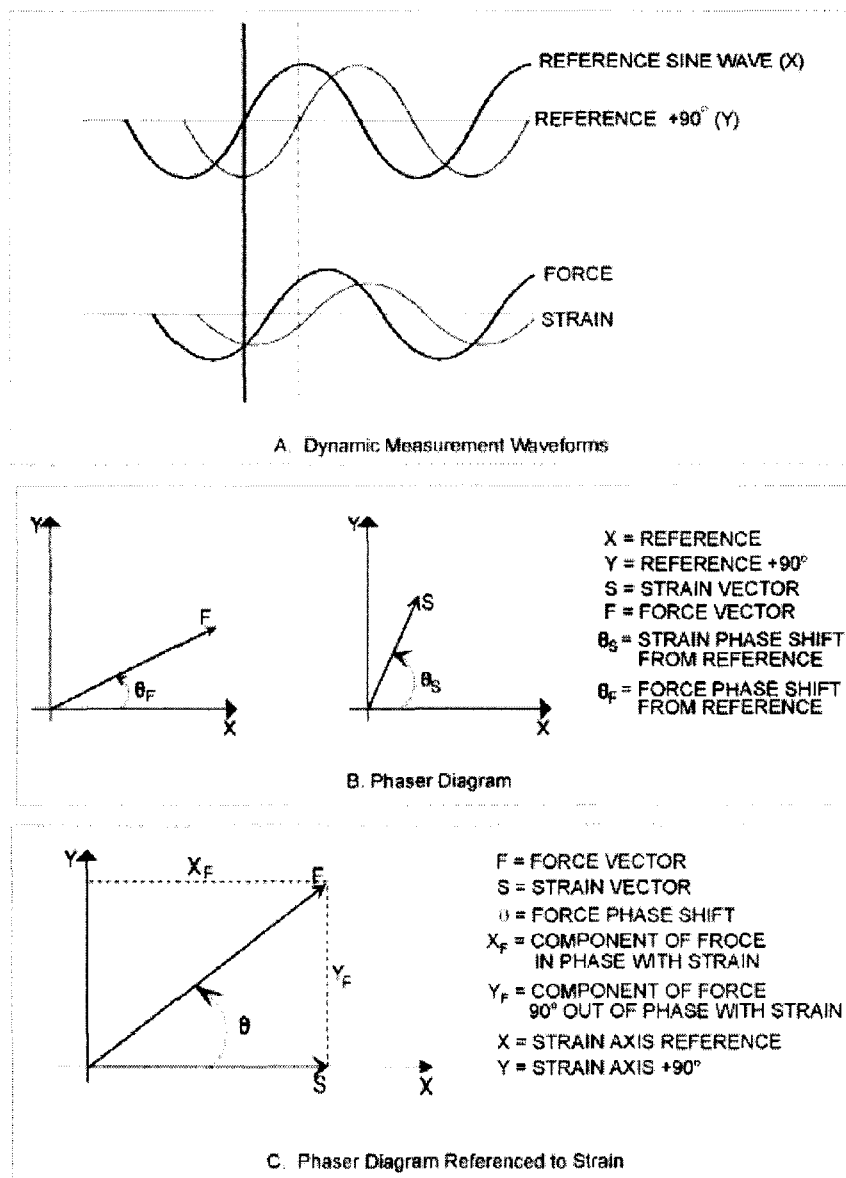


Figure 18. Normalized dynamic waveforms and vectors (TA Instruments, 2003)

The DMA test module “Dynamic Temperature Ramp Test” is used to ascertain T_g . In this test, temperature is automatically increased and decreased at selected ramp rates (in units of °C/min) from the initial to temperature limits, at a selectable constant frequency. A unique set of test conditions can be entered in up to eight temperature ranges, or "zones". In each temperature zone, a selectable thermal "soak time after ramp", which is the period of time the DMA holds at the final temperature before going into the next zone, ensures temperature stability prior to beginning the next ramp. The strain level in a temperature zone can be set to any value within the range of the instrument (as shown in the boundary window) but should not exceed the linear viscoelastic region of the sample material.

When setting up a temperature ramp test, enter a test frequency, an initial temperature, and each individual zone settings (i.e., final temperature, ramp rate, soak time, and strain). The total test duration is then calculated by the program. A typical set-up screen of the temperature sweep test in Orchestrator 7.1 for the RSA III DMA software package is shown in Figure 19. In order to rejuvenate the specimen and erase the effects of past aging, a dynamic temperature ramp test is performed on the specimen. The specimen is subjected to a sinusoidal strain of 0.035% ($350 \mu\epsilon$) at a frequency of 1 Hz as the temperature is swept to a final temperature approximately 5-10°C above T_g . The temperature rate is 6.0 °C/min and 3.5 °C/min for the regions below and above $\sim T_g - 25^\circ\text{C}$, respectively. The specimen is maintained at that temperature for 5 minutes for rejuvenation (rejuvenation is referred to as reestablishing thermodynamic equilibrium at temperature above T_g , see Figure 1). During this test, the storage modulus (E'), the loss

modulus (E'') and the ratio of the two ($\tan \delta = E''/E'$) are determined. In this dissertation, the temperature associated with the $\tan \delta$ peak is assumed to represent T_g . For PEEK films, the temperature ranges for the two zones are from room temperature to 120°C, and from 120°C to 148°C, respectively. For PPS films, the temperature ranges for zone 1 and 2 are room temperature to 70°C, and 70°C to 97°C, respectively. The parameter set for the T_g tests of PEEK and PPS are shown in Table 3.

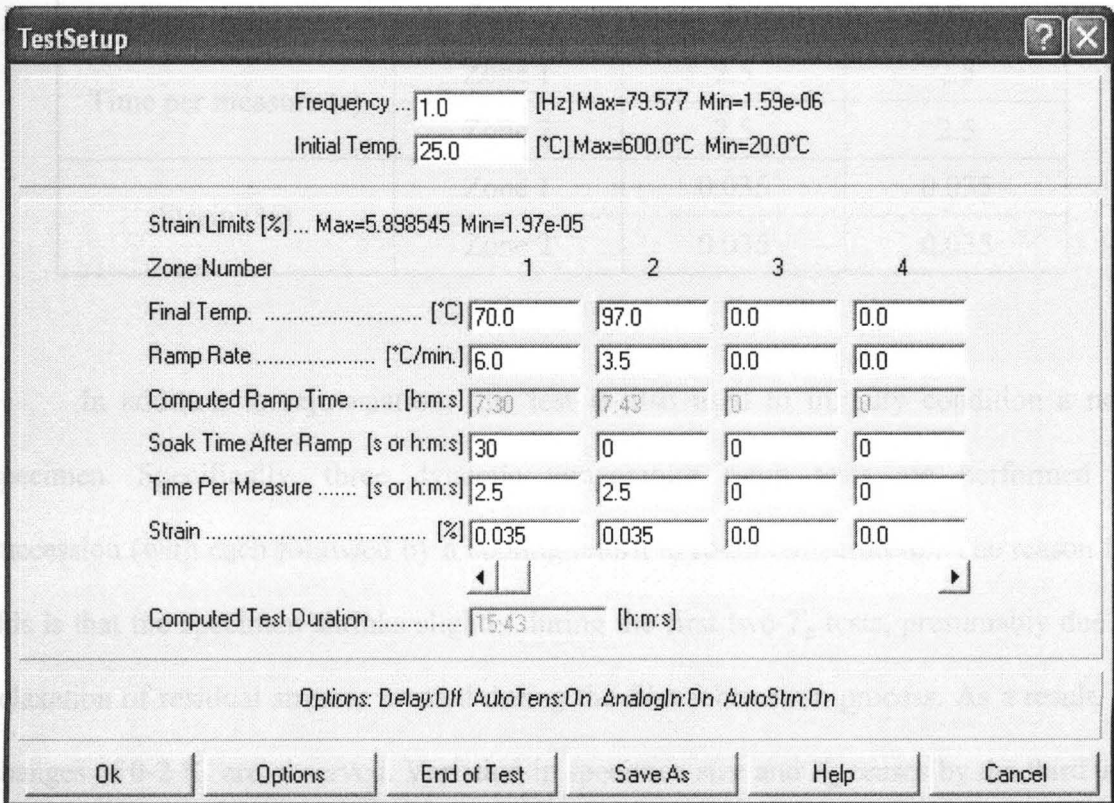


Figure 19. Dynamic temperature ramp test set-up screen

Table 3. Parameter set for the T_g tests

Material		PEEK	PPS
Initial Temperature (°C)		25	25
Final Temperature (°C)	Zone 1	120	70
	Zone 2	148	97
Ramp Rate (°C/min)	Zone 1	6	6
	Zone 2	3.5	3.5
soak time after ramp (s)	Zone 1	60	60
	Zone 2	0	0
Time per measure (s)	Zone 1	2.5	2.5
	Zone 2	2.5	2.5
Strain (%)	Zone 1	0.035	0.035
	Zone 2	0.035	0.035

In addition to rejuvenation, this test is also used to initially condition a new specimen. Specifically, three dynamic temperature ramp tests are performed in succession (with each followed by a cooling return to room temperature). The reason for this is that the specimen shrinks slightly during the first two T_g tests, presumably due to relaxation of residual stresses created during the film fabrication process. As a result, T_g changes of 0-2 °C are observed. Variation in specimen size and T_g ceases by the third test and the specimen is stable thereafter.

In the tests measuring the T_g , the RSA III DMA feature “Auto Tension” is applied. The auto tension maintains a static force that is greater than the peak force level reached in the dynamic oscillation. This feature accommodates the change in length of the specimen due to change in temperature by varying the distance between the grips, using

the RSA III control computer to monitor and control the static tension during a test. By maintaining a static force greater than the dynamic force, the DMA ensures that the film never goes into compression. This can lead to specimen buckling, and the stress signal will become truncated, which will adversely affect the quality of the data (Wang, 2007). This is illustrated in Figure 20.

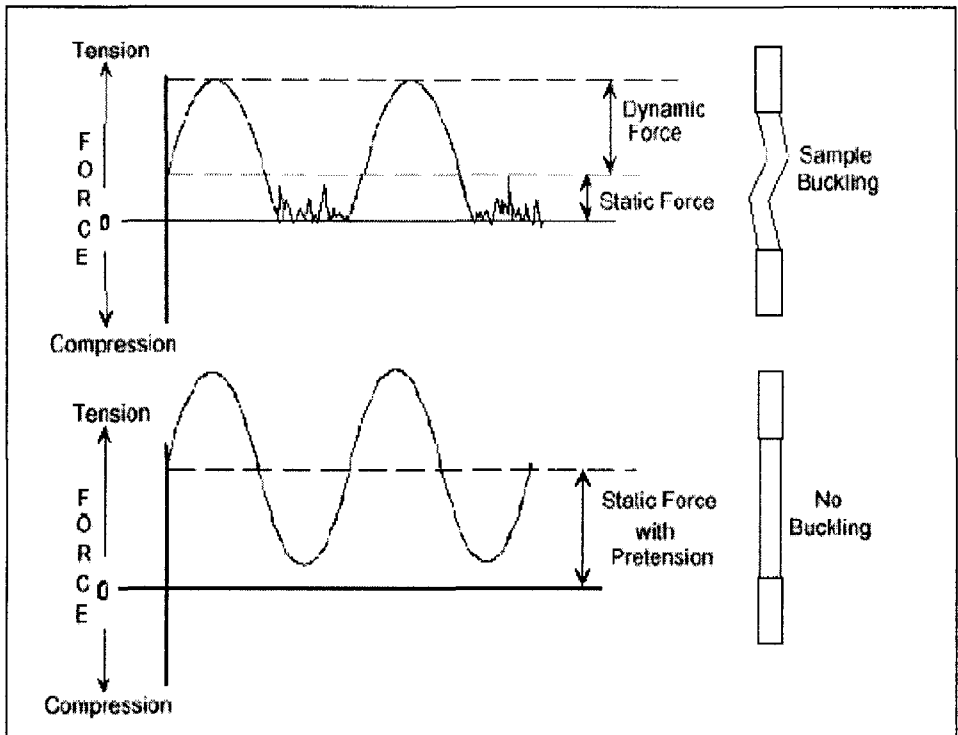


Figure 20. Effects of protection of auto tension adjustment (TA Instruments, 2003)

Auto tension parameters must be set in the Auto Tension Adjustment set-up screen in Orchestrator 7.1. Figure 21 shows the settings for auto tension adjustment for tested materials in this dissertation. The “Static Force Tracking Dynamic Force” mode seeks out a desired ratio of static force to the previous measured dynamic force based on supplied percentile to avoid buckling. The static force level is thereby controlled to be proportional to the measured dynamic force. This can be an advantage for tests run over a range of temperatures where the modulus of a material may change with varying

temperature (Instruments, 2003; TA Instruments, 2003). The initial static force is selected to 50 grams, which is approximately 50% greater than the maximum dynamic force during the temperature sweep tests for PEEK and PPS.

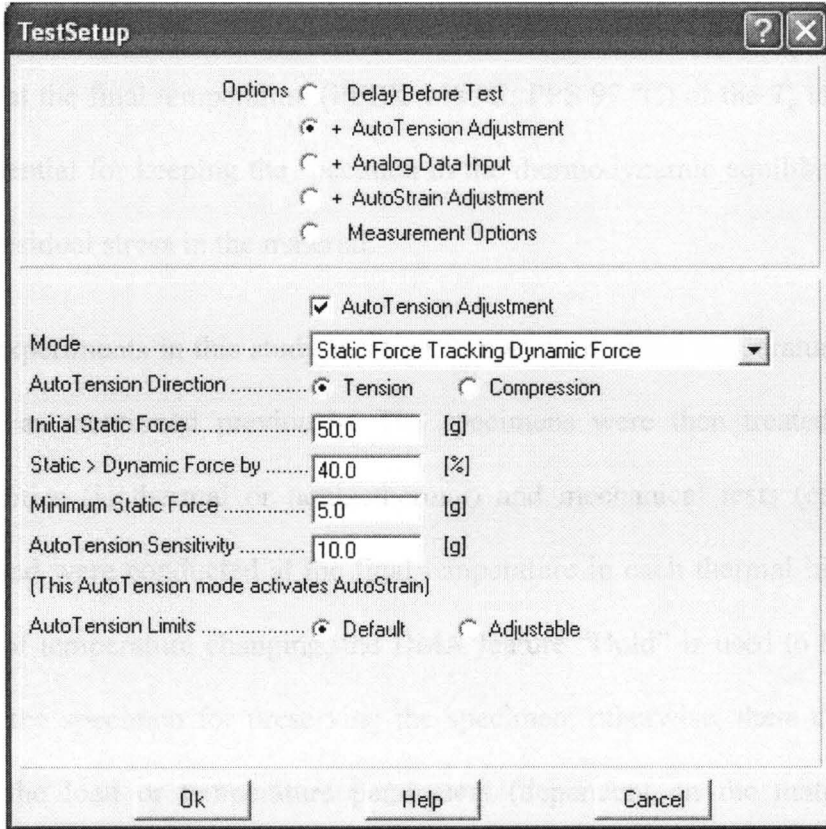


Figure 21. The setting of auto tension adjustment

"Minimum Static Force" represents the minimum pretension where the proportional force mode is to be used. This parameter prevents the static force levels from dropping below the sensitivity of the transducer or the stability of the sample; "Minimum static force" is set to 1 gram. "Auto Tension Sensitivity" is defined as the minimum change in static force that results in an adjustment to maintain the desired static force. If the applied static force is outside the sensitivity "window" (desired static force +/- sensitivity value), the applied static force is adjusted to try and match the desired

static force; otherwise no adjustment to the actual applied static force is made for that sample (TA Instruments, 2003). In the T_g experiments the auto tension sensitivity is set as 0.1 gram.

In the “End of Test” setting screen, as depicted in Figure 22, the oven holds the temperature at the final temperature (PEEK 148 °C; PPS 97 °C) of the T_g tests after each test. It is essential for keeping the specimen in the thermodynamic equilibrium state and erasing the residual stress in the material.

All experiments in this study were performed from three temperature sweep tests in sequence as mentioned previously. The specimens were then treated in designed thermal histories (isothermal or nonisothermal) and mechanical tests (creep or stress relaxation) and were conducted at the final temperature in each thermal history. During the process of temperature changing, the DMA feature “Hold” is used to hold the force constant on the specimen for preserving the specimen; otherwise, there can be sudden changes in the load or temperature parameters (dependent on the material and test conditions) as the specimen shrinks/expands under temperature changes. This feature maintains the small load on the specimen by moving the upper stage of the DMA appropriately, to keep the film in tension throughout the experiment and to avoid significant specimen length change lead by the quench or high heating rate (TA Instruments, 2003).

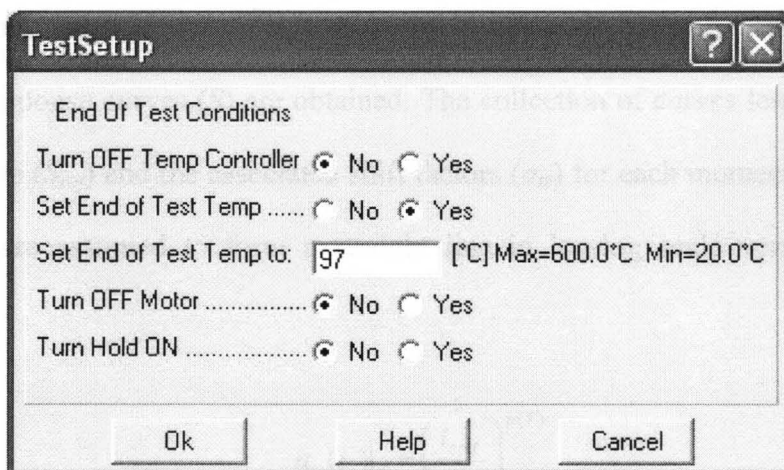


Figure 22. End of test settings of dynamic temperature sweep test

3.2.2 Creep and Stress Relaxation Test Method- Physical Aging

Struik (Struik, 1978) demonstrated that for thermorheologically simple materials undergoing isothermal physical aging, the momentary (short-term) response⁶ (S) is related to a momentary reference (master) curve (S_{ref}) by

$$S(t)|_{t_e, T} = S_{ref}(a_{te}t)|_{t_{eref}, T} \quad (42)$$

where t_{eref} is the isothermal aging time at which the reference curve was defined, t_e is the aging time at which the short-term test is taking place, T is the common isothermal temperature at which both the short-term test and the reference curve were obtained, and

⁶ The difference between “long-term” and “short-term” is based on the ratio of the test duration (t) to the aging time at the beginning of the test (t_e). In general, the short-term test is defined typically where the test duration t is limited to a time corresponding to $0.1 t_e$ (Struik, 1978) or $0.3 t_e$. The momentary curves are obtained from short-term tests (Tomlins, 1996; Tomlins and Read, 1998; Tomlins et al., 1994).

a_{te} is the horizontal shift factor⁷ due to physical aging. In isothermal aging tests, the momentary response curves (S) are obtained. The collection of curves leads to a suitable reference curve (S_{ref}) and the associated shift factors (a_{te}) for each momentary curve. The shift factors are assumed to form a straight line in log-log scale versus aging time according to

$$a_{te}(t_e)|_T = \left(\frac{t_{eref}}{t_e} \right)^{\mu(T)} \quad (43)$$

where μ is the shift rate at temperature T (Struik, 1978).

The approach above scales the time domain in order to obtain the momentary response at any aging time and is referred to as time-aging time superposition. It is similar to another approach, time-temperature superposition principle (discussed previously), that is used to relate the behavior of polymers at various temperatures to the behavior at a reference temperature by a horizontal temperature shift factor (a_T) (Ferry, 1980; O'Connell and McKenna, 1997). This approach can be combined with physical aging shift factors to predict the momentary response at one temperature (T) using a reference curve defined at a reference temperature (T_{ref}) as

$$S(t)|_{t_e, T} = S_{ref}(a_{te} a_T t)|_{t_{eref}, T_{ref}} \quad (44)$$

⁷ A small vertical shift is also sometimes needed in order to achieve ideal superposition (Sullivan et al., 1993). Such materials are not thermorheologically simple and require more complex methods of analysis. It should be noted that there is often no clear trend to the optimal vertical shift factors; in such cases, assuming thermorheological simplicity (i.e. no vertical shifting) is preferred (Bradshaw and Brinson, 1997a)

In order to construct a reference curve spanning several temperatures, reference curves are shifted together in log time to identify the appropriate temperature shift factors (a_T). Each of these individual curves must be at the same aging time (t_{eref}) so the resulting master curve represents the behavior of the material at that age (Barbero and Julius, 2004). These curves must also be momentary curves, otherwise the resulting master curve will not, in most cases, be useful to predict long-term data (Matsumoto, 1988).

One approach to characterizing physical aging behavior for a material is to perform a series of load-unload tests whose duration is short enough that the aging state does not change appreciably during the load segments. In all cases, the material is rejuvenated above T_g and quenched. For isothermal physical aging, the final temperature is $T < T_g$, and the aging time t_e is the time elapsed since the quench. For nonisothermal physical aging, all temperatures after quench are $T < T_g$ but can vary in time; the definition of aging time is less clear but in this dissertation is defined as the time elapsed since the last temperature jump. The load steps occur at particular moments of aging time to be characterized (t_{e0} , $2t_{e0}$, $4t_{e0}$, etc.) and have a duration of less than 10% of the aging time when they occur in order to keep the aging state approximately constant during the load step. The stress and strain levels during testing are also maintained in the linear viscoelastic range.⁸

Two types of testing will be used in this study to characterize the aging response.

⁸ High levels of stress applied to the material can affect the aging state; for example, Struik (1978) found that a large stress spike after isothermal aging effectively rejuvenates the specimen somewhat (i.e. erases part of the physical aging effects). As the loads remain in the linear viscoelastic range, it is assumed in this dissertation that there is no coupling between stress and the aging state.

The first is a creep test, in which the stress is constant during each step (σ_{creep} in load step, 0 in unload step). During both load and unload portions, the time-dependent strain response is monitored. The strain due to an individual load step is obtained as the measured value (ϵ) minus the extrapolated strain from the previous unload step (ϵ_{unload}); this is the strain that is presumed to occur had the current load not been applied. The momentary tensile compliance $D(t)$ for each load step is calculated as

$$i^{th} \text{ Load Step} \rightarrow t = t_e - t_{ei} ; D(t) = \frac{\epsilon(t) - \epsilon_{unload}(t)}{\sigma_{creep}} \quad (45)$$

where t_{ei} is the aging time at the start of the i^{th} load step and t is the time elapsed since the load was applied in the i^{th} load step. In this study, the momentary compliance curves are described using the shifted three parameter Kohlrausch model of the form expressed in Equation (39). Schematics of a isothermal and nonisothermal creep test are shown in Figure 23 and Figure 24, respectively.

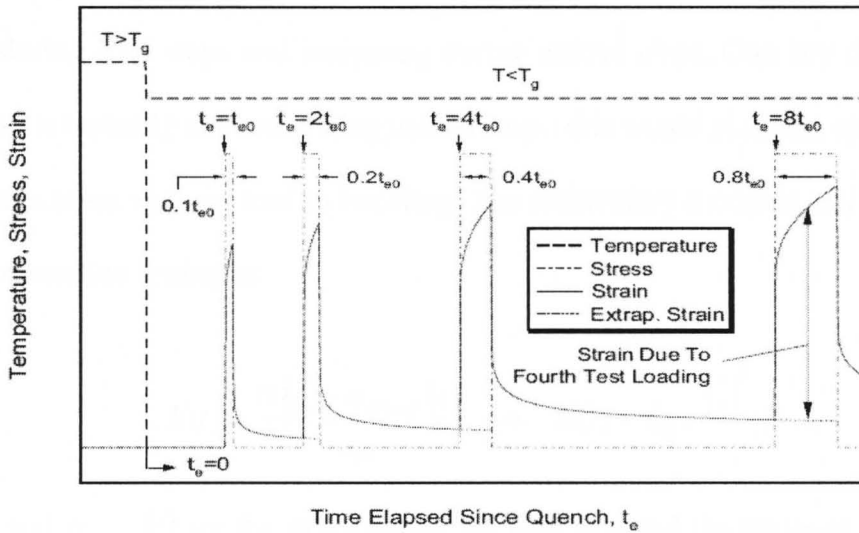


Figure 23. Short-term test method of isothermal creep testing (Bradshaw and Brinson, 1997e)

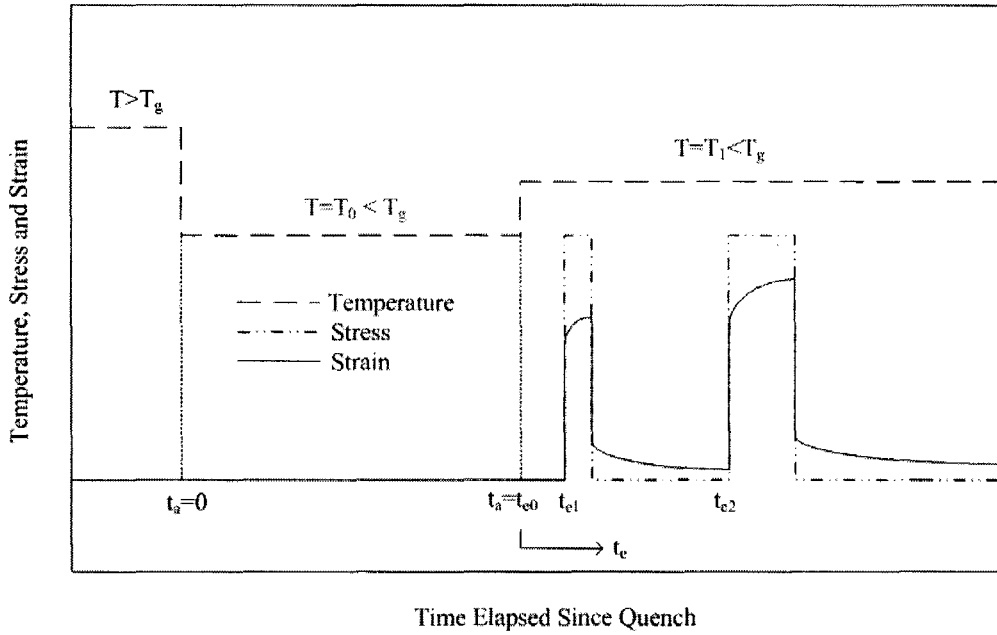


Figure 24. Schematic of up-jump nonisothermal creep test (Guo et al., 2009)

The second approach used is a stress relaxation test. This approach is similar to the creep test except that the stress and strain reverse positions. Specifically, the strain is held constant in each “load” and “unload” step and the stress varies throughout, decreasing during load steps and increasing during unload steps. One key difference is that the strain is typically not zero during unload steps; this would place the specimen in a state of compression and can lead to buckling. The momentary modulus $E(t)$ is obtained from stress relaxation testing as

$$E(t) = \frac{\sigma(t) - \sigma_{unload}(t)}{\epsilon_{sr}} \rightarrow E(t) = E_0 e^{-\left(\frac{t}{\tau}\right)^\beta} \quad (46)$$

where $\sigma(t)$ and $\sigma_{unload}(t)$ are the stress during the load step and the previous unload step (extrapolated), respectively, ϵ_{sr} is the portion of the strain responsible for $\sigma(t) - \sigma_{unload}(t)$,

and E_0 , τ and β are the initial modulus, relaxation time and shape parameter, respectively, for the reference curve (Kohlrausch function).

Once a series of momentary curves are obtained as described above, the reference curve and shift rate need to be obtained. One approach is to manually determine these values using visual means. It is preferable, however, to use an automated method that will lead to consistent, repeatable results across many experimental sets. This study uses the PHYAGE program to automatically determine the optimal reference curve and shift rate for a given set of data (Bradshaw and Brinson, 1997a). This program is designed to be used with compliance data but can also be applied to modulus data by appropriate adjustment of the data.⁹ Theoretically, the shift factors obtained should be the same for a given material whether creep or stress relaxation testing is used (Vleeshouwers et al., 1989).

3.2.3 Creep and Stress Relaxation Test – DMA settings

The RSA III DMA offers the “Program Test Sequence” module to carry out sequential tests designed by the user. This is the approach used to complete physical aging creep or stress relaxation tests in this dissertation. The sequential creep and stress relaxation tests consist of a series of creep and stress relaxation processes at various aging times. The individual creep and stress relaxation are performed by the DMA test module

⁹ The inverse of the modulus data is supplied to PHYAGE. The reference modulus is given by Equation (46) where E_0 is simply the inverse of the “compliance” value of S_0 obtained by PHYAGE and τ and β are the PHYAGE obtained values.

“Multiple Extension Mode” and “Stress Relaxation Test” respectively; a setup screen showing such a test sequence is provided in Figure 25. A typical “Multiple Extension Mode” set up is shown in Figure 26, which includes a load and an unload process to complete the test for one of the aging time conditions. Here, the zone numbers 1, 2, 3 and 4 represent the period of ramp to load, maintain load, ramp to unload and maintain unload, respectively.

The loads for physical aging tests need to remain in the linear region; this needs to be determined by experiments in order to choose a proper load level. Once chosen, the proper ram rate is also determined via experiment, or previous testing; the goal is for the load to approximately equal the desired applied load when the ramp concludes, with a minimum of overshoot or undershoot. The ramp rate is evaluated approximately by (Wang, 2007)

$$RampRate = \frac{\left(\frac{F}{100}\right) \times L_0}{\left(\frac{E'}{10}\right) \times H_0 \times W_0 \times \Delta t} \quad (47)$$

where F is force which is desired by DMA (g); E' is the storage modulus at the temperature considered from the T_g test, (dyne/cm²); L_0 is the original length (m); H_0 is original thickness of specimen (m); W_0 is original width of specimen (m); and Δt is zone time for loading or unloading (s). Each sub-test contains one load and unload process, specifying the strains to be used in the sub-test (load or unload value).

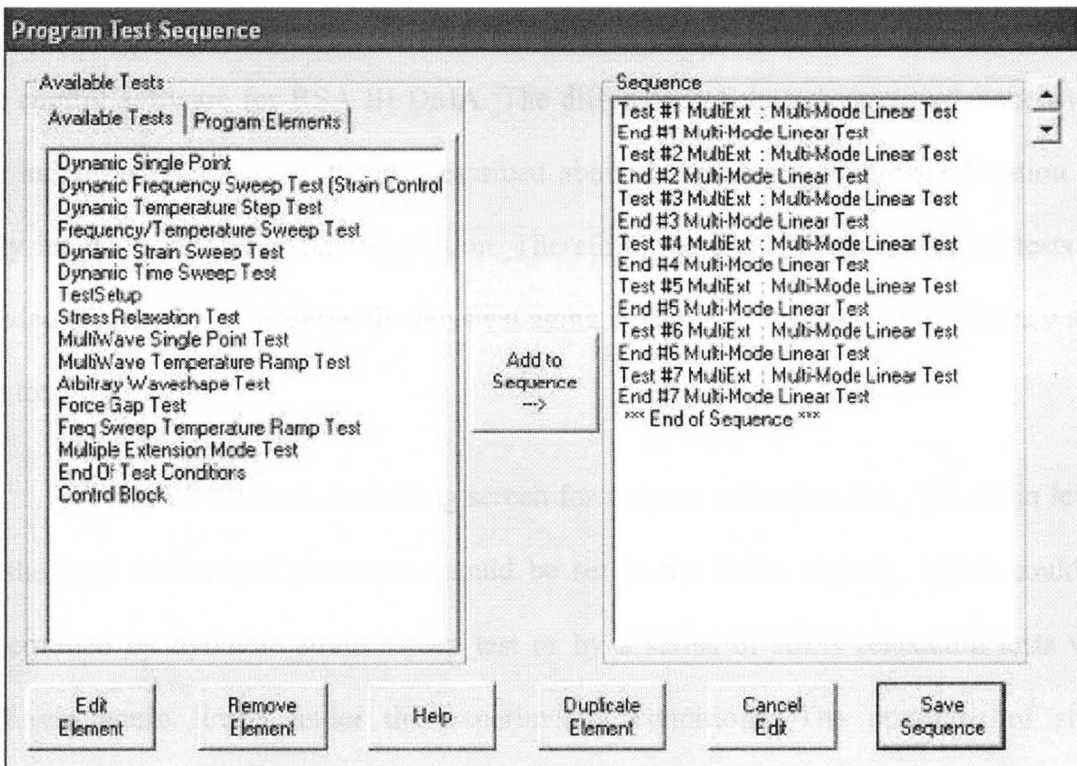


Figure 25. Test sequence design in RSA III DMA

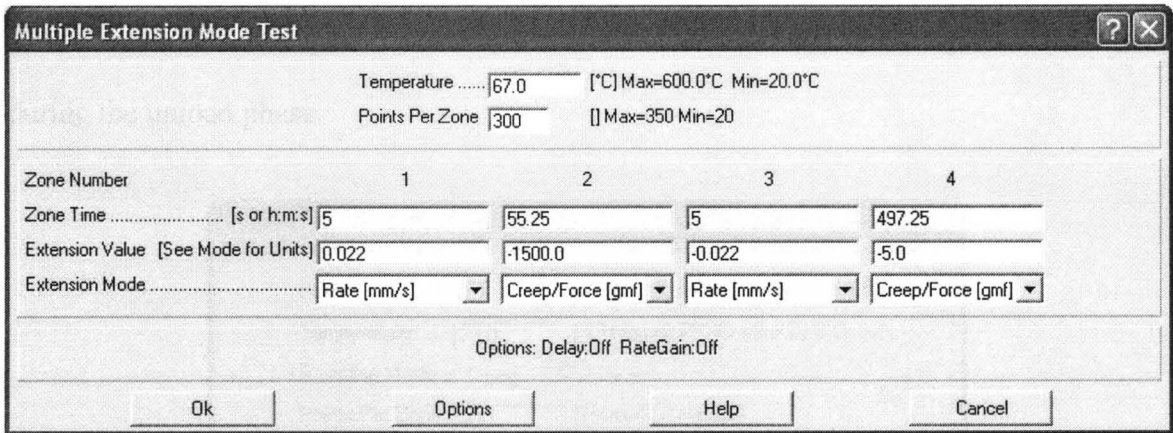


Figure 26. Multiple extension mode test set up screen for single creep-recovery test

The minus values of force in Figure 26 represent tension loading; Turn on window/graphic control in the standard (i.e. Struik) creep test protocol, as shown in Figure 26, the recovery period is 9 times longer than the load duration. The time elapsed in the load or unload ramp is 5 seconds for most creep and stress relaxation tests.

The stress relaxation tests are also organized by the “Program Test Sequence” in the control software for RSA III DMA. The difference of the sub stress relaxation with the individual creep-recovery test described above is that a single stress relaxation can only include the load or unload portion. Therefore, more sub stress relaxation tests are needed (Figure 25) to observe the physical aging behavior at the same aging times within the total time range.

Figure 27 displays the setting screen for a stress relaxation test. The strain levels in the load and unload processes should be set in the linear regions, which could be determined by dynamic strain sweep test or by a series of stress relaxation tests with different strain levels under the experimental conditions. The durations of stress relaxation tests are same as those in creep tests described previously. During stress relaxation, the auto tension adjustment is applied; the settings are shown in Figure 28. This ensures that the specimen always remains in tension and buckling does not occur during the unload phase.

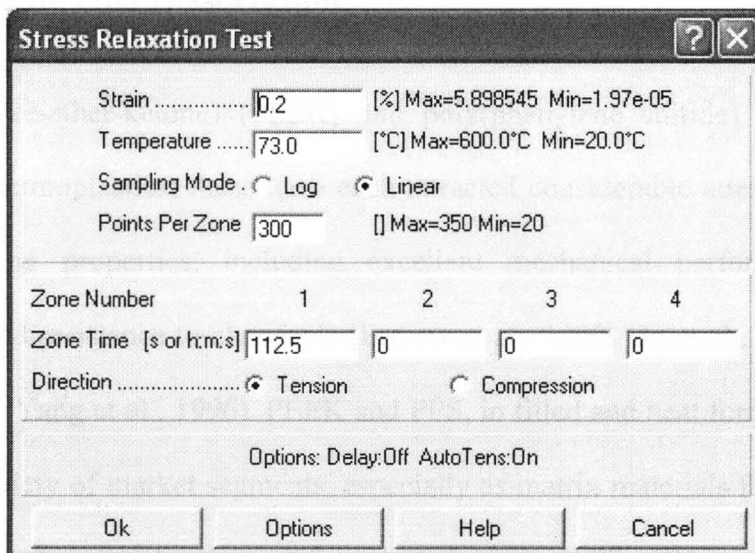


Figure 27. Stress relaxation test setting screen

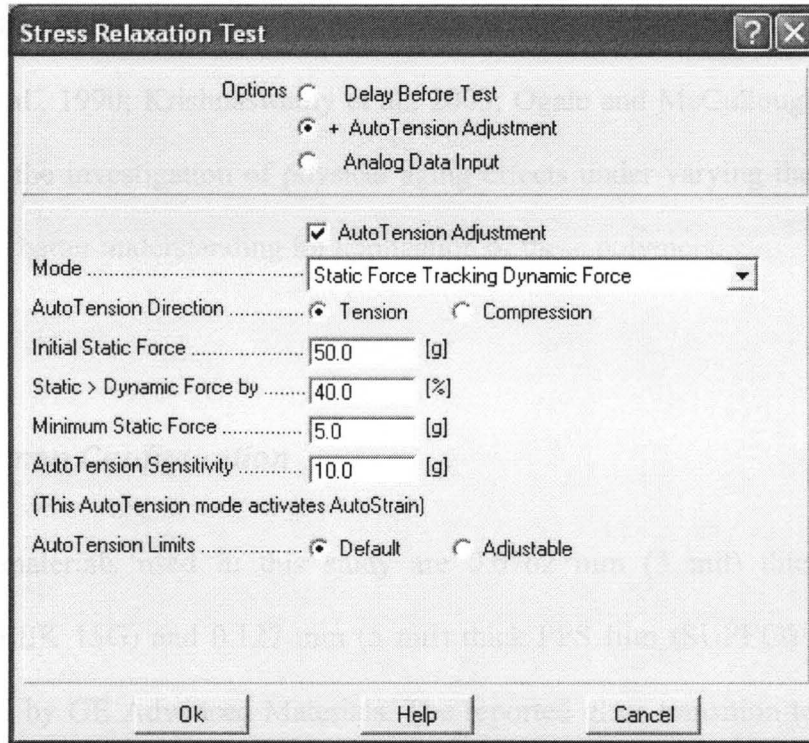


Figure 28. Auto tension setting screen for stress relaxation test

3.3 Materials in This Dissertation

Poly(ether-ether-ketone) (PEEK) and poly(phenylene sulfide) (PPS) are high performance thermoplastics; these have each attracted considerable attention because of their outstanding properties, including excellent mechanical performance at high temperatures and resistance to chemicals (Farrow et al., 1990; Hu et al., 2005; Kemmish and Hay, 1985; Yang et al., 1996). PEEK and PPS, in filled and neat forms, are currently utilized in a variety of market segments, especially as matrix materials for composites in elevated temperature applications (Choy and Leung, 1990; D'Amore et al., 1990;

D'Amore et al., 1994; D'Amore et al., 1991, 1993; Farrow et al., 1990). Although quite a few studies have been published on the characterization of PEEK/PPS-based materials (D'Amore et al., 1990; Krishnaswamy et al., 2003; Ogale and McCullough, 1987; Yang et al., 1996), the investigation of physical aging effects under varying thermal histories would lead to better understanding for application of these polymers.

3.3.1 Specimen Configuration

The materials used in this study are 0.0762 mm (3 mil) thick PEEK film (Vitrex® PEEK 15G) and 0.127 mm (5 mil) thick PPS film (SUPEC® PPS RESIN), both supplied by GE Advanced Materials. The reported glass transition temperatures of these two materials are 143°C and 92°C, respectively (Anonymous, 2001). Both PEEK and PPS specimens were obtained from 305 mm square sample sheets; these specimens were manually cut to be 25.4 mm long (in the load direction) and 12.7 mm wide. In the temperature sweep (T_g) tests, it is found that the change of specimen length (for both PEEK and PPS) depends on the direction of cutting from the sample sheet. In one direction the specimen gets longer after heating up, while in the direction perpendicular to this, the specimen is shorten in temperature sweep test. In experiments, specimens are prepared in the same direction which makes the specimen longer in tension during T_g tests. Minor variation in the actual specimen width dimension required normalization of the data. The film cutter, shown in Figure 29, showed good repeatability in cutting PEEK and PPS films. When cutting the films, clearance between the cutter and the edge of film sheet is fixed by three mechanical parts in order to generate 12.7 mm (0.5 inch) wide strip.

Experimental specimens were then cut by scissors from the strip to achieve 25.4 mm (1.0 inch) length.

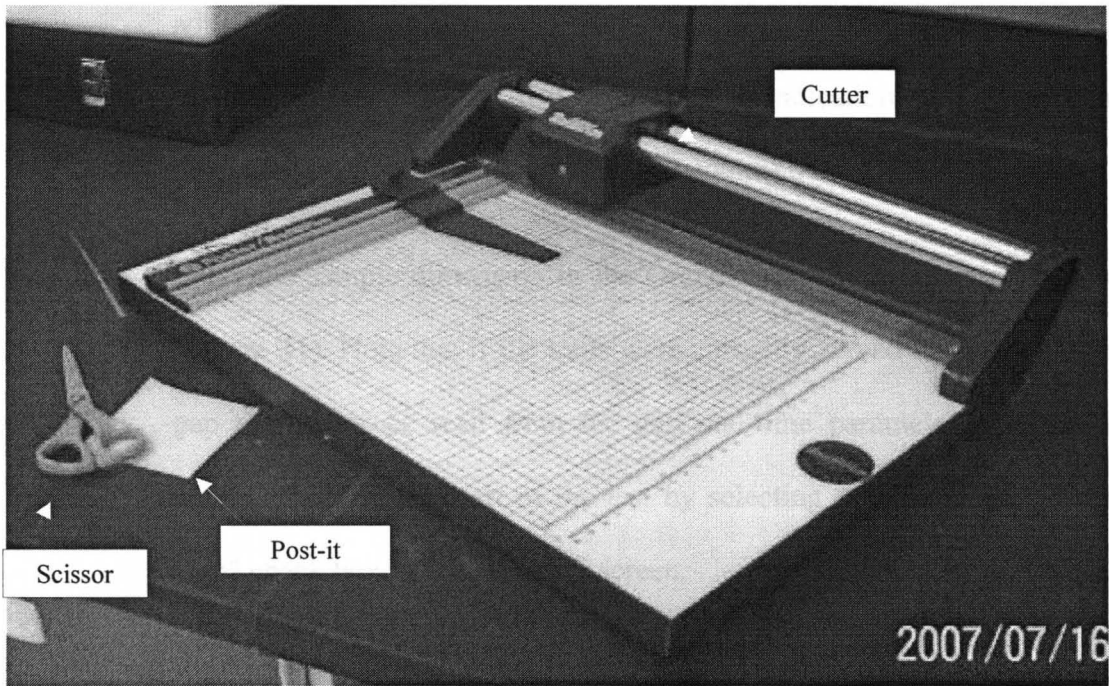


Figure 29. Tools for preparing the sample

Figure 30 shows a specimen mounted onto the film/fiber tension clamps. To install a specimen:

1. Open the oven, zero the fixture by controlling the transducer to the position let the top and bottom clamps contact slightly, and the moving the transducer up to set the gap between clamps a desired value (25.4 mm), this is completed by the options “Zero fixture” and “Set Gap” in Orchestrator software. Place the specimen between two jaws at the top/bottom clamps and tighten the tools screws.
2. Examine the sample to ensure that it exhibits neither wrinkles nor kinks. If

these are present the sample should be remounted.

- Using the stepper motor control buttons on the right side of the test station adjust the stage to provide a very slight tension (less than 5 grams) as indicated by the "NORMAL FORCE" meter indication on the front panel display of the control screen, or the gap control dialog tool.
- Enter the sample dimension in the Orchestrator "Test Geometry" screen (Figure 31). Note that if the tools were correctly zeroed the actual sample gap can either be read from the gap real-time parameter or measured automatically at the start of the test by selecting the "Read Test Fixture Gap" check box in the geometry screen.

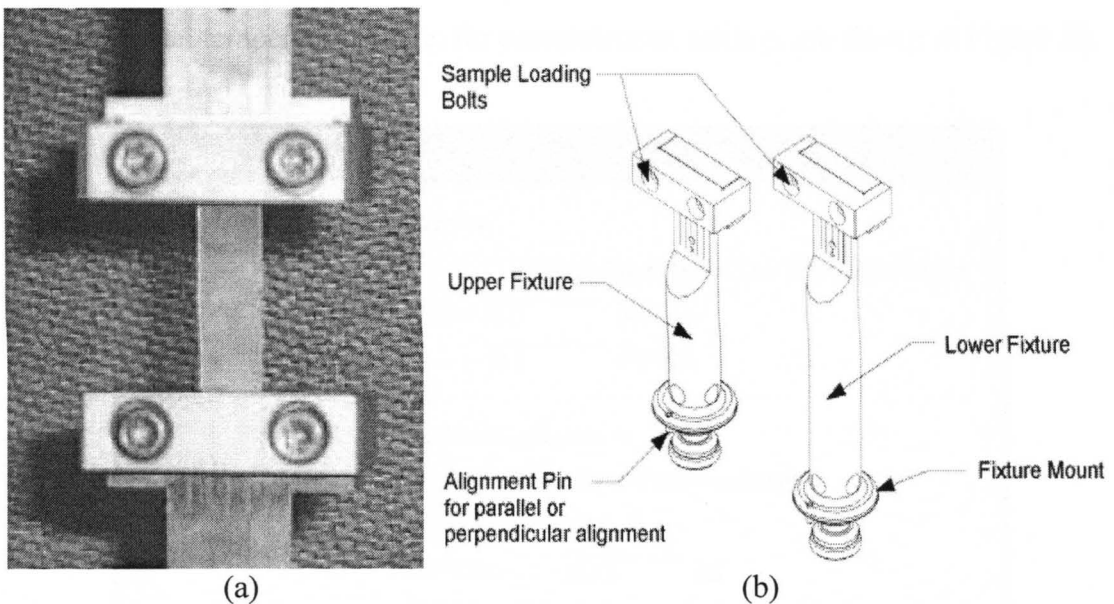


Figure 30. Specimen was mounted in the film/fiber tension clamps. (a) PPS specimen between top/bottom clamps; (b) Film and fiber tool component

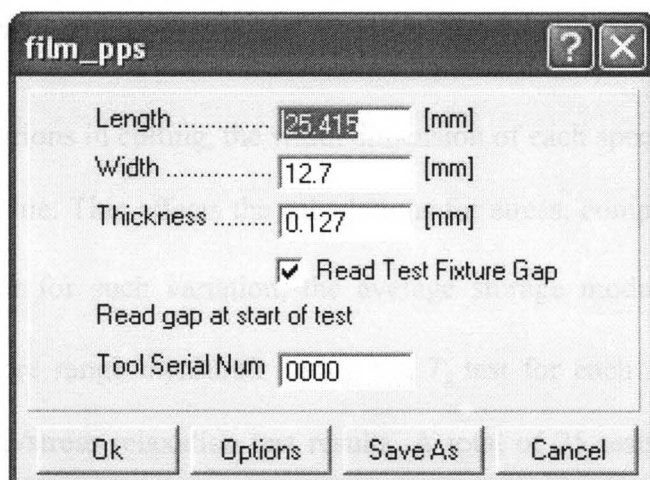


Figure 31. Specimen geometry input

In the “Options” menu in Figure 31, the tools constants can be entered by the user. For the film materials in this dissertation, the tool mass of the upper clamp is 92.6 gram. The “Tool Thermal Expansion Coefficient” and “Fixture Compliance” are negligible in the experimental temperature range; for completeness, settings are shown in Figure 32.

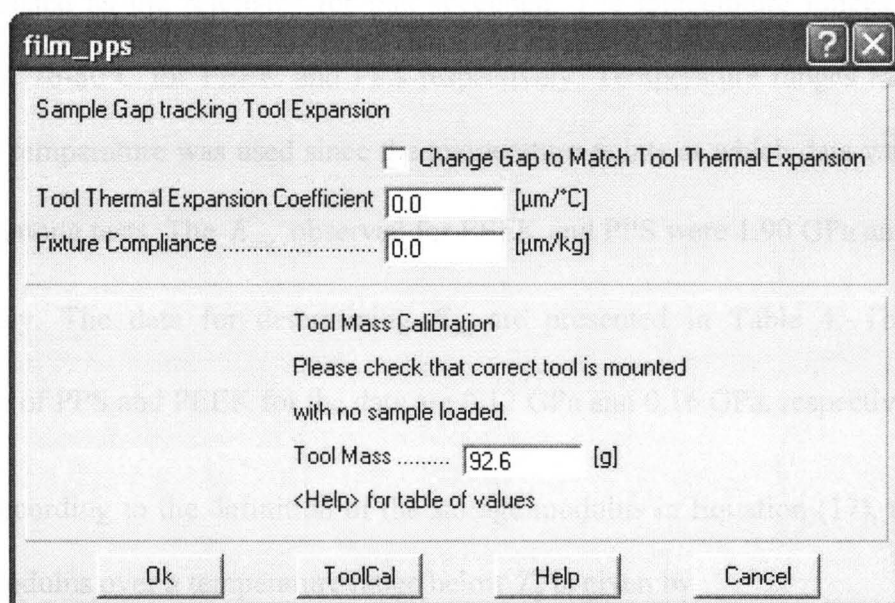


Figure 32. Tool constants input screen

3.3.2 Normalization of Experimental Results due to Dimension Variation

Due to variations in cutting, the width dimension of each specimen differs slightly from the desired value. This affects the calculations for stress, compliance and modulus. In order to account for such variation, the average storage modulus (E'_{ave}) value at specified temperature range measured during the T_g test for each specimen is used to normalize the creep/stress relaxation test results. A total of 25 tests were performed to establish the average value (E'_{ave}) for each polymer. The stress for a given specimen is then multiplied by the ratio E'_{ave}/E'_{spec} where E'_{spec} is the specimen value obtained during the T_g test at the identical temperature. This step reflects the idea that all specimens should have an identical E'_{spec} but do not due to specimen dimensional variation. For each PEEK and PPS specimen, the storage modulus value E'_{spec} in a short temperature range was calculated as the reference for that specimen. The temperature ranges were 130-134°C and 76-80°C for PEEK and PPS respectively. Temperature ranges rather than a particular temperature was used since the temperature points at which data was collected changed among tests. The E'_{ave} observed for PEEK and PPS were 1.90 GPa and 2.14 GPa respectively. The data for determining E'_{ave} are presented in Table 4. The standard deviations of PPS and PEEK for the data are 0.12 GPa and 0.16 GPa, respectively.

According to the definition of the storage modulus in Equation (17), the average storage modulus over a temperature range below T_g is given by

$$E'_{ave} = \frac{F_0}{\epsilon_0 W_{avg} H} \cos \delta \quad (48)$$

where F_0 is the amplitude of dynamic force oscillation, W_{avg} is the actual average width of the specimen, H is the thickness of the specimen, the latter being quite uniform for all specimens. During a glass transition temperature experiment for an individual specimen, the storage modulus is given by

$$E'_{spec} = \frac{F_0}{\varepsilon_0 W_N H} \cos \delta \quad (49)$$

where W_N is the nominal width (12.7mm) of the tested specimen. The compliance $D(t)$ from creep recovery experiment is expressed by Equation (45); in this equation, the applied stress is calculated using the nominal width of the sample and given by

$$\sigma_{creep}^N = \frac{P}{W_N H} \quad (50)$$

where P is the constant load on specimen. The actual specimen width is recovered using E'_{avg} and expressed as

$$\frac{E'_{avg}}{E'_{spec}} = \frac{W_N}{W_{spec}} \rightarrow W_{spec} = W_N \left(\frac{E'_{spec}}{E'_{avg}} \right) \quad (51)$$

To account for dimensional variation, the actual width needs to be adopted to obtain the creep compliance from experiments. This is achieved by applying Equations (48) and (49), with the normalized compliance for a specimen given by

$$D(t) = \frac{\varepsilon(t) - \varepsilon_{unload}(t)}{\sigma_{creep}^N} \times \left(\frac{E'_{spec}}{E'_{ave}} \right) \quad (52)$$

The experimental relaxation modulus can be normalized by an analogous procedure. The resulting modulus is given by

$$E(t) = \frac{\sigma(t) - \sigma_{unload}(t)}{\epsilon_{sr}} \times \left(\frac{E'_{ave}}{E'_{spec}} \right) \quad (53)$$

The test results are quite consistent after normalization is used in physical aging data analysis; this will be demonstrated in the next chapter.

Table 4. Average storage modulus over a temperature range for normalization

Material	PEEK	PPS
E' database (GPa)	1.83; 1.90; 1.83; 1.91; 1.96; 1.72; 1.89; 2.00; 2.15; 1.83; 1.71; 1.73; 1.89; 1.88; 1.94; 1.53; 1.58; 2.04; 2.08; 2.03; 1.93; 1.89; 2.04; 2.04; 2.10.	2.21; 2.22; 2.11; 1.81; 2.13; 2.17; 2.02; 2.13; 2.01; 2.21; 2.21; 2.28; 2.23; 2.20; 2.19; 1.93; 1.96; 2.27; 2.32; 2.16; 2.23; 2.14; 2.05; 2.29; 2.07.
E'_{ave} (GPa)	1.90	2.14

3.4 Other Aspects Related Experiments

3.4.1 Actual Temperature Ramp Rate

The specimen is rejuvenated to erase past aging effects as described previously. The specimen is then quenched to the desired aging temperature (isothermal) or reaches final temperature after a multi-step thermal history (nonisothermal). The aging clock begins ($t_e = 0$) when the specimen first reaches the desired aging temperature (isothermal) or final temperature (nonisothermal). In general, the cooling/heating rate can reach up to 50 °C/min according to the RSA III documentation. In testing at University of Louisville, the specimen reaches temperature very quickly. Figure 33 shows the experimental data of

temperature in the period of quenching, compared with the ideal temperature step curve. In this test, the PPS film was quenched from 97 °C to 57 °C, starting from time = 0 second, the temperature first reached 57 °C about 50 second after the starting of quench, and was steady at 57 °C within 30 seconds later. In this example, $t_e = 0$ at the 50 second point. This behavior is applicable to PEEK material as well. The manner of temperature up-jump is similar as this example. More generally, it is observed that in the first 3 minutes after reaching a desired temperature value, the temperature changed 0.5-1°C and remained within $\pm 0.1^\circ\text{C}$ thereafter.

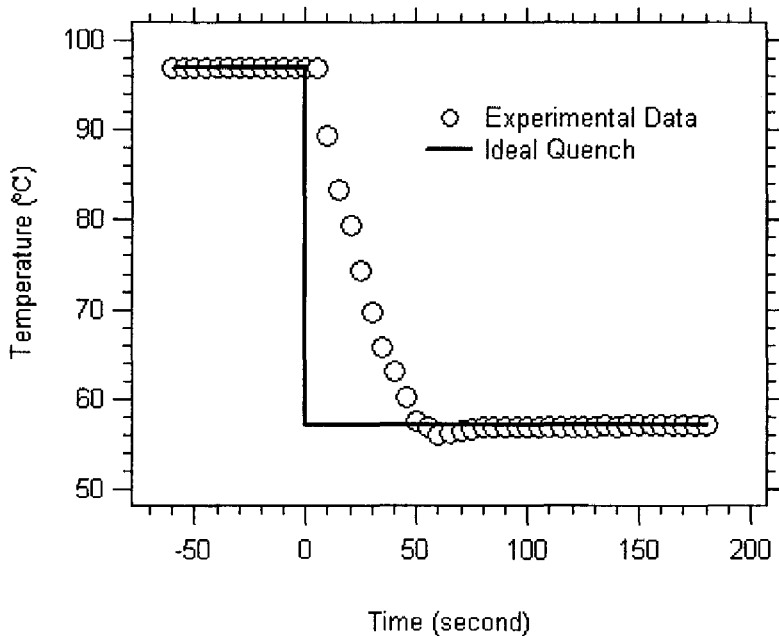


Figure 33. Temperature change during quench of PPS

3.4.2 Test Temperatures

For isothermal physical aging in Chapter IV, all tests were performed at

temperatures are approximately 15°C – 35°C below T_g . These values are such that changes in physical aging can be measured within a lab time scale suitable for this study (each test lasting 24–48 hours). The test temperatures used in the isothermal aging are 110°C, 120°C and 130°C for PEEK ($T_g = 143.5^\circ\text{C}$, details see next chapter) and at 57 °C, 67 °C, 73 °C and 77°C for PPS ($T_g = 92.2^\circ\text{C}$).

In nonisothermal physical aging tests, the temperatures range from room temperature to a temperature near below T_g . Chapter V demonstrates single step temperature up-jump creep testing and experiments after more complicated thermal histories for both PEEK and PPS materials. The final temperatures of these nonisothermal aging are selected from the temperatures at which isothermal creep or stress relaxation were performed. The nonisothermal thermal histories of PPS include:

97 °C (~5 °C above T_g) → 57 °C (14 hr) → 73 °C
97 °C → 63 °C (14 hr) → 73 °C
97 °C → 67 °C (14 hr) → 73 °C
97 °C → 57 °C (14 hr) → 67 °C
97 °C → 67 °C (14 hr) → 77 °C
97 °C → 57 °C (10 hr) → 67 °C (4 hr) → 73 °C
97 °C → 67 °C (4 hr) → 77 °C (10 hr) → 73 °C
97 °C → 67 °C (3 hr) → 77 °C (7 hr) → 57 °C (4 hr) → 73 °C
97 °C → 27 °C (12 hr) → 73 °C (1 hr) → 27 °C (1hr) → 73 °C
97 °C → 57 °C (4 hr) → 73 °C (6 hr) → 67 °C
97 °C → 75 °C (240 hr, equilibrium) → 83 °C
97 °C → 78 °C (12 hr, equilibrium) → 83 °C
97 °C → 80 °C (5 hr, equilibrium) → 83 °C
97 °C → 81 °C (3 hr, equilibrium) → 83 °C
97 °C → 84 °C (0.5 hr, equilibrium) → 83 °C

97 °C → 85 °C (0.5 hr, equilibrium) → 83 °C

97 °C → 86 °C (0.3 hr, equilibrium) → 83 °C

97 °C → 88 °C (0.3 hr, equilibrium) → 83 °C

The nonisothermal thermal histories of PPS include:

148 °C (~5 °C above T_g) → 110 °C (14 hr) → 130 °C

148 °C → 118 °C (14 hr) → 130 °C

148 °C → 120 °C (14 hr) → 130 °C

148 °C → 125 °C (14 hr) → 130 °C

148 °C → 110 °C (14 hr) → 120 °C

148 °C → 120 °C (4 hr) → 125 °C (10 hr) → 130 °C

Chapter VII shows aging behavior near glass transition temperature in PPS, including experiments on aging into equilibrium at various temperatures, for both isothermal and nonisothermal cases. The test temperatures in the isothermal aging are 78°C, 80°C, 81°C, 82°C, 83°C, 84°C and 85°C. All tests are performed within the linear viscoelastic range of the materials.

3.4.3 Linear Regions

As described in previous chapter, the stress/strain response of the material under a general load history was obtained by superposing the response of the material to a series of individual load steps via the Boltzmann superposition principle (Tschoegl, 1989). If the loads place the material outside of the linear viscoelastic range, the compliance/modulus will vary depending on stress/strain level, indicating that the material is in the nonlinear range (Gates et al., 1996).

Before exploring the effects of physical aging on the creep/stress relaxation properties, determination of the maximum stress level (for creep tests) or maximum strain level (for stress relaxation tests) in the linear viscoelastic range was established. Each specimen was repeatedly rejuvenated, quenched to the desired temperature and tested at an aging time of 5/16 hours at increasingly higher stress/strain levels. The transition from linear to nonlinear behavior is evident when the stress/strain level is such that significant changes in compliance/modulus are observed. In addition to compliance and modulus values, load and recovery data from several loadings at different stress levels also provide data for checking superposition (Gates and Feldman, 1995). It is straightforward to verify that Boltzman's superposition principle applies to the entire load/unload data set (another indication of linearity). Using the approach above, the linear viscoelastic range was determined at 110 °C, 120 °C and 130 °C for the PEEK films and at 57 °C, 67 °C, 73 °C, 77 °C, and 85 °C for PPS films. All subsequent tests are performed at stress/strain levels known to be in the linear viscoelastic range.

Linear viscoelastic ranges were established for PEEK and PPS films in both creep (maximum stress) and stress relaxation (maximum strain) by a series of tests at an aging time of 5/16 hours. A sample image for PEEK film at 130° C is shown in Figure 34; the compliance is similar for specimen loads of 1200 g and less but changes dramatically for a load of 1400 g. The resulting limits for linearity for each material and temperature are presented in Table 5.

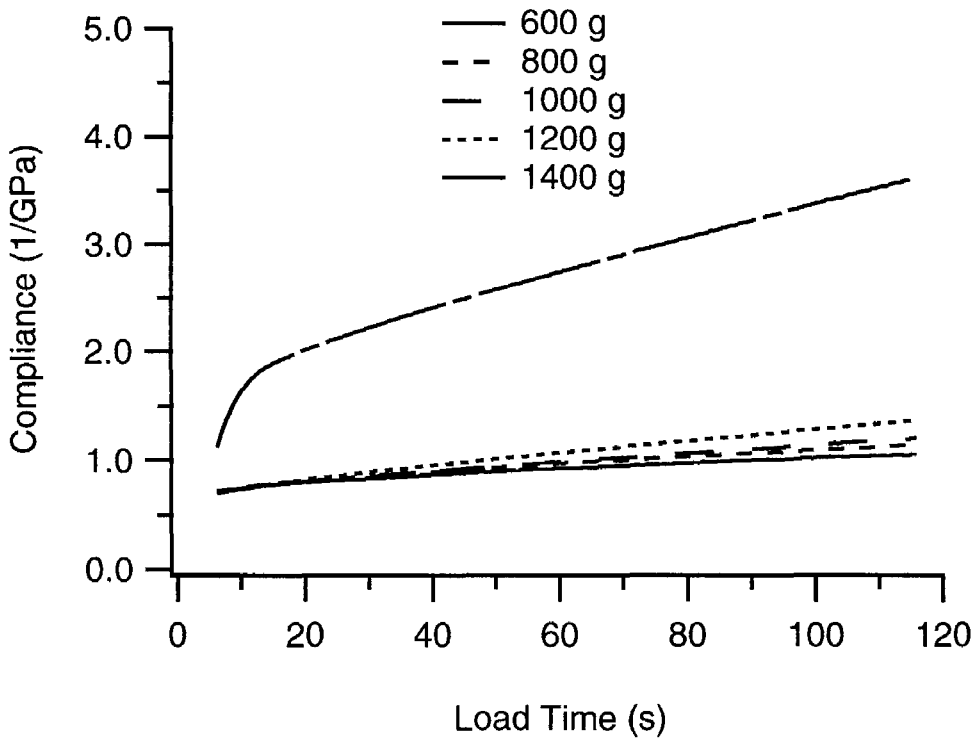


Figure 34. Linearity tests for PEEK at 130°C ($t_e = 5/16$ hours)

Table 5. Upper stress/strain limits of linear viscoelastic range ($t_e = 5/16$ hours)

Experiment conditions		Stress level (MPa)	Strain level (%)
Material	Temperature (°C)		
PEEK	110	16.20	0.55
	120	14.18	0.50
	130	12.15	0.40
PPS	57	12.15	0.57
	67	9.72	0.55
	73	8.20	-
	77	7.29	0.20
	85	1.22	-

CHAPTER 4

ISOTHERMAL PHYSICAL AGING OF PEEK AND PPS

In this chapter, the isothermal physical aging behavior of two polymer films (PEEK, PPS) has been assessed under both creep and stress relaxation using a DMA. The test methods for the instrument as well as the approach to account for minor specimen dimensional variation were developed. The compliance and modulus results developed using the test methods were extremely consistent for specimens at a given temperature and aging time. Comparison between compliance and modulus, using linear viscoelasticity theory to perform the material function conversion, also indicated excellent agreement between the results; this was also true of the shift rates and temperature shift factors. This finding demonstrates that the test and analysis methods used in this study are adequate to capture the physical aging behavior. These methods and database of physical aging test results will provide a useful foundation for the characterization and modeling of physical aging response under a complicated temperature history.

4.1 Background

Isothermal physical aging has been widely studied experimentally by dilatometry

(volume relaxation), differential scanning calorimetry (DSC) (enthalpy relaxation), mechanical tests (creep and stress relaxation). The pioneering work of Tool (Tool, 1946) and Kovacs (Kovacs, 1963) effectively established the phenomenology of volume relaxation, in particular the existence of a distribution of relaxation times, and the non-linearity of the response. Later studies on isothermal volume contraction have confirmed this phenomenology and have been aimed at a quantitative evaluation of the kinetics of volume relaxation in different polymer systems (Duran and McKenna, 1990; McKenna, 1994; McKenna, 1996; Robertson and Wilkes, 1998; Santore et al., 1991; Struik, 1997). In some papers, volume relaxation for the viscoelastic response was investigated by DSC and dynamic mechanical tests (Drozdov and Dorfmann, 2003; Muzeau et al., 1995; Robertson and Wilkes, 2000). Due to the lack of suitable commercial equipment, there are limited numbers of dilatometric studies. In contrast, DSC studies are extremely numerous. The technique of DSC is used to determine the enthalpy of a glassy polymer in order to characterize its structural state, and this is analogous to the volume determined by dilatometry. The DSC has been applied to determine the physical aging behavior of amorphous polymers and semicrystalline polymers (Cheng et al., 1991; Hourston et al., 1996; Hu et al., 2005). In recent years, several comparative studies of physical aging were reported by DSC and thermally stimulated current techniques (Canadas et al., 1998; Dong et al., 2004; Hernandez and Suarez, 2004). In the mechanical testing of physical aging, most researchers use creep experiments to observe the response of physical aging with differential aging time and temperature. Creep test measures the strain by holding the stress at a constant value. Since Struik (1978) developed the sequential test and data analysis method, many papers on the creep responses of polymers have been published

(Bradshaw and Brinson, 1999; Brinson and Gates, 1995; Miyano et al., 2000; Read et al., 1992; Schwarzl and Kaschta, 1998; Spinu and McKenna, 1994; Spinu and McKenna, 1997; Tomlins, 1996). Compared with Creep test, stress relaxation test received much less attention since it was difficult to control strain at a constant value precisely during the stress measurement. An earlier study on stress relaxation was reported by Cizmecioglu and co-workers (Cizmecioglu et al., 1981), the experimental results were “in accordance with” observations made by Struik for creep curves. McKenna and co-workers reported the stress relaxation response of epoxy glasses subjected to different thermal treatment (Lee and McKenna, 1990b) and investigated the time-temperature and time-aging time superposition of the stress relaxation data of polycarbonate (O'Connell and McKenna, 1997). Vleeshouwers (Vleeshouwers et al., 1989), McKenna (Lee and G.B., 1997) reported the effect of physical aging of epoxy by both the creep and stress relaxation test.

PEEK and PPS are both thermoplastic polymers that are potential substitutes for epoxy thermoset resins in high-performance composite materials (D'Amore et al., 1990). Characterizing the physical aging behavior of PEEK and PPS will provide important information in the development of high-performance PMCs; the methods developed to study this behavior can also be readily applied to other thermoplastic materials.

Several studies have been published on the characterization of PEEK and PEEK-based materials. Kemmish and Hay (Kemmish and Hay, 1985) examined the heat capacity and activation energy of amorphous PEEK using DSC. Ogale and McCullough (Ogale and McCullough, 1987) observed the effect of physical aging of PEEK at three levels of crystallinities by creep testing and DSC; however, correlation of the DSC and

creep experiments was not achieved due to the absence of an enthalpy relaxation peak for aged semicrystalline PEEK. Carfagna and co-workers analyzed the physical aging of amorphous PEEK by DSC, X-ray diffraction, water sorption and infrared spectroscopy; their work emphasized the free volume reduction and on the related morphological modifications (Carfagna et al., 1988). D'Amore and co-workers (D'Amore et al., 1990; D'Amore et al., 1991) investigated viscoelastic properties of PEEK and PEEK-based composite APC2 by creep and dynamic mechanical tests; shift rates and mechanical properties at 2-3 temperatures were presented for PEEK and APC2.

There are fewer publications on the physical aging of PPS. Ma and co-workers (Ma et al., 1992) studied the effect of physical aging on impact toughness of PPS-based composites. Krishnaswamy and others (Krishnaswamy et al., 2003) reported the influence of semicrystalline morphology on the physical aging characteristics of PPS.

The study in this chapter characterizes isothermal physical aging of PEEK and PPS using a DMA. PEEK was chosen since it is an ideal matrix material for PMCs; PPS was chosen since it has excellent temperature and chemical resistance, PPS-based composite may work well below 75°C. Typically, creep tests are used to characterize the aging mechanical response. This is a relatively straightforward test in which constant load (stress) is applied to the specimen (often by dead weight methods) and the specimen elongation (strain) is monitored. Another approach is to use stress relaxation testing, in which the specimen deformation (strain) is held constant and the change in specimen load (stress) is monitored. The chief reason that stress relaxation tests are not performed more often is that equipment providing precise strain control is required. In this study, both creep and stress relaxation testing is performed. The DMA provides adequate capability

to control either stress or strain while monitoring the other. This permits characterization of physical aging by two means to validate the anticipated viscoelastic relationships. Since the DMA allows both creep and stress relaxation test methods to be used, the ideal choice for a given situation can be chosen.

4.2 Results of Glass Transition Temperature

Typical glass transition test results are shown in Figure 35 for PEEK and PPS films. The figures present the storage modulus (E'), the loss modulus (E'') and the ratio of the two ($\tan \delta$). The peak of $\tan \delta$ is assumed to represent T_g ; this value is indicated in each figure. The glass transition results demonstrated minor variations in the third T_g test, leading to values of $143.5 \pm 0.3^\circ \text{C}$ and $92.2 \pm 0.5^\circ \text{C}$ for the PEEK and PPS films, respectively. They are virtually identical with values provided by the manufacturer. Note that the glass transition temperatures depicted in Figure 35 are test results from a single specimen for each material; the temperatures matching along with the peak of $\tan \delta$ are not exactly the average values above, but still in the reasonable data scattering range.

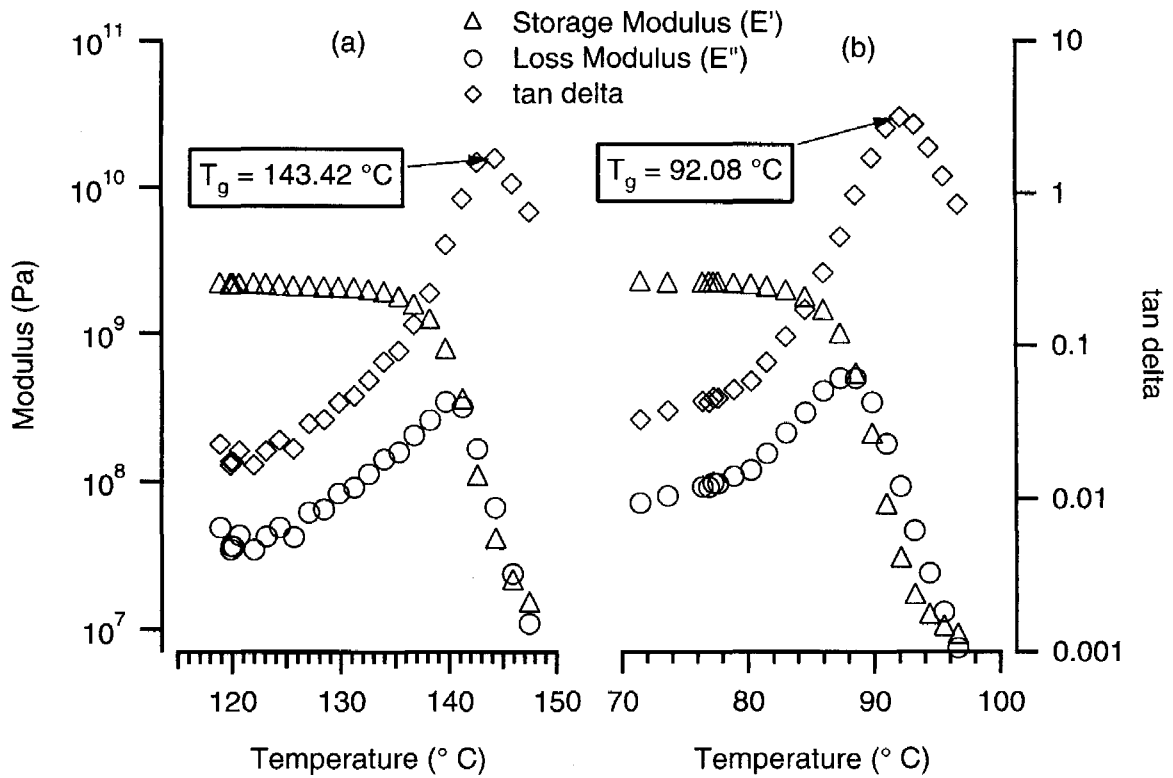


Figure 35. Representative glass transition temperature (T_g) test results:
 (a) PEEK film; (b) PPS film

4.3 Creep and Stress Relaxation Test Details

The isothermal aging tests were carried out in uniaxial extension following the procedure established by Struik (Struik, 1978) as described previously. All isothermal physical aging tests (both creep and stress relaxation) were short-term, with the ratio of loading time to aging time $t/t_e \leq 0.1$. Loading and displacement was controlled/monitored by the suitable test module using the motor and transducer of RSA3 DMA. The convection oven is designed for rigorous temperature control; temperature stability was found to be within $\pm 0.1^\circ\text{C}$.

In the sequenced tests, the aging time (t_e) at each load point was $5/16$, $5/8$,

5/4, 5/2, 5, 10 and 20 hours with the load applied for $0.1 t_e$ followed by an unload for t_e . For creep testing, each load–unload pair was performed using the multiple extension mode of the DMA with 4 zones (ramp to load, maintain load, ramp to unload, maintain unload) to minimize overshoot. For an individual creep step, the load is a value selected within the linear region upon the test temperature. In all creep and stress relaxation tests in this and next chapter, the loading and unloading durations are 5 seconds, the corresponding loading and unloading deformation rate are then determined as described previously. For stress relaxation tests, each load-unload pair simply specifies the strain to be used (i.e. no ramp is required). It is imperative for these tests that the specimen remains in tension to avoid buckling; as such, a suitable unload tensile strain was used (0.002%) rather than the ideal value of 0 strain.

4.4 Time-Aging Time Superposition and PHYAGE

In the short-term sequenced creep and stress relaxation test represented in Chapter II, the specimen is loaded and unloaded according to a specific schedule. The response due to each short-term load is then determined by subtracting away the extrapolated relaxation (which would have occurred had the load not been applied); this results in a short-term compliance and stress modulus curve for each loading segment at a given aging time. By repeating this process at different aging times, a family of momentary curves can be obtained. This approach significantly reduces the time required to generate test data, since a number of tests at various aging times can be completed for each rejuvenation cycle. In this study, the raw data of each creep or stress relaxation test

including the test time (second), the specimen length (mm), load (gram) and strain (%) were exported from Orchestrator software; the data during loading and unload process were then removed manually, since these parts are not required for establishing the creep or relaxation phenomenon. The remaining data were then used to find the compliance or relaxation modulus of the material.

MathCAD documents were developed and used to determine the compliance and relaxation modulus curve family of sequential tests. The resulting compliance and modulus were corrected by the normalization procedure represented in the previous section. It is appropriate to note that the strain in creep should be obtained by the instantaneous specimen length and the original length at the beginning of loading process in the first creep test. The strain values in the raw data sheet of Orchestrator are determined by refer to the initial specimen length in the current sub creep test, therefore, these strain output cannot be adopted directly in data analysis.

Once families of compliance or modulus curves at various aging times are collected from a series of creep tests, the time-aging time superposition can be applied to determine the aging shift factors, aging rate, etc. This analysis is performed by PHYAGE, a program developed by Bradshaw and Brinson (Bradshaw and Brinson, 1997a), which includes fitting the experimental data curve with an appropriate material function (Kohlrausch and Prony series), and finding the optimal reference curve, shift rates, and the associated shift factor function. The final output of the program is the reference curve; the shift rate describes the shift factor function and aging shift factors for each curve at specific aging times.

PHYAGE first fits each set of data with an optimal Kohlrausch curve. These curves are called the momentary curves (MCs). These MCs can be superposed onto a single momentary master (reference) curve (MMC) at a reference aging time. This superposition can be performed by shifting all the MCs horizontally (in log time) onto the MMC (Bradshaw and Brinson, 1997a). One significant characteristic of PHYAGE is that it can create the “total reference curve” which gathers information of all material response curves by an iterative fashion. If the reference curve onto which all the rest of the momentary curves are shifted is one of the individual momentary curves, the results will be biased to that MMC obtained from a single test. In such a case, all the future predictions will have the shape of that chosen MC. To improve upon this, the concept of total reference curve is introduced. The total reference curve uses all the short term compliance curves to determine the reference curve parameters. For determining the total reference curve, one of the momentary curves is initially chosen as the reference curve and the rest of the momentary curves are superposed onto it. All the curves that were superposed on to the reference curve are fit with another Kohlrausch function (for creep test). This is considered as the new reference curve. All the momentary curves are again shifted onto the new reference curve and are again fit with a Kohlrausch curve. This process is repeated until convergence occurs; the final reference curve obtained after convergence is called the total reference curve. The shift factors a_{te} , which best superpose each of the momentary curves onto the total reference curve, are calculated along with the shift rate, μ , by PHYAGE. Using this shift rate and the total reference curve, the physical aging of the material can be predicted (Bradshaw and Brinson, 1997a; Guo and Bradshaw, 2007).

The PHYAGE program also provides three alternate solution methods for utilizing upon specific purpose. These methods consist of: (1) using the MC at t_{eref} as the reference curve with horizontal shifting only; (2) using the MC at t_{eref} as the reference curve with both horizontal and vertical shifting; and (3) using the total reference curve with both horizontal and vertical shifting.

In this chapter, the reference curves in isothermal aging data analysis are chosen as the total reference curve at the longest aging time, i.e., $t_{eref} = 20$ hours.

4.5 Creep and Stress Relaxation Results

4.5.1 Isothermal Creep Test Results

This section presents the results from aging experiments using sequential creep and stress relaxation tests. Selections of the creep measurements under aging at different temperatures are shown in Figure 36 – Figure 38 for PEEK and Figure 39 – Figure 42 for PPS. The tests were performed with a maximum stress values which are within the linear viscoelastic range (see Table 5). For each family of curves, creep compliances are plotted versus load time for various aging times at constant temperature. As aging increases, the creep curves shift towards longer times. Time-aging time superposition is used to form a single master curve for all of the data; the reference aging time is 20 hours.

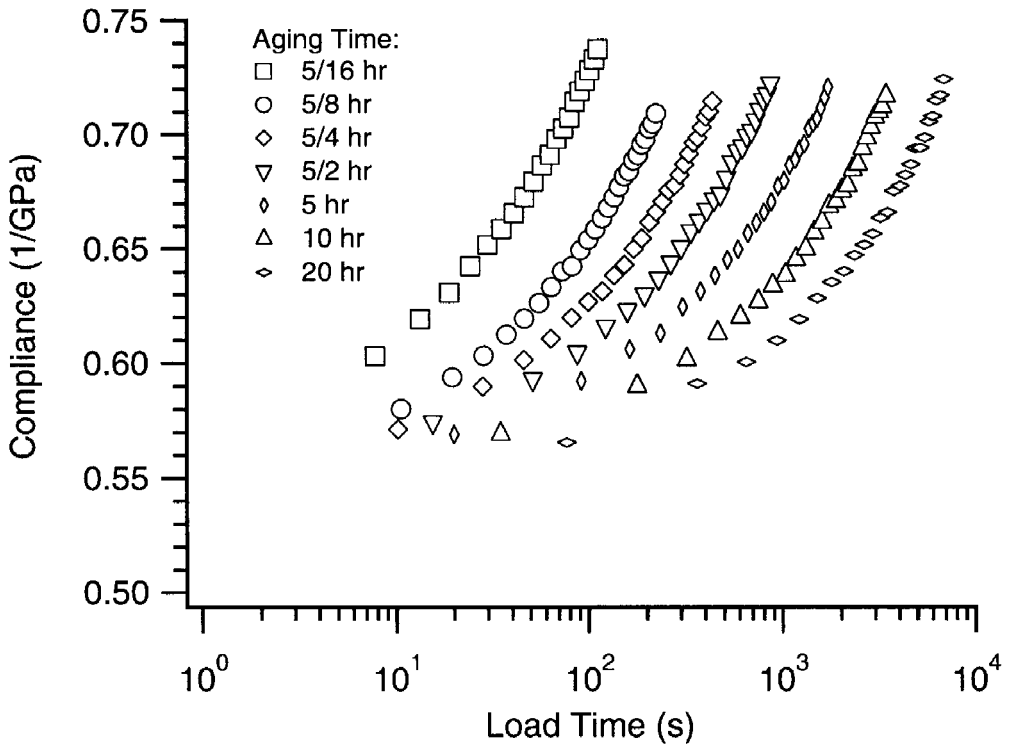


Figure 36. Isothermal creep test results for PEEK at 110°C

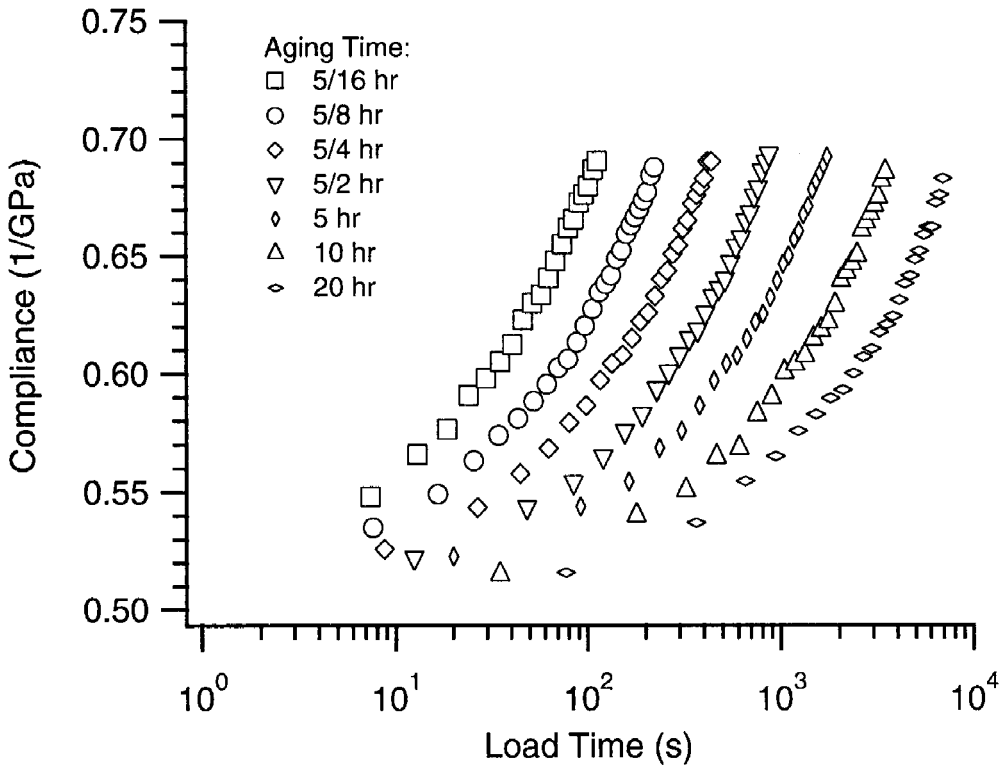


Figure 37. Isothermal creep test results for PEEK at 120°C

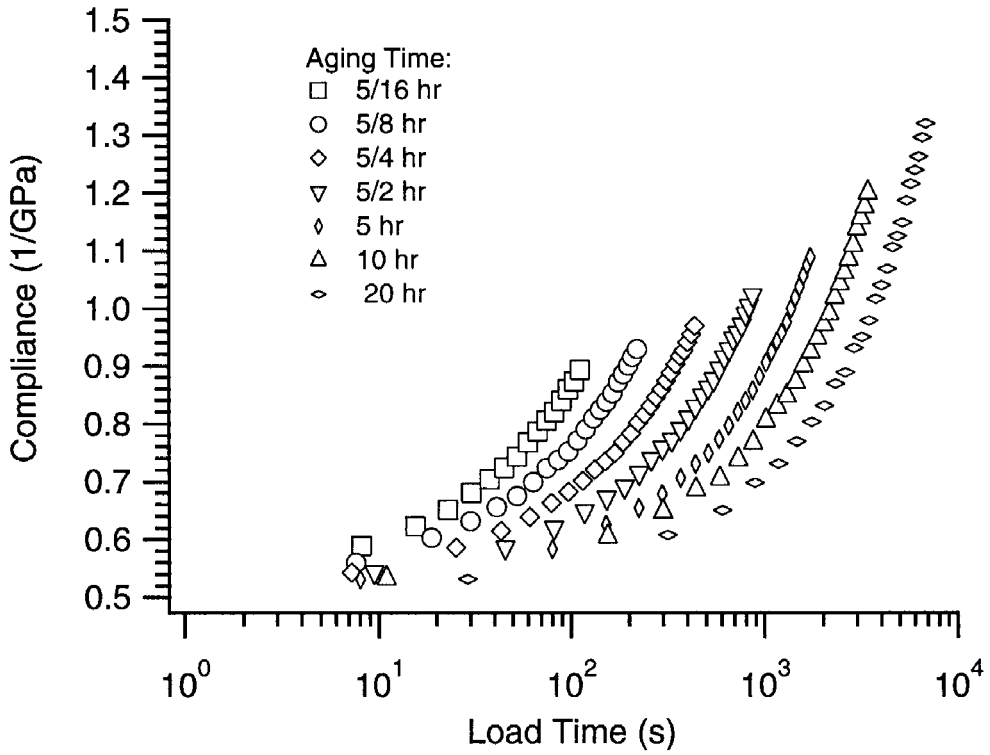


Figure 38. Isothermal creep test results for PEEK at 130°C

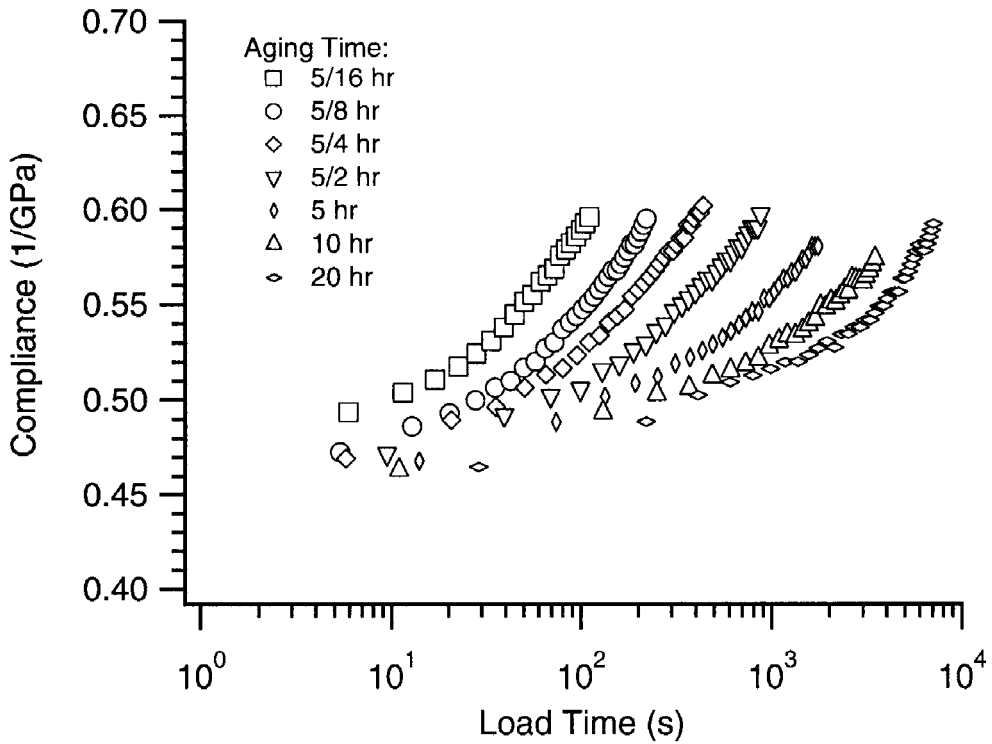


Figure 39. Isothermal creep test results for PPS at 57°C

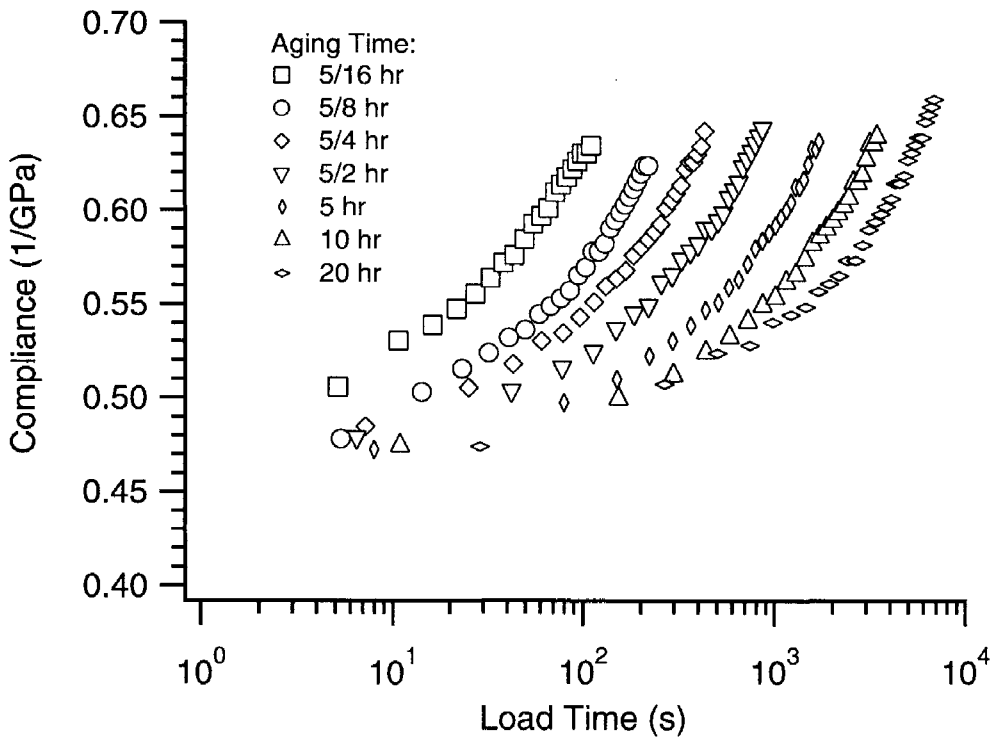


Figure 40. Isothermal creep test results for PPS at 67°C

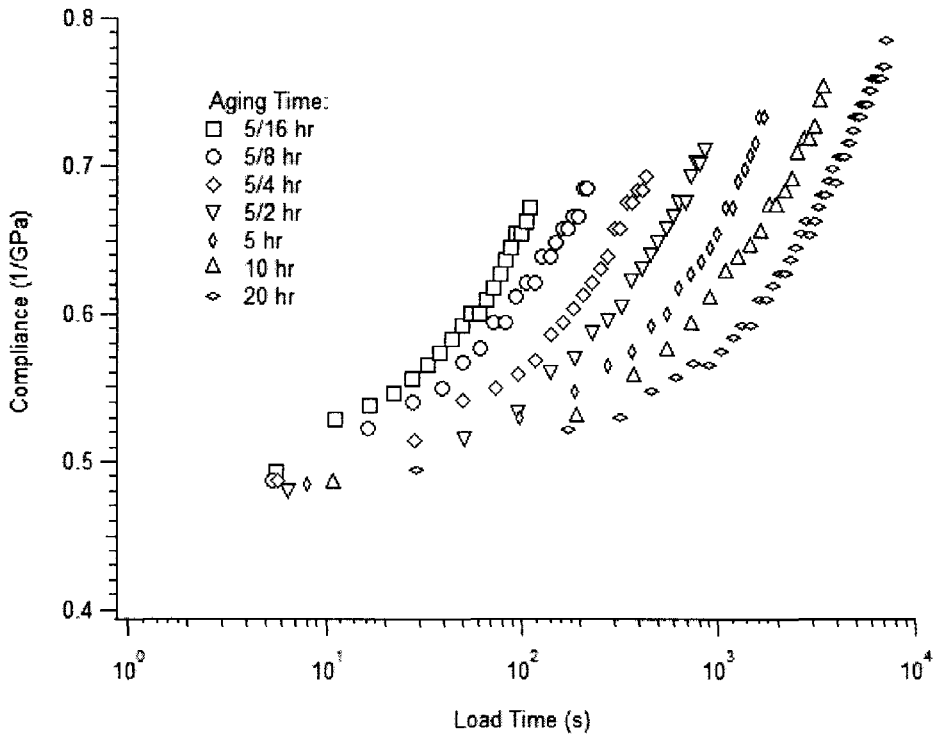


Figure 41. Isothermal creep test results for PPS at 73°C

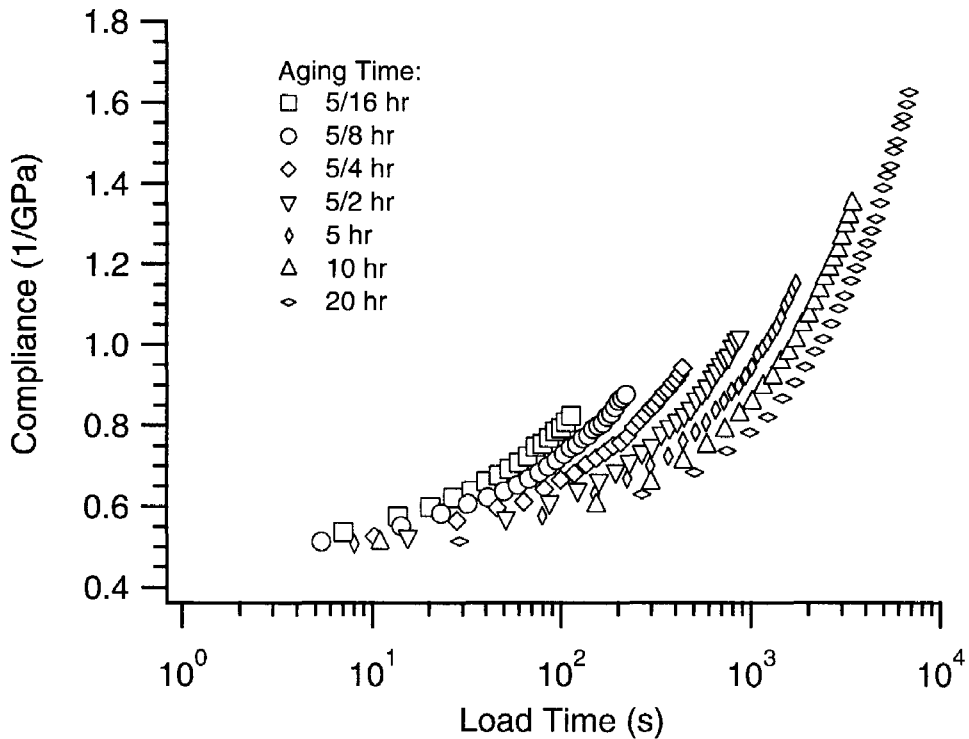


Figure 42. Isothermal creep test results for PPS at 77°C

4.5.2 Compliance Variation between Specimens

For each condition, at least 3 replicate tests were performed (different specimens, identical test conditions). In most tests, the values for all of the compliances could be measured with an absolute accuracy of $\pm 2\%$ (bias from average values) to the average compliance for all specimens.

Figure 43 shows the compliance variation between specimens of PEEK at 130°C, with aging time 5/16, 5/8 and 5/4 hours. The results at other experimental conditions have similar variations, except for PPS at 57°C, in which the variation of absolute accuracy is on the order of $\pm 3\%$.

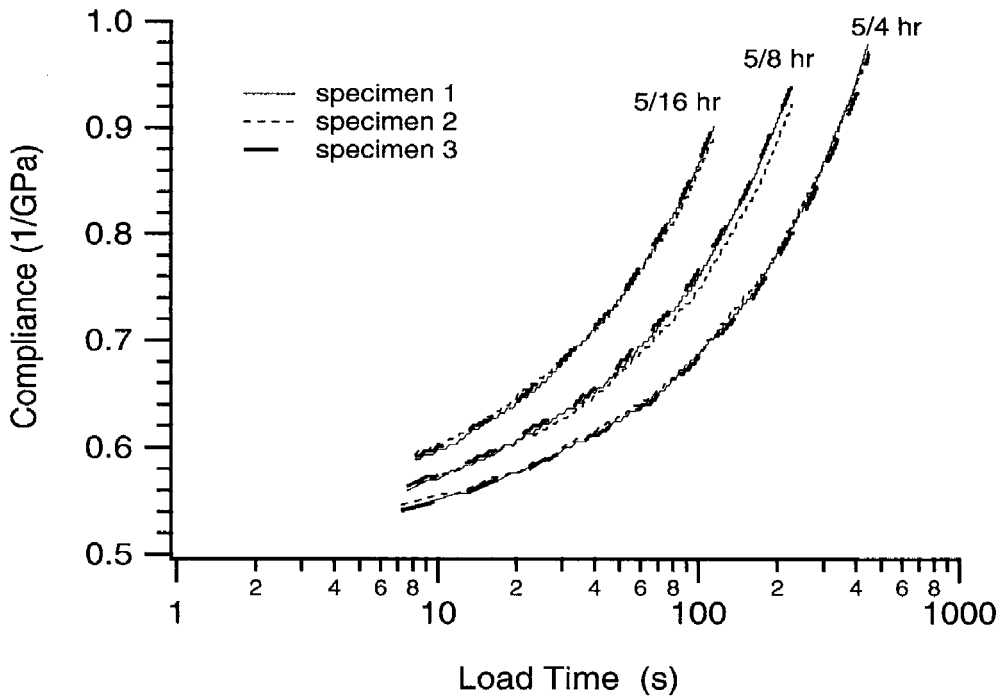


Figure 43. Variation between PEEK specimens in isothermal creep at 130°C

4.5.3 Creep Data Analysis

The optimal compliance reference curve and shift rate μ were determined using PHYAGE for the PEEK and PPS compliance results presented above. The resulting reference curve and shift rate values are listed in Table 6; each of the values represents an average of results from three tests. The results for across specimens were extremely consistent once the data was normalized by the storage modulus value as previously described. The shift factors obtained for each momentary curve along with the line prescribed by the obtained shift rate are shown in Figure 44 and Figure 45 for PEEK and PPS, respectively.

Table 6. Reference curve parameters obtained during isothermal creep tests at indicated temperature ($t_{ref} = 20$ hours, average values for 3+ replicates in each case)

Experiment conditions		D_0	τ	β	Shift Rate μ
Material	Temp. (°C)	(1 / GPa)	($\times 10^3$ s)	(unitless)	(unitless)
PEEK	110	0.515	118	0.449	0.955
	120	0.506	92.4	0.460	1.035
	130	0.512	7.87	0.531	0.745
PPS	57	0.452	1160	0.335	1.137
	67	0.461	90.9	0.441	0.958
	73	0.466	23.0	0.504	0.764
	77	0.474	3.61	0.429	0.450

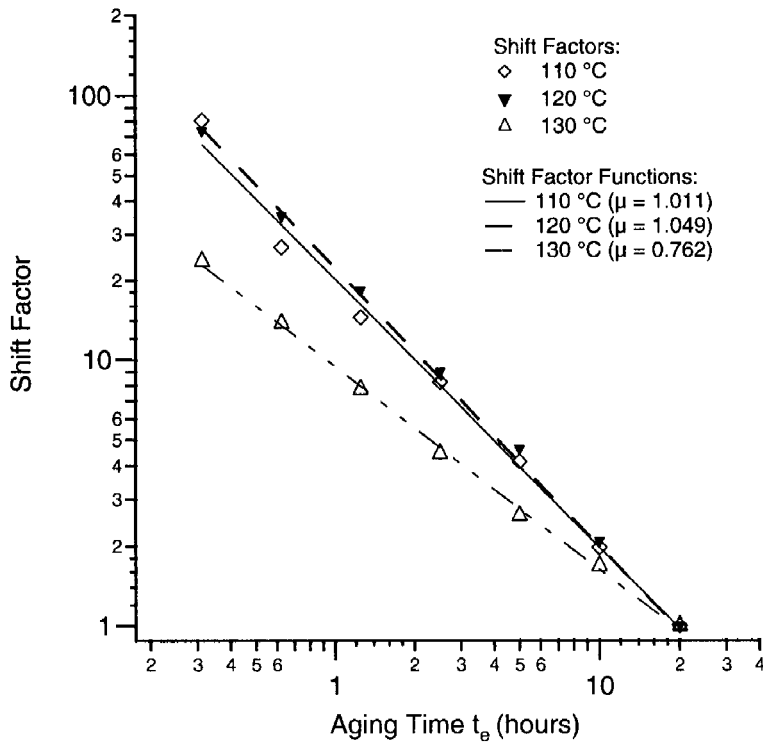


Figure 44. Shift factors and associated shift rates obtained from the creep tests for PEEK films at the temperatures indicated

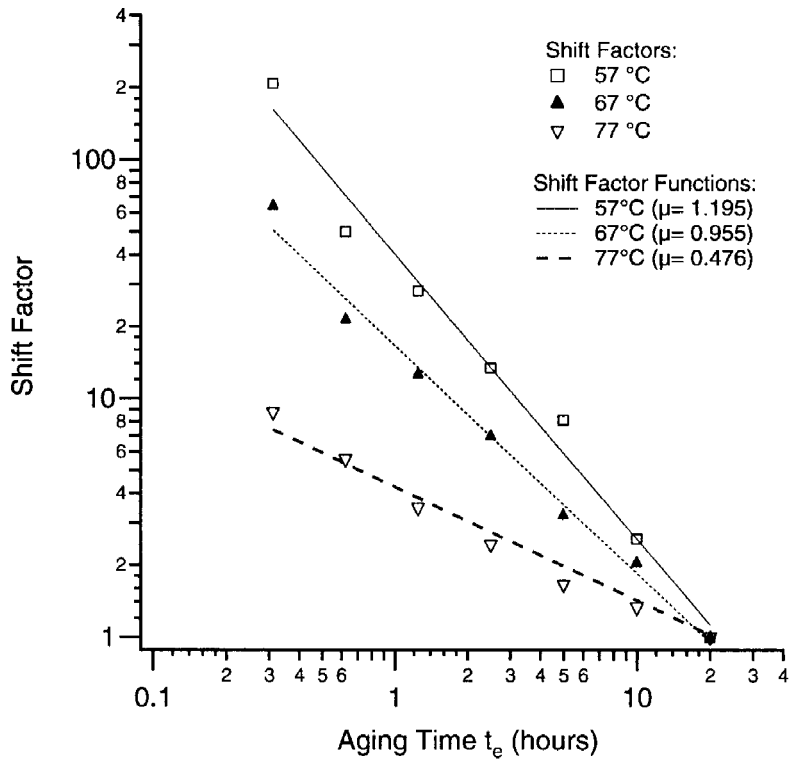


Figure 45. Shift factors and associated shift rates obtained from the creep tests for PPS films at the temperatures indicated

4.5.4 Isothermal Stress Relaxation Test Results

The stress relaxation tests for PEEK and PPS were performed in the same aging conditions as the compliance testing. For each stress relaxation test, the maximum strain value was chosen to be in the linear range; the minimum strain during the recovery was 5% percent of the maximum strain to maintain tension in the specimen.

Selections of the stress relaxation measurements under aging at different temperatures are shown in

Figure 46 – Figure 48 for PEEK and Figure 49 – Figure 52 for PPS. Each of these results show similar behavior, with modulus curves shifting in the time direction as aging

time proceeds. For each condition, at least 2 replicate tests were performed (different specimens, identical test conditions).

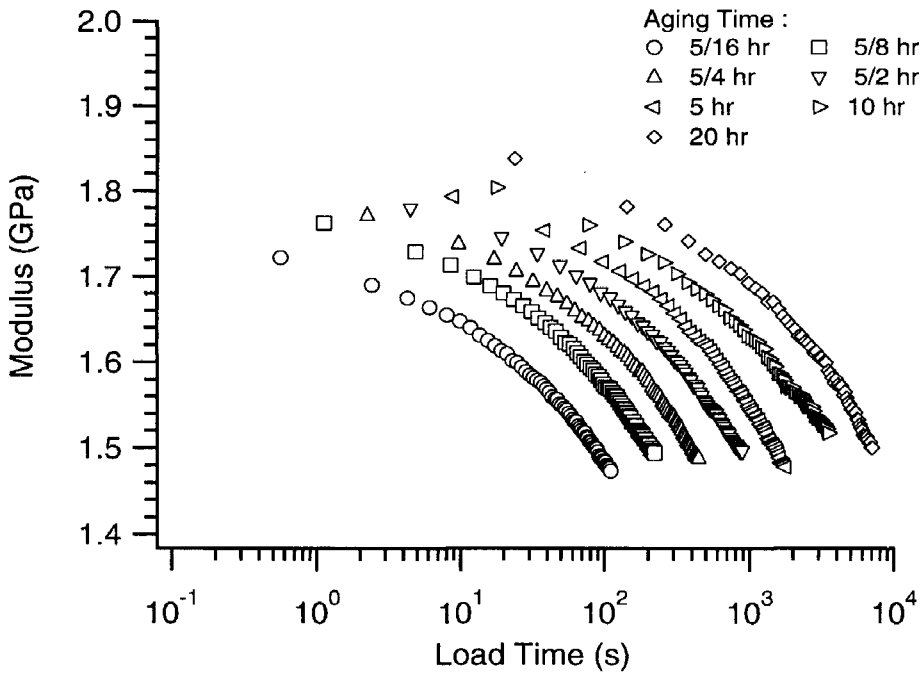


Figure 46. Isothermal stress relaxation test results for PEEK at 110°C

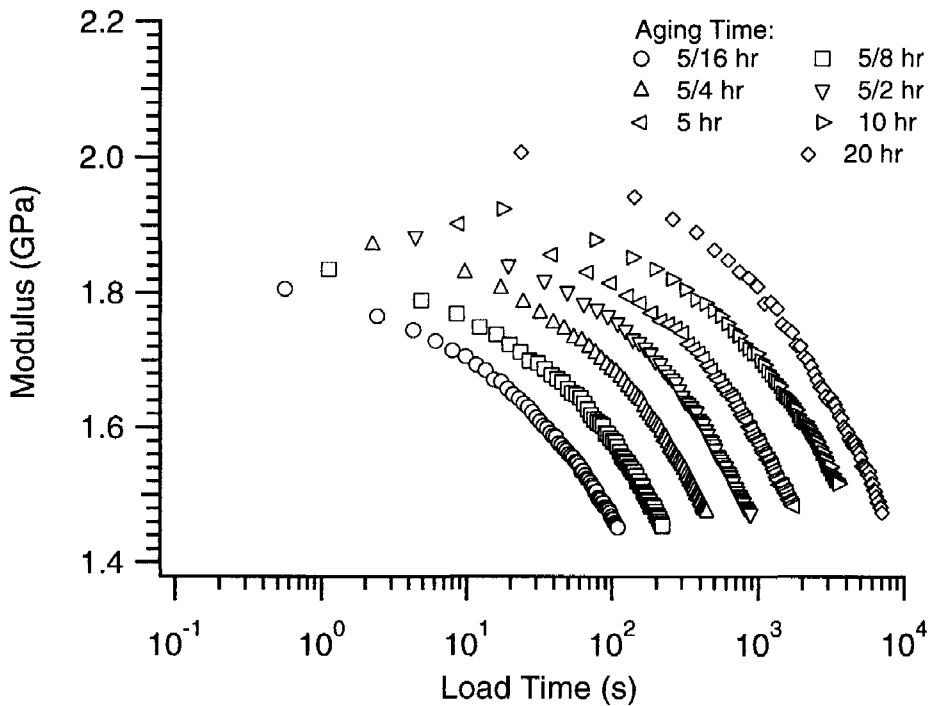


Figure 47. Isothermal stress relaxation test results for PEEK at 120°C

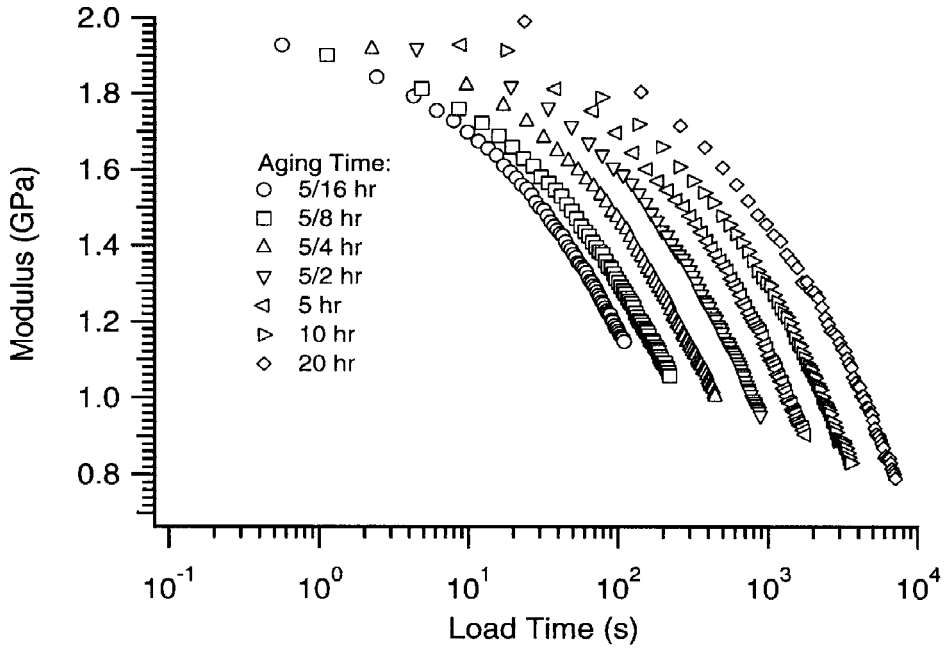


Figure 48. Isothermal stress relaxation test results for PEEK at 130°C

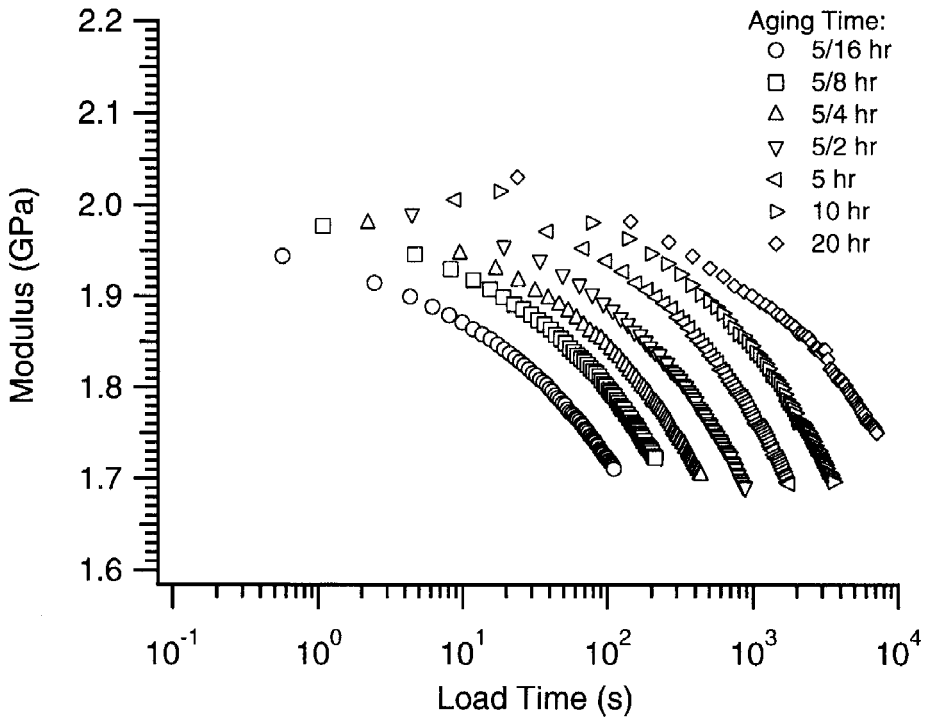


Figure 49. Isothermal stress relaxation test results for PPS at 57°C

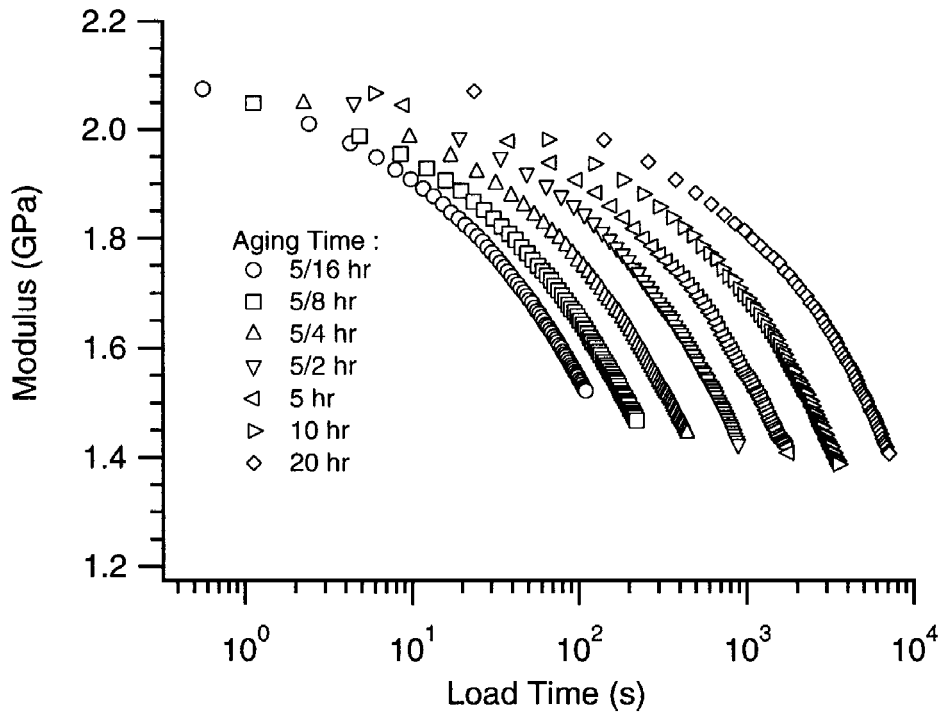


Figure 50. Isothermal stress relaxation test results for PPS at 67°C

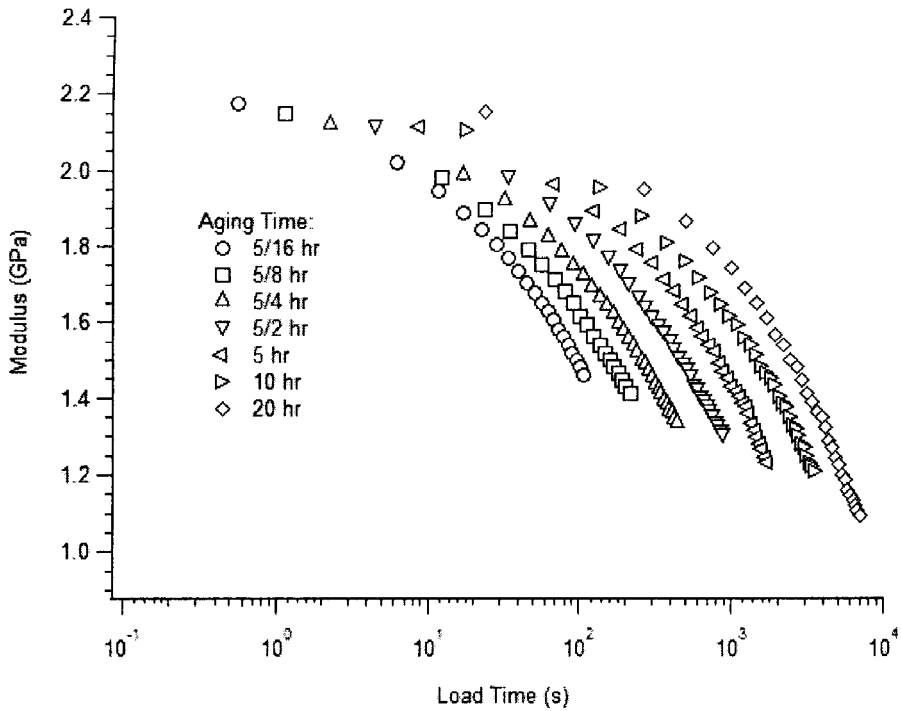


Figure 51. Isothermal stress relaxation test results for PPS at 73°C

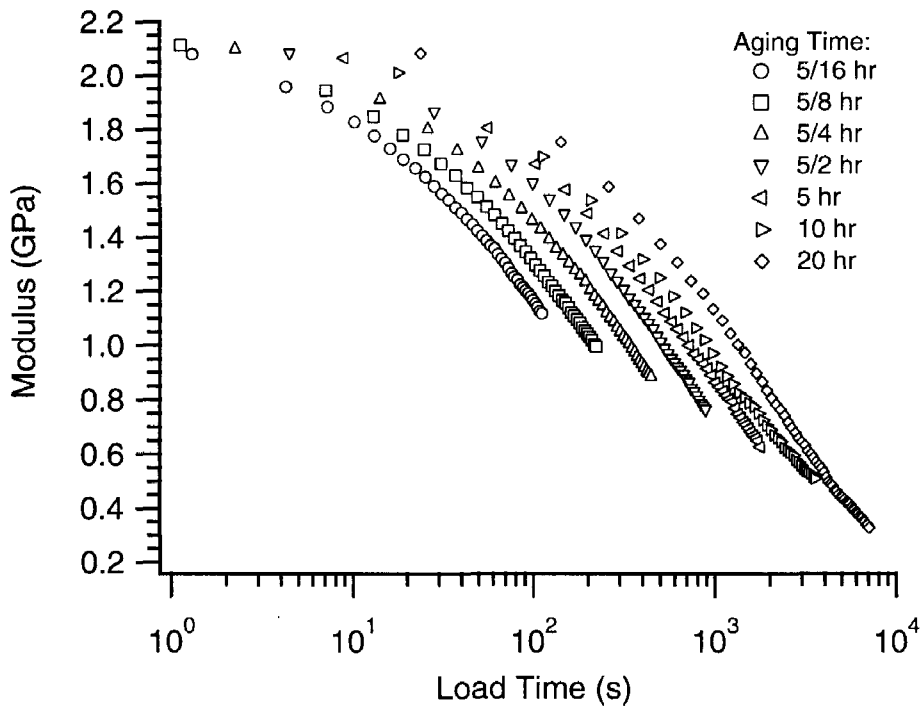


Figure 52. Isothermal stress relaxation test results for PPS at 77°C

4.5.5 Stress Relaxation Data Analysis

The optimal modulus reference curve (Kohlrausch function) and shift rate μ were determined using PHYAGE for the PEEK and PPS modulus results presented above. The resulting reference curve and shift rate values are listed in Table 7; each of the values represents an average of results from 2 - 3 tests. The results for across specimens were extremely consistent once the data was normalized by the storage modulus value as previously described. The shift factors obtained for each momentary curve along with the line prescribed by the obtained shift rate are shown in Figure 53 and Figure 54 for PEEK and PPS, respectively.

Table 7. Reference (master) curve parameters obtained during isothermal stress relaxation tests at indicated temperature ($t_{ref} = 20$ hours, average values for 2+ replicates in each case)

Experiment conditions		E_0	τ	β	Shift Rate μ
Material	Temp. (°C)	(GPa)	($\times 10^3$ s)	(unitless)	(unitless)
PEEK	110	1.884	1260	0.304	1.135
	120	2.007	161	0.413	1.065
	130	2.075	8.72	0.561	0.811
PPS	57	2.165	1360	0.347	1.143
	67	2.116	42.1	0.549	0.946
	73	2.154	14.6	0.564	0.782
	77	2.332	1.84	0.482	0.495

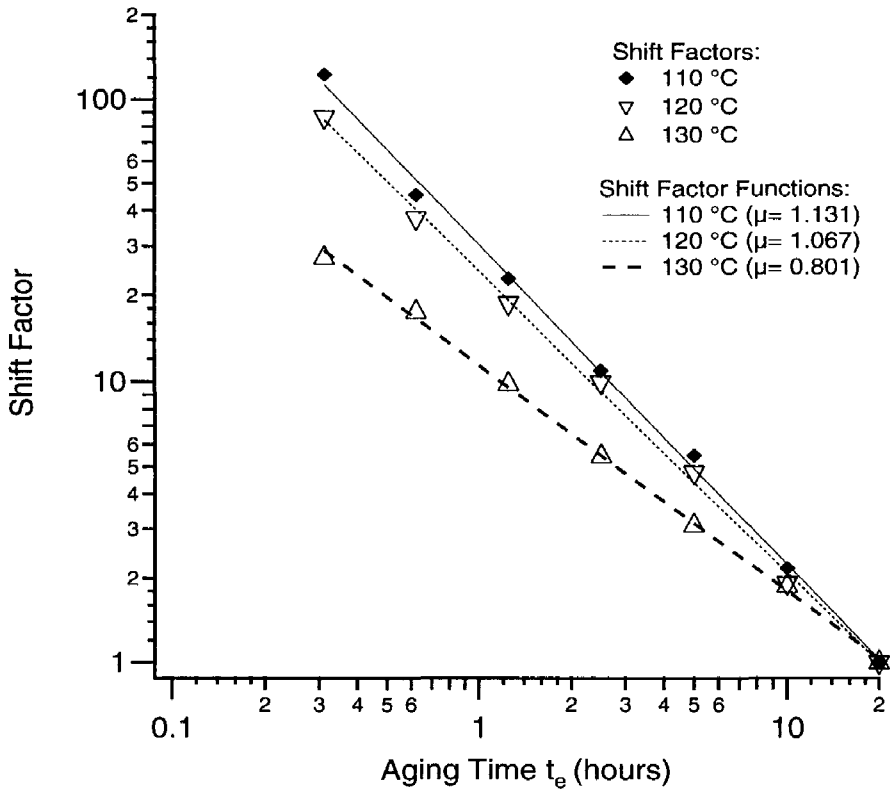


Figure 53. Shift factors and associated shift rates obtained from the stress relaxation tests for PEEK films at the temperatures indicated

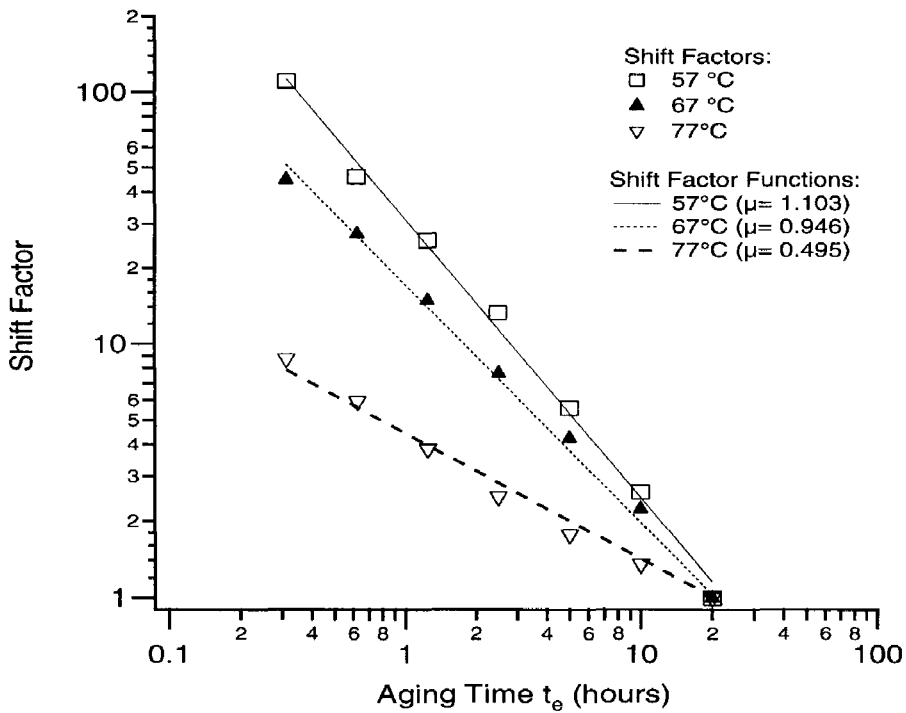


Figure 54. Shift factors and associated shift rates obtained from the stress relaxation tests for PPS films at the temperatures indicated

4.6 Temperature Shift Factors

Reference curves for creep and stress relaxation were previously presented for isothermal aging with a reference aging time of 20 hours. Time–temperature superposition should be possible for these reference curves; this allows a single master curve to be used to predict momentary response at any aging time and temperature (see Equation(40)).

Time–temperature superposition was successful using horizontal shifting alone for the PPS creep reference curves at 57 °C, 67 °C, 77 °C; the individual master curves shifted to the reference temperature of 77 °C are shown in Figure 55. The PEEK creep master curves at 110 °C, 120 °C and 130 °C are shown superposed at the reference

temperature of 130 °C in Figure 56; minor vertical shifting on the order of 2–4% was required. Time–temperature superposition of the stress relaxation curves are shown for PPS and PEEK in Figure 57 and Figure 58, respectively. These curves required greater vertical shifting (on the order of 9–16%). The need for vertical shifting in this case is also evident in the variation in the elastic modulus values (E_0) for both materials at the various temperatures (see Table 8). In addition to the shifted reference curves, Figure 55 - Figure 58 show the optimal reference curve resulting from each set of data; the coefficients for each of these curves are summarized in Table 8 (refer to Equation (39) or (46) for compliance and modulus, respectively).

Other researchers have observed that slight vertical shifts are often necessary to obtain time–temperature superposition of master curves (Matsumoto, 1988; O'Connell and McKenna, 1997). For the creep tests, the amount of vertical shift is on the same order as the variation witnessed in the individual creep test replicates. In this case, it is reasonable to expect that horizontal shifting alone is sufficient for time–temperature superposition were the experimental variation to be eliminated. The reason for larger vertical shifts required for both PEEK and PPS stress relaxation results is not clear at present. Additional investigation and repeat testing is needed to try and identify possible experimental reasons for the vertical shift.

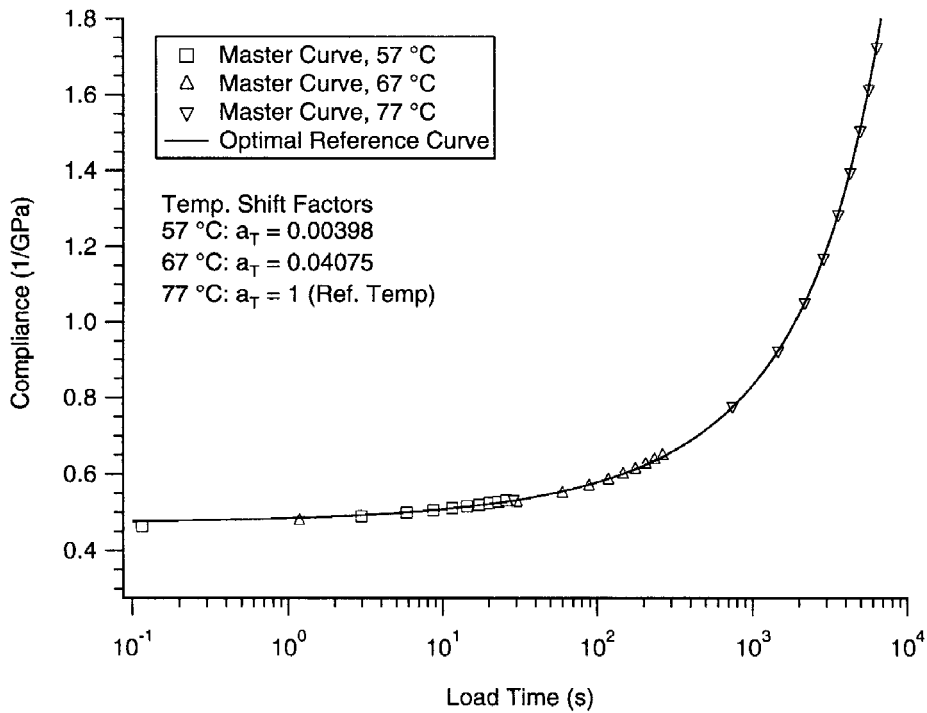


Figure 55. Time-temperature superposition of PPS creep master curves ($t_{ref} = 20$ hours, $T_{ref} = 77^\circ\text{C}$, temperature shift factors a_T as noted)

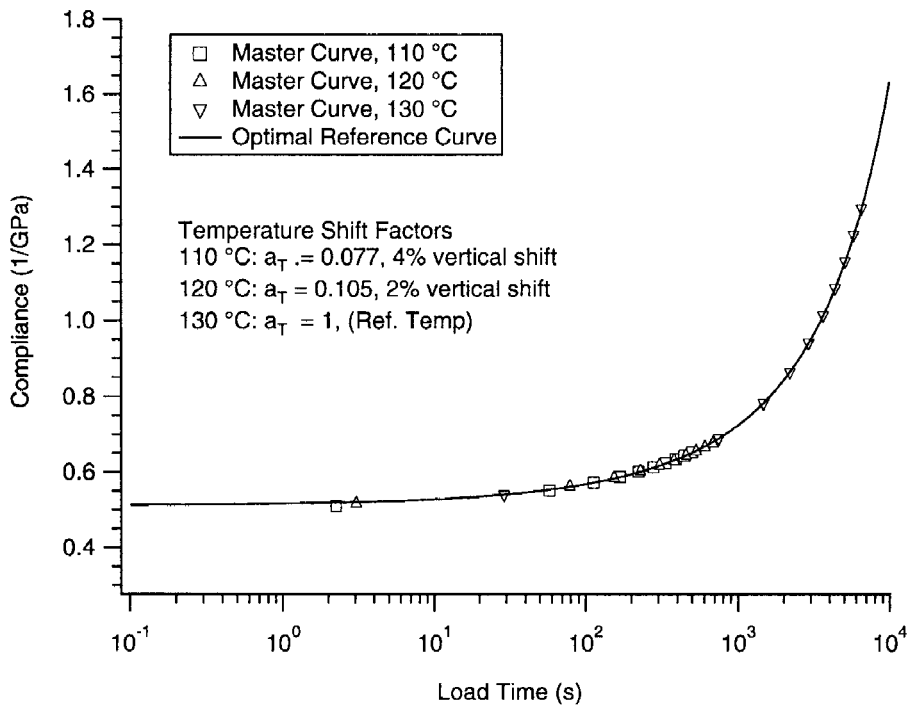


Figure 56. Time-temperature superposition of PEEK creep master curves ($t_{ref} = 20$ hours, $T_{ref} = 130^\circ\text{C}$, temperature shift factors a_T as noted)

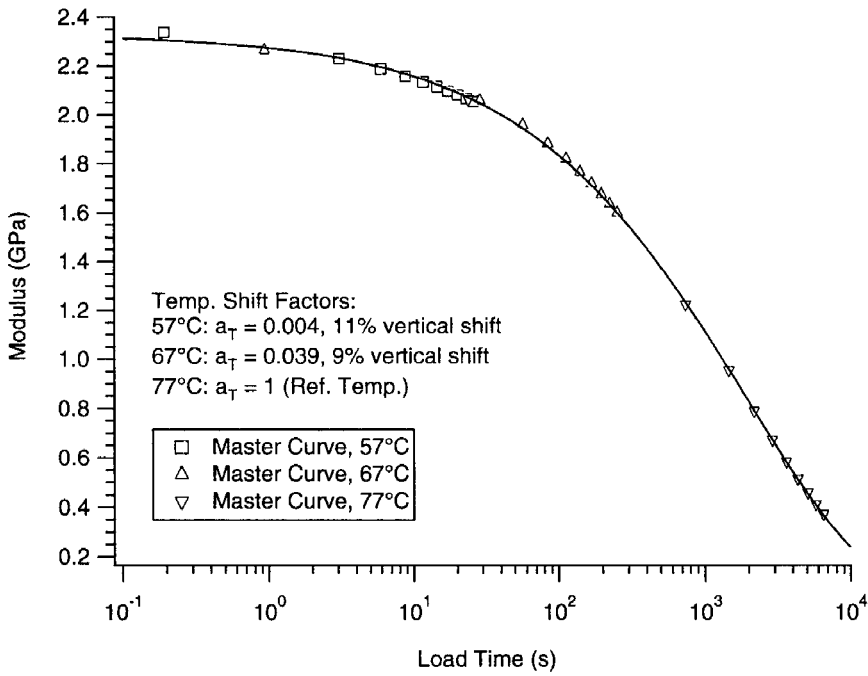


Figure 57. Time-temperature superposition of PPS stress relaxation master curves ($t_{ref} = 20$ hours, $T_{ref} = 77^\circ\text{C}$, temperature shift factors a_T as noted)

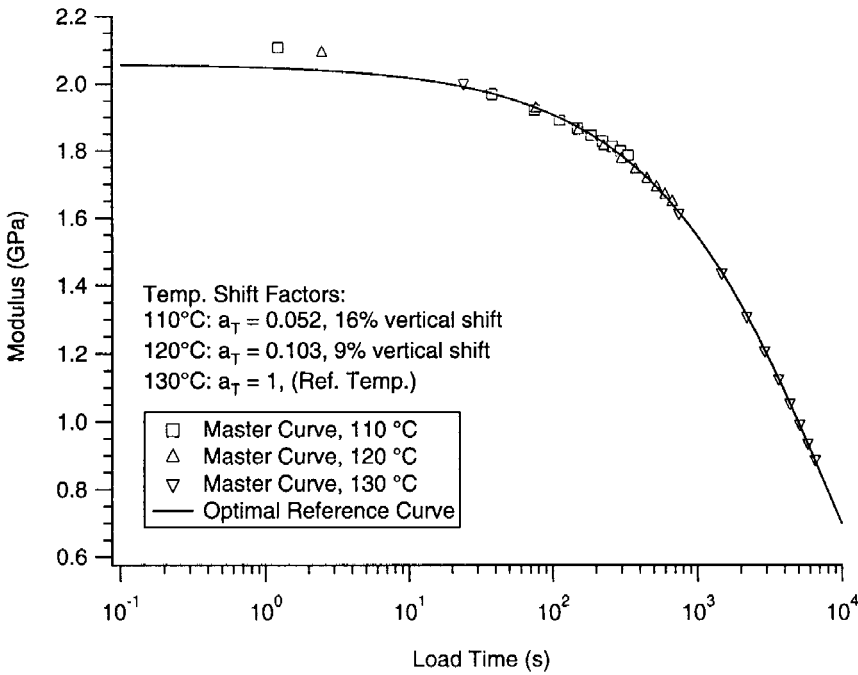


Figure 58. Time-temperature superposition of PEEK stress relaxation master curves ($t_{ref} = 20$ hours, $T_{ref} = 130^\circ\text{C}$, temperature shift factors a_T as noted)

Table 8. Optimal reference (master) curve parameters for PEEK and PPS obtained from time-temperature superposition at indicated temperature and aging time $t_{ref} = 20$ hours

Experiment conditions		D_0	τ	β
Material	Ref. Temp. (°C)	(1/GPa)	(s)	(unitless)
PPS	77	0.4728	3614	0.4454
PEEK	130	0.5116	7527	0.5241
Experiment conditions		E_0	τ	β
Material	Ref. Temp. (°C)	(GPa)	(s)	(unitless)
PPS	77	2.3308	1860	0.4903
PEEK	130	2.0582	8730	0.5771

4.7 Comparison of Creep and Stress Relaxation via Interconversion

Once stress relaxation testing is complete at a given isothermal aging condition, the obtained reference modulus function $E(t)$ can be converted to the compliance function $D(t)$ in accordance with Equation (22) using the program INVERT1D (Bradshaw and Brinson, 1997d). This program first converts the Kohlrausch function for modulus to a Prony series over the time domain of interest. It then uses the convolution integral in Equation (22) along with this Prony series to obtain the optimal Prony series for the unknown compliance function $D(t)$; this Prony series can then be converted back to a Kohlrausch function if desired.

Using this approach, the modulus results can be converted to compliance and compared to the compliance results obtained directly from creep testing. The results of both cases should match and the shift factors should also be identical. Figure 59 and

Figure 60 present the comparison of compliance obtained from creep and stress relaxation tests for PPS and PEEK, respectively. The similarity of the results validates both the use of linear viscoelasticity (source of Equation (22)) and the correctness of the test method used to perform the stress relaxation testing (source of $E(t)$ which is then converted to $D(t)$). It should also be noted that the findings in this study are consistent with the requirement that $D(t)E(t) \leq 1.0$. Specifically, for the temperatures and aging times considered in this work, it is observed that $0.9 < D(t)E(t) < 1.0$. This deviation from unity is very close to the predicted range $0.95 < D(t)E(t) < 1.0$ obtained from classical linear viscoelasticity theory (Vleeshouwers et al., 1989).

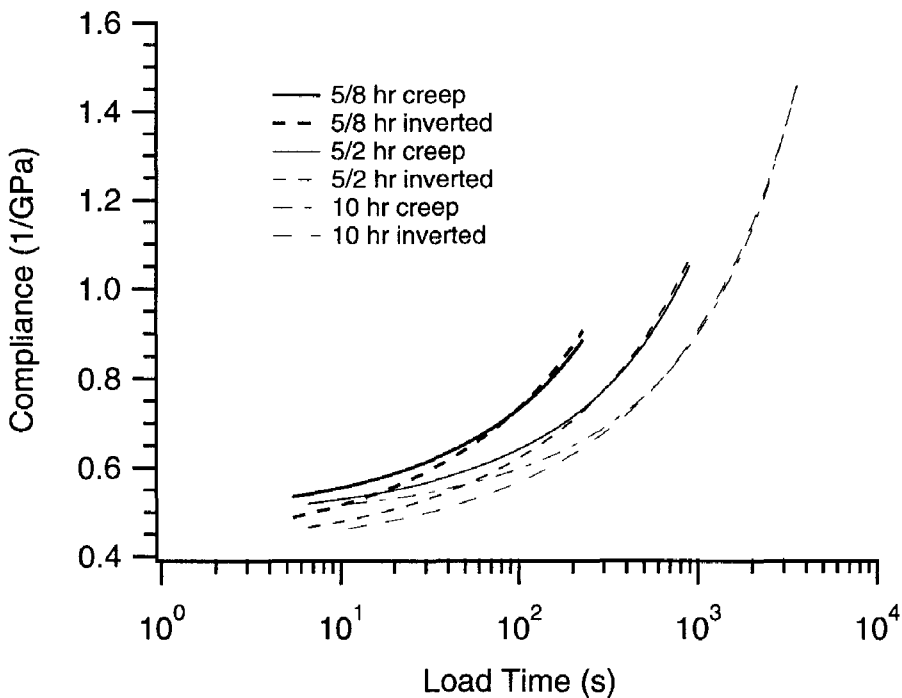


Figure 59. Comparison of compliance obtained by creep testing and stress relaxation testing for PPS isothermally aged at 77°C

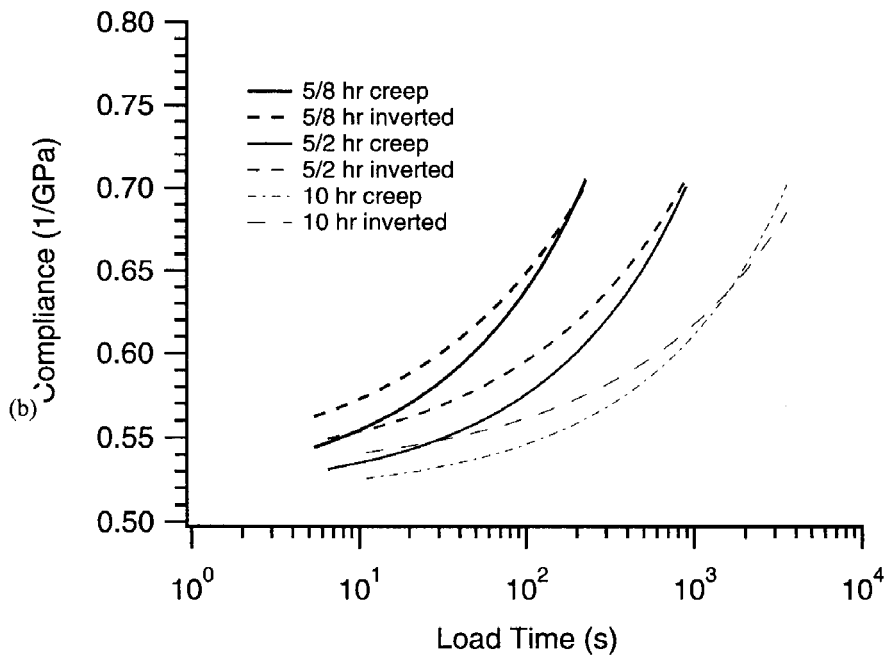


Figure 60. Comparison of compliance obtained by creep testing and stress relaxation testing for PEEK isothermally aged at 120°C

Figure 61 and Figure 62, respectively, illustrate the compliance curves and shift factors (shift rate) of PPS at 73 °C, at various aging times. The compliance curves obtained by creep tests and inverted from the stress relaxation tests using the convolution equation are compared in Figure 61. Since in this dissertation, the isothermal physical aging characterization provides the database and reference for the nonisothermal aging testing in next chapter, comparison of aging test results by two different methods validates that the experimental protocol built up for observe the physical aging effect by a DMA works well for these two materials.

In addition to compatible modulus and compliance material functions, the physical aging tests performed using creep and stress relaxation should also lead to similar shift rates and temperature shift factors. Results for shift rates and temperature shift factors are shown in Figure 63 and Figure 64, respectively, for both PPS and PEEK.

The values in all cases indicate good agreement. It is also observed that the shift rates tend towards 0 as the temperature approaches T_g ; this is expected from physical aging theory (Struik, 1978).

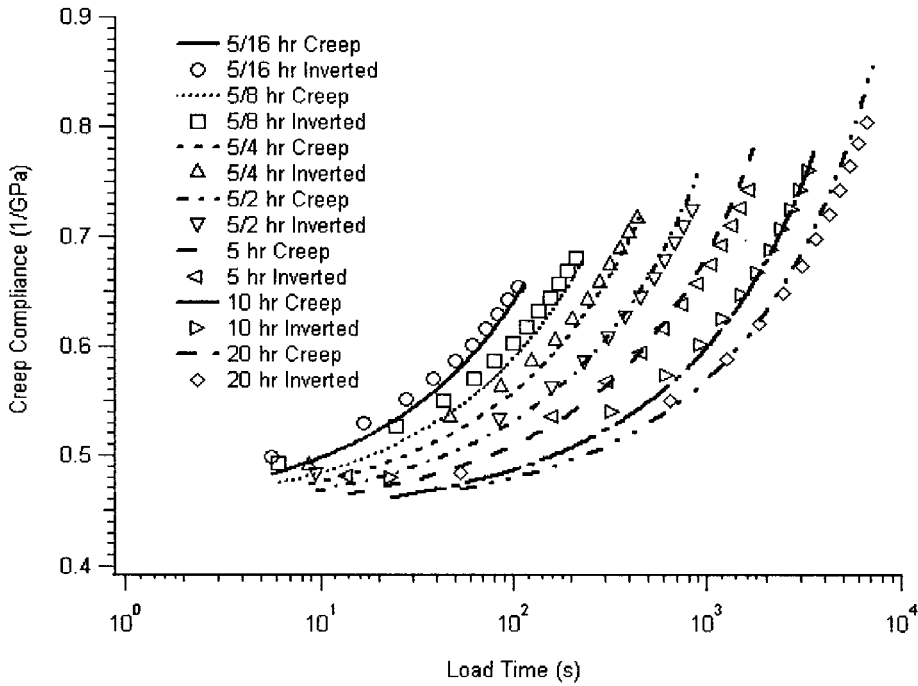


Figure 61. Compliances of creep test and inverted from stress relaxation in PPS and 73°C

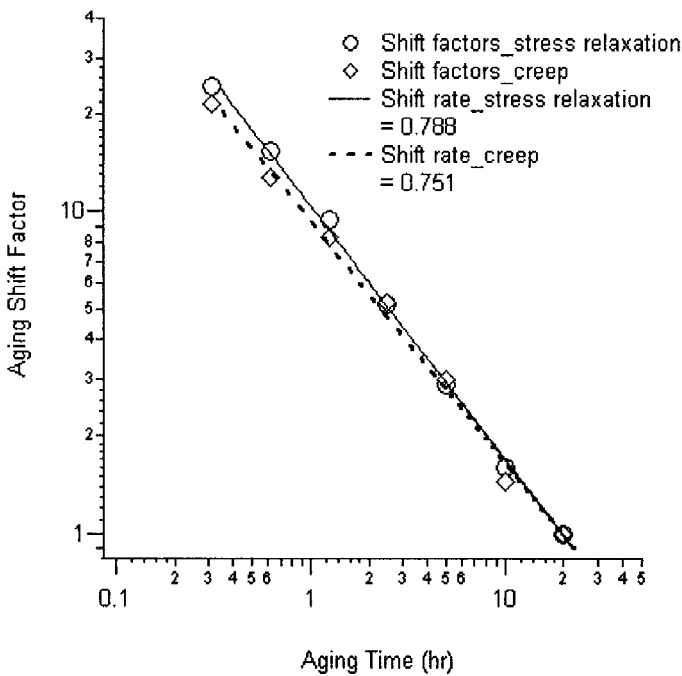


Figure 62. Shift rate comparison of creep and stress relaxation tests in PPS and 73°C

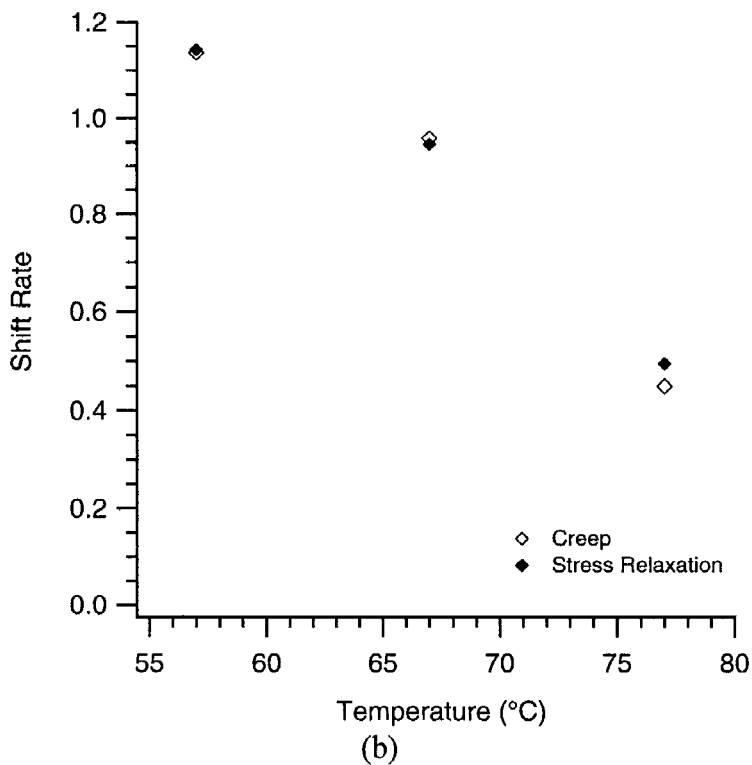
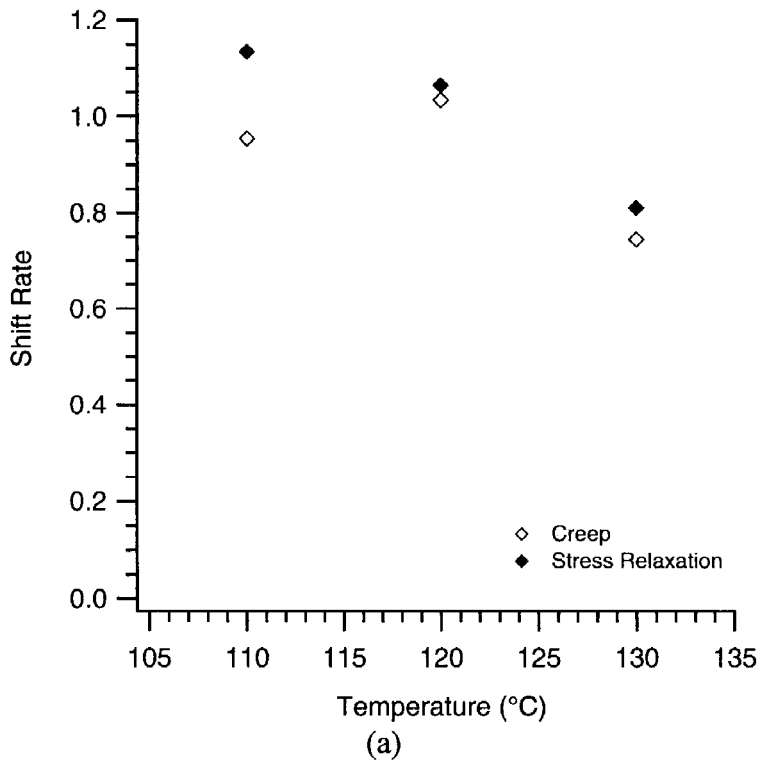


Figure 63. Comparison of shift rates obtained by creep and stress relaxation:
 (a) PEEK; (b) PPS

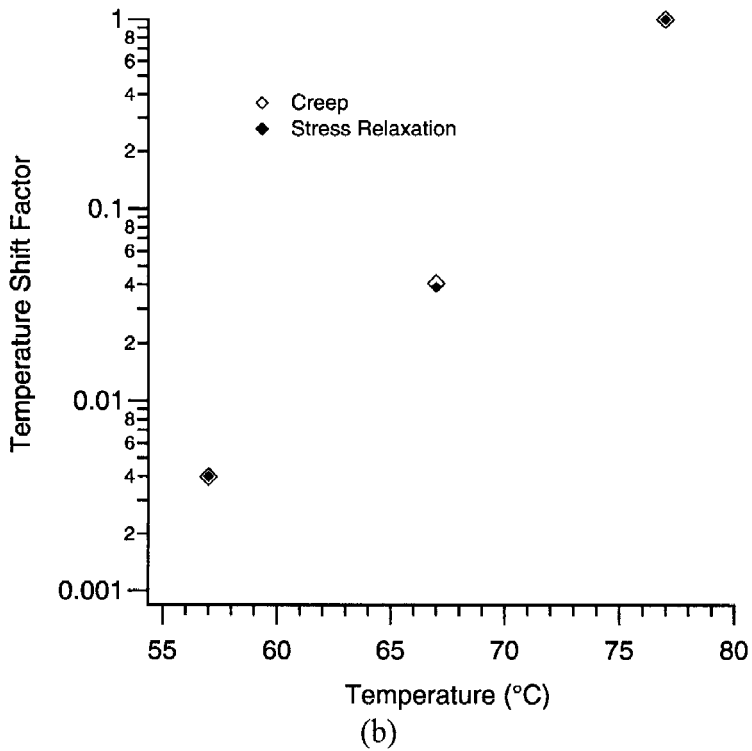
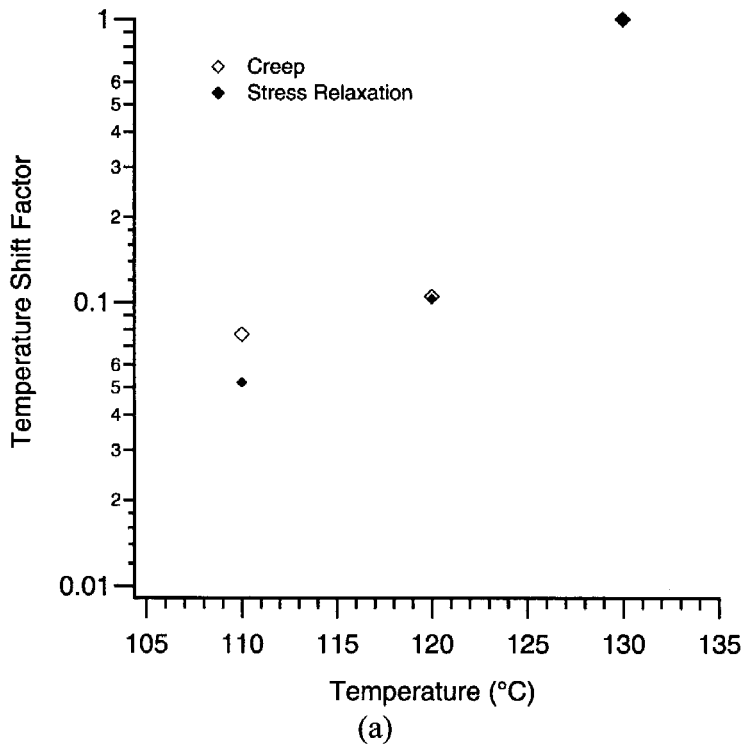


Figure 64. Comparison of temperature shift factors obtained by creep and stress relaxation:
 (a) PEEK; (b) PPS

CHAPTER 5

NONISOTHERMAL PHYSICAL AGING OF PEEK AND PPS

This chapter covers the testing details and results on nonisothermal physical aging of PEEK and PPS. The thermal histories include both one-step temperature up-jump and multi-step temperature changes following quenching. Short-term and long-term creep compliance and aging shift factors under such thermal conditions are summarized; these data form the database for modeling nonisothermal aging behavior in the next chapter.

5.1 Background

In the previous chapter, past and current research efforts studying isothermal physical aging in neat polymers and polymeric materials were discussed. Isothermal physical aging occurs when a polymeric material falls in an equilibrium state since a temperature jump away from a rubbery state into a glassy state. Generally, the equilibrium state is achieved by rejuvenating the material at $T \geq T_g$ and annealing at that temperature for a period. Under isothermal conditions below T_g , many researchers have performed experimental and analytical investigations on the nature of the mechanical response in a number of polymeric materials by various techniques. This has led to a

standard test method (developed by Struik) via creep or stress relaxation and a concise framework to analyze experimental results and predict mechanical response, which was discussed in the previous chapter.

For aging materials used in an actual structure, understanding only the isothermal response characteristics is likely insufficient for design. However, while the isothermal physical aging has been extensively studied, nonisothermal physical aging has received less scrutiny. As such, relatively few studies have been performed in both collecting experimental data and creating models to predict physical aging effects during an arbitrary temperature history. Most structures undergo complicated thermal histories during their service life; if aging effects are deemed significant for such structures, an analysis of the aging response to a nonisothermal condition must be undertaken. In this chapter, an experimental investigation of nonisothermal physical aging in glassy polymers PEEK and PPS will be presented. This work provides a database of viscoelastic response in polymers as effects of nonisothermal physical aging; this forms the basis for modeling complex material behavior under complicated thermal conditions (will be discussed in Chapter VI).

Compared to isothermal physical aging, a relatively small number of studies considering the mechanical response during nonisothermal physical aging have been undertaken in literature. Struik (1978; 1988) considered the aging shift factor a_{te} after temperature up-jump thermal histories after aging at lower temperatures since quenching (this experiment is referred as to single temperature up-jump test in this dissertation; see Figure 24). The test material was slowly heated up to a temperature above T_g and was

held at that temperature for 30 minutes to erase internal residual stress and to reach thermodynamic equilibrium state. The test specimen was then quenched from this temperature to a dwell temperature T_l for a period (120 hours for most of the studies) and then jumped to the final temperature below T_g . On the final temperature, both the volumetric and mechanical response of the material (in creep) was monitored during this nonisothermal physical aging. Studies were undertaken on polystyrene (PS), poly(vinyl chloride) (PVC) and polycarbonate (PC). Each data set consisted of the results for a common final temperature T_e with varying first temperature values T_l ; for each set, the dwell time t_l spent at T_l was the same in all cases. The shift factor a_{te} was determined by the time-aging time superposition principle with an isothermal reference curve at the final temperature T_e (at aging time 16/3 hours) to the nonisothermal creep data. This approach is identical to the isothermal method previously described in Equation (42); as such, a similar test method can be applied to characterize both isothermal and nonisothermal physical aging, with the only difference between these two kind of tests being temperature histories prior to testing. Struik found that, unlike isothermal physical aging, aging shift factors after the temperature up-jump treatments do not form a straight line in double logarithmic space. Instead, the aging shift factors initially increase (softer response) followed by a decrease (stiffer response). Typical compliance curves and aging shift factors are shown in Figure 65. With sufficient elapsed time since the temperature jump, the material “forgets” its past aging history and begins to act as though it was isothermally aged at the current temperature.

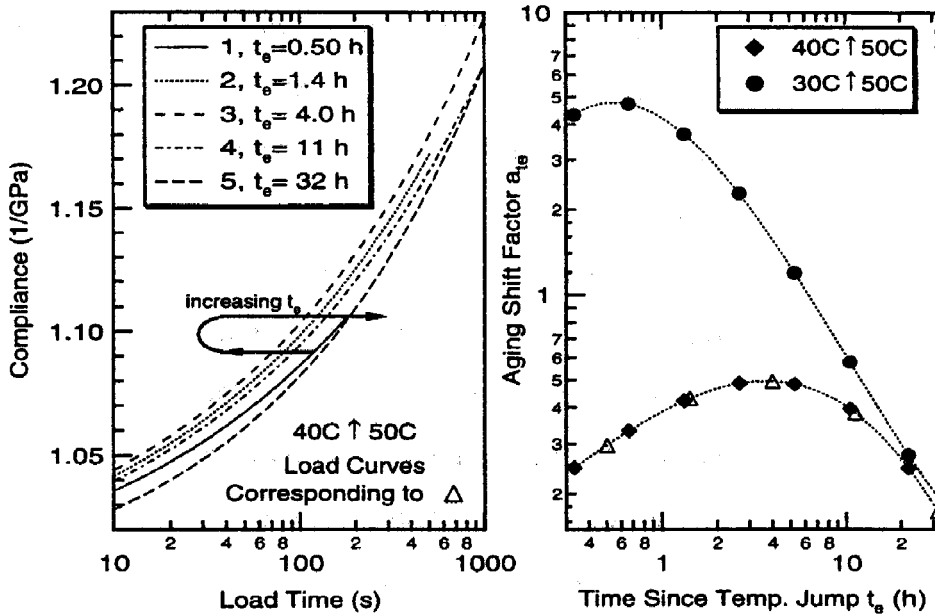


Figure 65. Compliance and shift factors for PVC after aging 120 hours at a lower temperature (30°C, 40°C) followed by jump to 50°C as performed by Struik (Bradshaw and Brinson, 1997c; Struik, 1988)

Struik also investigated material response during simultaneous volume recovery process along with nonisothermal physical aging under identical thermal conditions. In this test, the specific volume v (reciprocal of density) was monitored with aging time; the test protocol is demonstrated in Figure 66. The results of $\log a_{te}$ versus v of polycarbonate is depicted in Figure 67. Fairly good linear correlations were found at all test temperatures. This conclusion supports the argument that a common underlying phenomenon (free volume) drives both the volumetric and mechanical aging response of glassy solids. Struik's findings indicate that a relationship between the mechanical and thermodynamic properties exists during structural relaxation, though there is considerable scatter in his data of polystyrene for some temperature histories.

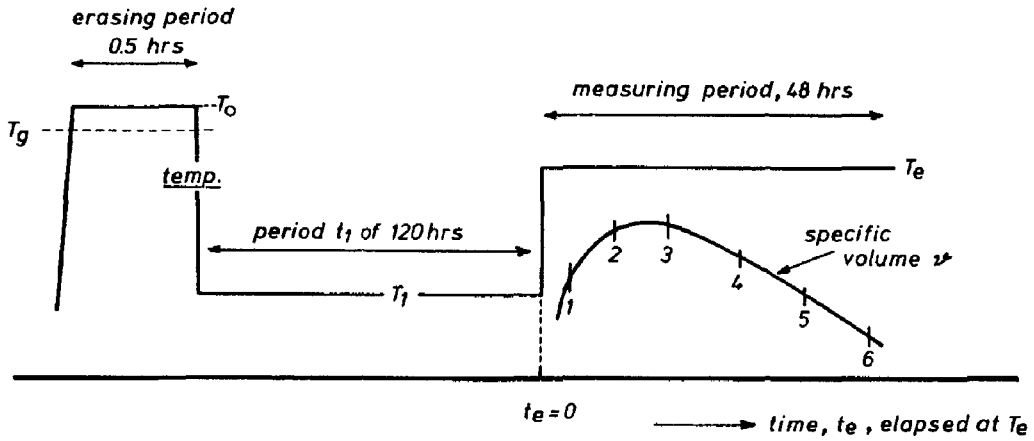


Figure 66. Single temperature up-jump test on volume recovery after aging at a lower temperature, studied by Struik for both volume and mechanical response (Struik, 1978)

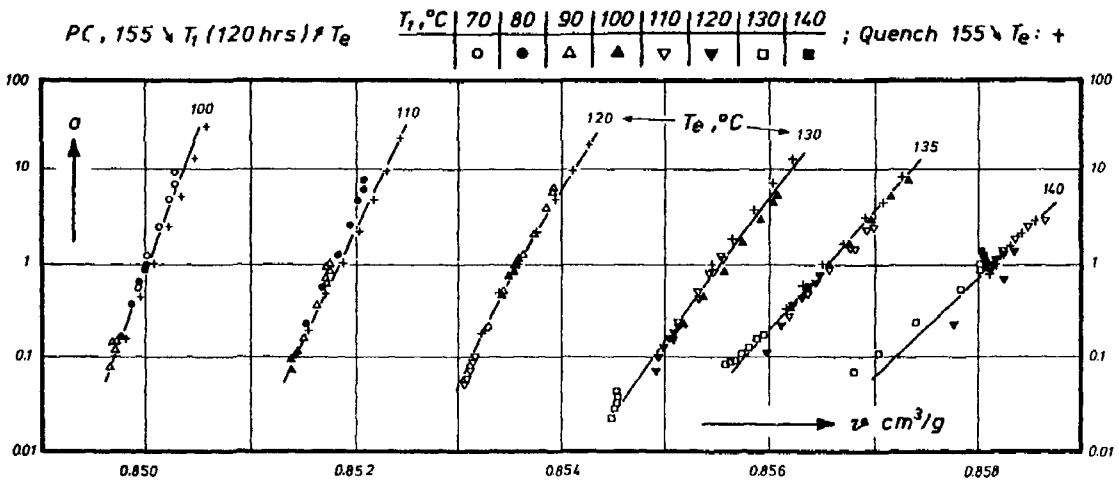


Figure 67. Correlation between a_{te} and specific volume v for polycarbonate during temperature up-jump histories (above T_g , quench to T_1 and hold 120 hr, jump to T_e) (Struik, 1988)

McKenna and coworkers have also considered nonisothermal mechanical response of glassy solids (McKenna et al., 1993, 1995; Schultheisz et al., 1995). These studies repeat the experiment described in Figure 24 and Figure 66 using an epoxy system and compare both the volumetric response δ and mechanical shift factor a_{te} ,

where δ is the normalized volumetric departure from equilibrium, defined as

$$\delta(t, T) = \frac{v(t, T) - v_{eq}(T)}{v_{eq}(T)} \quad (54)$$

and v_{eq} is the specific volume at equilibrium state (often referred as to v_{∞} in literature).

Strictly speaking, these experiments are isothermal since they consider only a single temperature jump away from a sub- T_g equilibrium state. In other words, the material was held at the dwell temperature T_l long enough, that the material reached the equilibrium state and was then jumped to a new temperature T_{θ} . In their tests, both temperature up-jump and down-jump were considered; this is not possible for the standard physical aging studies (equilibrium state above T_g) since an up-jump enters equilibrium instantaneously. These researchers observed differences in the behavior of a_{te} and δ , especially in the fact that the two properties appeared to reach equilibrium at different times (McKenna et al., 1995). Specifically, the mechanical response a_{te} reached equilibrium after the volumetric response in the up-jump experiments, while the opposite result occurred in the down-jump experiments. This point was used to argue that determination of the mechanical response a_{te} from the volumetric response δ is not appropriate, and that a different time scale governing the mechanical response process must be identified. It should be noted, however, this data also clearly showed reasonable linear relationships between a_{te} and δ in log-log scale away from the equilibrium state, consistent with the findings of Struik. Before reaching equilibrium (i.e. during the process of physical aging), a direct connection between a_{te} and δ may be acceptable.

Besides the studies above, Bradshaw and Brinson did a significant amount of work on effects of nonisothermal physical aging upon the mechanical response of IM7/K3B graphite reinforced thermoplastic polyimide composite (Bradshaw and Brinson, 1997b, 1999) with a T_g of approximately 240° C (Gates and Feldman, 1995). In their studies, nonisothermal aging tests were performed on the shear and transverse specimens by creep for single temperature up-jump and down-jump tests, using the protocol described previously in this dissertation. From a theoretical perspective, there are two notable contributions by these researchers. First, they developed a new continuous shift factor (CSF) method by using both the load and unload test data from an experimental data set (Bradshaw and Brinson, 1997b, 1999); this approach reduces the amount of tests that need to be run to characterize nonisothermal response as well as allowing more advanced analyses that are not possible with the standard method. A new parameter called the effective aging time was introduced to describe the state of aging throughout a nonisothermal history in a consistent and clear fashion. Figure 68 shows the calculated effective aging time of a temperature up-jump test, and the continuous shift factors obtained by CSF method as well as discrete shift factor points using the standard approach. It can be seen that the CSF method leads to reasonable predictions to recovering the mechanical shift factor function (a_{te}) from a nonisothermal aging experiment. Compared the result from standard approach, the CSF method yields a continuous curve of a_{te} rather than a series of discrete points, more data is obtained from each test. The second contribution of Bradshaw and Brinson in their investigation on nonisothermal aging is that they developed KAHR- a_{te} model (Bradshaw, 1997), which

assumes a correlation between volume response and mechanical properties in structural relaxation. The KAHR- a_{te} model extends the KAHR (Kovacs-Aklonis-Hutchinson-Ramos) model (Kovacs et al., 1979) to predict nonisothermal aging shift factors obtained from mechanical response testing. Since this chapter focuses on experimental characterization of nonisothermal aging, the details of the KAHR- a_{te} method will be presented in next chapter.

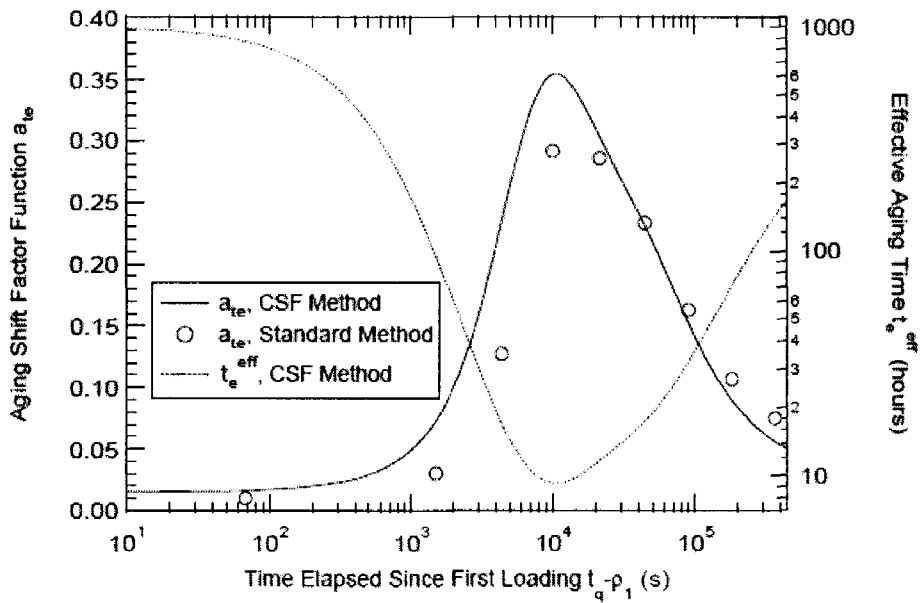


Figure 68. Aging shift factor a_{te} and effective aging time t_e^{eff} determined from the effective time for CSF method. Thermal history: aged 68 hours at 215°C, followed by up-jump to 225°C (Bradshaw, 1997)

Besides the experimental characterizations above and the studies performed for this dissertation presented below, little additional work has been performed by other researchers in determining the nonisothermal mechanical response of glassy polymers undergoing physical aging. The above studies show that there is some connection between volumetric and mechanical response, but that difficulties may ensue as the

equilibrium state is approached. Since structures in practice are unlikely to age into equilibrium, it may be possible to set aside this latter concern in developing a mechanical response model. The KAHR model was extended to deal with aging shift factors by Bradshaw and Brinson and the limited results presented were quite encouraging, indicating that the KAHR- a_{te} model is a promising basis to predict nonisothermal physical aging shift factors. Nonisothermal aging effects on various nonisothermal conditions of pure polymers are characterized; these results form the basis of nonisothermal modeling to take place in next chapter.

5.2 Experimental Results on Single Temperature Up-jump Tests

PEEK and PPS films have been tested in five different up-jump conditions as described in Chapter III. For each thermal history, at least three replicate tests are conducted. Compliance curves determined from one of these replicates for each thermal history will be presented in detail while discrete aging shift factors obtained by PHYAGE will be shown both as average and data limit bias for all replicates.

Figure 69 - Figure 72 illustrate the compliance curves of four up-jump thermal histories ending at 130°C, with the dwell temperatures of 110°C, 118°C, 120°C and 125°C, respectively. From these figures, as the dwell temperature decreases, the compliance response gets closer to isothermal response. For the same dwell period (14 hours), when the holding temperature prior to up-jump is high enough (>118°C), with increasing aging time, the material after up-jump will become initially softer first, and

then become stiffer with further aging. This reflects that the compliance curves in several figures below shift leftwards, and then rightwards as found in earlier work; e.g. Figure 65.

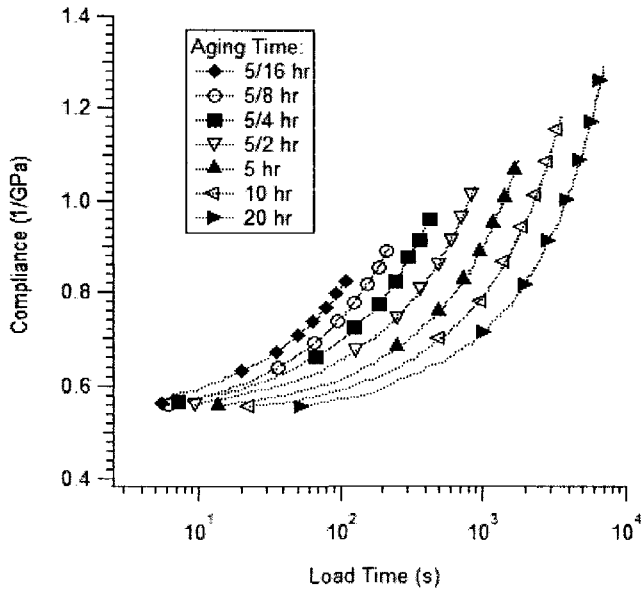


Figure 69. Creep compliance of PEEK after aging at 110°C for 14 h then jump to 130°C

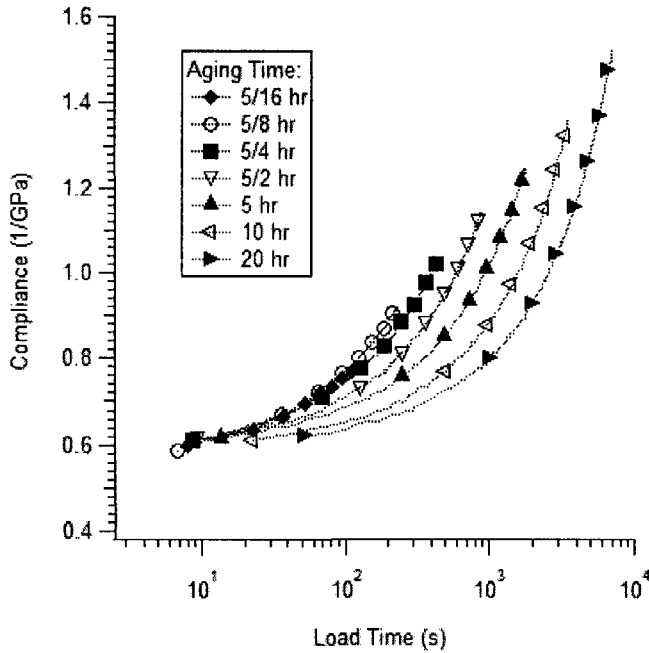


Figure 70. Creep compliance of PEEK after aging at 118°C for 14 h then jump to 130°C

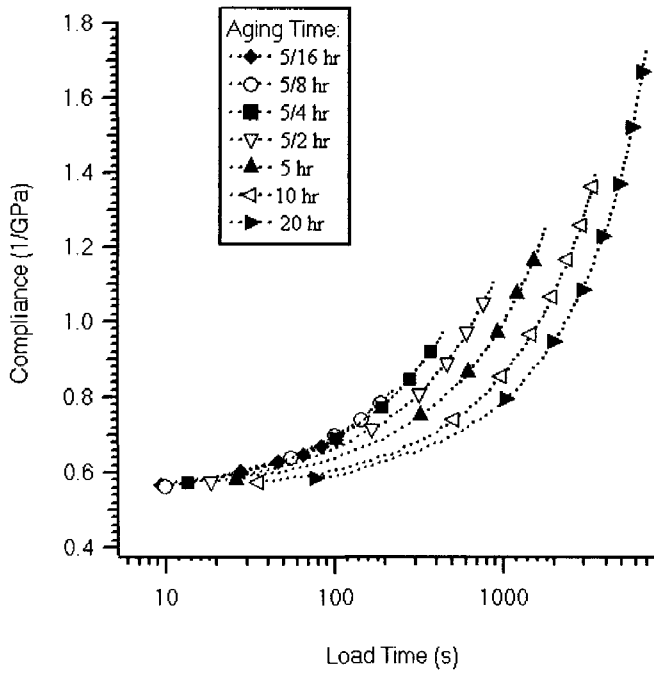


Figure 71. Creep compliance of PEEK after aging at 120°C for 14 h then jump to 130°C

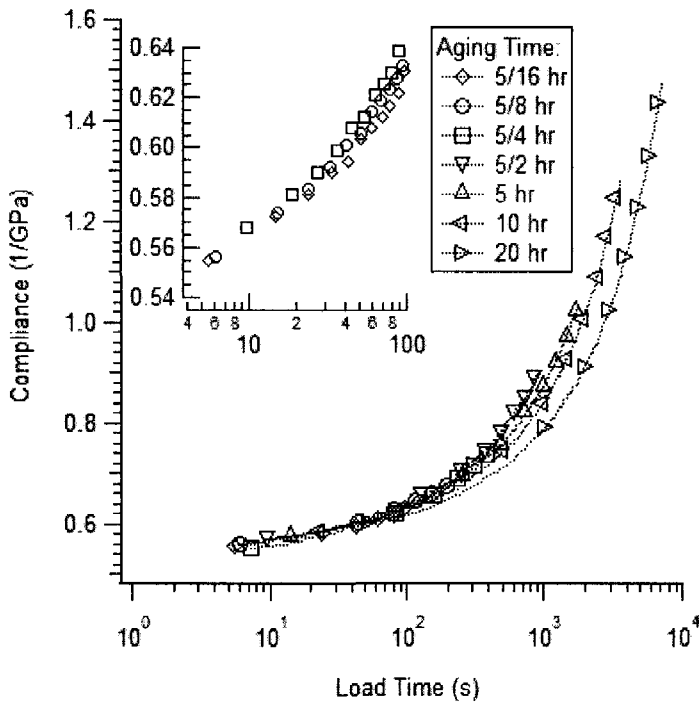


Figure 72. Creep compliance of PEEK after aging at 125°C for 14 h then jump to 130°C

The family of compliance curves shown above is obtained from the sequenced creep tests at several aging times from 5/16 hour to 20 hour; note that the aging time of nonisothermal aging in this dissertation is defined as the time elapsed from last temperature jump. It is clear by inspection that tests in Figure 70 - Figure 72 are not isothermal aging tests as the curves are not evenly spaced and moving to the right with aging. The compliances of up-jump 110°C-130°C in Figure 69 visually reveal little difference from isothermal responses; the reason for this is that the material aged at relatively low temperature (110°C) such that the aging state had not changed much before jump to the test temperature (130°C). As such, the aging prior to up-jump did not affect much on the thermodynamic state of the specimen, with the result that the material response looks quite similar to the aging response at isothermal 130°C. To clarify this point, an inset plot is made in Figure 72 to show the shifting tendency of compliance response at 5/16, 5/8 and 5/4 hour since temperature jump from 125°C at short times. It is clear that these curves shift to the left along the logarithmic time axis.

Besides the tests shown in Figure 69 - Figure 72, one more single temperature up-jump with thermal histories of 110°C-120°C are also considered in this study. For the sake of brevity, the compliance response is not presented here; associated aging shift factors will be exhibited in the next chapter.

The temperature up-jump thermal histories for creep tests in PPS include 57°C-73°C, 63°C-73°C, 67°C-73°C, 57°C-63°C and 67°C-77°C. Figure 73 - Figure 75 depict the compliance curves for the three up-jump tests ending at 73°C; the compliance curves of the last two thermal histories will not be shown due to similar response, although the

aging shift factors of these two tests will be used in the modeling work presented later. These experimental results are similar to those observed in the PEEK material. It should be noted that these data sets appear to have the strain occurring in a series of steps. The reason for this is that when the RSA3 DMA is used in transient mode, the specimen elongation occurs in $1 \mu\text{m}$ steps of the upper stage. For a specimen length of 25.4 mm, this corresponds to a strain step of 39 microstrain. This incremental nature of the applied strain is the reason for the “stair case” appearance of the compliance curve in Figure 73 and Figure 74 (and to a lesser extent in compliance of PEEK shown previously).

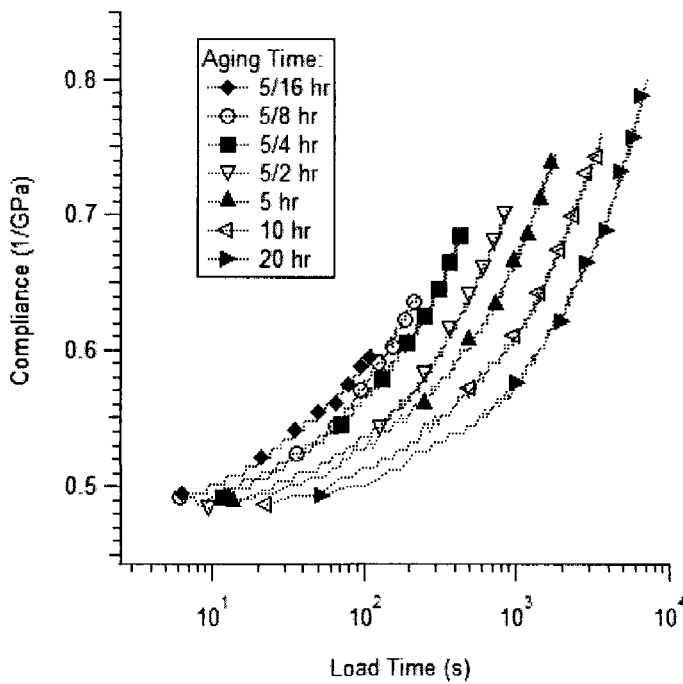


Figure 73. Creep compliance of PPS after aging at 57°C for 14 h then jump to 73°C

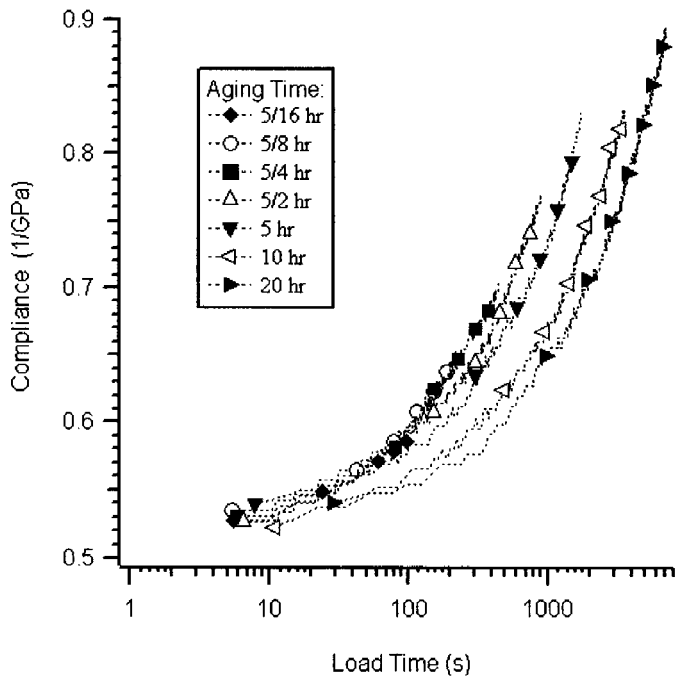


Figure 74. Creep compliance of PPS after aging at 63°C for 14 h then jump to 73°C

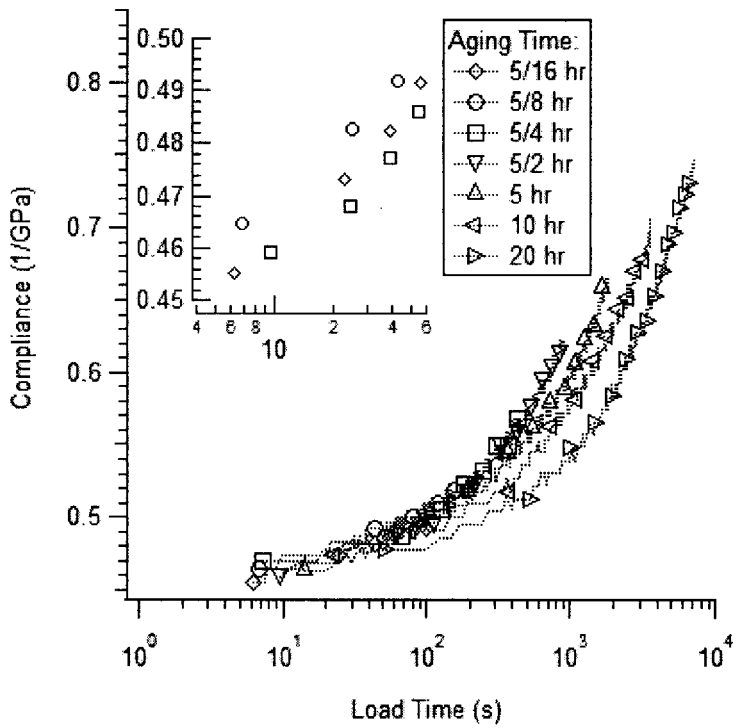


Figure 75. Creep compliance of PPS after aging at 67°C for 14 h then jump to 73°C

The aging shift factor for each compliance curve is then identified using the PHYAGE program with horizontal shifting alone. The shift factors obtained are relative to the isothermal aging reference curve at 130°C at $t_e = 20$ hours for PEEK and to the isothermal aging reference curve at 73°C at $t_e = 20$ hours for PPS; the reference curve is vertically shifted prior to the analysis as needed (typically ~5%) to bring it in line vertically with the longest aging time compliance in the data set¹⁰. The resulting shift factors for the data in Figure 70 are shown in Figure 76; these show the increase and decrease that is expected for an up-jump aging condition. For each experimental condition, at least three replicate tests were performed (different specimens, identical test conditions). In most tests, the compliance values were within $\pm 5\%$ of the average compliance for all specimens. The optimal horizontal shift factors were then obtained as described above. In Figure 76, the shift factors observed for 3 tests using PEEK for a set of test results 118°C (14 h) - 130°C are shown; the error bars indicate a 90% confidence interval (The confidence interval was calculated by the method $\left(\bar{X} \pm (S/\sqrt{n})t_{\alpha/2}(n-1)\right)$, where \bar{X} is the sample mean, S is the square root sample variation, n is the sample size, t is the student's t -distribution and α is the confidence level). The experimental results from other test conditions are similar to these in terms of data scatter.

¹⁰ In detail, the vertical shift for the isothermal reference curve ($t_e = 20$ hr) was made in this way: fit the reference curve and the compliance at the longest aging time ($t_e = 20$ hr) using the Kohlrausch function, shift the initial compliance D_{0ref} to the initial compliance of the data with the vertical shift factor D_{0data}/D_{0ref} .

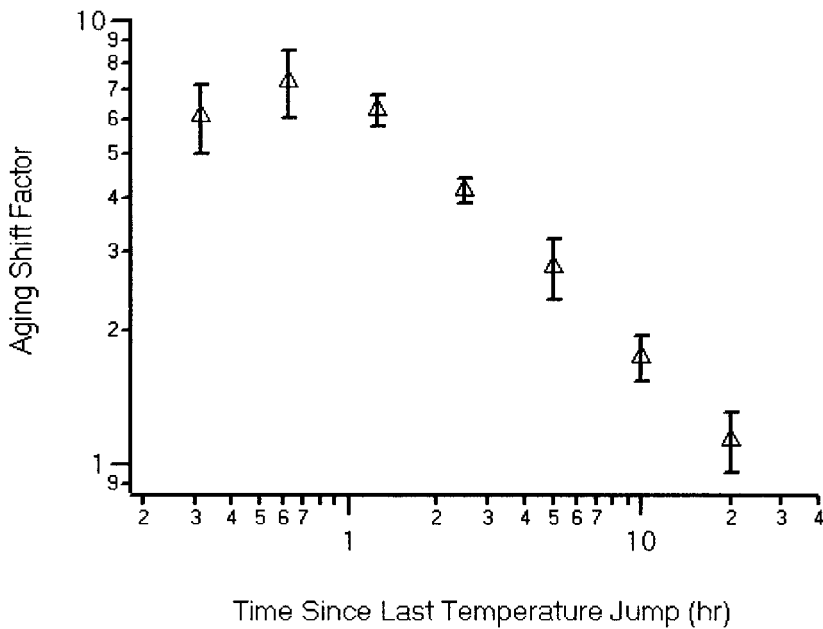


Figure 76. Average aging shift factors from three PEEK tests after aging at 118°C for 14 h followed by jump to 130°C; error bars indicate a 90% confidence level

Figure 77 and Figure 78 summarize the aging shift factors for temperature up-jump tests (with dwell temperature and test temperature pairs with 14 hour of aging prior to up-jump) for PEEK and PPS, respectively; the final temperatures are 130°C for PEEK and 73°C for PPS. For comparison, isothermal aging shift factors at these temperatures at similar aging times are also included. The nonisothermal aging shift factors in the single temperature up-jump cases manifest complex material behavior under such thermal conditions. The aging state of glassy polymers clearly depends on the thermal treatments. These curved nonisothermal aging shift factors need to be modeled, in order to describe mechanical behavior under such conditions. Once the aging shift factors can be predicted by a model, the compliance properties will be obtained by submitting the a_{te} information and reference curve parameters into Equation (42).

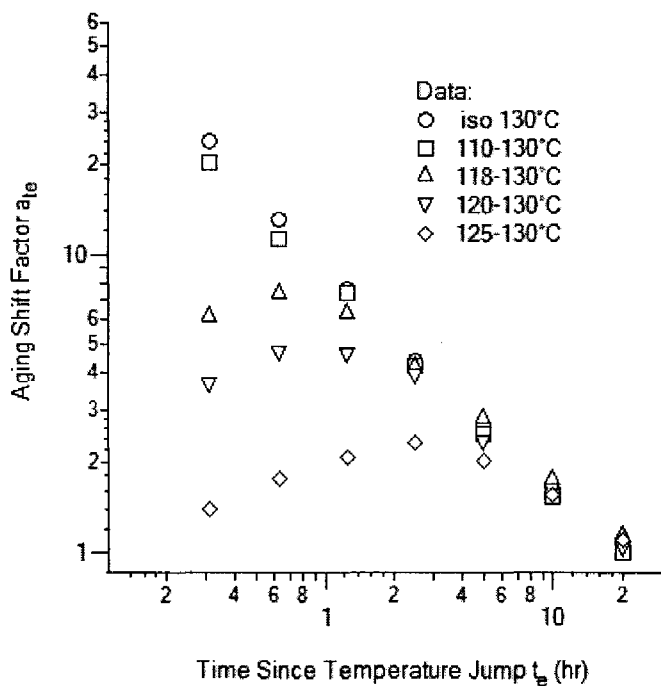


Figure 77. Aging shift factors of creep tests after temperature up-jump to 130°C for PEEK; isothermal aging shift factors at the same temperature reported for comparison

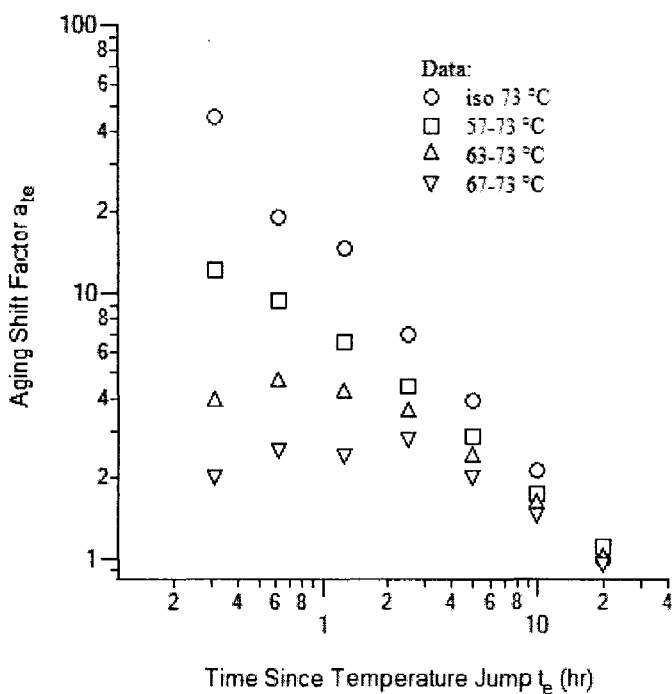


Figure 78. Aging shift factors of creep tests after temperature up-jump to 73°C for PPS; isothermal aging shift factors at the same temperature reported for comparison

5.3 Results for Complex Thermal Treatments

Since practical structures go through complex temperature conditions in applications, it is indispensable to investigate the viscoelastic properties after more involved thermal histories than a single temperature jump after quenching. In this study, nonisothermal physical aging tests were performed after multiple temperature jumps in PPS; predictions of the mechanical responses for various thermal histories using the single up-jump data set and the KAHR- a_{te} model will be provided in the next chapter.

The thermal histories of PPS film considered in this dissertation include:

97 °C (5 °C above T_g) → 57 °C (10 hr) → 67 °C (4hr) → 73 °C

97 °C → 67 °C (4hr) → 77 °C (10hr) → 73 °C

97 °C → 67 °C (3hr) → 77 °C (7hr) → 57 °C (4hr) → 73 °C

97 °C → 27 °C (12hr) → 73 °C (1hr) → 27 °C (1hr) → 73 °C

97 °C → 57 °C (4hr) → 73 °C (10hr) → 67 °C.

The creep test methodology is exactly the same as that in up-jump tests. At each loading point, the time elapsed from the last temperature jump was 5/16, 5/8, 5/4, 5/2, 5, 10, and 20 hrs, the duration of each load was 1/10 of these “aging times” from last temperature varying. The resulting aging shift factors of creep tests are demonstrated in Figure 79 and Figure 80. The aging shift factor data in these two figures are general curves which strongly depend on thermal histories. Unlike found in single temperature up-jump tests, the aging shift factors at 20 hr are not close to 1 for several thermal histories, it means the material at a long (20 hr) time after temperature jumps manifested quite different mechanical behavior compared with that in the isothermal case.

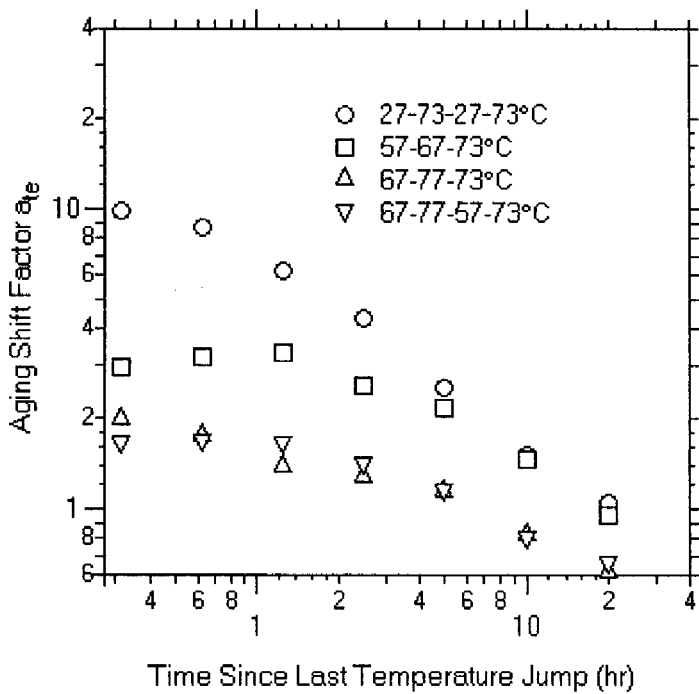


Figure 79. Mechanical shift factors during physical aging after multiple temperature steps for PPS with end temperature of 73 °C; experimental data are the average of three data sets of sequenced creep experiments

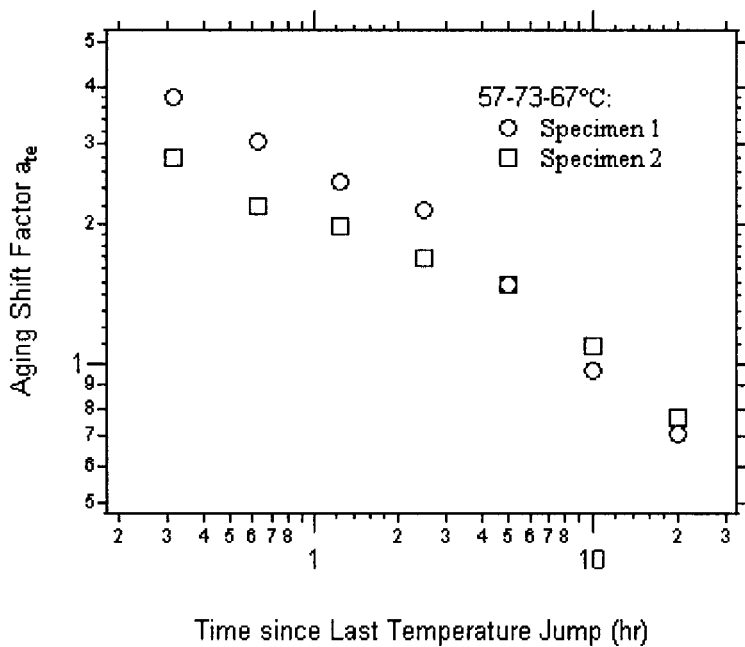


Figure 80. Mechanical shift factors during physical aging after multiple temperature steps for PPS with end temperature of 67 °C; experimental data are the average of three data sets of sequenced creep experiments

5.4 Long-term Nonisothermal Aging Response

5.4.1 Background

Long-term mechanical behavior of glassy polymers is a critical issue for many structural applications using polymer-based materials. During their service life, the viscoelastic properties of polymers can be strongly affected by physical aging, especially as temperatures approach the glass transition temperature T_g . Hence, the effects of physical aging on mechanical responses have received a great deal of attention in the past several decades. Struik (1978), McKenna (McKenna, 1995a), Tomlins (Tomlins, 1996; Tomlins et al., 1994) and other researchers (Dean et al., 1995; Kato, 1997; Veazie and Gates, 1997) have used creep tests of neat polymers and polymeric matrix composites (PMCs) to experimentally determine the long term effects of physical aging. Effective time approaches, developed by Hopkins and Haugh (Haugh, 1959; Hopkins, 1958), can also be used to predict long-term behavior from short-term tests. For example, Struik (1978) has shown fairly good predictive capabilities for long-term creep response of PVC at constant temperatures.

In recent years, investigators put forward several models in order to describe long-term data with good accuracy for specific materials or applications. Read and Tomlins (Read and Tomlins, 1997; Tomlins, 1996) used a stretched exponential Kohlrausch function, combined with an equation of the relaxation time over wide ranges of aging time and loading time to represent long-term compliance; their numerical results provided reasonable predictions of long-term data on polypropylene and PVC. Arnold

and White (Arnold and White, 1995) compared the θ concept model and the so-called universal formula (Kohlrausch function) method to long-term creep data in PMMA; they reported that the universal formula method produced a satisfactory fit, with the effects of aging being taken into account through the use of an effective time, while the θ concept model was not very successful. Skrypnik and co-workers (Skrypnik et al., 2000) introduced a constitutive model for long-term behavior of thermoplastics that integrates effective time theory with a generalized Schapery model (Schapery, 1969); the model led to good long-term predictions for multi-step stress loading and recovery tests for polypropylene. Another constitutive model derived from the effective time concept was proposed by Zheng and Meng (Zheng and Weng, 2002). The authors claimed that this model is identical with classical effective time theory when the aging time is sufficiently long; however, at short times, the former is more suitable for chrono-rheologically simple materials since it can account for the transition to the asymptotic state. This model was used to predict tests for a glass fiber/Derakane resin composite (30 vol.% glass fibers and Novolac vinyl ester resin (Dow Derakane 470-36)) and the results matched the experimental findings.

Most investigations above have attempted to develop models based on classical effective time theory; these approaches have been largely focused on improving predictive abilities or calculating the long-term response for specific materials at constant or varying stress levels. It is a remarkable fact that all of research on long-term viscoelastic response of polymers in the literature is conducted at isothermal conditions; this means that the material is quenched from a temperature above the glass transition

temperature (T_g) to a temperature $T < T_g$ and held at this temperature until the long-term test is complete. While isothermal long-term physical aging has been extensively studied, long-term mechanical properties with physical aging effects after a varying temperature history has received far less scrutiny. In this section, we address the nonisothermal long-term creep response of PPS films and provide a database for the further modeling work presented in next chapter.

5.4.2 Long-term Creep Results During Nonisothermal Aging

Long-term nonisothermal creep tests are performed for several thermal histories; these are identical to those considered in short-term testing and include both single temperature up-jump and multi-step temperature conditions. The thermal histories of PPS film considered in this dissertation include:

97 °C (5 °C above T_g) → 57 °C (14 hr) → 73 °C

97 °C → 63 °C (14 hr) → 73 °C

97 °C → 67 °C (14 hr) → 73 °C

97 °C → 73 °C (isothermal aging)

97 °C → 57 °C (10 hr) → 67 °C (4 hr) → 73 °C

97 °C → 67 °C (4 hr) → 77 °C (10 hr) → 73 °C

97 °C → 27 °C (12 hr) → 73 °C (1 hr) → 27 °C (1hr) → 73 °C

97 °C → 57 °C (4 hr) → 73 °C (6 hr) → 67 °C

At the final temperature in a thermal history, characterization of the aging state occurs using a long-term creep and recovery test. All creep tests begin 0.5 hours from the instant at which the specimen has first reached the final temperature (t_{e0}). Creep tests are performed in tension and generally last for at least 10 hours ($t/t_{e0} \geq 20$).

Long-term creep tests are conducted at the final temperature (73 °C or 67 °C) in the thermal histories above. It should be emphasized that long-term in this context means that the load duration is such that the aging state changes appreciably during the loading history (i.e. the creep tests do not consist a series of short-term load steps during which the aging shift factor remains approximately constant). The stress level applied to the specimens (4.87 MPa) remains in the linear viscoelastic regions at 73 °C and 67 °C; details on determining linear ranges are presented elsewhere (Guo et al., 2009).

The long-term creep data were collected in two successive time zones. The first time zone covers the time scale from the starting of loading ($t = 0$) to $t = 180$ seconds and the second time zone is the remainder of total loading time. The data collected in time zone 1 is considered as the short-term response of creep ($t/t_e \leq 0.1$); this data is utilized by the nonisothermal effective time theory for predicting the long-term response. The whole data set of compliance curve represents the long-term response of nonisothermal physical aging; it will be compared with numerical results to validate the effective time theory under complicated thermal histories in the next chapter.

Figure 81 - Figure 83 depict long term creep responses for six thermal histories. For each thermal history, test results from three replicates are plotted. The creep tests last

for at least 10 hours, while the aging time since last temperature jump is 0.5 hour. It is clear that the long-term creep compliance curves are consistent with each other under the same experimental condition; the maximum deviation of compliance values between any individual data set and the average was found less than 5%, while the average deviation is less than 2%. Note that the creep data are evenly distributed in real time; this is the reason that in Figure 81 -Figure 83, one sees more data points near the ends of both time zones (x axis is in logarithmic scale).

Long-term creep results for the other two thermal histories are similar as those shown in Figure 81- Figure 83, compliance curves from different specimens are consistent each other, these results will be presented later comparing with the predictions from effective time theory.

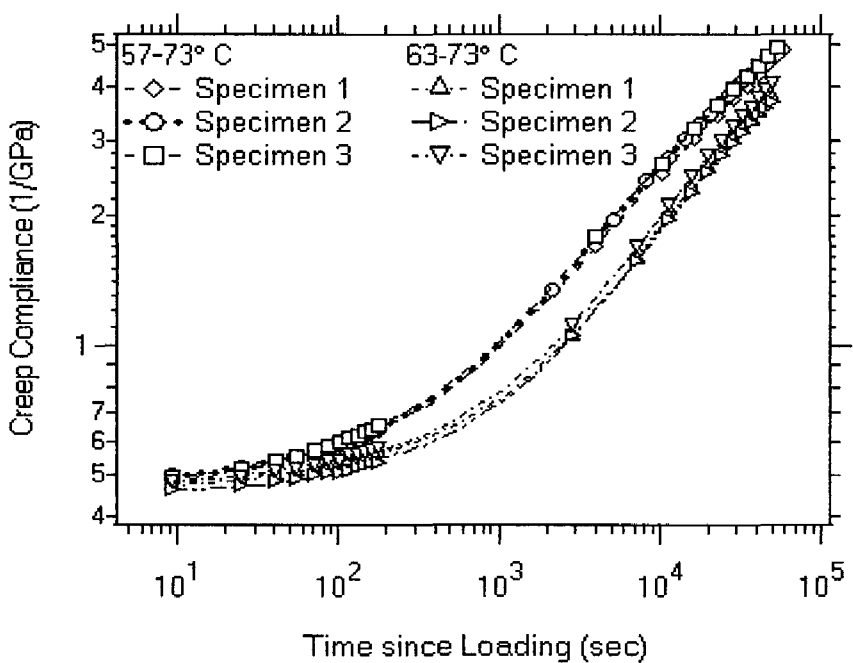


Figure 81. Long-term creep compliance curves of two thermal histories: 97 °C → 57 °C → 73 °C and 97 °C → 63 °C → 73 °C

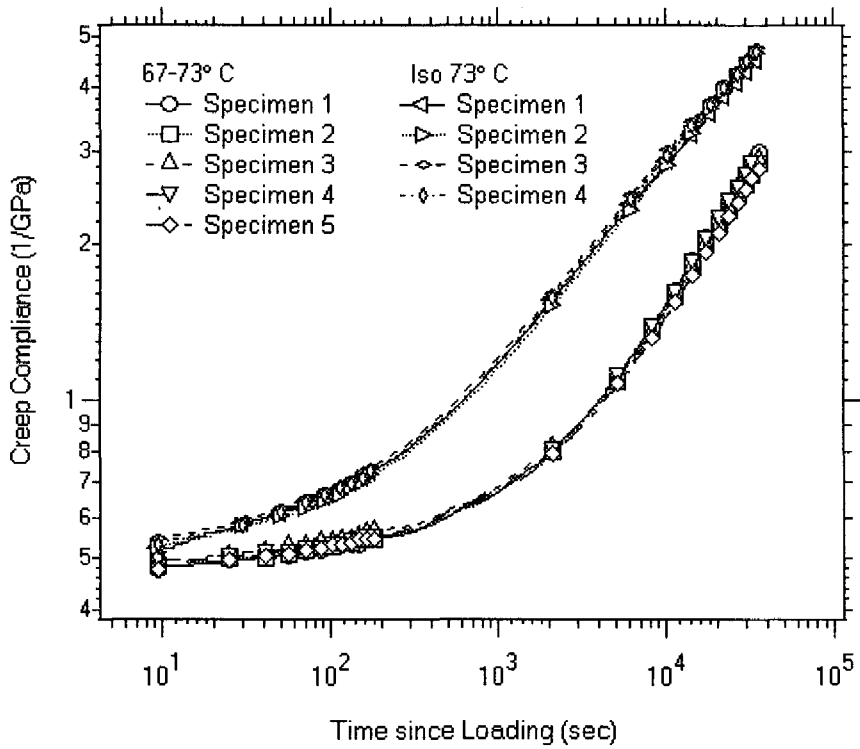


Figure 82. Long-term creep compliance curves of two thermal histories: 97 °C → 67 °C → 73 °C and isothermal aging at 73 °C

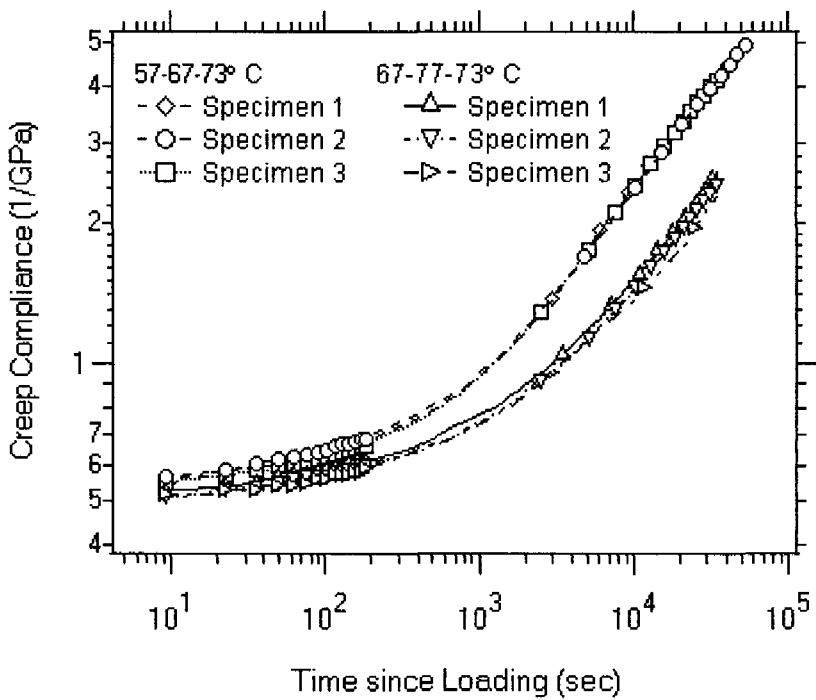


Figure 83. Long-term creep compliance curves of two thermal histories: 97 °C → 57 °C → 67 °C → 73 °C and 97 °C → 67 °C → 77 °C → 73 °C

CHARTER 6

MODELING NONISOTHERMAL PHYSICAL AGING

6.1 Background

Most previous work on nonisothermal behavior of glassy polymers has concentrated on volumetric response or enthalpy recovery, including several theories on specific volume (Kovacs et al., 1979; Ramos et al., 1984), free volume (Robertson, 1979; Robertson, 1992; Robertson et al., 1984), fictive temperature (Moynihan et al., 1991; Narayanaswamy, 1971; Tool, 1946), and relaxation time (Ngai, 2000; Ngai, 2003; Rendell and Ngai, 1987; Rendell et al., 1987). The Kovacs-Aklonis-Hutchinson-Ramos (KAHR) model, the Tool-Narayanaswamy-Moynihan (TNM) model, Ngai-Rendell's coupling model and Robertson-Simha-Curro (RSC) theory, are able to capture many of the experimental observations associated with the glass transition and structural recovery. The volume and enthalpy responses of polymers are important from a practical view because the changing "thermodynamic state" of the non-equilibrium glass impacts the mechanical response of the polymer in physical aging (McKenna and Simon, 2000). Therefore, the structural recovery models above represent a good starting point for predicting nonisothermal mechanical properties; In particular, this dissertation focuses on extension of the KAHR model, which has successfully described the major features of structural recovery.

In the 1960's, Kovacs (Kovacs, 1963) developed a series of experimental techniques to illustrate the kinetics of glasses in structural (volume) recovery after temperature jumps. These techniques include: (1) the intrinsic isothermal experiment; (2) the asymmetry of approach experiment; and (3) the memory experiment (McKenna, 1995a; McKenna, 2007; McKenna and Simon, 2000); these are discussed in greater detail in the next chapter for materials aged near T_g . The structural recovery phenomenon has been investigated by many researchers, and several reviews have been written (Hutchinson, 1995; McKenna, 1989).

In recent years, McKenna and co-workers have studied structural recovery and physical aging responses of polymer glasses subsequent to plasticizer jumps, including the effects of relative humidity and carbon dioxide pressure (Alcoutlabi et al., 2004; Alcoutlabi, 2002; McKenna, 2007, 1995b; Zheng and McKenna, 2003; Zheng et al., 2004). They reported the volume responses under these conditions have similar phenomenology to, but different kinetics from, those obtained by temperature jumps. Clearly, studies of structural (volume) recovery provide many valuable insights into the long-term behavior of polymer glasses. As stated in the previous chapter, researchers have found that there is some kind of correlation between volumetric response and simultaneous aging shift factors; the KAHR- a_{te} model was developed based on this fact.

6.2 KAHR- a_{te} Model

6.2.1 The KAHR Model

In the KAHR model, the volume recovery behavior can be expressed by the normalized departure from equilibrium δ , which is defined as in Equation (54). The volume response (specific volume change during physical aging was demonstrated in the Chapter I) is determined as (Kovacs et al., 1979):

$$\delta(z) = -\Delta\alpha \int_0^z R(z-\zeta) \frac{dT}{d\zeta} d\zeta \quad (55)$$

where $\Delta\alpha = \alpha_l - \alpha_g$ is the difference in coefficient of thermal expansion between the liquid and glassy state, T is temperature, $R(z)$ is a normalized retardation function that ranges between 1 at $z = 0$ and 0 at $z = \infty$, and z is the reduced time defined as:

$$z = \int_0^t \frac{d\xi}{a_T a_\delta} \quad (56)$$

where t is time, a_T is the temperature shift factor, and a_δ is the structural shift factor.

In this work, $R(z)$ is chosen as a normalized sum of Kohlrausch modulus functions of the form:

$$R(z) = \left(\sum_{q=1}^K R_q \right)^{-1} \left(\sum_{k=1}^K R_k e^{-\left(\frac{z}{\tau_k}\right)^{\beta}} \right) \quad (57)$$

where K is the number of elements of $R(z)$ and R_k , τ_k and β_k are the k^{th} coefficient, relaxation time and exponential parameter, respectively. This expression is normalized such that $R(0) = 1$ as required in the KAHR model (Kovacs et al., 1979).

The shift factors a_T and a_δ follow the exponential forms suggested by KAHR (Kovacs et al., 1979):

$$a_T = \exp(-\Delta\alpha\zeta e^b(T - T_r)); a_\delta = \exp(-\zeta\delta) \quad (58)$$

$$e^{-b} = 1 - x; \zeta = \frac{(1 - x)\theta}{\Delta\alpha} \quad (59)$$

where T_r is a reference temperature, x is a partition parameter ($0 \leq x \leq 1$), and θ is a material constant; note that b and ζ are introduced to simplify the solution in the case of $T = T_r$ (i.e., a_T is fixed at unity and a_δ is related to a single parameter ζ) (Bradshaw, 1997).

6.2.2 KAHR- a_{te} Model of Aging Shift Factor

The KAHR model can be extended to predict mechanical response shift factors a_{te} if a relationship between a_{te} and δ (or ν) could be ascertained. Based on the findings of Struik (Struik, 1988) (see Figure 67) and McKenna (1995), the logarithmic a_{te} data appears to be well-represented by a straight line versus δ (or ν) for materials that do not reach thermodynamic equilibrium. Assuming this behavior, the relationship between a_{te} and δ can be expressed as:

$$a_{te} = e^{r_0(T) + r_1(T)\delta} \quad (60)$$

where r_0 describes the equilibrium value of the shift factor a_{te} and r_1 describes how a_{te} changes with a departure from volume equilibrium ($\delta \neq 0$). Recalling the expression for a_δ in Equation (58), this expression was written by Bradshaw (1997) as:

$$a_{te}(a_\delta, T) = e^{r_0(T)} \left(\frac{1}{a_\delta} \right)^{r_1(T)/\zeta} \quad (61)$$

The dependence of r_0 and r_1 on the temperature T can take on any number of forms. In this dissertation, they are assumed to take on the form below

$$a_{te}(a_\delta)|_T = \left(\frac{c_0}{a_\delta} \right)^{c_1}; \quad c_0, c_1 > 0 \quad (62)$$

where constants c_0 and c_1 are specific to the temperature at which the mechanical responses were measured. Generalization of this expression to a wider variety of temperatures (i.e. expressions for c_0 and c_1 for any temperature) is considered later.

This equation indicates a temperature-dependent linear relationship between a_{te} and a_δ in log-log plot. At a given temperature, mechanical response (a_{te}) can be evaluated if the thermal history is known. This relationship is assumed based on the experimental findings of Struik (Struik, 1978, 1988) and McKenna (McKenna, 1995b); as will be shown in a later section, the predictions obtained using this approach are validated by the nonisothermal physical aging test results presented here.

6.2.3 KAHR- a_{te} Model Solution Algorithm

There are two basic problems of interest for the KAHR- a_{te} model formation: (1) prediction of mechanical aging shift factor a_{te} for a given set parameters; (2) determination of those parameters to fit a known mechanical response data set. This section focuses on the first problem.

An essential step for the first problem is to determine the reduced time z . This derivation follows that presented by Bradshaw (1997). Once the z is obtained, volume response and then aging shift factors can be found by using KAHR- a_{te} model parameters. Differentiating Equation (56) we find:

$$\frac{dz}{dt} = \frac{1}{a_T(z)a_\delta(z)} \quad (63)$$

Substituting δ from Equation (55), a_T and a_δ from Equation (58) and a_{te} from Eq. (62) leads to:

$$\frac{dz}{dt}(z) = e^{\Delta\alpha\zeta e^b(T(z)-T_r)} e^{\left[-\Delta\alpha\zeta \int_0^z R(z-\zeta) \frac{dT}{d\zeta} d\zeta\right]} \quad (64)$$

This represents an ordinary differential equation in z that can be solved using suitable numerical methods.

If the temperature history is restricted to a series of temperature jumps since the material was at $T = T_g$ (i.e. the last moment it was in equilibrium before quenching to $T < T_g$), Equation (64) can be further simplified. Specifically, a temperature history consisting of M temperature jumps can be expressed as a function of the time since the quench from T_g (t_a) as:

$$T(t_a) = T_g + \sum_{m=0}^{M-1} H(t_a - \theta_m) \Delta T_m \quad (65)$$

$$\theta_0 = 0 \quad ; \quad \Delta T_m = \begin{cases} T_0 - T_g & m = 0 \\ T_m - T_{m-1} & m > 0 \end{cases}$$

where ΔT_m and θ_m is the temperature change and time at the m^{th} step, respectively, and $H(t)$ is the Heaviside function. Substituting this into Equation (64) leads to the following

simplified differential equation for z :

$$t_a \in [\theta_p, \theta_{p+1}) \rightarrow \frac{dz}{dt}(z) = e^{\Delta\alpha\zeta e^b(T_p - T_r)} e^{\left[-\Delta\alpha\zeta \sum_{m=0}^p \Delta T_m R(z - \tilde{\theta}_m)\right]} \quad (66)$$

where $p \in [0, M-1]$, $\tilde{\theta}_m = z(\theta_m)$ and $\theta_m = \infty$.

The expression in Equation (66) is an ordinary differential equation. Since the initial condition at time $t_a = 0$ is known to be $z(0) = 0$, this represents an initial value problem that can be solved using a variety of approaches. In this work, the reduced time z is evaluated using a 5th order Runge-Kutta method with the Cash-Karp parameters as detailed in a reference (Press et al., 1992); further details regarding the solution method are available elsewhere (Bradshaw, 1997). Once z is obtained, all quantities of interest (δ , a_δ , a_{te} , etc.) are obtained by algebraic evaluation.

The code for the KAHR- a_{te} model was written by C language. Most of the code used in this study was developed by Bradshaw (1997) and the main body and a few functions were programmed by me.

6.2.4 Optimal KAHR- a_{te} Model Parameters

The second problem seeks the parameters that lead to the best fit of the data using the KAHR- a_{te} model. In this case, a data set (t_i and a_{tei}) have been obtained from the testing, the problem here is that how to find proper KAHR- a_{te} model parameters to get a best description for the given data. Model parameters were found by minimizing the χ^2 error between the desired fitting functions and the data expressed as:

$$\chi^2(F) = \sum_{n=1}^N \left(\frac{f(t_n; F) - g_n}{\sigma_n} \right)^2 \quad (67)$$

where g_n is the value of the data point under consideration, $f(t_n; F)$ is the fitting function prediction at associated time t_p using the current set of model parameters F , and σ_n is the standard deviation of the n^{th} data point. The minimization of χ^2 is performed using the Levenberg-Marquardt algorithm (Press et al., 1992), in which the derivatives of the model function with respect to the fitting parameters are used to step iteratively towards the optimal parameter set. For the current work, the data always remains substantially larger than zero and we can safely set $\sigma_n = g_n$ (the value of the associated data point); this then relates χ^2 to the root mean square (RMS) percent error as:

$$\text{RMS}(F) = 100 \sqrt{\frac{\chi^2(F)}{N}} \quad (68)$$

The RMS error will be used to compare the model predictions and experimental data in next section of this chapter.

6.3 Application of KAHR- a_{te} Model to Nonisothermal Data

6.3.1 KAHR- a_{te} Model Parameters

The difference between the liquid and glass thermal expansion coefficients ($\Delta\alpha$) is provided as material constant to the model. For PEEK, $\Delta\alpha$ is $4.5 \times 10^{-4} \text{ K}^{-1}$, calculated from the data reported by Farrow et al. (Farrow et al., 1990). However, a comparable source for the thermal expansion coefficients of PPS on both sides of T_g was not found in

the literature. The linear thermal expansion coefficient of PPS in the glassy state was reported by Plastics International Company (Anonymous, 2001); with the assumption of isotropy, the volumetric α_g was determined to be $2.16 \times 10^{-4} \text{ K}^{-1}$. The corresponding value in the liquid state (α_l) is typically 2-3 times larger than α_g (Ferry, 1980); thus, the value of $\Delta\alpha = \alpha_l - \alpha_g$ is expected to be in the range $2.16\text{-}4.32 \times 10^{-4} \text{ K}^{-1}$. Based upon the reported $\Delta\alpha$ values of other polymers, this work assumes $\Delta\alpha = 4 \times 10^{-4} \text{ K}^{-1}$ for PPS in our application using the KAHR- a_{te} model.

Ideally the volumetric coefficients of thermal expansion (CTE) would be obtained directly for the materials studied, one possibility is to perform this test using a TMA in order to obtain the linear CTE (α_L); the volume change rate with respect to temperature, α_V , is then calculated from the measurements of the length change of the sample (i.e., $\alpha_V = 3\alpha_L$). This is based on the assumption that the length changes in all dimensions are isotropic for thin films. This was observed experimentally by Fleming and Koros (Fleming and Koros, 1986) and was used by others in the literature (Alcoutlabi et al., 2004; Alcoutlabi, 2002). Due to time constraints, this work has not been pursued; minor differences in $\Delta\alpha$ will likely change the KAHR- a_{te} model parameters for a set of data but is anticipated to still lead to good fits shift factors a_{te} .

The normalized retardation function $R(z)$ is described as a series of stretched exponential functions. In this study, only the case of a single element ($K = 1$) is considered; this fixes the coefficient R_1 at unity, which leaves six parameters needed for the KAHR- a_{te} model ($\zeta, b, c_0, c_1, \tau, \beta$). Cases using two elements ($K = 2$) have also been considered. The relaxation times were fixed to reasonable values for the data under

consideration (i.e. $\tau_1 = 500$ s and $\tau_2 = 1000$ s) to speed the solution. Little, if any, improvement was observed relative to the single element model; these results are not presented in the interest of brevity.

In tests intended to identify the KAHR- a_{te} model parameters, the thermal history consists of an up-jump test with two temperature steps ($T_g \rightarrow T_0$ at $t_a = 0$ and $T_0 \rightarrow T_1$ at $t_a = 14$ hours = 50400 s. The reference temperature T_r is selected to be the final temperature after the up-jump (T_1). Predictions using the obtained model parameters are also demonstrated for more complicated thermal histories involving both up-jumps and down-jumps.

6.3.2 KAHR- a_{te} Model Parameter Identification

In order to obtain a sufficient number of aging shift factor data points to fit the KAHR- a_{te} model, the experimental data were first fitted using polynomials with MATLAB; the resulting functions were used to create a data set consisting of more aging shift factor points than the 7 values obtained for each test. Optimal parameters of KAHR- a_{te} model for the each data set were then obtained by the Levenberg-Marquardt method; the parameters obtained from PEEK thermal histories of 118-130°C and 120-130°C, and PPS thermal histories of 63-73°C and 67-73°C (PPS) are listed in Table 9. These parameter sets are used for model predictions that follow in the next section.

Table 9. Optimal parameters of KAHR- a_{te} model from single temperature up-jump tests.

Parameter	Thermal Histories (PEEK)		Thermal Histories (PPS)		
	Obtained	118-130°C	120-130°C	63-73°C	67-73°C
ζ (unitless)		965.64	855.25	260.08	273.28
b (unitless)		0.000536	0.001675	0.904045	0.746357
c_0 (unitless)		0.567246	0.493083	0.662666	0.715915
c_1 (unitless)		3.0434	4.3365	10.7613	10.4957
$\tilde{\tau}$ (sec)		780.12	171.25	609.20	777.44
$\tilde{\beta}$ (unitless)		0.1738	0.1177	0.1110	0.1411

6.3.3 Aging Shift Factor Predictions for Up-jump Tests

The optimal parameters for PEEK from the tests from 118-130°C and 120-130°C are used to predict the aging shift factors for five different thermal histories; in each case, this means that four experimental conditions are predicted using parameters from a different test condition. These results are shown in Figures 84-85. In all of the cases, the predicted shift factors match the data sets quite well.

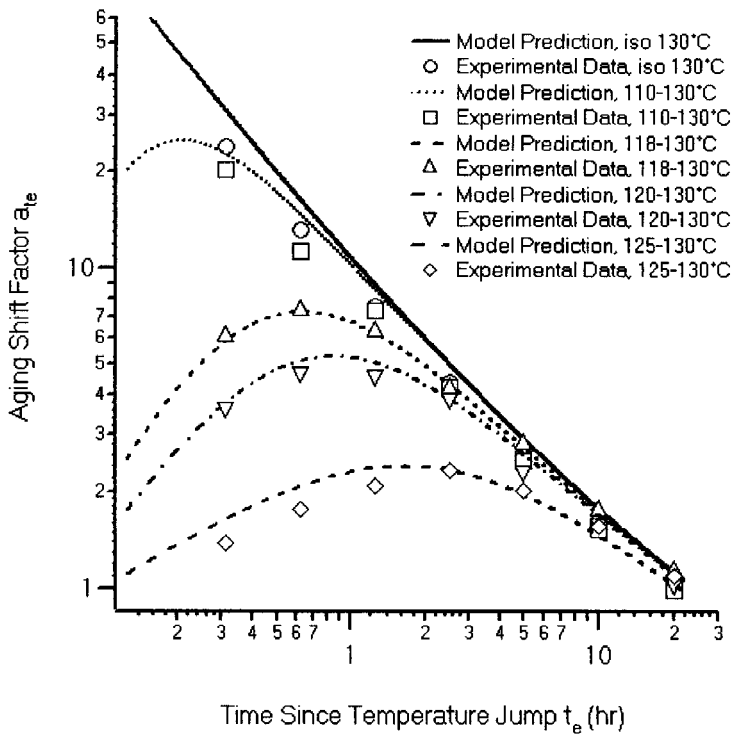


Figure 84. Prediction of mechanical shift factor for PEEK using KAHR- a_{te} model parameters obtained from 118-130°C

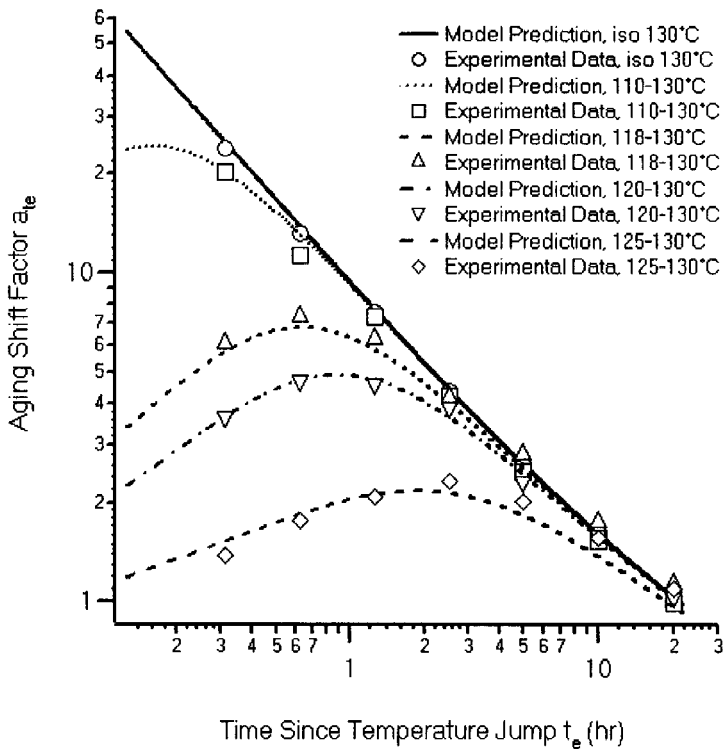


Figure 85. Prediction of mechanical shift factor for PEEK using KAHR- a_{te} model parameters obtained from 120-130°C

Similarly, the optimal parameters for PPS from the tests from 63-73°C and 67-73°C are used to predict the aging shift factors for five different thermal histories; as before, this means that four experimental conditions are predicted using parameters from a different test condition. Figure 86 demonstrates the predictions obtained using the KAHR- a_{te} parameters obtained from the 63-73°C tests; the predictions are quite good in most cases. Figure 87 demonstrates the same except using the parameters obtained from the 67-73°C tests; these results do not match the other data sets as well as the 63-73°C case. The chief reason for this difference appears to be the unusually low aging shift factor data point at aging time $t_e = 2.5$ hr in the 67-73°C tests; for example, the 63-73°C KAHR- a_{te} parameters predict the 67-73°C data well except for this one. The optimal KAHR- a_{te} parameters for the 67-73°C alter the shape of the prediction to pass through the point at $t_e = 2.5$ hr; in doing so, the resulting parameters perform worse for other conditions. To demonstrate this, the KAHR- a_{te} model parameters were obtained for the 67-73°C data set with the $t_e = 2.5$ hr point excluded; the resulting prediction of five temperature histories is shown in Figure 88; as expected, these predictions shows improved agreement with the data sets.

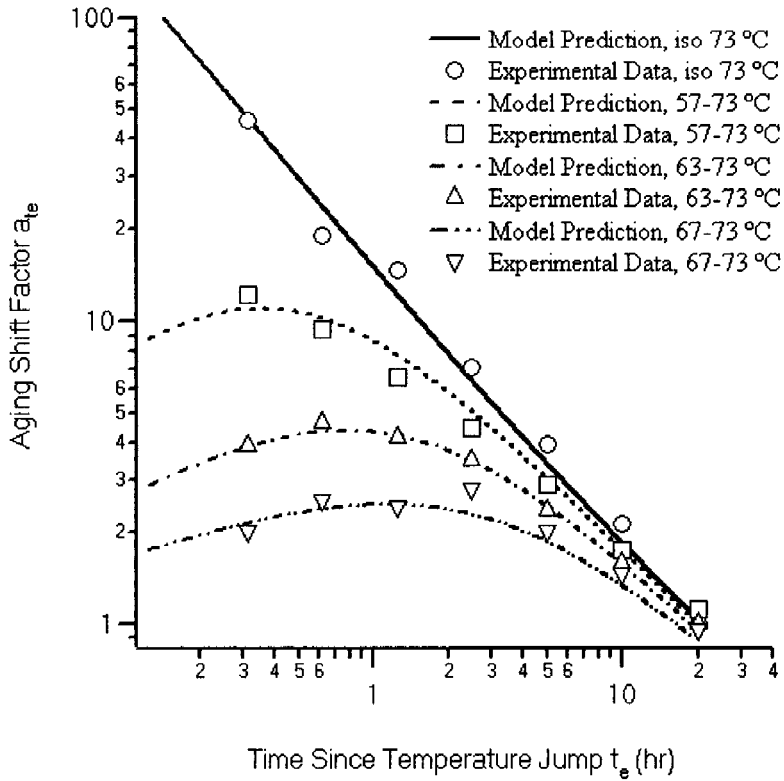


Figure 86. Prediction of mechanical shift factor for PPS using KAHR- a_{te} model parameters obtained from the 63-73°C tests

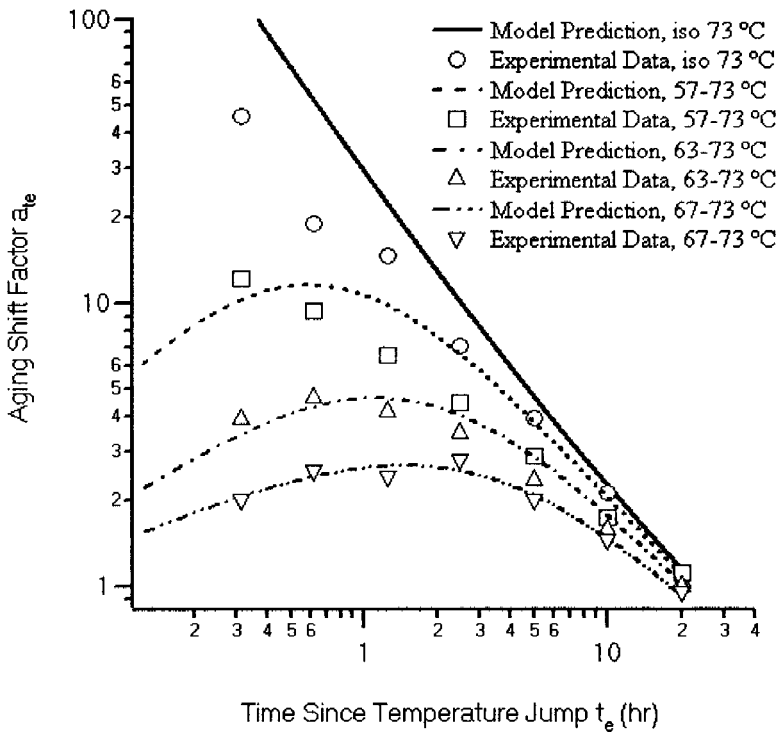


Figure 87. Prediction of mechanical shift factor for PPS using KAHR- a_{te} model parameters obtained from the curve fitting of the entire data points of 67-73°C tests

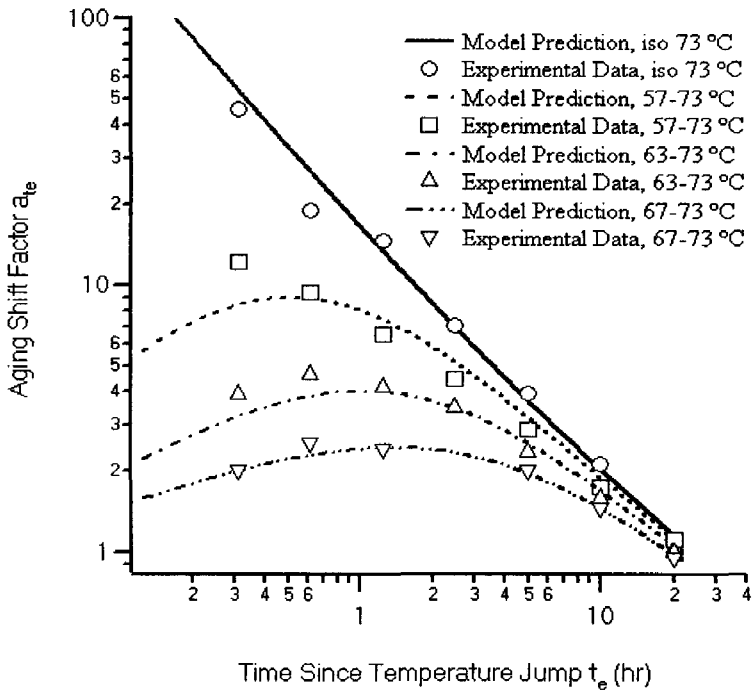


Figure 88. Prediction of mechanical shift factor for PPS using KAHR- a_{te} model parameters obtained from the curve fitting of 67-73°C tests except excluding the $t_e = 2.5$ hr point; KAHR- a_{te} model parameters are $\zeta = 347.38$, $b = 0.567146$, $c_0 = 0.668579$, $c_1 = 8.4406$, $\bar{\tau} = 262.79$, and $\tilde{\beta} = 0.1185$

In order to quantify the degree of fit between the model and the data, the RMS percent errors between each prediction¹¹ and each experimental data set were calculated using Equation (68) (RMS error was calculated between the original aging shift factor data points and the model predictions at the same aging time); the resulting values are listed in Table 10. The RMS value corresponding to the case used to obtain KAHR- a_{te} model parameters is highlighted; not surprisingly, these show the lowest RMS error for a given set in most cases. These results demonstrate that within the time and temperature scale of our experiments, the KAHR- a_{te} model can be used to successfully predict the

¹¹ The predictions use the parameters in Table 9 except that the 67-73°C case uses the parameters obtained from removing the odd point at $t_e = 2.5$ hr; these parameters are described in Figure 88.

aging shift factors of different thermal histories, including both nonisothermal and isothermal cases. The fact that good agreement is obtained for a family of temperature history results (average RMS error 6-10%) based on model parameters from a single test condition indicates that the model is capable of capturing the phenomena that occur during the nonisothermal aging and volume recovery experiments.

Table 10. RMS error between data and prediction of KAHR- a_{te} model, $K = 1$

PEEK		RMS Error (%)	PPS		RMS Error (%)
Pred. from 118-130°C	110-130°C	18.39	Pred. from 63-73°C	57-73°C	5.63
	118-130°C	0.55		63-73°C	0.93
	120-130°C	7.51		67-73°C	8.42
	125-130°C	7.86		Iso 73°C	7.81
	Iso 130°C	16.47			
Average Error		10.16	Average Error		5.70
Pred. from 120-130°C	110-130°C	8.92	Pred. from 67-73°C	57-73°C	10.62
	118-130°C	7.37		63-73°C	8.81
	120-130°C	2.23		67-73°C	4.67
	125-130°C	11.99		Iso 73°C	3.82
	Iso 130°C	6.56			
Average Error		7.41	Average Error		6.98

Although good agreement is demonstrated in Table 10, it is clear that the results preferentially fit those data sets used to obtain the parameters at the expense of the fit quality for the other data sets. Ideally, the KAHR- a_{te} model parameters could be obtained that optimally fit an arbitrarily large collection of data sets at the same time; such an optimization procedure will be presented in next section.

As the model parameters are determined, the response of structural relaxation δ or a_δ can be evaluated by Equation (54) – (59). The compliance tests also provide the aging shift factors a_{te} . As such, the relationship between a_{te} and a_δ (or δ) in Equation (62) can

be examined. According to Equation (58) and Equation (62), the KAHR- a_{te} model assumes linear relationship between $\log a_{te}$ and δ . Figure 89 and 90 give examples for PEEK and PPS, respectively. In these figures, the δ values were calculated using the model parameters obtained from 120-130 °C and 67-73 °C for several different thermal histories. The correlation (curve fit) between aging shift factors and δ in these thermal histories was plotted as a linear function of $\log a_{te}$ vs. δ ; it should be emphasized that δ (a normalized measure of specific volume) has not been directly determined by experiment in this study. In these plots, linear relationships between aging shift factors and volumetric response are demonstrated. Note that these results are consistent with the findings of Struik as shown in Figure 67.

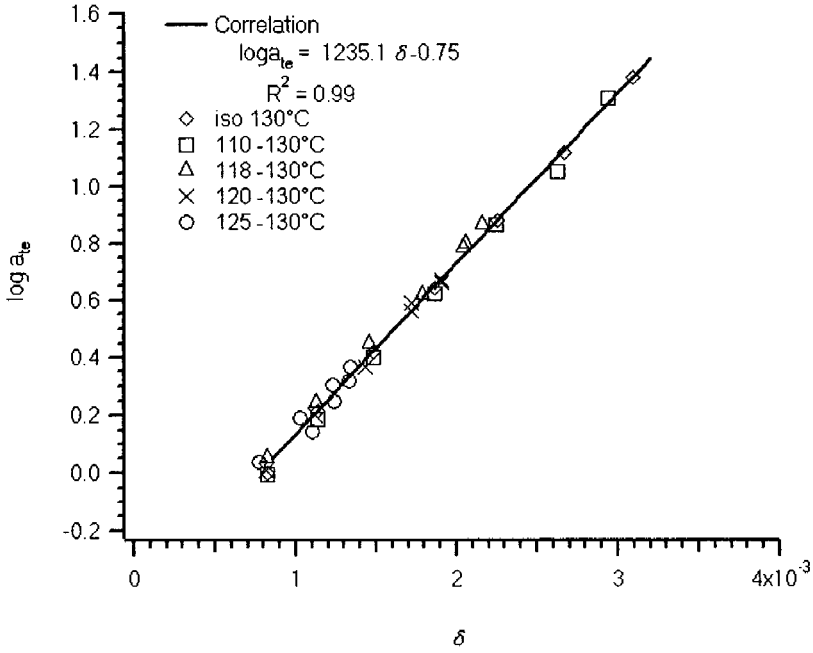


Figure 89 Correlation between $\log a_{te}$ and δ of PEEK for several thermal histories; δ is calculated by model parameters from 120-130°C

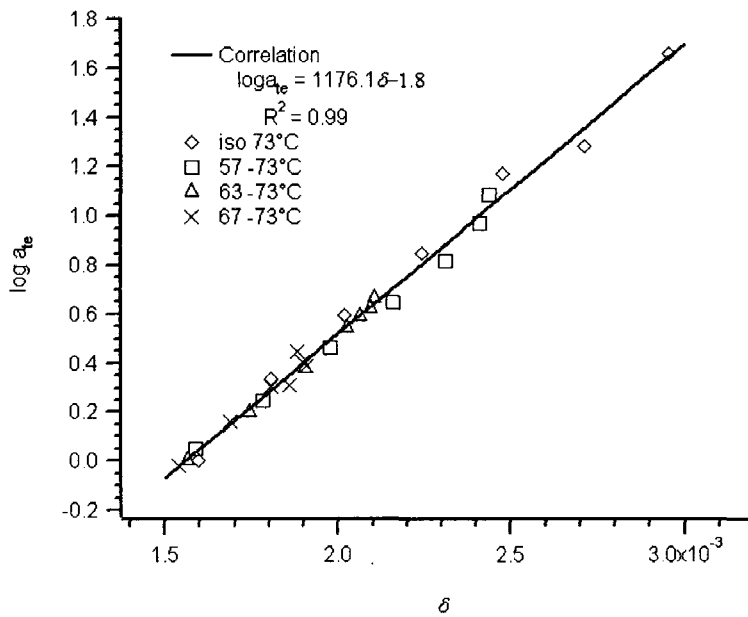


Figure 90 Correlation between $\log a_{te}$ and δ of PPS for several thermal histories; δ is calculated by model parameters from 63-73°C

6.3.4 Aging Shift Factor Predictions for Complex Thermal Histories

The KAHR- a_{te} model with optimal parameters from single up-jump temperature history has been applied to predict aging shift factors on more complex thermal conditions for PPS material. Figure 91 shows the model prediction and experimental data (average of three replicates) of thermal history 97 °C → 57 °C (10 hr) → 67 °C (4hr) → 73 °C. This thermal history includes up-jumps only except the quenching from 97 °C to 57 °C. Figure 91 demonstrates that the model prediction accords with experimental results throughout the testing duration.

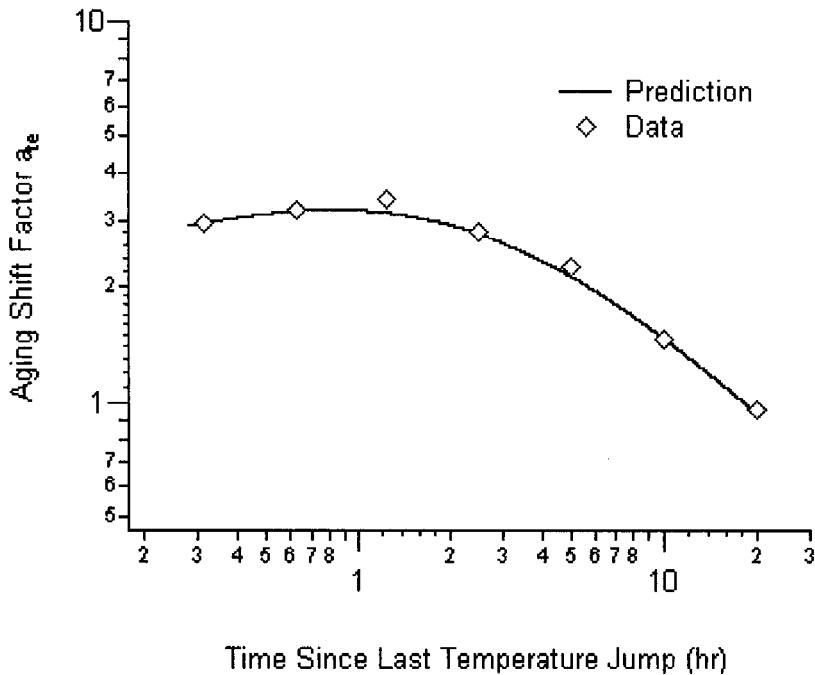


Figure 91. Aging shift factor of creep tests on PPS for thermal history 97°C → 57°C (4hr) → 67°C (10hr) → 73°C; KAHR- a_{te} model parameters obtained from the single up-jump 63-73°C, as listed in Table 9

Besides the case above, two more complex thermal histories are presented below. Figures 92 and 93 compare the aging shift factors obtained from KAHR- a_{te} model prediction and experiments on the temperature histories 97 °C → 67 °C (3hr) → 77 °C (7hr) → 57 °C (4hr) → 73 °C and 97 °C → 27 °C (12hr) → 73 °C (1hr) → 27 °C (1hr) → 73 °C, respectively. Figures 92 and 93 indicate that the aging shift factors after these temperature jumps can be predicted effectively by the model. The thermal histories in these two figures include a series of up-jumps and down-jumps as would likely occur in actual structures, in order to examine the predicting capacity of the model. Figure 92 represents the temperature changing within a range of 16 - 40 °C below T_g while Figure 93 covers the temperature range from room temperature to $T_g - 20^\circ\text{C}$. The predictions for a_{te} after 3-step and 4-step temperature jumps were obtained using parameters obtained

from the single up-jump test; the fact that fairly good agreement between the model and data were obtained demonstrate the potential for predicting mechanical response for complicated thermal histories based on model parameters identified from tests involving relatively simple thermal histories. Note that while the results in this dissertation show good agreement between the data and the KAHR- a_{te} model with suitable parameters, this should not be interpreted that aging shift factors can be predicted for any arbitrary thermal history. Comparison between the model results and experiments on temperature ranges consisting of the regions of interest should be pursued to assess the applicability of the model before applying to general cases of interest.

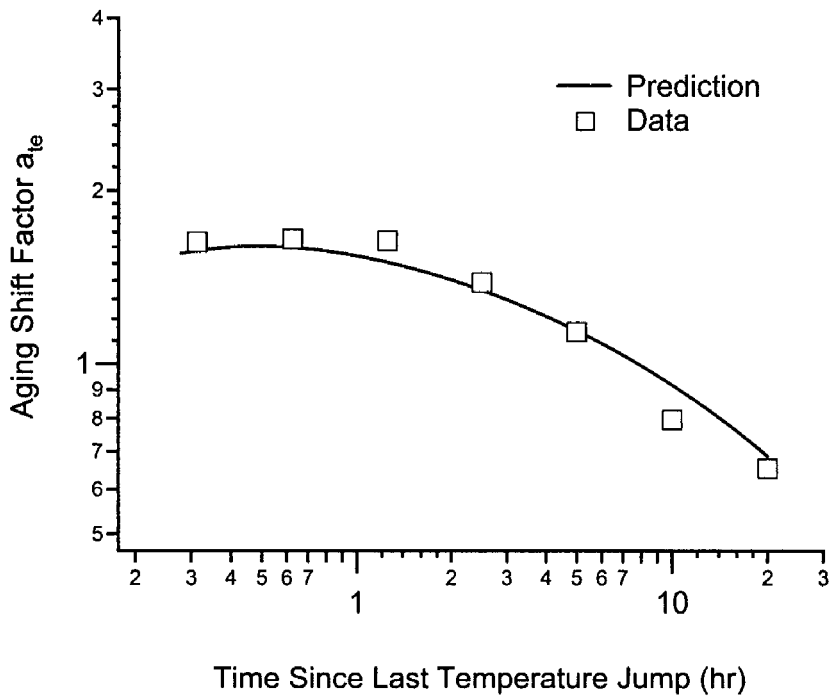


Figure 92. Aging shift factor of creep tests on PPS, thermal history 97 °C → 67 °C (3hr) → 77 °C (7hr) → 57 °C (4hr) → 73 °C; KAHR- a_{te} model parameters obtained from the single up-jump 63-73°C, as listed in Table 9

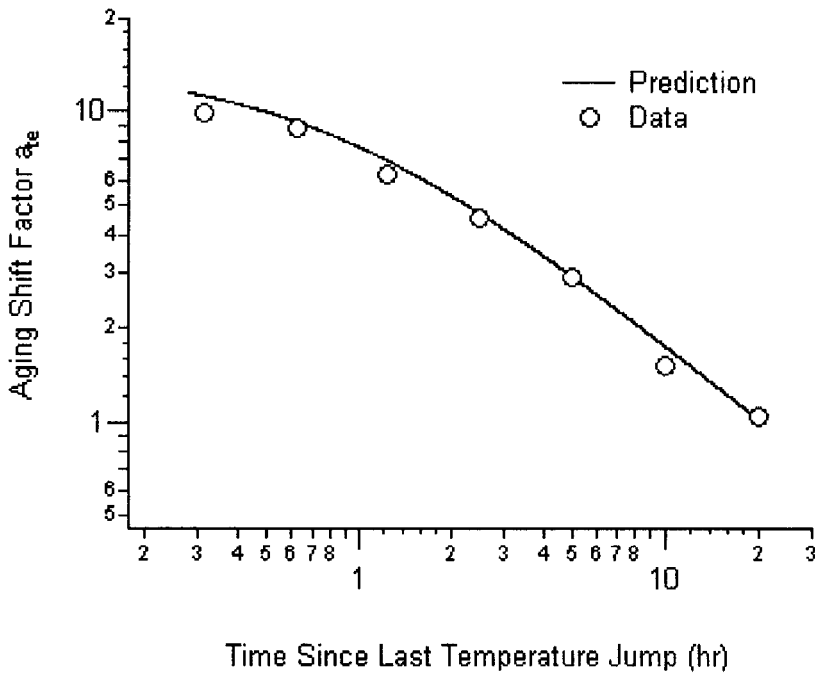


Figure 93. Aging shift factor of creep tests on PPS for thermal history 97 °C → 27 °C (12hr) → 73 °C (1hr) → 27 °C (1hr) → 73 °C. KAHR- a_{te} model parameters obtained from the single up-jump 63-73°C, as listed in Table 9

6.4 Optimization of KAHR- a_{te} Model Parameters

In previous section, the KAHR- a_{te} model of nonisothermal physical aging shift factors in glassy polymers was introduced and experimentally validated. The objective in the current section is to present a method for finding the optimal parameters of the KAHR- a_{te} model which provide best description of multiple data sets from various thermal histories. The optimization is performed in an iterative approach, in which the model parameters are determined in three steps, with this procedure repeated until the whole parameter set converges. At that point, it is assumed that the optimal parameters for the entire set are determined. This optimization method is applied to the data of nonisothermal physical aging for poly(ether ether ketone) (PEEK) and polyphenylene

sulfide (PPS) films below, the prediction results using the identified parameters are presented along with comparison to the results from the last section.

6.4.1 Optimization Procedure

As described in the previous section, the KAHR- a_{te} model can seek values of any/all of the model parameters from a single nonisothermal condition. Of course these parameters can be used to predict mechanical response for some other thermal histories; however, the RMS error levels of predictions for other experimental conditions are much higher than that for the thermal history used for parameter identification (Table 10). This indicates that parameters from a single temperature history have a best description only for the mechanical response on the identical thermal treatment, and they can also give reasonable predictions for other conditions. In order to find a optimal parameter set based on several experimental findings, a optimization procedure was developed in this dissertation. The optimization procedure finds the optimal parameters in three steps:

(1) Determine starting value of c_0 and c_1 .

Run the numerical program for KAHR- a_{te} model to obtain the optimal parameters ζ , b , c_0 , c_1 , τ , and β for each nonisothermally experimental condition. Note that the $\log a_{te}$ and δ have the following linear relationship:

$$\log a_{te} = \frac{c_1}{\ln 10} (\ln c_0 + \zeta \delta) = p + m\delta \quad (69)$$

This equation provides optimal description for the data of individual nonisothermal

temperature history under the current KAHR- a_{te} model. Based on the identified parameter frame, the volume recovery responses δ can be evaluated for other nonisothermal experiments. Plot the δ responses versus their associated aging shift factors (a_{te}) together; a linear regression is then performed as described below..

If the number of nonisothermal temperature histories used for identifying the optimal parameters is N , there will be N linear regression equations. The assumed relationship is shown in Equation (69). Therefore, the slope and intercept of the i^{th} line are m_i and p_i , they have the following form:

$$m_i = \frac{1}{\ln 10} c_{1,i} \zeta_i \quad (70)$$

$$p_i = \frac{1}{\ln 10} c_{1,i} \ln c_{0,i} \quad (71)$$

We use the average value of m , p , and ζ to evaluate the initial guess of c_0 and c_1 for the optimization procedure:

$$m = m_{avg} = \frac{\sum_{i=1}^N m_i}{N} = \frac{1}{\ln 10} c_{1,initial} \frac{\sum_{i=1}^N \zeta_i}{N} \quad (72)$$

$$p = p_{avg} = \frac{\sum_{i=1}^N p_i}{N} = \frac{1}{\ln 10} c_{1,initial} \ln c_{0,initial} \quad (73)$$

The initial values of c_0 and c_1 can be calculated by these equations.

(2) Determine initial values of $\tilde{\tau}$ and $\tilde{\beta}$.

In this step, the values c_0 and c_1 are fixed to the initial values obtained above. Now the

procedure seeks the optimal retardation functions $R_i(z)$, ζ_i and b_i ($i = 1, 2, 3, \dots, N$) for each nonisothermal case. This optimization method uses the average value of $R_i(z)$ from various thermal histories as the initial value of retardation function. The parameters $\tilde{\tau}$ and $\tilde{\beta}$ are acquired from $R_{avg}(z)$; note since $R(z)$ is a stretched exponential function, it is not sufficient/proper to simply average $\tilde{\tau}$ and $\tilde{\beta}$.

Assuming a single Kohlrausch term for $R(z)$, this expression can be reformulated algebraically as:

$$R(z) = \exp\left(-\left(\frac{z}{\tilde{\tau}}\right)^{\tilde{\beta}}\right) \rightarrow \ln(-\ln R(z)) = \tilde{\beta}(\ln z - \ln \tilde{\tau}) \quad (74)$$

Equation (74) appears as a straight line in the scale $\ln z$; with slope $\tilde{\beta}$ and intercept $-\tilde{\beta} \ln \tilde{\tau}$. Data from all N cases are then plotted; parameters $\tilde{\tau}$ and $\tilde{\beta}$ can be determined by linear regression.

(3) Determine the material parameters ζ and b .

At this point, values c_0 , c_1 , $\tilde{\tau}$, and $\tilde{\beta}$ have been determined. The remaining parameters for each thermal history (ζ_i and b_i) can be found using the KAHR- a_{te} model. These values can then be averaged as ζ and b .

(4) Convergence check.

If ζ_i and b_i converge at some fixed values, then stop the optimization, the average value of ζ_i and b_i are defined as the optimal parameters in this procedure. The following convergence criterion was used: The average percent error of ζ_i and b_i less than 10% and

the maximum percent error less than 15%, these coefficients are convergent; otherwise, they are non-convergent at here, in this situation, go back to the first step, and increase the initial c_0 and c_1 by a stepsize of 10%.

The structure of optimization procedure above is represented in Figure 94. This procedure works well to determine optimal parameters from several nonisothermal aging conditions for both PEEK and PPS. The ζ and b directly converge at constant values in the calculation, so the convergence check loop was not be used for PEEK and PPS.

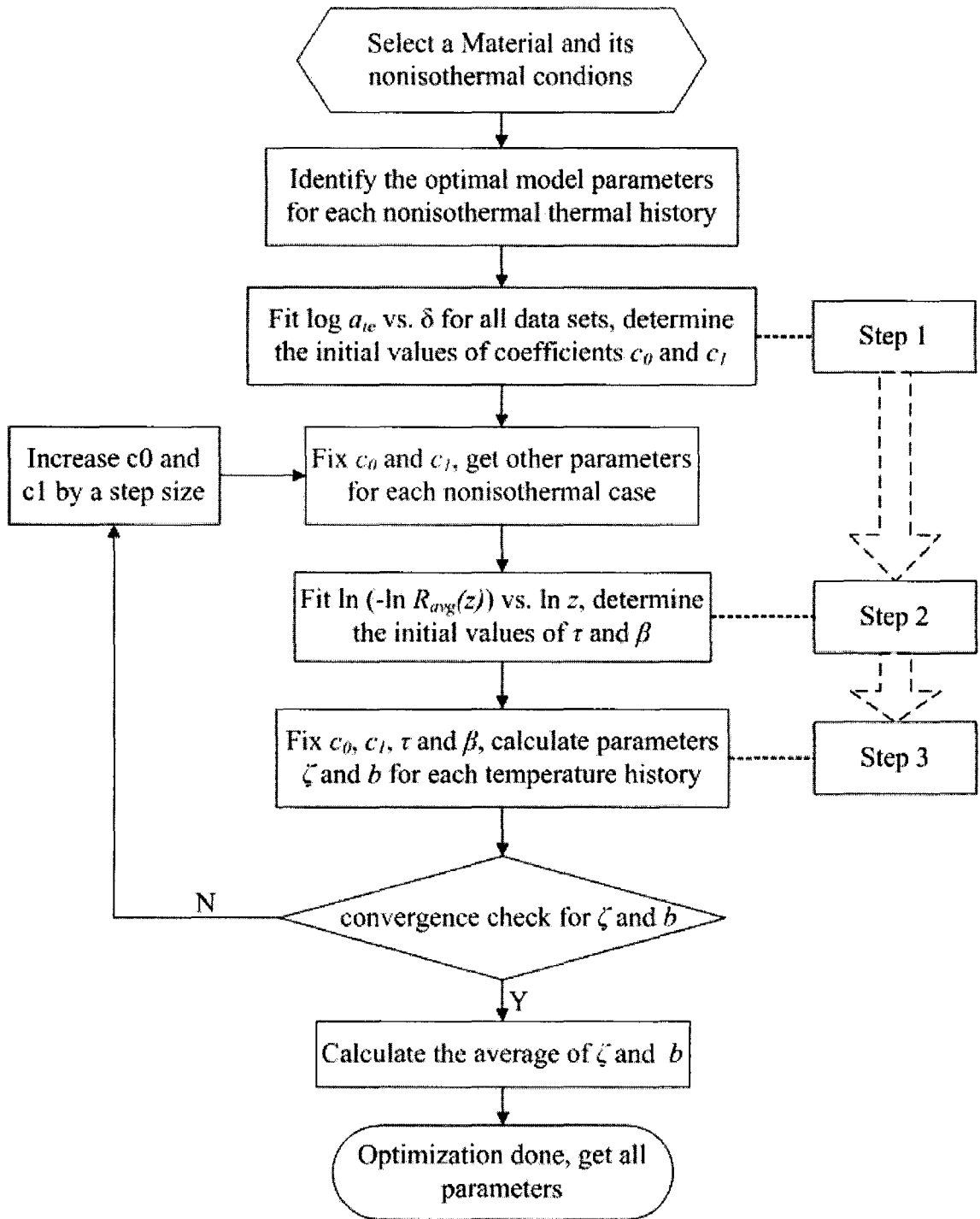


Figure 94. Schematic representation of optimization procedure

6.4.2 Optimal Parameter Determination

In this section, the results of optimization for PPS and PEEK are reported step by step using the procedure described above. In the interest of brevity, the results of PPS are represented in detail while the results of PEEK are summarized at the end of this section.

(1) Determine c_0 and c_1

The optimal parameters of the KAHR- a_{te} model with one-element retardation function are listed in Table 11. Using these parameter sets, the aging shift factor and simultaneous volume response are calculated for 57-73°C, 63-73°C, and 67-73°C, PPS; the log a_{te} versus δ are plotted in Figure 95 - Figure 97. In these figures, the correlation lines are calculated via Equations (70) and (71) utilizing linear regression. Moreover, according Equations (72) and (73), we get the initial values of c_0 and c_1 at 0.633 and 12.423, respectively.

Table 11. Parameters of KAHR- a_{te} model, one-element retardation function

Parameter	PEEK			PPS		
	118-130°C	125-130°C	120-130°C	63-73°C	67-73°C	57-73°C
ζ	965.6	1361.3	855.2	260.1	347.4	171.4
b	5.360×10^{-4}	5.308×10^{-3}	1.675×10^{-3}	0.904	0.567	1.413
c_0	0.567	0.319	0.493	0.663	0.669	0.631
c_1	3.043	1.717	4.337	10.761	8.441	19.839
$\tilde{\tau}$	780.1	495.9	171.2	609.2	262.8	3319.3
$\tilde{\beta}$	0.174	0.123	0.118	0.111	0.119	0.067

$$c_{1,initial} = \frac{\sum_{i=1}^3 m_i}{\sum_{i=1}^3 \zeta_i} \ln 10 = 12.422 \quad (75)$$

$$c_{0,initial} = \exp \left(\frac{\sum_{i=1}^3 p_i}{3c_{1,initial}} \ln 10 \right) = 0.633 \quad (76)$$

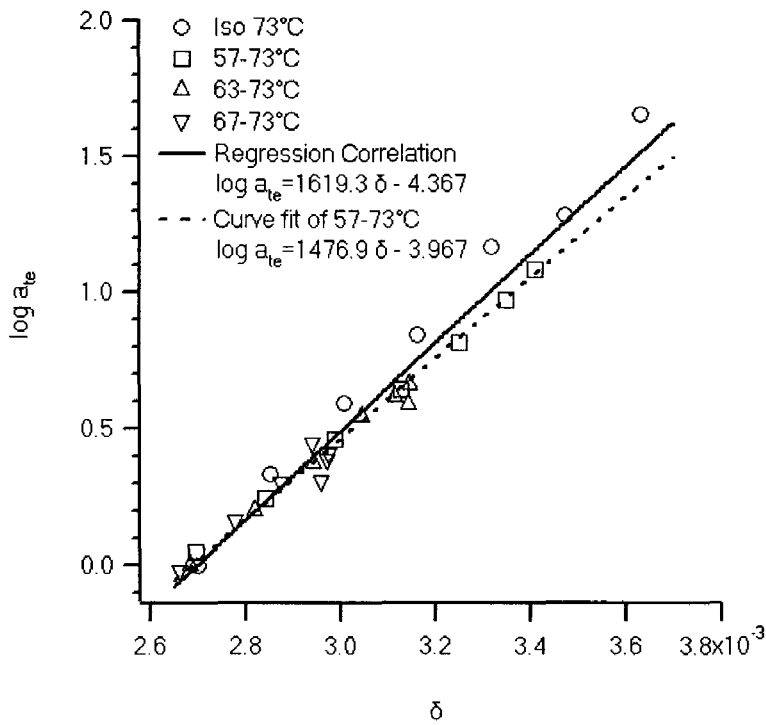


Figure 95. Correlation of $\log a_{te}$ and δ for PPS, based the parameter frame of 57-73°C

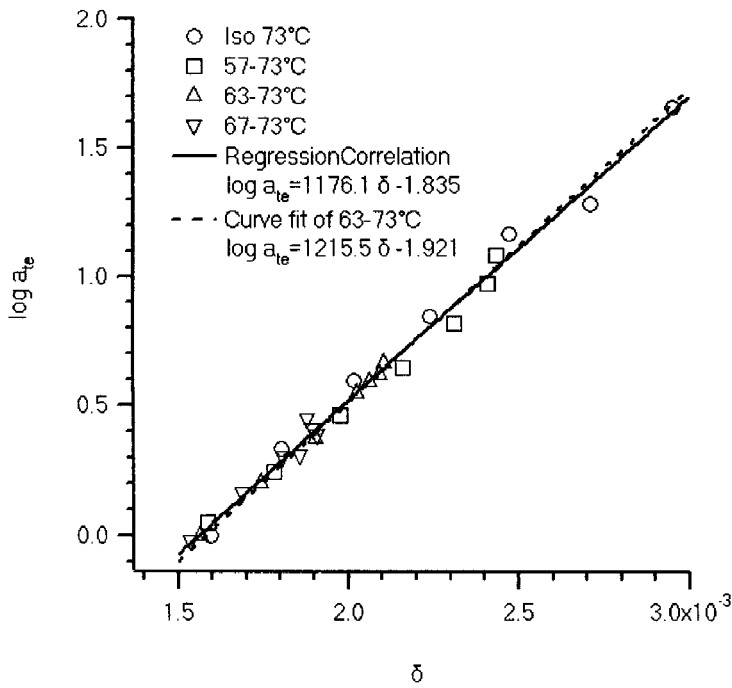


Figure 96. Correlation of $\log a_{te}$ and δ for PPS, based the parameter frame of 63-73°C

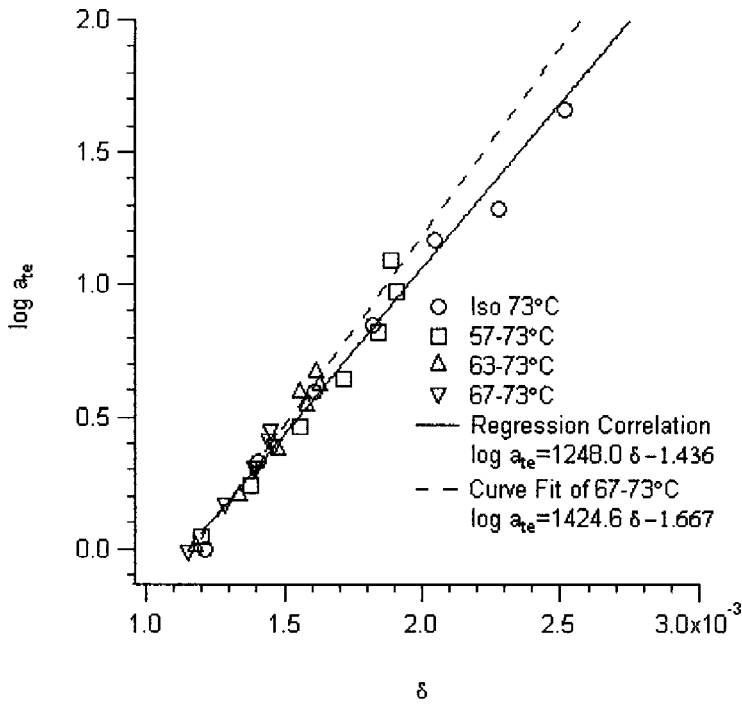


Figure 97. Correlation of $\log a_{te}$ and δ for PPS, based the parameter frame of 67-73°C
 Fix c_0 and c_1 with these numbers, other four parameters, shown in Table 12, are found by the curve fitting program

(2) Determine $\tilde{\tau}$ and $\tilde{\beta}$

The KHAR- α_{te} program is then run using c_0 and c_1 fixed to the values determined above. The resulting model parameters are shown in Table 12. Applying the parameters in Table 12, the stretched exponential functions $R(z)$ of 57-73°C, 63-73°C, 67-73°C and their average ($R_{avg}(z)$) are depicted in Figure 98. The reduced time z is evaluated by resolving the ordinary differential equation Equation (66) for each experimental condition. Numerically, calculate the $\ln z$ and corresponding $\ln(-\ln R_{avg}(z))$, then plot them in Figure 99. The linear regression of the data indicates a formulation of the straight line. Using Equation (74), the initial $\tilde{\tau}$ and $\tilde{\beta}$ are found from the regression function in Figure 99.

$$\tilde{\beta} = 0.0916 \quad (77)$$

$$\tilde{\tau} = e^{\left(\frac{0.565}{\tilde{\beta}_{initial}}\right)} = 477.289 \quad (78)$$

Table 12. Parameters of KAHR- α_{te} model, PPS; with $c_0 = 0.633$, $c_1 = 12.422$

Parameter	Thermal History		
	63-73°C	67-73°C	57-73°C
ζ	297.5	362.2	176.5
b	0.757	0.437	1.416
$\tilde{\tau}$	106.7	57.8	9913.1
$\tilde{\beta}$	0.0855	0.0903	0.105

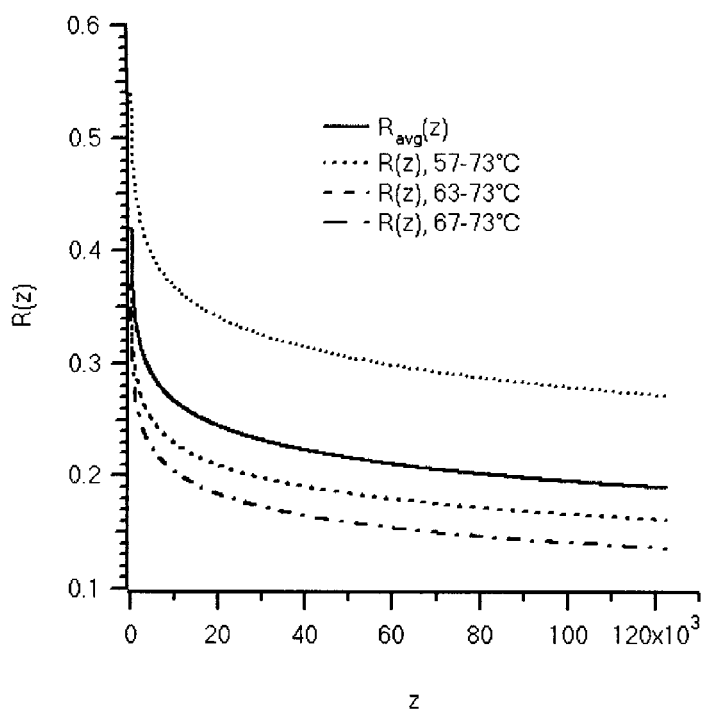


Figure 98. Average retardation function and retardation functions of three individual up-jump thermal histories for PPS

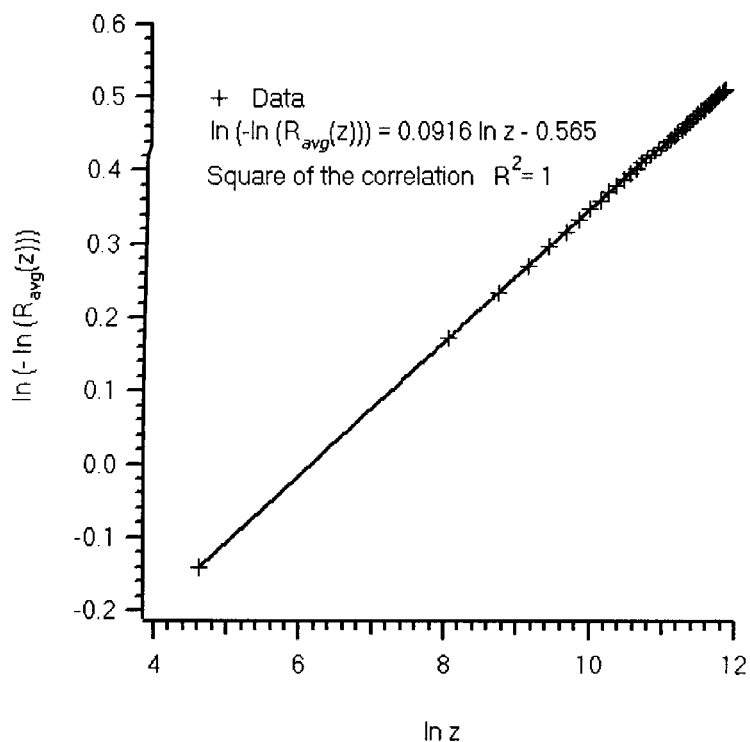


Figure 99. Data and regression of $\ln(-\ln R_{avg}(z))$ vs. $\ln z$ for PPS

(3) Determine ζ and b

At this point, parameters c_0 , c_1 , $\tilde{\tau}$ and $\tilde{\beta}$ are known for this optimization cycle. Next, ζ_i and b_i are finally determined by the curve fitting program for KARRH- a_{te} model using the fixed values of c_0 , c_1 , $\tilde{\tau}$ and $\tilde{\beta}$; the results are shown in Table 13. The average and maximum percent error are less than the limit of convergence criterion; this indicates the parameters are converged. As such, the optimization procedure is complete and the average ζ_i and b_i in Table 13 become ζ and b for the optimal values.

Table 13. KARRH- a_{te} model values ζ and b , PPS; with $c_0 = 0.633$, $c_1 = 12.422$, $\tilde{\tau} = 477.289$, and $\tilde{\beta} = 0.0916$

Parameter	Fits				Error (%)	
	57-73 °C	63-73 °C	67-73 °C	Average	Avg.	Max.
ζ	251.358	252.703	257.390	253.817	0.939	1.408
b	0.976	0.924	0.858	0.919	4.461	6.638

By the same method, the optimal parameters for PEEK can be identified using nonisothermal temperature histories 118-130°C, 120-130°C, and 125-130°C. The resulting values c_0 , c_1 , $\tilde{\tau}$ and $\tilde{\beta}$ from the first two steps for PEEK are 0.568, 4.447, 986.831, and 0.155, respectively. In the third step, the KARRH- a_{te} model finds the ζ and b for each thermal history; these are listed in Table 14. According the convergence criterion, the average values of ζ and b in Table 14 are considered as the optimal parameters and the procedure is stopped.

Table 14. KAHR- a_{te} model values ζ and b , PEEK; with $c_0 = 0.568$, $c_1 = 4.447$, $\bar{\tau} = 986.831$, and $\tilde{\beta} = 0.155$

Parameter	Fit				Error (%)	
	118-130 °C	120-130 °C	125-130 °C	Average	Avg.	Max.
ζ	647.356	630.852	705.102	661.103	4.427	6.625
b	0.226	0.258	0.211	0.232	7.615	11.207

6.4.3 Aging Shift Factor Prediction

The parameters identified by the optimization method are applied to predict aging shift factors under both isothermal and nonisothermal conditions. The results of PEEK and PPS are shown in Figure 100 and Figure 101; the fits obtained between the data and predictions are excellent for all cases. This can be quantified using the RMS percent error between the prediction and fitting curve of experimental data; these are listed in Table 15.

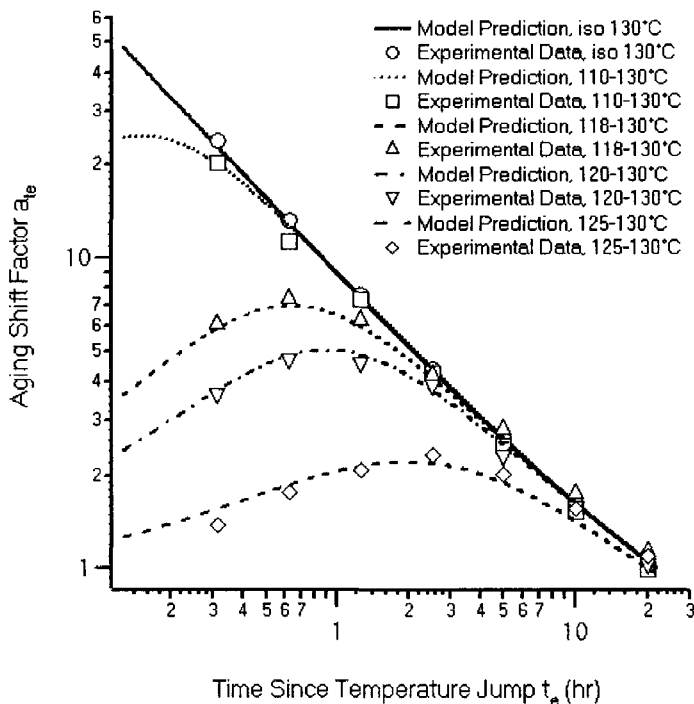


Figure 100. Prediction of aging shift factor for PEEK using optimal KAHR- a_{te} model

parameters

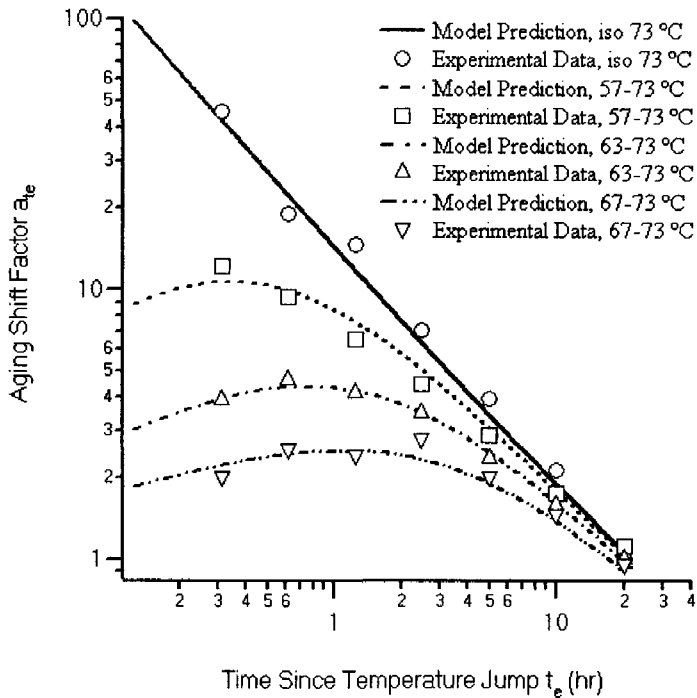


Figure 101. Prediction of aging shift factor for PPS using optimal KAHR- a_{te} model parameters

Table 15. RMS error between data and prediction of KAHR- a_{te} model

PEEK	RMS Error (%)	PPS	RMS Error (%)
110-130°C	7.53	57-73°C	5.69
Prediction of 118-130°C	3.50	Prediction of 63-73°C	2.55
Optimization 120-130°C	8.30	Optimization 67-73°C	6.26
Method 125-130°C	9.15	Method Iso 73°C	6.21
Iso 130°C	4.80		
Average Error	6.66	Average Error	5.18

The average RMS errors in Table 15 are smaller than all of errors obtained from the predictions using parameters fitted single thermal history as reported in Table 10. The prediction curves can capture all of the experimental findings very well. These validate

that the optimization method can seek a single parameter set which provides a better description of the data over various thermal histories versus those from any single test set.

For completeness, the optimal model parameters for PPS and PEEK are listed in Table 16. Comparison of model predictions and testing results for other temperature scenarios for PPS is shown in Figure 102. It is clear that the optimal parameter set of KAHR- a_{te} model successfully characterizes nonisothermal physical aging after several temperature jumps. Since the model coefficients were determined from a series of single temperature jump histories, this work demonstrates that the KAHR- a_{te} model has the capacity of predicting material response for more complicated thermal conditions.

Table 16. Optimal KAHR- a_{te} model parameters for PPS and PEEK obtained from three up-jump data sets by an optimization procedure

Material	ζ (unitless)	b (unitless)	θ (K ⁻¹)	c_0 (unitless)	c_1 (unitless)	$\bar{\tau}$ (second)	$\bar{\beta}$ (unitless)
PPS	253.8	0.919	0.255	0.633	12.422	477.3	0.092
PEEK	661.1	0.232	0.375	0.568	4.447	986.8	0.155

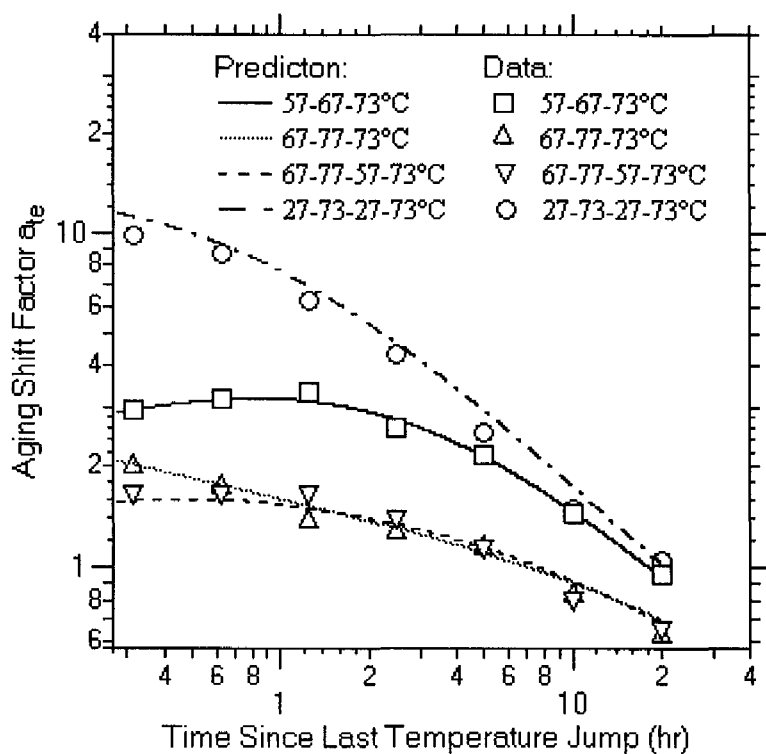
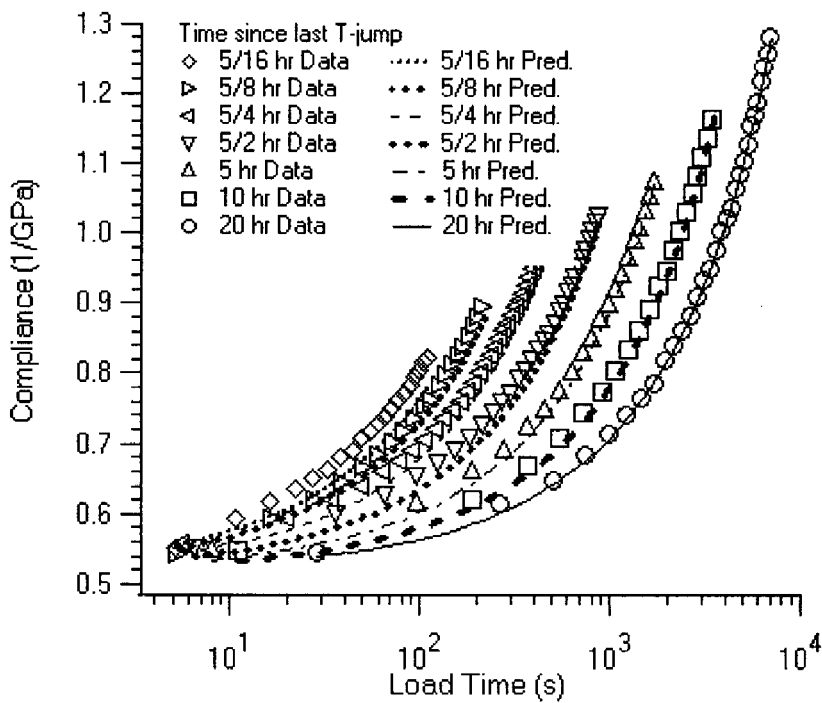


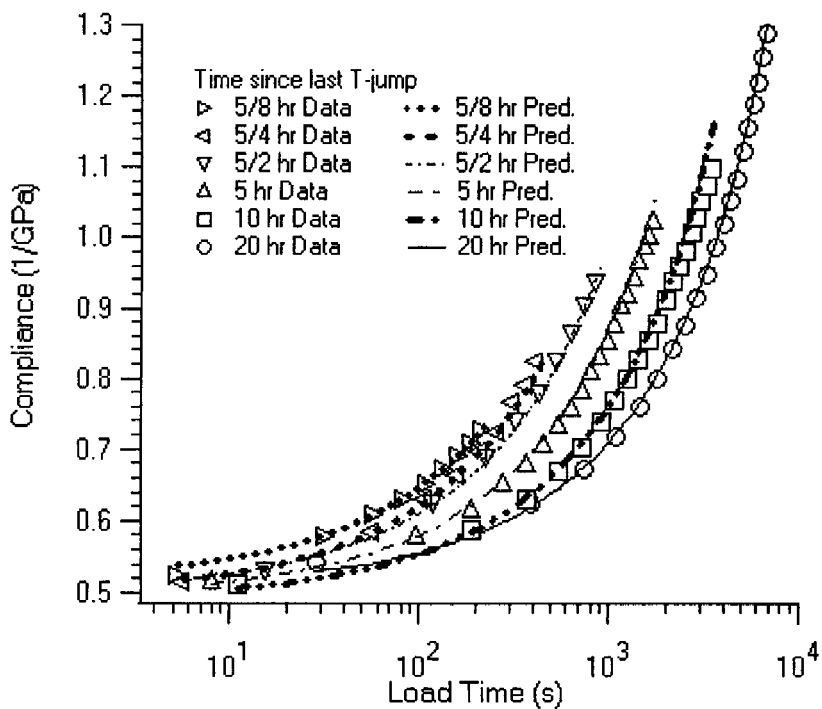
Figure 102. Prediction of mechanical aging shift factor by KAHR- a_{te} model for various complex thermal histories in PPS

6.4.4 Prediction of Compliance after Temperature Jumps

According to the shift factors output from the KAHR- a_{te} model, compliance curves can be predicted for each thermal condition. Figure 103 illustrates creep responses for 110-130 °C and 120-130 °C of PEEK, maximal %2 and %5 vertical shifts are applied for these two thermal histories, respectively. The predicted compliance can demonstrate the data very well except for the first curve of the whole family. The reason for that is that the compliance value close to the change of temperature is affected by the dwell temperature, at which the specimen aged for a period.



(a)



(b)

Figure 103. Compliance of experimental data and model predictions for PEEK:
 (a) 110-130°C; (b): 120-130°C

Since the compliance predictions for PPS material have similar results as shown above for PEEK, the results for PPS will not be presented for the purpose of brevity.

6.5 Prediction of Aging Shift Factors at Various Temperatures

The creep properties of nonisothermal aging discussed so far were examined at a single temperature (130 °C and 73 °C for PEEK and PPS, respectively) after multiple temperature steps. This means that the KAHR- a_{te} model parameters were developed from tests at a single temperature following various thermal histories. Although the model parameters were determined by single step temperature up jumps with the identical final temperature, it is possible to extend the predictive ability of KAHR- a_{te} model to other final temperatures.

In order to accomplish this, a temperature shift factor $a_{T,\delta}$ must be introduced to allow parameters c_0 and c_1 to relate the predicted a_δ with the aging shift factors a_{te} at another temperature. The reason for $a_{T,\delta}$ is that the reference curve of a_{te} is currently defined on the non-equilibrium state of polymers at a particular aging time (t_{ref}) and a particular temperature (T_{ref} , 130 °C and 73 °C for PEEK and PPS in previous examples, respectively). In other words, the reference curves for a_{te} depend on thermal histories while the temperature shift factor a_T and structural shift factor a_δ in the KAHR model are defined to link the retardation time at a reference temperature T_r in equilibrium ($\delta = 0$) to the retardation time at temperature T and $\delta \neq 0$. This significant difference requires a shift factor, $a_{T,\delta}$ which scales a_δ at the reference aging time from the temperature under

consideration to the reference temperature; this permits the use of the model parameters obtained from the reference temperature to predict material response at different temperatures.

As described above, $a_{T,\delta}$ is defined as:

$$a_{T,\delta} = \frac{a_{\delta,iso}(T_r, t_{ref})}{a_{\delta,iso}(T, t_{ref})} \quad (79)$$

where the $a_{\delta,iso}(T_r, t_{ref})$ is the isothermal structural shift factor at the reference aging time t_{ref} at temperature T_r , at which the KAHR- a_{te} model parameters were identified. Similarly, $a_{\delta,iso}(T, t_{ref})$ is the isothermal structural shift factor at the reference aging time at temperature T using those same parameters. Thus, the correlation of a_{te} and a_{δ} is:

$$a_{te}(a_{\delta})|_T = \left(\frac{c_0}{a_{\delta} a_{T,\delta}} \right)^{c_1}; \text{ constants } c_0, c_1 > 0 \quad (80)$$

The KAHR- a_{te} model maps structural shift factor a_{δ} to aging shift factor a_{te} by parameters c_0 and c_1 at the reference temperature. The aging temperature factor $a_{T,\delta}$ couples predicted a_{δ} and a_{te} for the reference curves at other temperatures and therefore enables the model to predict aging shift factors in wider temperature ranges.

As proposed in Equation (80), the KAHR- a_{te} model assumes parallel linear relationships between a_{δ} and a_{te} in log-log space for different final temperatures below T_g , with parameter c_1 being the slope of these straight lines and $c_0 / a_{T,\delta}$ representing the intercept. Equations (79) and (80) are applied to predict viscoelastic response at 67 °C for PPS. Figure 104 shows the experimental data and prediction of a_{te} on thermal history

97 °C → 57 °C → 73 °C → 67 °C, model parameters are listed in Table 16. The structural shift factor at reference aging time on 67 °C, $a_{\delta}(67^{\circ}\text{C}, t_e = 72000\text{sec})$ is equal to 0.5673; similarly, the reference structural shift factor on reference temperature $a_{\delta}(73^{\circ}\text{C}, 72000\text{sec}) = 0.6300$. Therefore, $a_{T,\delta} = 0.5673/0.6300 = 0.9005$. As shown in Figure 104, the model involving the $a_{T,\delta}$ term results in excellent prediction. Hence, this approach is validated by experiment on the specific thermal history whose final temperature is different (but not far away) from the temperature at which model parameters were identified.

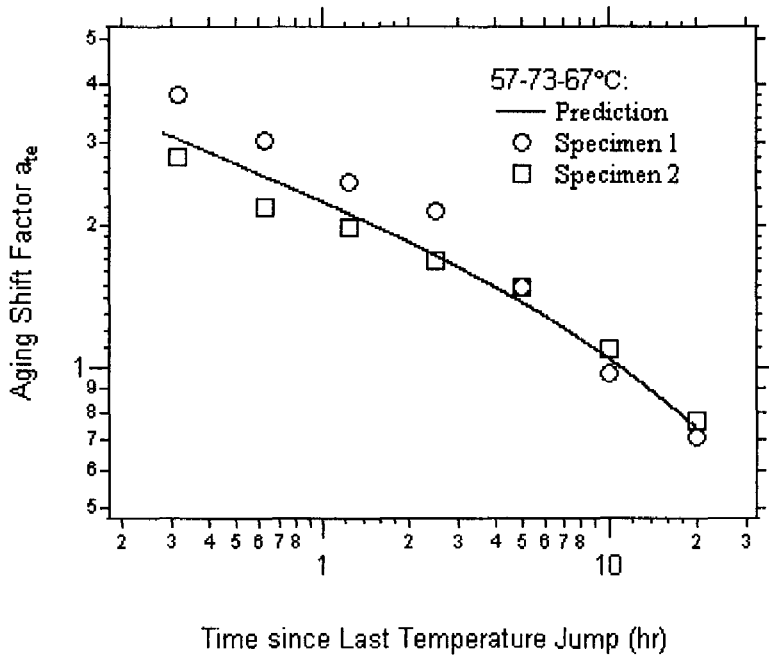


Figure 104. Prediction of mechanical aging shift factor of PPS by KAHR- a_{te} model for thermal history: 97° C → 57° C (4hr) → 73° C (6hr) → 67° C. Reference curve is the isothermal compliance response at 67 °C with aging time = 20 hours

Two additional examples for predictions of nonisothermal mechanical shift factors at different temperatures are shown in Figure 105 and Figure 106. The predictions also match experimental data quite well. These encouraging results indicate that this

“parallel line” assumption (Equation (80)) is valid within our experimental range. The retardation function $R(z)$ utilized in this study considered a single Kohlrausch (stretched exponential) function; including additional terms as either a Kohlrausch or Prony series might better describe the viscoelastic response after complex thermal treatments. These considerations will be examined in future work.

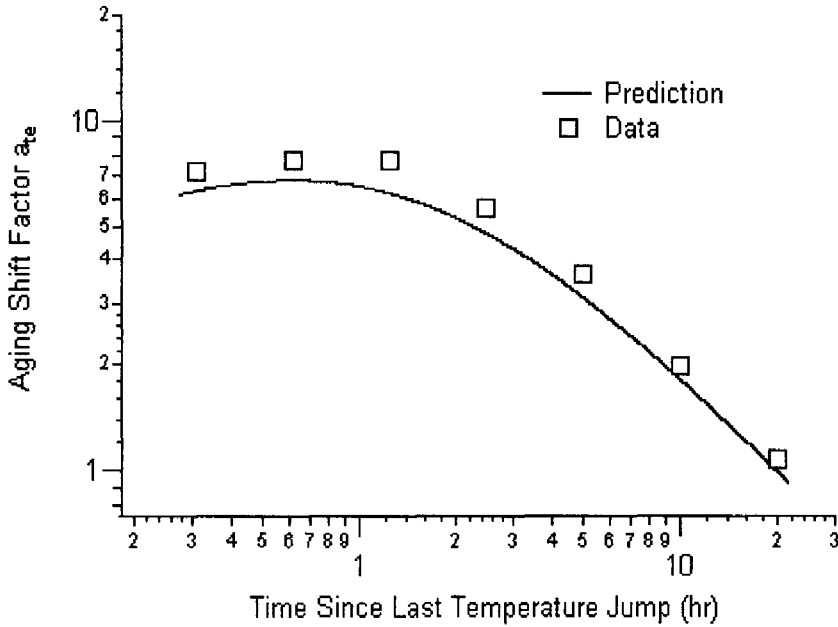


Figure 105. Prediction of mechanical aging shift factor of PPS by KAHR- a_{te} model for thermal history: $97^{\circ}\text{C} \rightarrow 57^{\circ}\text{C}$ (14hr) $\rightarrow 67^{\circ}\text{C}$; reference curve is the isothermal compliance response at 67°C with aging time = 20 hours and KAHR model uses parameters from Table 16

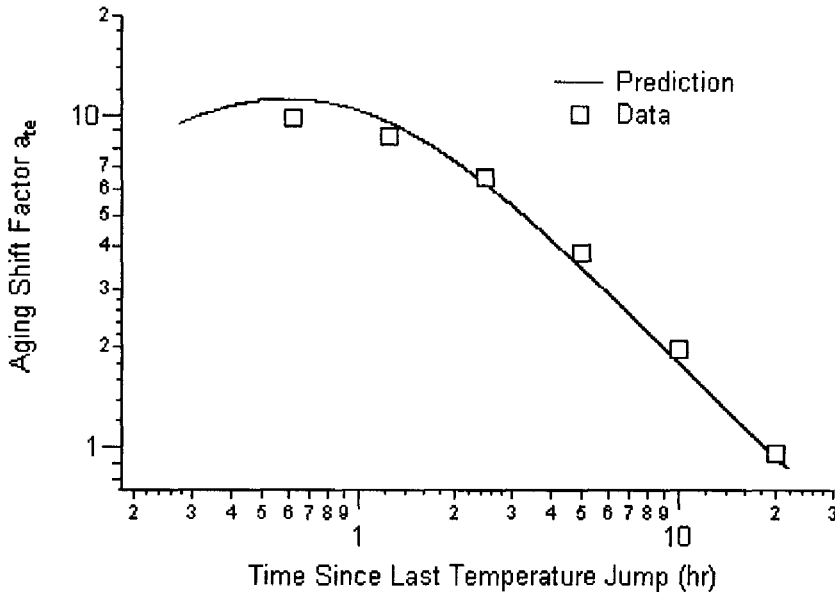


Figure 106. Prediction of mechanical aging shift factor of PEEK by KAHR- a_{te} model for thermal history: 148° C → 110° C (14hr) → 120° C; reference curve is the isothermal compliance response at 120° C with aging time = 20 hours and KAHR model uses parameters from Table 16

6.6 Prediction of Long-Term Response of PPS in Nonisothermal Aging

Long-term mechanical behavior of glassy polymers is a critical issue for many structural applications using polymer based materials. During their service life, the viscoelastic properties of polymers can be strongly affected by physical aging, especially as temperatures approach the glass transition temperature T_g . Hence, the effects of physical aging on mechanical responses have received a great deal of attention in the past several decades. While isothermal long-term physical aging has been extensively studied, long-term mechanical properties with physical aging effects after a varying temperature history has received far less scrutiny. This section represents the study on long-term response of PPS in nonisothermal physical aging, experimental results and predictive method will be reported below.

6.6.1 Effective Time Theory

Consider an isothermal aging creep test with an initial aging time of t_e^0 . At a later moment in the test, the aging time will be $t_e^0 + t$, where t is the time elapsed from load initiation (stress or strain, corresponding to creep or stress relaxation, respectively). When the testing time t approaches and exceeds the value of the initial aging time t_e^0 , one would expect deviation of the long-term creep/stress relaxation response from the momentary (i.e. short-term) response due to the change in the material aging state. Taking the initial aging time t_e^0 to be the reference aging time ($t_{ref} = t_e^0$) of the reference (momentary master) curve, the shift factor at any instant in time can be defined based on the shift rate μ (Struik, 1978):

$$a_{te}^0(t) = \left(\frac{t_e^0}{t_e^0 + t} \right)^\mu \quad (81)$$

To account for the cumulative effects of aging, the effective time increment $d\lambda$ corresponding to a real time increment dt is then defined:

$$d\lambda = a_{te}^0(t)dt \quad (82)$$

By integration, the total test time can be related to the effective time, $\lambda(t)$:

$$\lambda(t) = \int_0^t a_{te}^0(\xi)d\xi \quad (83)$$

Using the effective time in place of real time in the Kohlrausch function

$$D(t) = D_0 e^{(\lambda/\tau)^\beta} \quad (84)$$

results in a prediction of long-term creep response, where D_0 is initial compliance, τ is the relaxation time, and β is the stretch parameter of the MMC at $t_e^0 = t_{ref}$.

In isothermal physical aging, the shift rate is defined as $\mu = -d \log a_{te} / d \log t_e$; this reflects the fact that the shift factors a_{te} versus t_e form a straight line in log-log space. However, in nonisothermal cases, the plot of $\log a_{te}$ with $\log t_e$ is no longer a line, thus the shift rate is not constant but a function of time. Bradshaw and Brinson (1997d) introduced the concept of “effective aging time” to account for the nonlinear aging effects following a temperature jump. In their work, continuous aging shift factor information under single temperature up-jump or down-jump condition was exacted using effective time theory. This method might be used to predict long-term response for nonisothermal aging.

In current work, an alternate approach is considered. During nonisothermal physical aging, aging shift rate is denoted as $\mu^*(\xi)$, the effective time $\lambda^*(t)$ is given by:

$$a_{te} = \left(\frac{t_e^0}{t_e^0 + t} \right)^{\mu^*(\xi)} \rightarrow \lambda^*(t) = \int_0^t \left(\frac{t_e^0}{t_e^0 + \xi} \right)^{\mu^*(\xi)} d\xi \quad (85)$$

Note that $\mu^*(\xi)$ should approach the isothermal shift rate μ of the final temperature if time is long enough since the last temperature jump.

6.6.2 Determination of μ^* and λ^*

In order to create long-term predictions, the effective time $\lambda^*(t)$ must first be

obtained from a given shift factor data set obtained from either a nonisothermal physical aging test or from KAHR model predictions. One approach to determine λ^* would be to evaluate the integral in Equation (83) directly, using either a_{te} data points (approximated by a suitable, integrable function) or KAHR- a_{te} predictions of a_{te} . Alternately, the nonisothermal aging shift rate μ^* could first be evaluated based upon the a_{te} data / prediction and then utilized in Equation (85). Both approaches lead to similar results; findings utilizing the aging shift rate μ^* are considered to below to highlight one aspect of the long-term test results.

The aging shift rate can be written by:

$$\mu^*(t_e) = -\frac{d \log a_{te}}{d \log t_e}; t_e = t_e^0 + t \quad (86)$$

where t_e is the nonisothermal aging time, defined as the time elapsed since last temperature jump, t_e^0 is initial aging time when a long-term creep test starts, t is the loading time of the creep test. Note that the shift rate μ^* after multiple temperature jumps is a function of the test time t in long-term experiments. If the test time t is long enough, μ^* at a distant time after the changes of temperature should approach the isothermal shift rate μ_{iso} of the test temperature; this is equivalent to the “fading memory” concept, in which the material held at a single temperature long after various temperature steps begins to act as though it were only subjected to isothermal physical aging. Consequently, μ^* can be separated into two parts as $\mu^*(t) = \mu_{iso} + \tilde{\mu}(t)$, where $\tilde{\mu}(t)$ represents the difference of aging shift rate in isothermal and nonisothermal conditions.

The shift rate function $\mu^*(t_e)$ can be obtained from the predicted aging shift factors or experimental data. In this study, KAHR- a_{te} predictions are used to determine shift rates after various temperature histories. Once the numerical values of shift rate are attained by Equation (86), suitable curves are chosen to fit the shift rate values over the loading time of creep tests for most thermal history cases. Figure 107 demonstrates aging shift rates for several nonisothermal cases right after the material reaching the final temperature (73 °C).

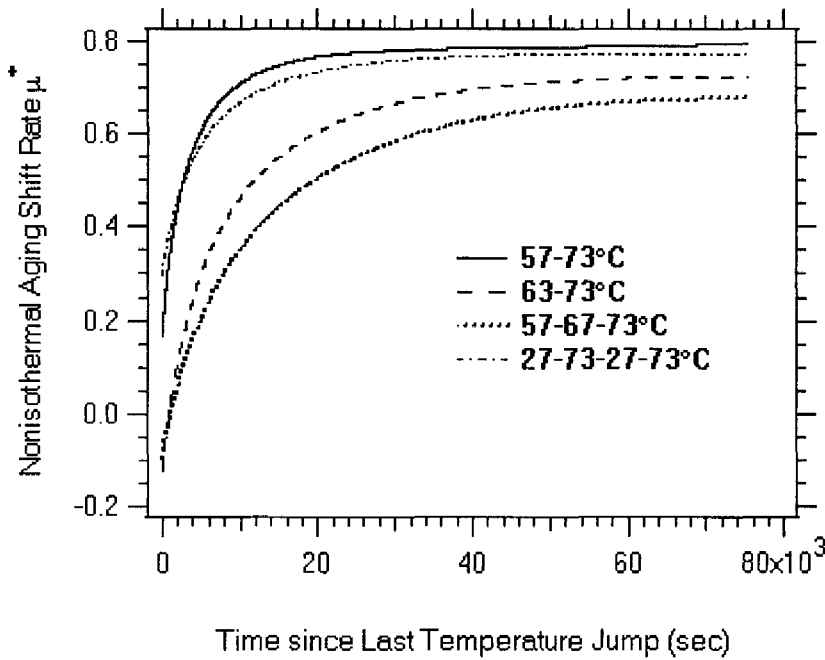


Figure 107. Nonisothermal aging shift rate μ^* for complex thermal histories, values of μ^* are calculated using the predicted a_{te} from KAHR- a_{te} model

Once suitable functions for μ^* are obtained, the effective time was found using a MATLAB program. Once the effective time has been evaluated, the long-term creep response subjected complicated thermal history can be predicted by Equation (84). Figure 108 shows calculated effective time over our long-term creep durations for several

thermal histories.

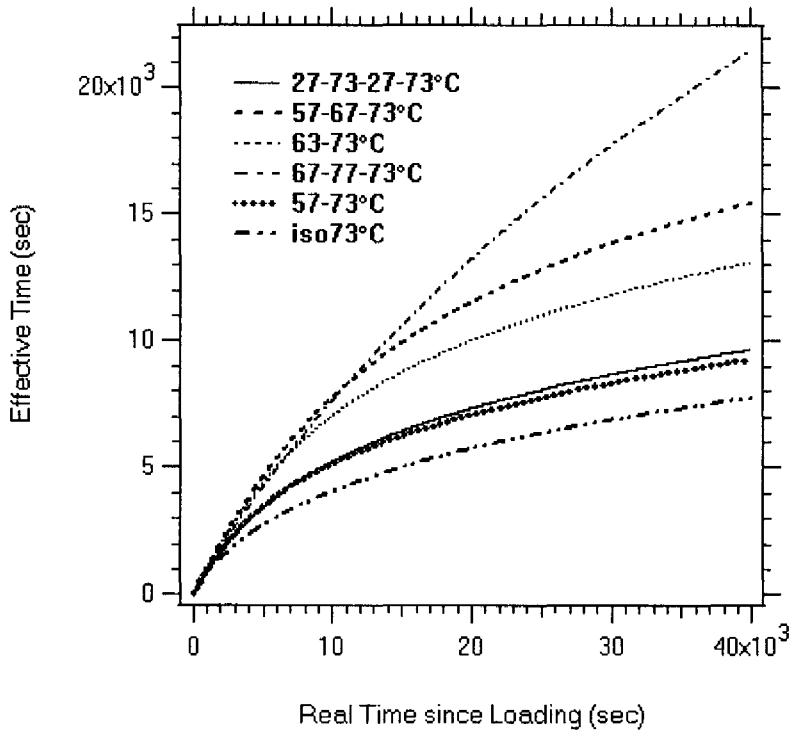


Figure 108. Calculated effective time for several isothermal and nonisothermal conditions

6.6.3 Predictions Long-term Response for Various Thermal Histories

Once the effective time λ^* has been calculated, it can be used to predict long-term response of a polymer during nonisothermal physical aging. From the short-term creep test results demonstrated above (compliance in time zone 1), Kohlrausch function parameters D_0 , τ and β were identified. Using these parameters and effective time λ^* in Equation (84), the long-term compliance prediction is obtained. Figure 109 and Figure 110 illustrate compliance predictions for long-term creep by using Kohlrausch function (Equation (84)). Parameters D_0 , τ and β from the short-term data are listed in Table 17. For the purpose of comparison, Kohlrausch functions in the effective time and real time

domain are shown in these two figures. It is clear that the model predictions based effective time theory lead to good agreement with the experimental findings in this dissertation in all of the thermal histories considered. The results from original Kohlrausch equation, which capture short time response very well, depart from the experimental data when the loading time is long enough. (i.e. $t_e^0 + t \gg t_e^0$)

In order to predict the long-term creep behavior after a nonisothermal temperature history, one needs to first perform a short-term test under the identical thermal condition and then obtain Kohlrausch function parameters of the short-term compliance curve. The aging shift factors a_{te} in the duration of long-term test are predicted by the KAHR- a_{te} model using parameters in Table 16. These a_{te} are with Equation (85) - (86) to calculate effective time λ^* . The long-term compliance is finally predicted by Equation (84) by inserting λ^* and Kohlrausch function parameters D_0 , τ and β from the short-term test.

Table 17. Parameters of Kohlrausch function to fit short-term creep response

Thermal History	D_0 (1/GPa)	τ (second)	β (unitless)
97 °C→57 °C→73 °C	0.453	1603	0.478
97 °C→63 °C→73 °C	0.461	3287	0.523
97 °C→57 °C→67 °C→73 °C	0.528	3176	0.469
97 °C→67 °C→77 °C→73 °C	0.523	6463	0.437

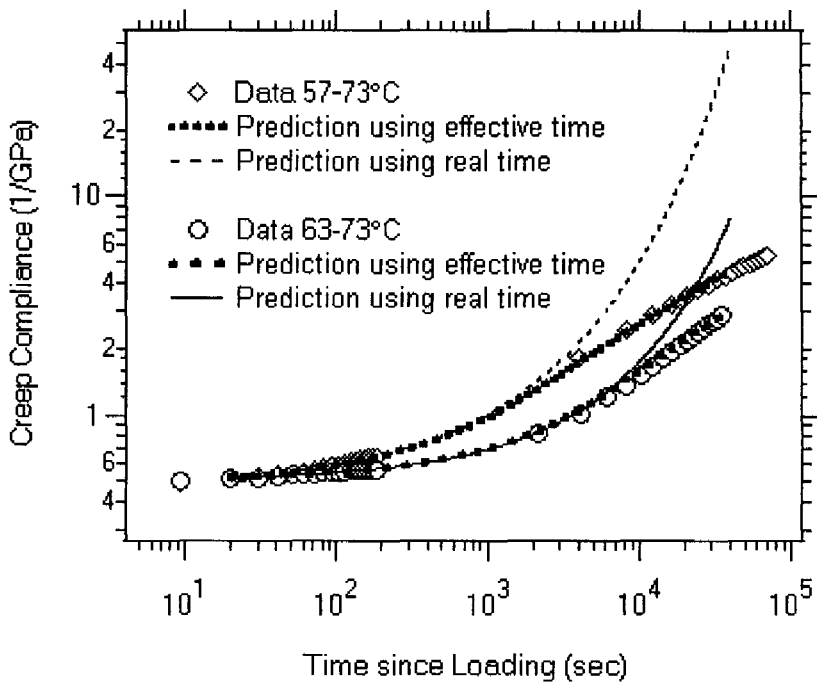


Figure 109. Long-term creep predictions by effective time theory and original Kohlrausch function from short-term response; thermal Histories: 97 °C → 57 °C → 73 °C and 97 °C → 63 °C → 73 °C

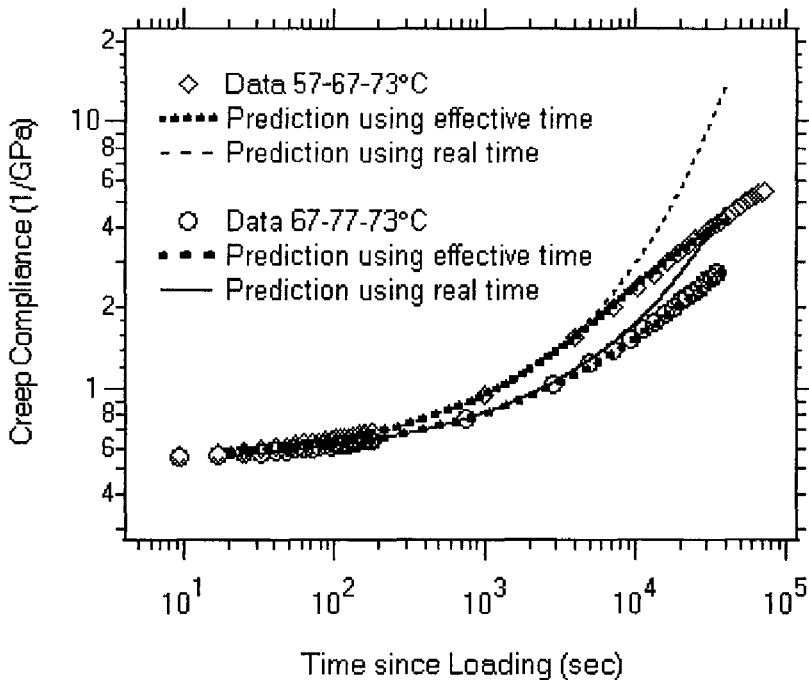


Figure 110. Long-term creep predictions by effective time theory and original Kohlrausch function from short-term response; thermal Histories: 97 °C → 57 °C → 67 °C → 73 °C and 97 °C → 67 °C → 77 °C → 73 °C

Figure 111 depicts the prediction and data for a more complicated thermal treatment: 97 °C → 27 °C (12 hr) → 73 °C (1 hr) → 27 °C (1 hr) → 73 °C. In this test, the specimen experienced temperature changes in a wide range; and the creep duration was 100 hours. The aim for this investigation is to examine the capacities of nonisothermal effective time theory when the creep process is rather long, subjected to elevated varying thermal circumstances. As in Figure 109 and Figure 110, the predictions made using the unaged Kohlrausch function and with nonisothermal effective time theory using the KAHR- a_{te} model are plotted in Figure 111; good agreement is obtained between the data and the KAHR- a_{te} model prediction. In order to demonstrate the importance of properly assessing the aging state, Figure 111 also contains a prediction using effective time theory under isothermal conditions (i.e. Equation (81) and (83) using the isothermal shift rate). In a previous publication (Guo and Bradshaw, 2007), we identified the (isothermal) shift rate $\mu = 0.811$ via isothermal creep tests at 73 °C. As Figure 111 clearly demonstrates, the predictions using isothermal effective time theory overestimates the creep compliance after 1300 seconds since loading and is in significant disagreement with test data by the end of the test (more than 100% error). This indicates that isothermal physical aging approaches cannot be used to predict nonisothermal physical aging test data without significant modification. On the other hand, the numerical result utilizing the KAHR- a_{te} model matches the experimental finding fairly well, with errors at 10 and 100 hours since loading being 5.1% and 12.9%, respectively. Consider that the prediction is made by using the information from the first 180 seconds of this creep test and aging shift factors from KAHR- a_{te} calculation, this example shows good predictive abilities of nonisothermal effective time theory.

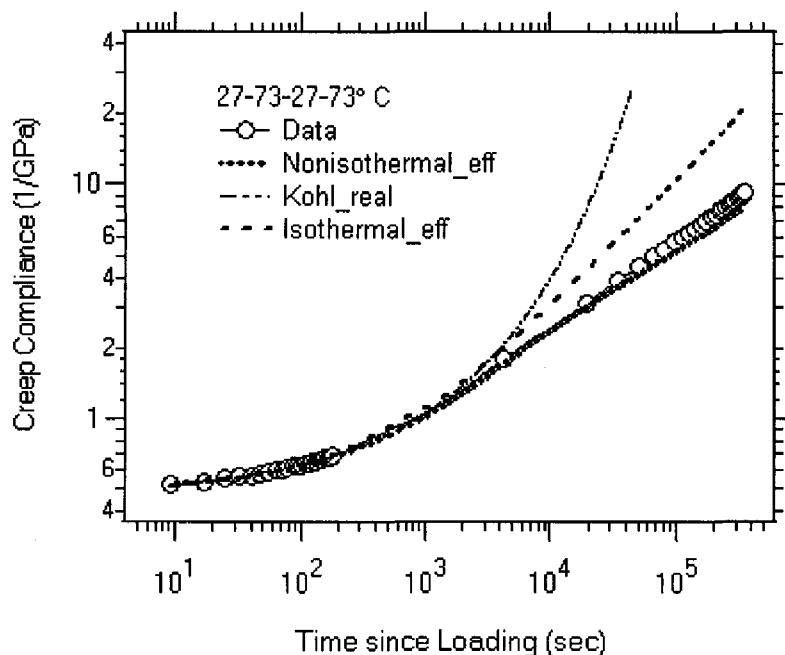


Figure 111. Long-term creep predictions by isothermal and nonisothermal effective time theory and original Kohlrausch function from short-term response; thermal histories: 97 °C → 27 °C → 73 °C → 27 °C → 73 °C. Kohlrausch function parameters: $D_0 = 0.460 \text{ GPa}^{-1}$, $\tau = 1593 \text{ second}$, and $\beta = 0.417$

Nonisothermal effective time based on predicted aging shift factors in Figure 104 for this thermal treatment was calculated for the long-term creep starting from 0.5 hour after reaching the final temperature (67° C). The long-term creep data sets and prediction by effective time theory are illustrated in Figure 112 with the associated Kohlrausch short-term fit parameters listed in the caption. The resulting long-term predictions are compared with the material responses found in two experiments using different samples. Due to the data scatter among individual tests revealed in previous section, the second data set in Figure 112 was shifted vertically by the amount of 4.5% prior to comparison to bring the short-term behavior in line for both data sets.

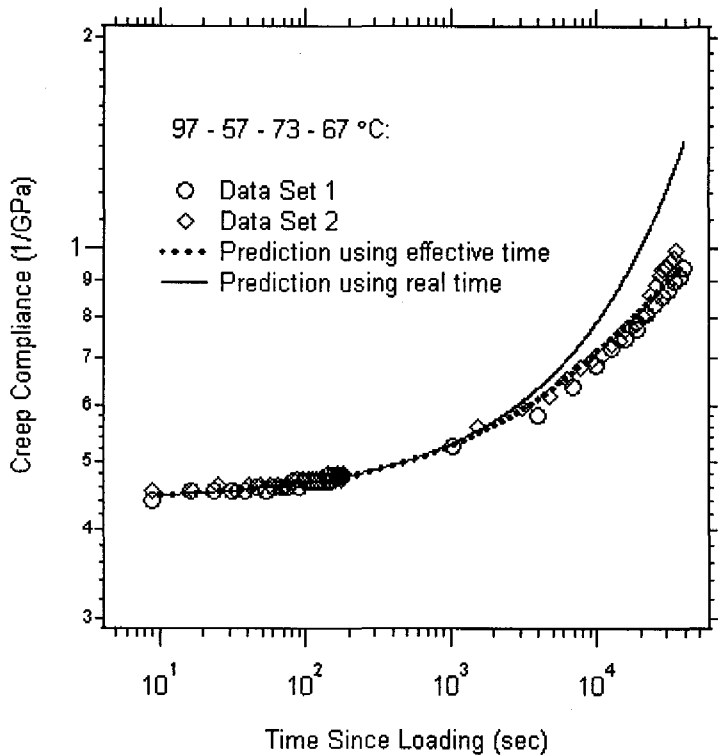


Figure 112. Long-term creep predictions by nonisothermal effective time theory and original Kohlrausch function from short-term response; the thermal history is: 97 °C → 57 °C → 73 °C → 67 °C. Kohlrausch function parameters: $D_0 = 0.432 \text{ GPa}^{-1}$, $\tau = 48929 \text{ second}$, and $\beta = 0.410$

These results demonstrate good agreement between nonisothermal effective time theory and long-term creep response data after multiple-step temperature histories. Note that the KAHR- a_{te} model plays a key role in modeling long-term viscoelastic properties, since it describes isothermal and nonisothermal aging shift factors, which are the basis for the calculation of effective time.

Although the prediction on the thermal history 97 °C → 57 °C → 73 °C → 67 °C match the experimental findings quite well, this should not be interpreted as meaning that the model can provide reliable results to arbitrary thermal histories ending at any temperature. The example shown in Figure 112 indicates the theory is applicable when the final temperature is not far from the reference temperature at which the model

parameters are identified; moreover, Equation (79) and (80) need to be examined in a wider temperature range in future work to better understand the limitations of this approach.

CHAPTER 7

PHYSICAL AGING NEAR GLASS TRANSITION TEMPERATURE

Physical aging near the glass transition temperature of PPS will be presented in this chapter. The test temperature close to T_g allows the specimen reach equilibrium after isothermal or nonisothermal temperature jumps, as such, the classic phenomenology of structural relaxation mentioned previously can be pursued by mechanical testing (physical aging) in a temperature range near T_g .

7.1 Aging into Equilibrium under Isothermal Conditions

This section focuses upon investigation of physical aging behavior of thermoplastics PPS near T_g , in order to provide kinematic observation of mechanical properties of polymers when they approach to the structural equilibrium states at various temperatures. The phenomenon of aging into equilibrium at several constant temperatures will be examined by the current work.

7.1.1 Background

Most of past investigations on physical aging were conducted at temperature at least 15 °C below T_g ; in this case, the material is in nonequilibrium state throughout the experiments and aging into equilibrium phenomenon could not likely be observed in the lab time scale. Therefore, there relatively are few data sets which demonstrate that the time required to reach structural equilibrium in physical aging and the temperature dependence of aging shift rate near glass transition. Lee and McKenna reported the aging shift factors at several aging times from small-strain stress relaxation tests of polypropylene oxide/DGEBA networks, at temperatures from 30°C to 5°C below T_g (Lee and McKenna, 1988). They observed aging into equilibrium near T_g (10°C and 5°C below) according to the change of aging shift rate, and the time of reaching equilibrium t^* was obtained. Interestingly, their experimental results of aging shift factors after t^* are slightly time-dependent and can be fitted by a straight line with a much lower slope than μ ; in this context t^* is defined as the point of intersection of the lines in the aging and slight aging regions (Lee and McKenna, 1988). Similar feature of aging shift factors from creep tests was also presented in another article by Lee and McKenna (Lee and McKenna, 1990a). Theoretically, aging shift factors should remain constant value when the material reaches the equilibrium state; however, their findings are relatively consistent with the finding of slight time-dependence. The reason for time dependence of a_{te} after t^* might be that material is still in the process of approaching final equilibrium at a slower rate as equilibrium is approached.

7.1.2 Test Method

This test method is similar to Struik's test method but with a significant modification. One common problem in the creep tests at temperature near T_g is that a small stress level applied to the specimen caused a very large strain if maintained for $t_e/10$ (standard Struik protocol). This is true even if the stress is known to be in the linear range. This leads to a very large calculated compliance value that may be inaccurate, especially if the large strain values cause the material to enter the nonlinear regime.

In order to correct this difficulty, the compliance limit method was developed to improve the physical aging tests performed near T_g (Wang, 2007). The difference between Struik's standard method and the compliance limitation method is in the loading time. The standard method uses 10% of the aging time at load application as loading time. In the compliance limitation method, however, a suitable compliance limit value is chosen based on creep test results. In this approach, the goal is to limit the amount of specimen deformation that occurs to ensure that the behavior remains in the linear regime. In order to accomplish this, the corresponding loading time for each aging creep test is specified appropriately. These loading times can be obtained by a full sequence test using the standard method or by limited testing.

The compliance limitation method is demonstrated based on compliance data in Figure 113 from Wang (2007). In this case, seven creep tests were performed using standard method, leading to the seven compliance curves shown. The initial and final compliances are about 0.7 and 1.8 GPa^{-1} , respectively; each of these can be converted to strain by multiplying by the applied stress σ_0 . A compliance limit value of 1.1 GPa^{-1} is

chosen; this limits the strain that will be achieved in every creep test by removing the load before the compliance value reaches 1.1 GPa^{-1} . The corresponding loading time is found for every test as 32 s, 50 s, 92 s, 165 s, 292 s, 523 s, and 1129 s compared to 112.5 s, 225s, 450 s, 900 s, 1800 s, 3600 s, and 7200 s for Struik's method at aging times 5/16, 5/8, 5/4, 5/2, 5, 10 and 20 hours, respectively. Clearly, the new loading times are much shorter than the standard ones and ensure that the observed compliances (or strains) are approximately within the limit of 1.1 GPa^{-1} initially specified. It should also be noted that this example is largely chosen for ease of illustration; in many cases close to T_g , the compliances obtained using the standard method are 1-2 orders of magnitude greater than the initial compliance and are likely well beyond the limitations of linear viscoelasticity (Wang, 2007).

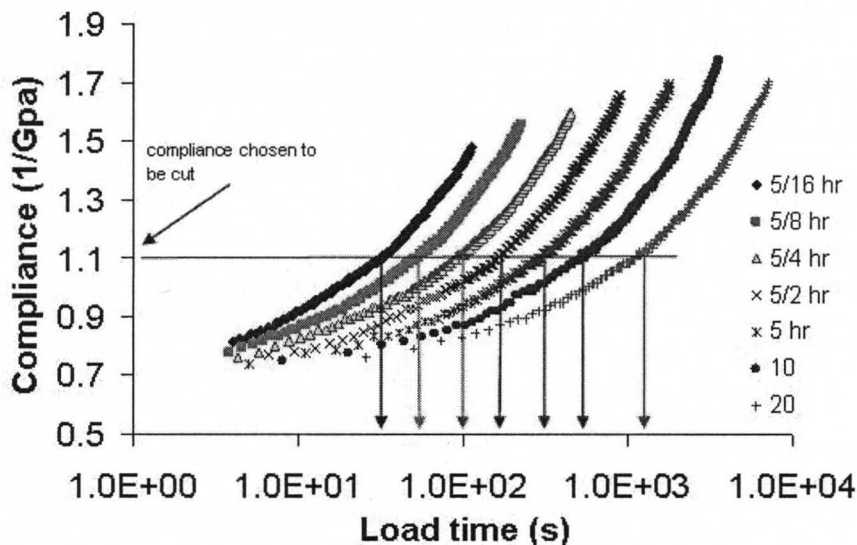


Figure 113. Compliance limitation physical aging test (Wang, 2007)

In this work, isothermal aging is characterized at 81°C , 82°C , 83°C , 84°C , and 85°C . At each temperature, aging times of the sequential creep tests start with 0.039 hours and end at aging times between 1.25 hours and 20 hours depending on the time

required to reach equilibrium. The compliance limit method was applied to determine the loading time after reaching equilibrium. Before equilibrium, loading times of creep were set as $0.1 t_e$ according to Struik standard method, since in these cases the loading time is short enough that no significant deformation occurs during momentary creep tests. Stress levels applied in creep tests keep within linear viscoelastic regions at the test temperatures. For each temperature, at least three separate tests were performed using different specimens to validate that the experiments are reproducible. Further experimental details will be presented in next section.

7.1.3 Results and Discussion

Sequential creep tests lead to compliance curves at various aging times, as described by Equation (45). Figure 114 depicts the compliance curves of a specimen at 82°C , with aging times varying from 0.039 hours to 5 hours. It is readily apparent that at first several aging times the compliance curves shift to right with increasing aging time; after 1.25 hour of aging the creep curves no longer shift to longer aging time, this indicates that the material attains the equilibrium state. The T_g of this material was determined by the peak of $\tan \delta$ and is 92.2°C . The applied stress is 1.22 MPa.

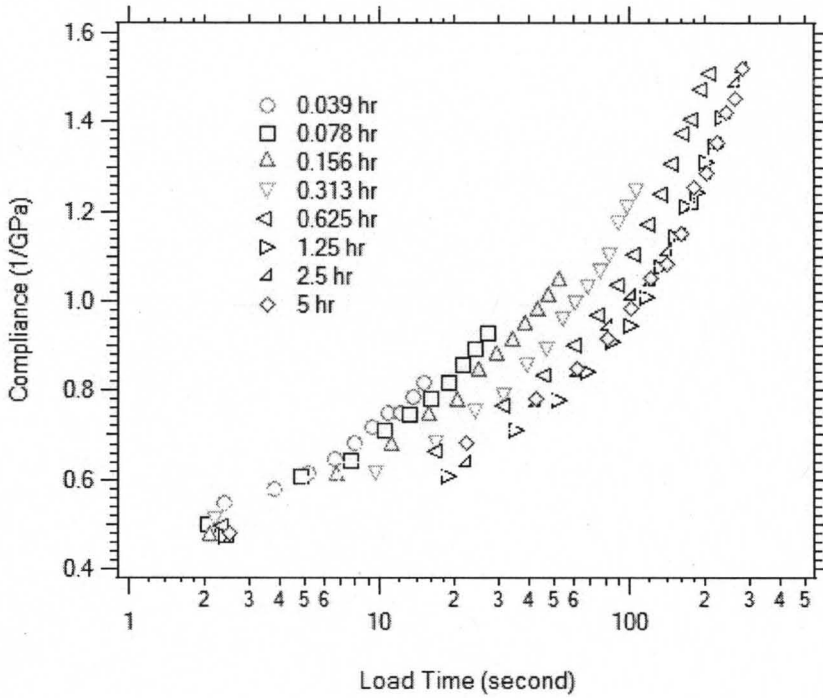


Figure 114. Compliance curves of PPS at 82°C for aging times from 0.039 hr to 5 hr

The associated aging shift factors of the compliance curves in Figure 114 were obtained by the time-aging time superposition principle. Reference aging time t_{eref} was selected as the longest aging time in the experiment, which is 5 hours in the case above. The corresponding aging shift factors versus aging time are plotted in double-logarithmic space, as shown in Figure 115. It can be seen that there is a sharp transition where the shift rate μ ($\mu = -\log a_{te} / \log t_e$) changes from a constant value (0.401) to virtually zero (0.0312). The time required to reach equilibrium t^* is 1.036 hour, determined by the intersection of line fits.

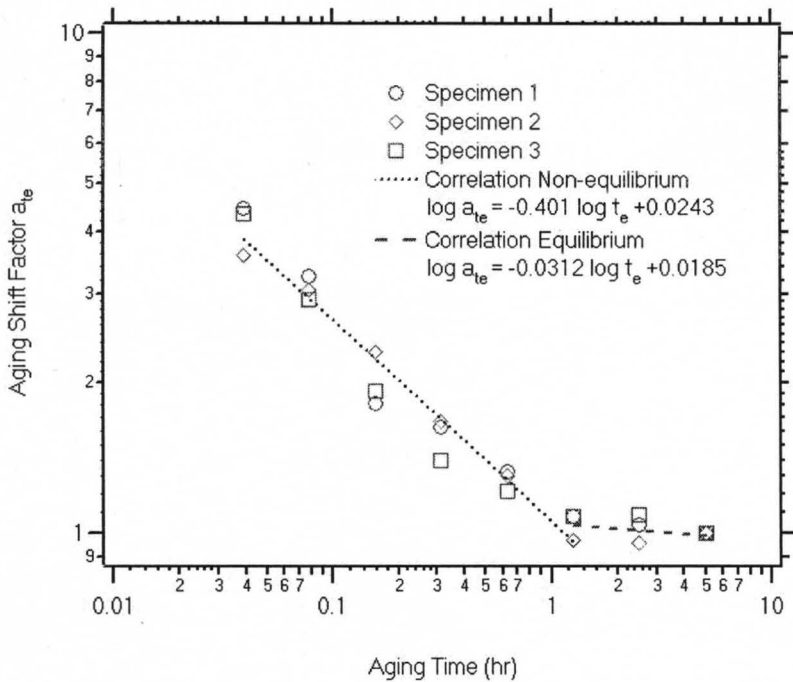


Figure 115. Log a_{te} versus log t_e for PPS aged at 82°C. The transition from aging to approximate non-aging behavior is illustrated by the abrupt change of shift rate.

Sequential creep tests are also performed at other temperatures mentioned above. At each temperature, t^* is determined, and the shift rate before and after t^* are also obtained. Another example of creep curves and associated aging shift factors at 84°C are demonstrated by Figure 116 and Figure 117. From these results, one can see the time required for attaining equilibrium t^* and aging shift rate μ prior to reaching equilibrium decreases when test temperature increases. The t^* and μ at 84°C are 0.147 hours and 0.308, respectively. The T_g of this material was determined by the peak of $\tan \delta$ and is 92.2°C. The applied stress is 1.22 MPa.

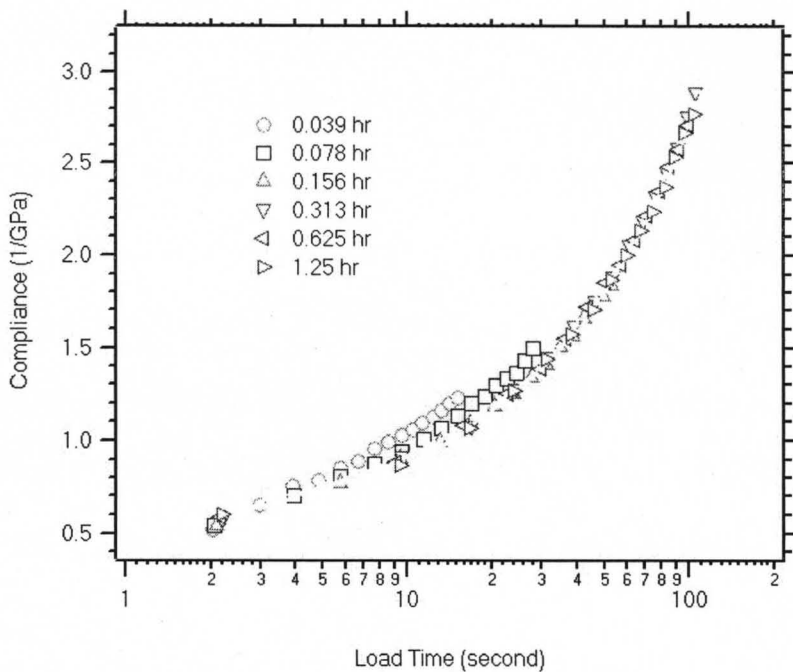


Figure 116. Compliance curves of PPS at 84°C for aging times from 0.039 hr to 1.25 hr

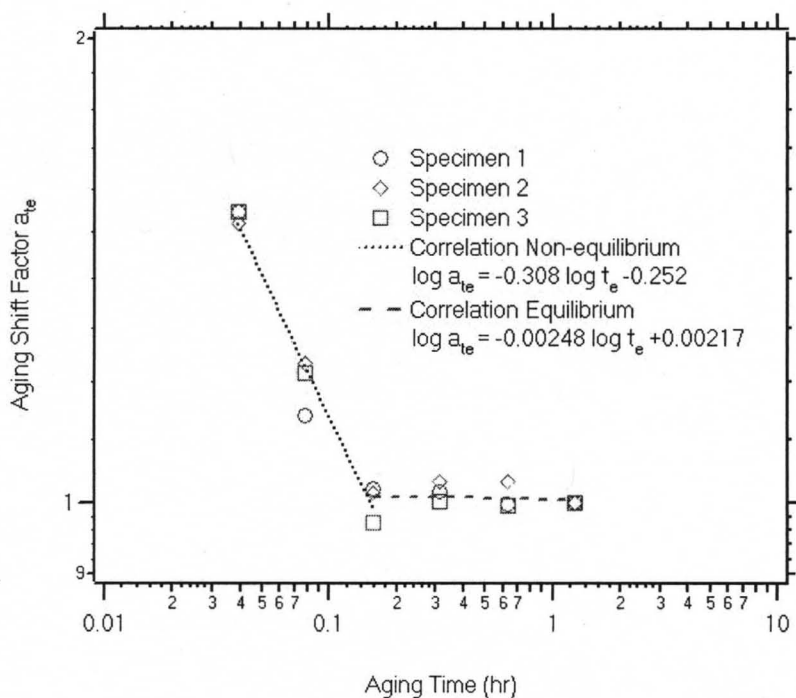


Figure 117. $\log a_{te}$ versus $\log t_e$ for PPS aged at 84°C; the transition from aging to approximate non-aging behavior is illustrated by the abrupt change of shift rate

Besides these examples at 82°C and 84°C, isothermal aging behavior of PPS is

also characterized at 81°C, 83°C, and 85°C. Figure 118 summarizes the transition of aging shift factors (aging into equilibrium) at each temperature; the curves represent the linear equilibrium and non-equilibrium fits of the data sets (e.g. see correlation curves in Figure 117) over the aging times from 0.01 hours to 20 hours. The aging shift rates as well as the t^* are listed in Table 18. It is clear that the aging shift rate and time needed to reach equilibrium decreases with increasing temperatures. When test temperature is 85°C, 7°C below T_g , the material will reach non-aging state at the time after 5.1 min from quenching; while the temperature 11°C below T_g , PPS needs more than 2 hours to reach equilibrium.

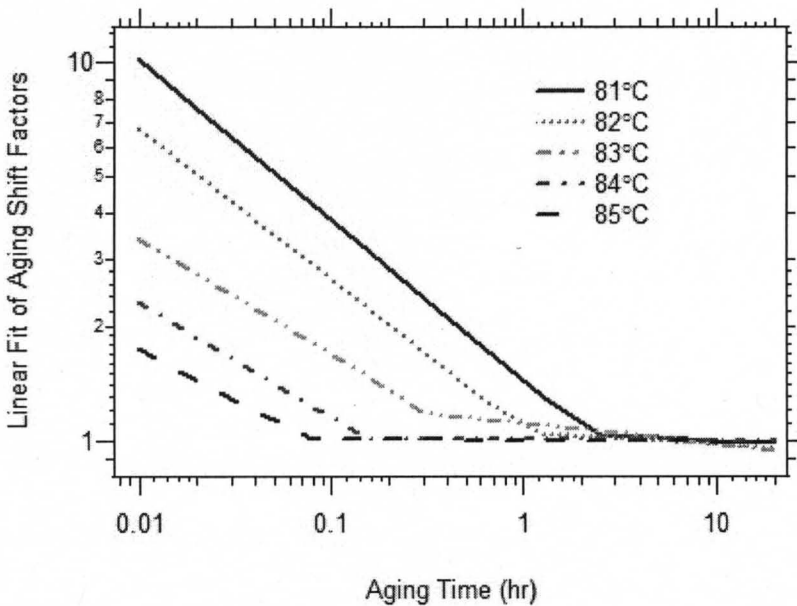


Figure 118. Linear fit of aging shift factors in aging and non-aging regions of PPS, at temperatures 81°C, 82°C, 83°C, 84°C and 85°C

Table 18. Time required to reaching equilibrium t^* and shift rates changing before and after t^* for PPS

Temperature (°C)	t^* (hr)	Shift Rate before t^*	Shift Rate after t^*	Ratio
81	2.185	0.426	0.0192	22.2
82	1.036	0.401	0.0312	12.8
83	0.285	0.378	0.0527	7.17
84	0.147	0.308	0.00248	124
85	0.0856	0.273	0.00489	55.8

To describe and predict equilibrium time t^* from quench below the glass transition temperature, one needs to find the relationship between t^* and the test temperature. One method to obtain this relationship is to plot t^* in logarithmic scale versus the temperature difference $T-T_g$, as presented in Figure 119. In this figure, the $\log t^*$ versus $T-T_g$ of PPS can apparently be expressed by a linear fit with high R-square value. From Figure 119, an equation to describe t^* of PPS material can be found as:

$$t^* = 0.5878 \times 10^{-0.3662(T-T_g)} \quad (87)$$

This line might be used to evaluate the time to equilibrium time at temperatures farther below T_g than the current data set. Experimental work is ongoing to examine how well this method can predict t^* at such temperatures. Note that the glass transition temperature T_g varies if different characterization methods are applied, in this equation, T_g is the temperature corresponding the peak of $\tan \delta$ at 1 Hz.

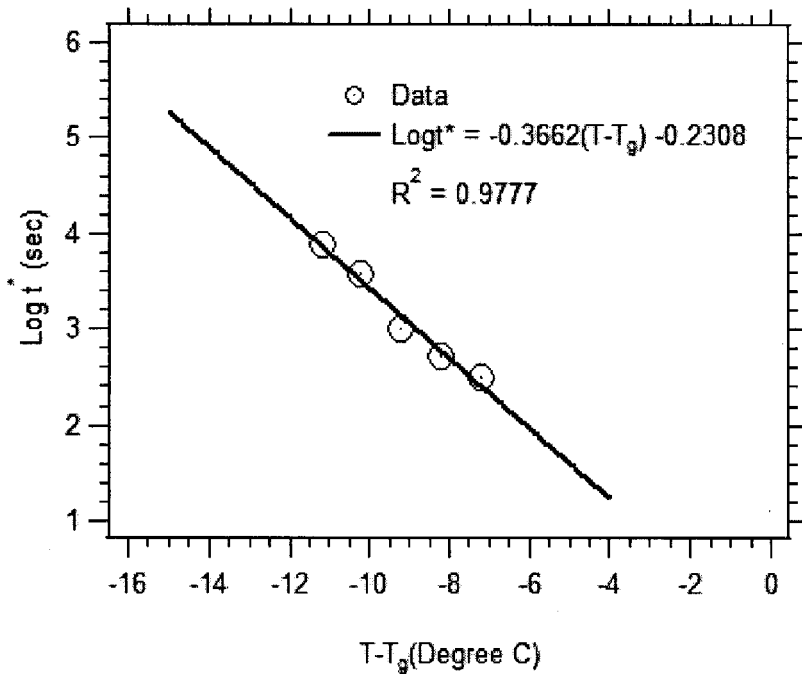


Figure 119. Temperature dependence of the time necessary for attainment of equilibrium t^* of PPS, in isothermal physical aging

7.2 Asymmetry of Approaching Equilibrium

After determining the times need to reach equilibrium at temperatures near T_g , several kinds of nonisothermal aging tests were performed. One of these is a mechanical tests similar to the famous “asymmetry of approaching” found by Kovacs (1963) in 1960’s for specific volume. The relationship between mechanical and thermodynamic properties might be found in these proposed experiments. For example, Kovacs data for specific volume is represented in Figure 120. In this figure, the material (Poly(vinyl acetate) (PVAc)) was allowed to reach equilibrium at the two temperatures labeled T_0 . Subsequently, the material was subjected to a temperature change to 35°C . Note that although the magnitude of the temperature jump in both cases is 5°C , the volume recovers much more rapidly towards equilibrium in the down-jump experiment than it

does in the up-jump experiment. This result shows the inherent nonlinearity of the structural recovery process and has been widely interpreted to imply that the material response (relaxation time) depends upon the instantaneous state or structure of the glass. An example of asymmetry of approaching is shown in Figure 121 via creep tests of PPS. The films were aged to equilibrium at 80, 81 or 85°C, then jumped to 83°C; the aging shift factors were then determined. Figure 121 illustrates a_{te} data sets of several thermal histories and their Prony series fits over aging time from 200 seconds from temperature jump to reaching equilibrium at the final temperature (83°C). These plots show similarities of the thermodynamic and mechanical properties as the response of structural relaxation. This provides the new evidence for the validity of predicting mechanical behavior of polymers using the existing models developed via the thermodynamic methods.

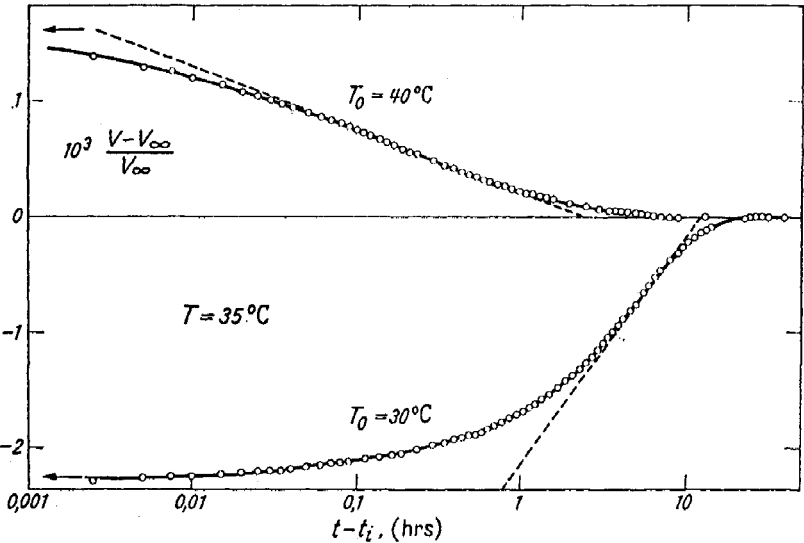


Figure 120. Normalized volumetric response of PVAc after single temperature jump (Kovacs, 1963)

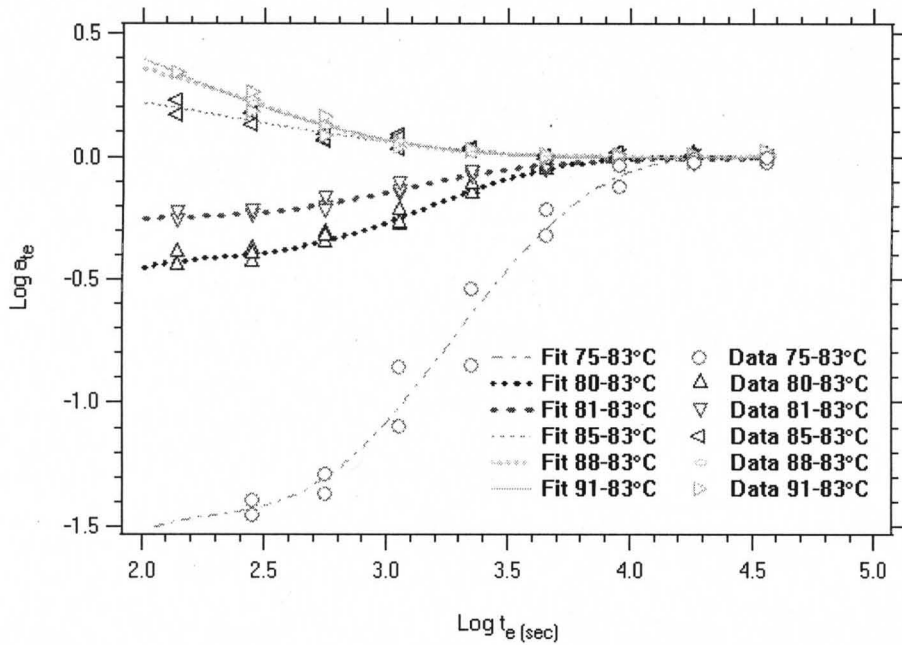


Figure 121. Asymmetry of approaching equilibrium of aging shift factors of PPS

7.3 Effective Relaxation Time Paradox

Kovacs analyzed a series of data sets from asymmetry of approach experiments, including the data shown in Figure 120, using a parameter that he referred to as effective relaxation time (τ_{eff}), which was defined in terms of time derivative of δ as:

$$\tau_{eff}^{-1} = -\frac{1}{\delta} \frac{d\delta}{dt} \quad (88)$$

As a material approaches equilibrium state at a temperature, Kovacs et al. (1979) have shown that τ_{eff} should approach a common constant in either an up-jump or down-jump history using their multiple retardation time KAHR model. However, this was not supported by experiments. In plots of negative log τ_{eff} versus δ , Kovacs observed an apparent paradox: while the values of τ_{eff} converge nicely as δ approaches to zero (i.e. equilibrium) for the down-jump cases, they tend to different values (expansion gap) in the

up-jump cases. The $-\log \tau_{eff}$ data close to equilibrium at several temperatures are demonstrated in Figure 122. The value labeled on the each curve is the temperature at equilibrium before the jump (T_0 in Figure 120), and the value T is the temperature after the jump.

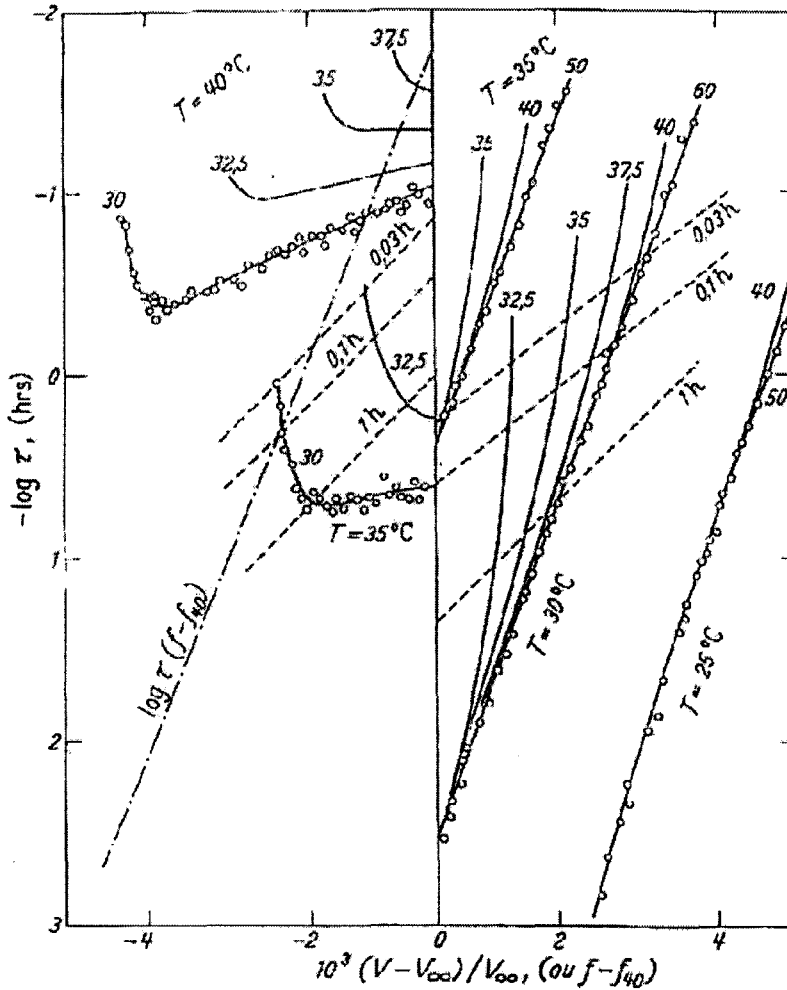


Figure 122. Original τ -effective plot from Kovacs for poly(vinyl acetate). Unlabeled values are equilibrium temperature before the jump, values T are temperatures after the jump, and both lines and circles are experimental data. Left part presents the results for up-jump tests; while the right part shows the results of down-jump experiments (Kovacs, 1963)

McKenna and co-workers examined the Kovacs's data published in 1963 and some unpublished data from the same era, as well as some more recent data from the

Institut Charles Sadron (McKenna et al., 1999). They analyzed these data by several different statistical methods and concluded that an expansion gap did exist for the up-jumps. Simon *et al.* (Kolla and Simon, 2005) studied volumetric response of up-jump and down-jump experiments in an epoxy material at two different final temperatures, after reaching equilibrium on a couple of other temperatures. The results are consistent with those of Kovacs; the τ_{eff} paradox was found at the highest aging temperature but it does not exist at the lowest aging temperature.

The expansion gap and τ_{eff} paradox are important because the phenomenon is not predicted by the most widely used empirical models of structural recovery, the KAHR model and the Tool-Narayanaswamy-Moynihan (TNM) model. These two multiple retardation time models are thermorheologically simple, hence the relaxation time should tend towards a common value at equilibrium. On the other hand, the coupling model developed by Ngai and co-workers was able to predict the expansion gap (Rendell et al., 1987). This model is alternatively derived from a coupled rate equation approach, and such modification causes the model to be thermorheologically complex and allows for successful prediction of the τ_{eff} paradox; however, further work applying the model to structural recovery has not been performed.

As presented in the previous section, the aging shift factors in this dissertation also manifest the characteristics of asymmetry of approaching equilibrium (see Figure 121). After a thorough literature search, the author believes this is the first report on the investigation of aging shift factors on up-jump and down-jump tests after reaching equilibrium. Since this phenomenon is similar to the findings on volume response, it is

reasonable to wonder if an equivalent τ_{eff} paradox can be derived from the aging shift factor data shown in Figure 121 from mechanical testing. Recall the definition of τ_{eff} in Equation (88), the effective relaxation time in mechanical aging shift factors can be given as:

$$\tau_{eff,a_{te}}^{-1} = \frac{1}{\log a_{te}} \frac{d \log a_{te}}{d \log t_e} \quad (89)$$

According to this equation, effective relaxation time based of aging shift factors are calculated using the Prony series fit of a_{te} and $\log t_e$ shown in Figure 121, the results are demonstrated in Figure 123. The left part of this figure clearly shows so-called expansion gap of the up-jump tests as the aging effective relaxation time does not converge when the material is approaching equilibrium ($\log a_{te} \cong 0^-$; see Figure 121). The results of down-jump tests shows that the $\tau_{eff,a_{te}}$ tends to reach a fixed value when the material reaches equilibrium ($\log a_{te} \cong 0^+$), but the curves cross over a little bit before reaching equilibrium. Note that the curves are obtained from curve fitting of discrete aging shift factors. Because limited data points of a_{te} are available from sequential mechanical testing, the changing of a_{te} with increasing aging time could not be precisely described based on the data in Figure 121. Specifically, aging shift factors of thermal histories 88°C equilibrium - 83°C and 91°C equilibrium - 83°C are very close at the same aging time; as such the a_{te} fit for both cases are quite similar.

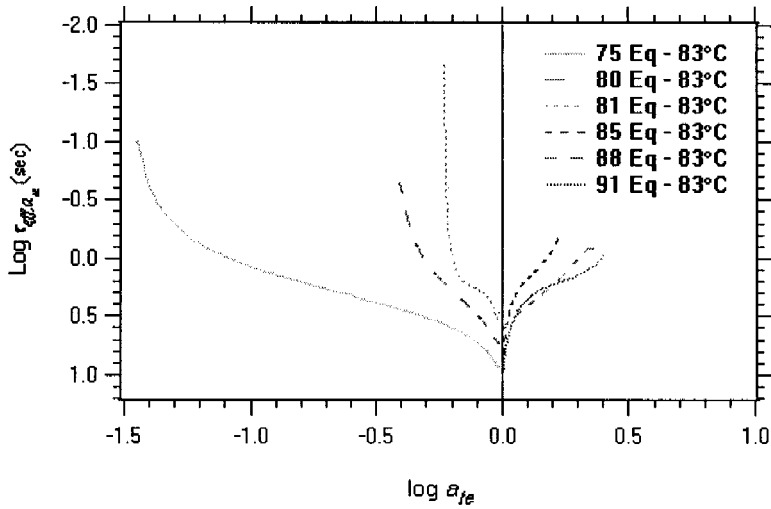


Figure 123. Logarithmic effective relaxation time at 83°C for PPS, the results are obtained from mechanical test results for up-jump and down-jump from equilibrium at various temperatures.

The expansion gap of aging from mechanical tests in Figure 123 is consistent with the findings by Simon and co-workers on an epoxy, as depicted in Figure 124. In this figure, the values of the initial temperatures (T_0) from which each jump was made are indicated. An expansion gap is observed for the largest up-jumps.

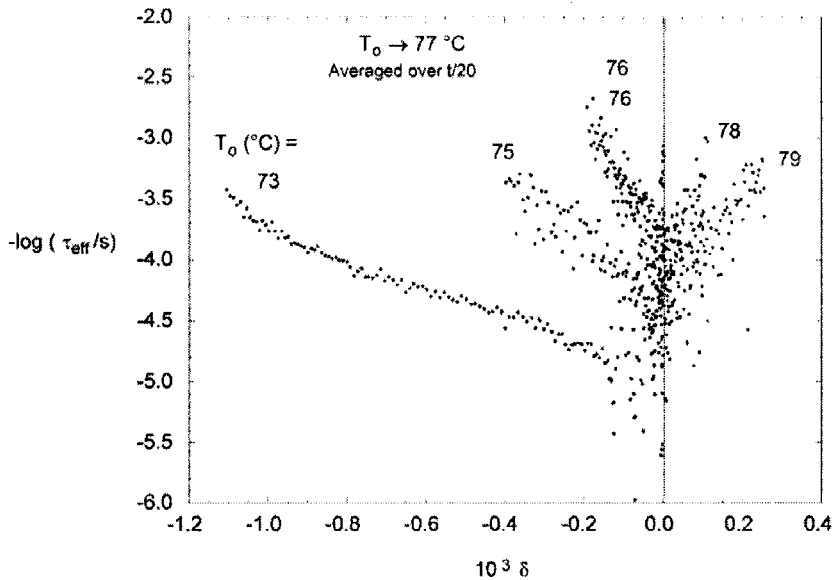


Figure 124. τ -effective plot for an epoxy aging at 77 °C. The values of τ_{eff} were determined from $(d\delta/dt)$ and average δ value obtained from time t to $1.05t$ (i.e. over a logarithmic time interval of 0.02) for the volume recovery curves (Kolla and Simon, 2005)

7.4 Comparison of Mechanical and Volumetric Phenomenology

Note that the kinetics of volume recovery in glassy polymers exhibits a richness of behaviors that offers a severe test of any model (McKenna, 1989; McKenna, 2007; McKenna and Simon, 2002). In order to model these material behaviors, there are three types of physical phenomenology in glassy polymers which must be understood: (1) structural recovery kinetics in the intrinsic isotherm; (2) the nonlinearity of structural recovery in the asymmetry of approach experiment; and (3) the relaxation process in the memory experiment. These three aspects are recognized by researchers from the investigation of volume recovery. Asymmetry of approaching equilibrium in volume response has been shown in Figure 120.

Figure 125 and Figure 126 illustrate the thermal history and volume response of other two classes of experiments. Figure 125 depicts the volume departure from equilibrium on the ordinate and the logarithm of the time after the beginning of the quench on the abscissa, This result was reported by Simon and co-workers (Simon et al., 2001), the test material is polystyrene. Lines in this figure are fits to the TNM model of structural recovery. This result shows that volume response approaching equilibrium under isothermal conditions has similar behavior as the results in Figure 118 from mechanical testing of physical aging.

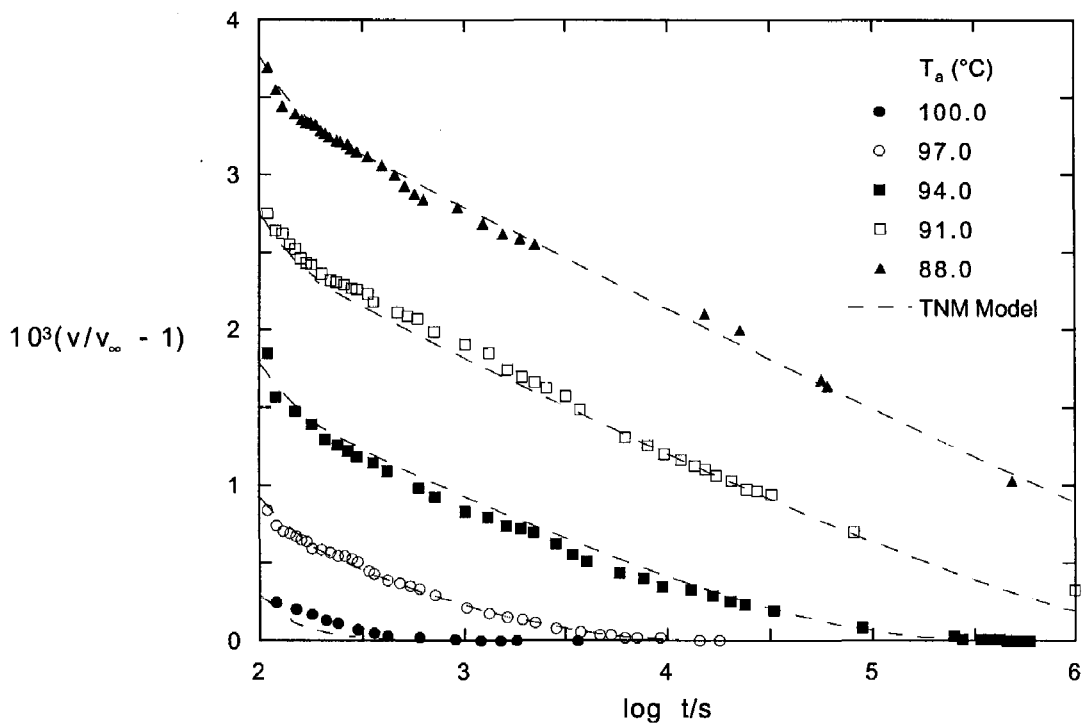


Figure 125. Volume recovery in a polystyrene during isothermal physical aging at various indicated temperatures (Simon et al., 2001)

Figure 126 shows volume response of PVAc following isothermal and several non-equilibrium temperature up-jump tests. For case 2 - 4, material was aged at a lower temperature for a period t_{dwell} and the jumped to the test temperature 30°C. The value t_{dwell} is such that the volume immediately after the jump to 30°C is approximately equal to the equilibrium volume at 30°C (hence, δ is close to 0 at short times for curves 2 - 4). As shown in Figure 126, the δ data go from (or through) a zero value and continue to evolve (cross over), finally merge into the isothermal response. These experimental results are evidence for the existence of a non-exponential relaxation or recovery process.

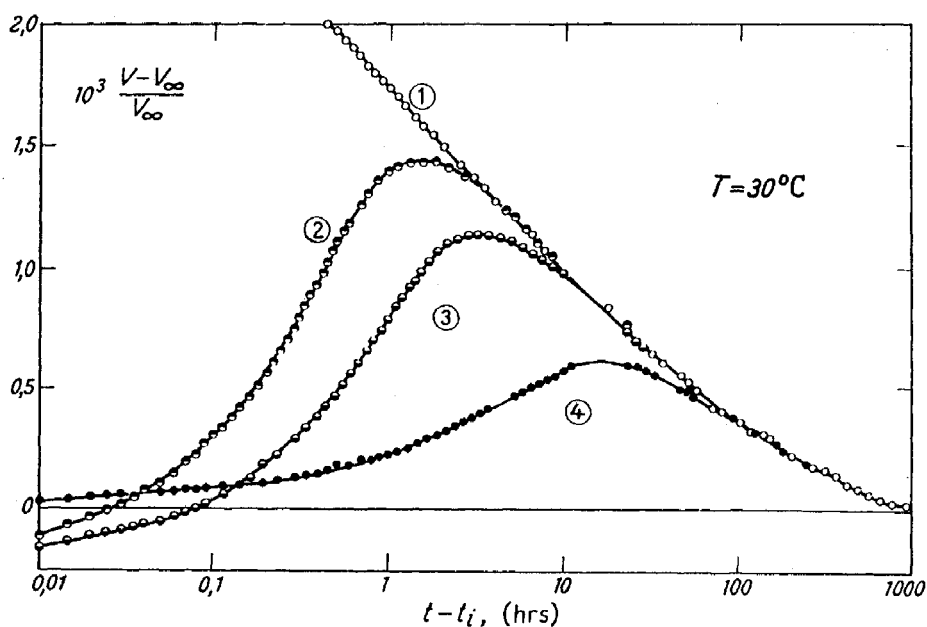


Figure 126. The “memory effect” for volumetric response δ in a poly(vinyl acetate) on several thermal histories. (1): quench from 40°C to 30°C (isothermal aging); (2): quench from 40°C to 10°C for 160 h followed by up-jump to 30°C; (3): quench from 40°C to 15°C for 140 h followed by up-jump to 30°C and (4): quench from 40°C to 25°C for 90 h followed by up-jump to 30°C. $t - t_i$ is the time elapsed since the jump to 30°C (Kovacs, 1963)

The experiments of physical aging near glass transition temperature indicate that the similarity between mechanical and volume properties for the three classes of volume recover experiments above. Comparing the data in Figure 126 with the single temperature up-jump test results in previous chapter, one can find that the non-equilibrium up-jump lead to “memory effect” on aging shift factors, the behavior of nonisothermal aging shift factors has similar response to the volume response. Moreover, Figure 118 and Figure 125 exhibit the same kind results on α_{te} and δ during isothermal aging into equilibrium. As stated before, the asymmetry of approaching equilibrium also exists in mechanical tests (Figure 121).

Studies on physical aging of glassy polymers have shown the similarity between

the volume response and mechanical aging shift factors in all of the three classes experiments found by Kovacs, which constitute the most physical phenomenology for this material. The aging shift factors in both experiments near the glass transition and experiments after non-equilibrium temperature up-jump provide further validation of this idea. These results offer another valuable approach to investigate the relationship between the mechanical response and thermodynamic properties (volume, enthalpy, etc.) during structural relaxation of glassy materials.

CHAPTER 8

SUMMARY AND CONCLUSIONS

In this dissertation, nonisothermal physical aging behavior of glassy polymers has been systemically investigated over a temperature range from $T_g-35^\circ\text{C}$ to $T_g-7^\circ\text{C}$. A sequential creep test method using a DMA was developed and utilized to characterize the effect of physical aging on various thermal histories. The KAHR- a_{te} model was modified by adopting a series of equations describing correlation between mechanical properties and volume response and successfully predicted material behavior under complicated thermal conditions. In addition, all of classic physical phenomenology during structural recovery (intrinsic isotherm, asymmetry of approaching equilibrium and memory effect) on mechanical response was systemically reported in this dissertation, the famous expansion gap was first found from mechanical response. The findings in this dissertation provide methodology to model and predict the time-dependent mechanical behavior of polymeric materials under varying temperature conditions, this will be helpful to design and use neat polymers and polymer matrix composites under complicated thermal environments.

The first portion of this dissertation (Chapter I – III) introduced the background of physical aging in polymers and investigated techniques to characterize mechanical response of polymer materials such as compliance and modulus by using a DMA. A series of test methods were developed to determine: glass transition temperature of a

thermoplastics; linear viscoelastic regime at constant temperature; compliance and modulus properties from creep and stress relaxation testing. In this section, various test protocols used in this study were demonstrated in details, basic polymer viscoelasticity was also presented in the second chapter as background knowledge of this dissertation.

In the second portion of this dissertation (Chapter IV), the physical aging behavior of two polymer films (PEEK, PPS) has been assessed under both creep and stress relaxation. This required the development of approaches to account for minor specimen dimensional variation. It is demonstrated that compliance and modulus results developed using the test methods were extremely consistent for specimens at a given temperature and aging time. Comparison between compliance and modulus, using linear viscoelasticity theory to perform the material function conversion, also indicated excellent agreement between the results; this was also true of the shift rates and temperature shift factors. This finding demonstrates that the test and analysis methods used in this study are adequate to capture the physical aging behavior. These methods and database of physical aging test results will provide a useful foundation for the characterization and modeling of physical aging response under an arbitrary temperature history.

The third portion of the dissertation (Chapter V and VI) considered the mechanical responses of nonisothermal physical aging of polymer films (PEEK and PPS) by experiments and the KAHR- a_{te} model. The short-termed creep tests after single temperature up-jump and more complicated temperature histories were performed at 35-15°C below T_g for PEEK and PPS, in the linear viscoelastic region. Besides the experimental findings, KAHR- a_{te} model was introduced to predict the mechanical

behavior of glassy polymers. The KAHR- a_{te} model is based upon the idea that a correlation exists between volume recovery and physical aging, an assumption which has been verified away from equilibrium by some experimental results. By assuming a form for the correlation, the KAHR model for volume recovery can be extended to predict mechanical response.

The KAHR- a_{te} can be used to predict aging shift factors in multiple nonisothermal conditions in our testing temperature scale, the results of prediction fit the experimental data very well for all of the thermal histories studied in this dissertation. Besides short-term response, long-term creep tests of PPS are performed after complex thermal histories. Effective time theory along with the KAHR- a_{te} model using parameters obtained in up-jump tests were applied to predict long-term creep response after multi-step temperature jumps. The results show clearly that the nonisothermal effective time theory successfully characterizes long-term mechanical behavior during physical aging. As such, it is anticipated that this approach can be used to successfully model the long-term physical aging response of PMCs under nonisothermal service temperature histories.

Prediction of the mechanical behavior of nonisothermal physical aging in polymers is one of the great unsolved problems in the plastics industry and the KAHR- a_{te} model provides a method to predict aging shift factors of polymeric materials subject to complex temperature histories.

The last portion of this work (Chapter VII) describes effect of physical aging near the glass transition temperature. Since aging occurs at elevated temperatures, aging into

equilibrium can be realized at these temperatures. In this dissertation, both isothermal physical aging and nonisothermal physical aging are studied for PPS.

Isothermal physical aging of PPS near the glass transition temperature has been characterized by creep tests by the compliance limit test method. Compliance curves and resulting aging shift factors are analyzed at 81°C, 82°C, 83°C, 84°C, and 85°C, from 11.2°C to 7.2°C below T_g . At each test temperature, the transition of aging shift factor was detected; this suggests that the material has been aged into equilibrium. The time required to reach equilibrium t^* is obtained by the abrupt change of aging shift rate. The temperature dependence of t^* can be expressed by an equation, from the line fit of the data $\log t^*$ verse $T-T_g$. This equation might be used to predict the equilibrium time of PPS polymer at temperature below T_g .

On nonisothermal physical aging, after reaching equilibrium at various temperatures near T_g , up-jump and down-jump were conducted to a common temperature and then creep tests were performed at the final temperature. Like the results reported in volume recovery, asymmetry of approaching equilibrium of mechanical shift factors was found in up-jump and down-jump tests. Based on this finding, effective relaxation time paradox in mechanical behavior was first presented in this dissertation. The study in this section provides experimental evidence on the similarity of phenomenology on mechanical behavior and thermodynamic properties, during the process of structural relaxation. Further research on correlation between these material functions will be useful to predict the material response in many particular forms (volume, enthalpy, creep, relaxation, etc.)

With the above findings, this dissertation has constructed a framework from which predictions of the mechanical response of glassy polymers undergoing nonisothermal physical aging can be obtained. In addition, this dissertation first provided database on mechanical response in all of the three aspects (intrinsic isotherm; asymmetry of approach; and memory effect) of basic physical phenomenology of glassy materials.

REFERENCES

- Aklonis, J. J., and MacKnight, W. J. (1983). Introduction to Polymer Viscoelasticity, John Wiley & Sons, New York.
- Alcoutlabi, M., Banda, L., and McKenna, G. B. (2004). A comparison of concentration-glasses and temperature-hyperquenched glasses: CO₂-formed glass versus temperature-formed glass. *Polymer* 45(16), 5629-5634.
- Alcoutlabi, M., Briatico-Vangosa, F. and McKenna, G. B. (2002). Effect of chemical activity jumps on the viscoelastic behavior of an epoxy resin: Physical aging response in carbon dioxide pressure jumps *JOURNAL OF POLYMER SCIENCE PART B-POLYMER PHYSICS* 40(18), 2050-2064.
- Anonymous (2001). Material Properties Database, Thermal Properties. Plastics International Company.
- Apitz, D., Pedersen, T. G., and Johansen, P. M. (2004). Organic Holographic Materials and Applications II. (K. Meerholz, ed.), Vol. 5521, pp. 181-188. SPIE.
- Arnold, J. C., and White, V. E. (1995). Predictive models for the creep-behavior of PMMA. *Materials Science and Engineering A: Structural materials properties microstructure and processing* 197(2), 251-260.
- Barbero, E. J., and Julius, M. J. (2004). Time-Temperature-Age Viscoelastic Behavior of Commercial Polymer Blends and Felt-Filled Polymers. *Mechanics of Advanced Materials and Structures* 11(287-300).
- Bradshaw, R. D. (1997). Characterization and Modeling of Viscoelastic Composite Laminates with Nonisothermal Physical Aging. Ph.D. Dissertation, Northwestern University, Evanston, IL.
- Bradshaw, R. D., and Brinson, L. C. (1997a). Physical aging in polymers and polymer composites: An analysis and method for time-aging time superposition. *Polymer Engineering and Science* 37(1), 31-44.
- Bradshaw, R. D., and Brinson, L. C. (1997b). Recovering nonisothermal physical aging shift factors via continuous test data: Theory and experimental results. *Journal of Engineering Materials and Technology-Transactions of the Asme* 119(3), 233-241.
- Bradshaw, R. D., and Brinson, L. C. (1997c). Recovering nonisothermal physical aging shift factors via continuous test data: Theory and experimental results. *Journal of Engineering Materials and Technology-Transactions of the ASME* 119(3), 233-241.
- Bradshaw, R. D., and Brinson, L. C. (1997d). A Sign Control Method for Fitting and Interconverting Material Functions for Linearly Viscoelastic Solids. *Mechanics of Time-Dependent Materials* 1(85-108).
- Bradshaw, R. D., and Brinson, L. C. (1997e). A Sign Control Method for Fitting and Interconverting Material Functions for Linearly Viscoelastic Solids. *Mechanics of Time-Dependent Materials* 1(1), 85-108.

- Bradshaw, R. D., and Brinson, L. C. (1999). Mechanical response of linear viscoelastic composite laminates incorporating non-isothermal physical aging effects. *Composites Science and Technology* 59(9), 1411-1427.
- Brinson, H. F., and Brinson, L. C. (2008). *Polymer Engineering Science and Viscoelasticity: An Introduction*, Springer, New York.
- Brinson, L. C., and Gates, T. S. (1995). Effects of physical aging on long-term creep of polymers and polymer matrix composites. *International Journal of Solids and Structures* 32(6-7), 827-846.
- Canadas, J. C., Diego, J. A., Mudarra, M., and Belana, J. (1998). Comparative TSPC, TSDC and DSC physical ageing studies on PET-a. *Polymer* 39(13), 2795-2801.
- Carfagna, C., Amendola, E., Damore, A., and Nicolais, L. (1988). Physical aging of amorphous poly(etheretherketone) (PEEK). *Polymer Engineering and Science* 28(18), 1203-1206.
- Catsiff, E., and Tobolsky, A. V. (1955). Stress-relaxation of polyisobutylene in the transition region. *Journal of Colloid Science* 10(4), 375-392.
- Cheng, S. Z. D., Heberer, D. P., Janimak, J. J., Lien, S. H. S., and Harris, F. W. (1991). Structure and thermal history dependent enthalpy relaxation at the glass transition of semicrystalline polyimides. *Polymer* 32(11), 2053-2059.
- Choy, C. L., and Leung, W. P. (1990). Thermal expansion of poly (ether-ether-ketone) (PEEK). *Journal of Polymer Science: Part B: Polymer Physics* 28(11), 1965-1977.
- Cizmecioglu, M., Fedors, R. F., Hong, S. D., and Moacanin, J. (1981). Effect of physical aging on stress relaxation of poly(methyl methacrylate). *Polymer Engineering and Science* 21(14), 940-942.
- Crawford, R. J. (1992). *Plastics Engineering*, Pergamon, New York.
- D'Amore, A., Cocchini, F., Pompo, A., Apicella, A., and Nicolais, L. (1990). The effect of physical aging on long-term properties of poly-ether-ketone (PEEK) and PEEK-based composites. *Journal of Applied Polymer Science* 39(5), 1163-1174.
- D'Amore, A., Pompo, A., Mijovic, J., and Nicolais, L. (1994). The kinetics of volume relaxation and related property changes during physical aging of poly(ether ether ketone) (PEEK). *Composite Structures* 27(1-2), 45-49.
- D'Amore, A., Pompo, A., and Nicolais, L. (1991). Viscoelastic effects in poly(ether ether ketone) (PEEK) and PEEK-based composites. *Composites Science and Technology* 41(3), 303-325.
- D'Amore, A., Pompo, A., and Nicolais, L. (1993). Volume relaxation and related dynamic mechanical property changes during physical aging of poly-ether-ether-ketone (PEEK). In "Makromolekulare Chemie-Macromolecular Symposia", Vol. 68, pp. 203-212. HUETHIG & WEPF VERLAG.
- Dean, G. D., Tomlins, P. E., and Read, B. E. (1995). A model for nonlinear creep and physical aging in poly(vinyl chloride). *Polymer Engineering and Science* 35(16), 1282-1289.
- Dong, Y., Ruan, Y., Wang, H., Zhao, Y., and Bi, D. (2004). Studies on glass transition temperature of chitosan with four techniques. *Journal of Applied Polymer Science* 93(4), 1553-1558.
- Doolittle, A. K. (1951). Studies in newtonian flow. 2. the dependence of the viscosity of liquids on free-space. *Journal of Applied Physics* 22(12), 1471-1475.
- Drozdov, A. D., and Dorfmann, A. (2003). Physical aging and the viscoelastic response of

- glassy polymers: Comparison of observations in mechanical and dilatometric tests. *Mathematical and Computer Modelling* 37(7-8), 665-681.
- Duran, R. S., and McKenna, G. B. (1990). A torsional dilatometer for volume change measurements on deformed glasses: instrument description and measurements on equilibrated glasses. *Journal of Rheology* 34(6), 813-839.
- Eisele, U. (1990). Introduction to Polymer Physics, Springer-Verlag, New York.
- Emri, I., and Knauss, W. G. (1986). Pressure induced ageing of polymers. In *Nonlinear constitutive relations for high temperature applications*, pp. 77-88. NASA.
- Farrow, G. J., Wostenholm, G. H., Darby, M. I., and Yates, B. (1990). Thermal expansion of PEEK between 80 and 470 K. *Journal of Materials Science Letters* 9(6), 743-744.
- Ferry, J. D. (1980). Viscoelastic Properties of Polymers, Wiley, New York.
- Finley, W. N., Lai, J. S., and Onaran, K. (1976). Creep and relaxation of nonlinear viscoelastic materials, North-Holland Publishing Company, Amsterdam.
- Fleming, G. K., and Koros, W. J. (1986). Dilation of Polymers by Sorption of Carbon Dioxide at Elevated Pressures. 1. Silicone Rubber and Unconditioned Polycarbonate. *Macromolecules* 19(8), 2285-2291.
- Gates, T. S., and Feldman, M. (1995). The effects of physical aging at elevated temperatures on the viscoelastic creep of Im7/K3b. *Journal of Composites Technology & Research* 17(2), 177-178.
- Gates, T. S., Veazie, D. R., and Brinson, L. C. (1996). A Comparison of Tension and Compression Creep in a Polymeric Composite and the Effects of Physical Aging on Creep (NASA-TM-110273), Rep. No. NASA-TM-110273. NASA.
- Guo, Y., and Bradshaw, R. D. (2007). Isothermal Physical Aging Characterization of Polyether-ether-ketone (PEEK) and Polyphenylene Sulfide (PPS) Films by Creep and Stress Relaxation. *Mechanics of Time-Dependent Materials* 11(1), 61-89.
- Guo, Y., Wang, N., Bradshaw, R. D., and Brinson, L. C. (2009). Modeling mechanical aging shift factors in glassy polymers during nonisothermal physical aging. I. experiments and KAHR- a_{te} model prediction. *Journal of Polymer Science Part B: Polymer Physics* 47(3), 340-352.
- Haugh, E. F. (1959). Time, temperature, and linear viscoelasticity. *Journal of Applied Polymer Science* 1(2), 144-149.
- Haward, R. N., and Young, R. J., eds. (1997). The physics of glassy polymers. Springer, London.
- Hernandez, M. C., and Suarez, N. (2004). Physical aging effects on high temperature relaxation of poly(DTH carbonate) and poly(DTO carbonate) monitored by TSPC and TSDC. *Polymer* 45(25), 8491-8499.
- Herzog, B., Gardner, D. J., Lopez-Anido, R., and Goodell, B. (2005). Glass-transition temperature based on dynamic mechanical thermal analysis techniques as an indicator of the adhesive performance of vinyl ester resin. *Journal of applied polymer science* 97(6), 2221-2229.
- Hiemenz, P. C., and Lodge, T. P. (2007). Polymer Chemistry, CRC Press, New York.
- Hopkins, I. L. (1958). Stress relaxation or creep of linear viscoelastic substances under varying temperature. *Journal of Polymer Science* 28(118), 631-633.
- Hourston, D. J., Song, M., Hammiche, A., Pollock, H. M., and Reading, M. (1996). Modulated differential scanning calorimetry: 2. studies of physical ageing in

- polystyrene. *Polymer* 37(2), 243-247.
- Hu, W., Liu, B., Wu, W., Jiang, Z., Zhang, W., and Wu, Z. (2005). Physical aging behavior of 6F-PEEK and m-TPEEK studied by modulated differential scanning calorimetry. *Journal of Applied Polymer Science* 96(2), 312-317.
- Hutchinson, J. M. (1995). Physical Aging of Polymers. *Progress in Polymer Science* 20(4), 703-760.
- Instruments, T. (2003). RSA3 Rheometrics System Analyzer, New Castle, DE.
- Kato, K. (1997). Creep response calculation of rubber-like polymers using ADINA. *Computers and Structures* 64(5-6), 1013-1024.
- Kemmish, D. J., and Hay, J. N. (1985). The Effect of Physical Aging on the Properties of Amorphous PEEK. *Polymer* 26(6), 905-912.
- Knauss, W. G., and Emri, I. (1981). Non-linear viscoelasticity based on free volume consideration. *Computers and Structures* 13(6), 123-128.
- Knauss, W. G., and Emri, I. (1987). Volume change and the nonlinearly thermo-viscoelastic constitution of polymers. *Polymer Engineering and Science* 27(1), 86-100.
- Kohlrausch, F. (1863). Ueber die elastische nachwirkung bei der torsion. *Poogendorff's Annalen der Physik und Chemie* 119(7), 337-368.
- Kolla, S., and Simon, S. L. (2005). The tau-effective paradox: new measurements towards a resolution. *Polymer* 46(3), 733-739.
- Kovacs, A. J. (1958). La contraction isotherme du lolume des polymeres amorphes. *Journal of Polymer Science* 30(121), 131-147.
- Kovacs, A. J. (1963). Transition vitreuse dans les polymeres amorphes. etude phenomenologique. In *Fortschritte der Hochpolymeren-Forschung*, Vol. 3, pp. 394-507.
- Kovacs, A. J., Aklonis, J. J., Hutchinson, J. M., and Ramos, A. R. (1979). Isobaric volume and enthalpy recovery of glasses. 2. A transparent multiparameter theory. *Journal of Polymer Science: Polymer Physics Edition* 17(7), 1097-1162.
- Kreyszig, E. (2005). *Advance engineering mathematics*, 9th/Ed. Wiley, New York.
- Krishnaswamy, R. K., Geibel, J. F., and Lewis, B. J. (2003). Influence of semicrystalline morphology on the physical aging characteristics of poly(phenylene sulfide). *Macromolecules* 36(8), 2907-2914.
- Leaderman, H. (1943). *Elastic and creep properties of filamentous materials and other high polymers*, The Textile Foundation, Washington D. C.
- Lee, A., and G.B., M. (1997). Anomalous aging in two-phase systems: creep and stress relaxation differences in rubber-toughened epoxies. *Journal of Polymer Science* 35(8), 1167-1174.
- Lee, A., and McKenna, G. B. (1988). Effect of crosslink density on physical aging of epoxy networks. *Polymer* 29(10), 1812-1817.
- Lee, A., and McKenna, G. B. (1990a). The physical aging response of an epoxy glass subjected to large stresses. *Polymer* 31(3), 423-430.
- Lee, A., and McKenna, G. B. (1990b). Viscoelastic response of epoxy glasses subjected to different thermal treatments. *Polymer Engineering and Science* 30(7), 431-435.
- Ma, C. C. M., Lee, C. L., Chang, M. J., and Tai, N. H. (1992). Effect of physical aging on the toughness of carbon fiber-reinforced poly(ether ether ketone) and poly(phenylene sulfide) composites. *Polymer Composites* 13(6), 441-447.

- Mark, J. E., Ngai, K. L., Graessley, W. W., Mandelkern, L., Samulski, E. T., Koenig, J. L., and Wignall, G. D. (2004). *Physical Properties of Polymers*, Third/Ed. Cambridge University Press, Cambridge.
- Matsumoto, D. S. (1988). Time-temperature superposition and physical aging in amorphous polymers. *Polymer Engineering and Science* 28(20), 1313-1317.
- Mazurin, O. V., and Gankin, Y. V. (2007). Glass transition temperature: problems of measurements and analysis of the existing data, International Congress on Glass, July 1-6, Strasbourg, France.
- McKenna, G. B. (1989). Glass Formation and Glassy Behavior. In *Comprehensive Polymer Science: The Synthesis, Characterization, Reactions and Applications of Polymers* (C. Booth and C. Price, eds.), pp. 311-362. Pergamon Press, Oxford.
- McKenna, G. B. (1994). Dilatometric evidence for the decoupling of glassy structure from the mechanical stress field. *Journal of Non-Crystalline Solids* 172-174(Part 2), 756-764.
- McKenna, G. B. (1995a). Dynamics and mechanics below the glass transition: the non-equilibrium state. *Computational materials science* 4(4), 349-360.
- McKenna, G. B. (1996). Comments on "Isobaric volume and enthalpy recovery of glasses. II. a transparent multiparameter theory," by A. J. Kovacs, J. J. Aklonis, J.M. Hutchinson, and A. R. Ramos, *J. Polym. Sci., Polym. Phys. Ed.*, 17, 1097 (1979). *Journal of Polymer Science Part B: Polymer Physics* 34(15), 2463-2465.
- McKenna, G. B. (2007). Glassy states: Concentration glasses and temperature glasses compared. *Journal of Non-Crystalline Solids* 353(41-43), 3820-3828.
- McKenna, G. B., Leterrier, Y., and Schultheisz, C. R. (1993). The evolution of material properties during physical aging. In *Use of Plastics and Plastic Composites: Materials and Mechanics Issues (ASME MD-Vol. 46)* (V. K. Stokes, ed.), pp. 245-260, New York.
- McKenna, G. B., Leterrier, Y., and Schultheisz, C. R. (1995). The evolution of material properties during physical aging. *Polymer Engineering and Science* 35(5), 403-410.
- McKenna, G. B., Leterrier, Y. and Schultheisz, C.R. (1995b). The Evolution of Material Properties During Physical Aging. *Polymer Engineering and Science* 35(5), 403-410.
- McKenna, G. B., and Simon, S. L. (2000). Time Dependent Volume and Enthalpy Responses in Polymers. In *Time Dependent and Nonlinear Effects in Polymers and Composites, ASTM STP 1357* (R. A. S. a. C. T. Sun, ed.), pp. 18-46. American Society for Testing and Materials, West Conshohocken, PA.
- McKenna, G. B., and Simon, S. L. (2002). The glass transition: its measurement and underlying physics. In *Handbook of Thermal Analysis and Calorimetry* (S. Z. D. Cheng, ed.), Vol. 3 Applications to Polymers and Plastics. Elsevier Science.
- McKenna, G. B., Vangel, M. G., Rukhin, A. L., Leigh, S. D., Lotz, B., and Straupe, C. (1999). The tau-effective paradox revisited: an extended analysis of Kovacs' volume recovery data on poly(vinyl acetate). *Polymer* 40(18), 5183-5205.
- Mehta, P. K., and Monteiro, P. J. M. (1993). *Concrete structure, properties, and materials*, Prentice-Hall, Englewood Cliffs.
- Menard, K. P. (1999). *Dynamic Mechanical Analysis*, CRC Press, Boca Raton.
- Miyano, Y., Nakada, M., Kasamori, M., and Muki, R. (2000). Effect of physical aging on

- the creep deformation of an epoxy resin. *Mechanics of Time-Dependent Materials* 4(1), 9-20.
- Moynihan, C. T., Crichton, S. N., and Opalka, S. M. (1991). Linear and Non-linear Structural Relaxation. *Journal of Non-Crystalline Solids* 131(11), 420-434.
- Muzeau, E., Vigier, G., Vassoille, R., and Perez, J. (1995). Changes of thermodynamic and dynamic mechanical properties of poly(methyl methacrylate) due to structural relaxation: low-temperature ageing and modelling. *Polymer* 36(3), 611-620.
- Narayanaswamy, O. S. (1971). Model of Structural Relaxation in Glass. *Journal of the American Ceramic Society* 54(10), 491-497.
- Ngai, K. L. (2000). Short-time and Long-time Relaxation Dynamics of Glass-forming Substances: A Coupling Model Perspective. *Journal of Physics: Condensed Matter* 12(29), 6437-6451.
- Ngai, K. L. (2003). An Extended Coupling Model Description of the Evolution of Dynamics with Time in Supercooled Liquids and Ionic Conductors. *Journal of Physics: Condensed Matter* 15(11), S1107-S1125.
- O'Connell, P. A., and McKenna, G. B. (1997). Large deformation response of polycarbonate: Time-temperature, time-aging time, and time-strain superposition. *Polymer Engineering and Science* 37(9), 1485-1495.
- Ogale, A. A., and McCullough, R. L. (1987). Physical aging characteristics of polyether ether ketone. *Composites Science and Technology* 30(2), 137-148.
- Plazek, D. J. (1965). Temperature dependence of the viscoelastic behavior of polystyrene. *Journal of Physical Chemistry* 69(10), 3480-3487.
- Press, W. H., Teukolsky, S. A., Vetterling, W. T., and Flannery, B. P. (1992). *Numerical Recipes in C: The Art of Scientific Computing*, Cambridge University Press, Cambridge.
- Ramos, A. R., Hutchinson, J. M., and Kovacs, A. J. (1984). Isobaric Thermal Behavior of Glasses during Uniform Cooling and Heating. 3. Predictions from the Multiparameter KAHR model. *Journal of Polymer Science: Polymer Physics Edition* 22(9), 1655-1696.
- Read, B. E., Dean, G. D., Tomlins, P. E., and Lesniarekhamid, J. L. (1992). Physical aging and creep in PVC. *Polymer* 33(13), 2689-2698.
- Read, B. E., and Tomlins, P. E. (1997). Creep and physical aging of injection molded, fiber reinforced polypropylene. *Polymer Engineering and Science* 37(9), 1572-1581.
- Rendell, R. W., and Ngai, K. L. (1987). Coupling Model Interpretation of Dielectric Relaxation of Poly(vinyl acetate) near T_g. *Journal of Chemical Physics* 87(4), 2359-2362.
- Rendell, R. W., Ngai, K. L., and Fong, C. R. (1987). Volume recovery near the glass transition temperature in poly(vinyl acetate): predictions of a coupling model. *Macromolecules* 20(5), 1070-1083.
- Resapu, R. R. (2005). Isothermal and nonisothermal aging of polymers. M.S. Thesis, University of Louisville, Louisville, KY.
- Riande, E., Diaz-Calleja, R., Prolongo, M. G., Masegosa, R. M., and Salom, C. (2000). *Polymer Viscoelasticity: Stress and Strain in Practice*, Marcel Dekker, New York.
- Robertson, C. G., and Wilkes, G. L. (1998). Refractive index: a probe for monitoring volume relaxation during physical aging of glassy polymers. *Polymer* 39(11),

2129-2133.

- Robertson, C. G., and Wilkes, G. L. (2000). Physical aging behavior of miscible blends containing atactic polystyrene and poly(2, 6-dimethyl-1, 4-phenylene oxide). *Polymer* 41(26), 9191-9204.
- Robertson, R. E. (1979). Effect of Free Volume Fluctuations on Polymer Relaxation in the Glass State 2. Calculated Results. *Journal of Polymer Science: Polymer Physics Edition* 17(4), 597-613.
- Robertson, R. E. (1992). Free-Volume Theory and Its Application to Polymer Relaxation in the Glass State. In *Computational Modeling of Polymers* (J. Bicerano, ed.). Marcel Dekker Inc., New York.
- Robertson, R. E., Simha, R., and Curro, J. G. (1984). Free Volume and Kinetics of Aging of Polymer Glasses. *Macromolecules* 17(4), 911-919.
- Santore, M. M., Duran, R. S., and McKenna, G. B. (1991). Volume recovery in epoxy glasses subjected to torsional deformations: the question of rejuvenation. *Polymer* 32(13), 2377-2381.
- Schapery, R. A. (1969). On the characterization of nonlinear viscoelastic materials. *Polymer Engineering and Science* 9(4), 295-310.
- Scherer, G. W. (1986). Relaxation in glass and composites, Wiley, New York.
- Schultheisz, C. R., McKenna, G. B., Leterrier, Y., and Stefanis, E. (1995). A comparison of structure and aging time shift factors from simultaneous volume and mechanical measurements. In "Proceedings of 1995 SEM Spring Conference on Experimental Mechanics", pp. 329-335.
- Schwarzl, F. R., and Kaschta, J. (1998). Physical aging and shear creep of poly(carbonate). *Mechanics of Time-Dependent Materials* 2(1), 13-36.
- Simon, S. L., Sobieski, J. W., and Plazek, D. J. (2001). Volume and enthalpy recovery of polystyrene. *Polymer* 42(6), 2555-2567.
- Skrypnik, I. D., Spormaker, J. L., and Kandachar, P. (2000). A constitutive model for long-term behavior of polymers. In *Time dependent and nonlinear effects in polymers and composites* (R. A. Schapery and C. T. Sun, eds.), pp. 71-82. American Society for Testing and Materials, West Conshohocken.
- Sperling, L. H. (2005). Introduction to physical polymer science, Fourth /Ed. Wiley-Interscience, New York.
- Spinu, I., and McKenna, G. B. (1994). Physical aging of nylon-66. *Polymer Engineering and Science* 34(24), 1808-1814.
- Spinu, I., and McKenna, G. B. (1997). Physical aging of thin films of nylon and PET. *Journal of Plastic Film and Sheeting* 13(4), 311-326.
- Struik, L. C. E. (1978). Physical Aging in Amorphous Polymers and Other Materials, Elsevier Scientific Publishing Co., Amsterdam.
- Struik, L. C. E. (1988). Dependence of relaxation times of glassy polymers on their specific volume. *Polymer* 29(8), 1347-1353.
- Struik, L. C. E. (1997). On volume-recovery theory .2. Test on Kovacs's original delta vs t data. *Polymer* 38(20), 5233-5241.
- Sullivan, J. L. (1990). Creep and Physical Aging of Composites. *Composites Science and Technology* 39(3), 207-232.
- Sullivan, J. L., Blais, E. J., and Houston, D. (1993). Physical Aging in the Creep-Behavior of Thermosetting and Thermoplastic Composites. *Composites Science*

- and Technology* 47(4), 389-403.
- Svoboda, R., Pustkova, P., and Malek, J. (2008). Structural relaxation of polyvinyl acetate (PVAc). *Polymer* 49(13-14), 3176-3185.
- TA Instruments (2003). RSA3 Rheometrics System Analyzer, New Castle, DE.
- Tant, M. R., and Wilkes, G. L. (1981). An Overview of the Non-Equilibrium Behavior of Polymer Glasses. *Polymer Engineering and Science* 21(14), 874-895.
- Tomlins, P. E. (1996). Comparison of different functions for modeling the creep and physical ageing effects in plastics. *Polymer* 37(17), 3907-3913.
- Tomlins, P. E., and Read, B. E. (1998). Creep and physical ageing of polypropylene: A comparison of models. *Polymer* 39(2), 355-367.
- Tomlins, P. E., Read, B. E., and Dean, G. D. (1994). The Effect of Temperature on Creep and Physical Aging of Poly(Vinyl Chloride). *Polymer* 35(20), 4376-4381.
- Tool, A. Q. (1946). Relation between inelastic deformability and thermal expansion of glass in its annealing range. *Journal of the American Ceramic Society* 29(9), 240-253.
- Tran, L. T. (1996). Stress relaxation in polymer matrix composites. Ph.D. Dissertation, University of California at Berkeley, Berkeley, CA.
- Tschoegl, N. W. (1989). The Phenomenological Theory of Linear Viscoelasticity: An Introduction, Springer-Verlag, Berlin.
- Turnbull, D., and Cohen, M. H. (1961). Free-volume model of the amorphous phase: glass transition. *Journal of Chemical Physics* 34(1), 120-125.
- Veazie, D. R., and Gates, T. S. (1997). Compressive creep of IM7/K3B composite and the effects of physical aging on viscoelastic behavior. *Experimental Mechanics* 37(1), 62-68.
- Vleeshouwers, S., Jamieson, A. M., and Simha, R. (1989). Effect of physical aging on tensile-stress relaxation and tensile creep of cured epon-828 epoxy adhesives in the linear viscoelastic region. *Polymer Engineering and Science* 29(10), 662-670.
- Wang, N. (2007). Isothermal physical aging characterization and test methodology for neat and nanotube-reinforced poly(methyl methacrylate) (PMMA) near the glass transition temperature. M.S. Thesis, University of Louisville, Louisville, KY.
- Ward, I. M. (1983). Mechanical Properties of Solid Polymers, John Wiley & Sons, New York.
- Williams, M. L., Landel, R. F., and Ferry, J. D. (1955). The temperature dependence of relaxation mechanisms in amorphous polymers and other glass-forming liquids. *Journal of American Chemical Society* 77(14), 3701-3707.
- Yang, Y., D'Amore, A., Di, Y. W., Nichols, L., and Li, B. Y. (1996). Effect of physical aging on phenolphthalein polyethersulfone/poly(phenylene sulfide) blend. I. mechanical properties. *Journal of Applied Polymer Science* 59(7), 1159-1166.
- Zheng, S. F., and Weng, G. J. (2002). A new constitutive equation for the long-term creep of polymers based on physical aging. *European Journal of Mechanics A: Solids* 21(3), 411-421.
- Zheng, Y., and McKenna, G. B. (2003). Structural recovery in a model epoxy: Comparison of responses after temperature and relative humidity jumps. *Macromolecules* 36(7), 2387-2396.
- Zheng, Y., Priestley, R. D., and McKenna, G. B. (2004). Physical Aging of an Epoxy Subsequent to Relative Humidity Jumps Through the Glass Concentration.

CURRICULUM VITAE

NAME: Yunlong Guo

ADDRESS: Department of Mechanical Engineering, Speed School of
Engineering, University of Louisville, Louisville, KY 40292

DATE OF BIRTH: October 23, 1977, Beijing, P. R. China

EDUCATION: B.S. Automotive Engineering
Tsinghua University
1996-2000
M.S. Mechanical Engineering
Tsinghua University
2000-2003
Ph.D., Mechanical Engineering
University of Louisville
2003-2009

AWARD/HONORS: Sigma Xi Scientific Honor Society, Student member, since
2008
Who's Who among Students in American Universities and
Colleges, 2008
Hsing Chuang Award for Excellence in Graduate Study,
University of Louisville, 2007
Grosscurth Fellowship, University of Louisville, 2003-2005
Guang Hua Scholarship for Graduate Students, 2nd Prize,
Tsinghua University, 2001

General Scholarship for Graduate Study, Ministry of
Education of China, 2000-2003
Scholarship for Excellence, 3rd Prize, Tsinghua University,
1998

PROFESSIONAL SOCIETIES:

American Society of Mechanical Engineers (ASME)
Society for Experimental Mechanics (SEM)
Materials Research Society (MRS)
Society of Plastics Engineers (SPE)
American Association for the Advancement of Science (AAAS)

RESEARCH EXPERIENCE:

- (1) Experimental Investigation of Glassy Polymers using DMA. Developed experimental protocols of essential test methods (creep, stress relaxation, dynamic temperature ramp, etc.) used by dynamic mechanical analyzer. 2000+ hours experience on testing viscoelastic properties of polymers, including both isothermal/nonisothermal and short-term/long-term responses. Performed experiments on variety of polymeric materials such as PC, PPS, PEEK, PEI, PVC, PMMA, SWNT-PMMA, etc.
- (2) KAHR-ate Model. Co-author of KAHR-ate model. The KAHR-ate model describes time-dependent mechanical behavior for the nonisothermally structural relaxation. My work includes: found and represented a correlation between thermodynamic and mechanical properties in non-equilibrium state upon different thermal histories; first applied the KAHR-ate model to predict physical aging of glassy polymers upon complicated thermal histories; developed an optimization procedure to determine optimal (error minimization) model parameters for various temperature scenarios.
- (3) Nonisothermal Long-term Response of Polymers (To be published). Obtained

the long-term creep response of glassy polymers during nonisothermal physical aging. Successfully described and predicted these long-term behaviors found in the experiments, by expanding the effective time theory from constant temperature into complex thermal conditions.

- (4) Physical Aging near Glass Transition (To be published). Investigated physical aging behavior of glassy polymers near the glass transition temperature, found the similarity of mechanical and thermodynamic properties in isotherm, asymmetry and memory effect.

PUBLICATIONS:

Refereed Journal Articles

- Guo, Y. and Bradshaw, R.D. “Structural Relaxation in Glassy Polymers: Comparison of Mechanical and Thermodynamic Properties,” manuscript in preparation.
- Guo, Y. and Bradshaw, R.D. “Long Term Creep of Polyphenylene Sulfide (PPS) subjected to Complex Thermal Histories: the Effects of Physical Aging,” *Polymer*, Manuscript submitted, March, 2009.
- Guo, Y. and Bradshaw, R.D. “Modeling Mechanical Aging Shift Factors in Glassy Polymers during Nonisothermal Physical Aging: Part 2. Optimization of KAHR-ate Model Parameters,” *Polymer Bulletin*, to be submitted, April, 2009.
- Guo, Y., Wang, N., Bradshaw, R.D., and Brinson, L.C. “Modeling Mechanical Aging Shift Factors in Glassy Polymers during Nonisothermal Physical Aging: Part 1. Experiments and KAHR-ate Model Prediction,” *Journal of Polymer Science, Part B: Polymer Physics*, 2009, 47(3), 340-352.
- Guo, Y. and Bradshaw, R.D. “Isothermal Physical Aging Characterization of Polyether-ether-ketone (PEEK) and Polyphenylene sulfide (PPS) Films by Creep and Stress Relaxation,” *Mechanics of Time-Dependent Materials*, 2007, 11(1), 61-89.

- Guo, Y. and Zhao, Y. “Power Shaft Design for Dynamic Engine Test Bed,” Internal Combustion Engine Engineering (in Chinese), 2003, 24(6), 37-41.

Full-Length Conference Papers

- Guo, Y. and Bradshaw, R.D. “Physical Aging Characterization of PPS Near the Glass Transition Temperature,” Society for Experimental Mechanics Annual Conference, June 2009, Albuquerque, NM. To be submitted.
- Guo, Y. and Bradshaw, R.D. “Modeling Physical Aging of PPS Subjected to Complex Thermal Histories,” Society for Experimental Mechanics Annual Conference, June 2008, Orlando, FL.
- Guo, Y. and Bradshaw, R.D. “Creep Behavior of a Glassy Polymer during Nonisothermal Physical Aging,” Mechanics of Time-Dependent Materials Conference, March 2008, Monterey, CA.

Conference Presentations (Presenter's name bolded)

- **Guo, Y.**, Wang, N., Bradshaw, R.D. “Modeling Nonisothermal Physical Aging in Polymers and Polymer Matrix Composites,” 4th Annual Kentucky Innovation and Enterprise Conference, July 2008, Lexington, KY.
- Guo, Y. and **Bradshaw, R.D.** “Modeling Physical Aging of Polymers Subjected to Complex Thermal Histories,” Society for Experimental Mechanics Annual Conference, June 2008, Orlando, FL.
- **Guo, Y.** and Bradshaw, R.D. “Creep Behavior of a Glassy Polymer During Nonisothermal Physical Aging,” Mechanics of Time-Dependent Materials Conference, March 2008, Monterey, CA.
- Guo, Y., Wang, N., **Bradshaw, R.D.** “Nonisothermal Physical Aging of Glassy polymers: Experimental data and KAHR-ate model Predictions,” 2007 Joint ASME/ASCE/SES Conference on Mechanics and Materials, June 2007, Austin, TX.

Technical Reports (Non-Proprietary)

- Bradshaw, R.D., Guo, Y., Wang, N. and Resapu, R.R. “Summary Project Report – Modeling Nonisothermal Physical Aging in Polymers and Polymer Matrix Composites,” report to Kentucky Science and Engineering Foundation (KSEF) under grant number KSEF-148-502-05-136, June 12, 2007.
- Bradshaw, R.D., Guo, Y., Wang, N. and Resapu, R.R. “Annual Project Report – Modeling Nonisothermal Physical Aging in Polymers and Polymer Matrix Composites,” report to Kentucky Science and Engineering Foundation (KSEF) under grant number KSEF-148-502-05-136, May 1, 2006.